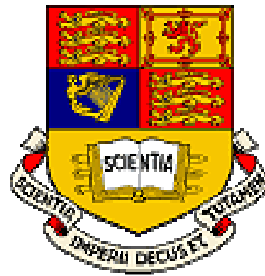


**SLDV TECHNOLOGY FOR MEASUREMENT OF MISTUNED BLADED
DISC VIBRATION**

A thesis submitted to the University of London
for the degree of Doctor of Philosophy



By
Dario Di Maio

Department of Mechanical Engineering
Imperial College London

May 2007

Abstract

Bladed discs are very sensitive structures and the amplitude vibration of each blade can vary significantly from blade to blade due to a series of factors such as geometrical inhomogeneity between blades or material properties. These factors lead to bladed disks mistuned thus the forced response amplitudes can be much higher than the level predicted for a tuned assembly.

Designed models need to be “validate” to predict the response of a real bladed disc within the tolerances set by the manufactures and this process is very expensive as well as difficult. The validation process needs “reference data” as fundamental input against what all predictions can be compared and validated. Data that can be provided both under stationary conditions and under rotating conditions and the latter is the most difficult to achieve, especially for bladed disc assemblies which are very sensitive to any structural modification as it could be attaching a transducer to measure vibrations. There are contact-less measurement techniques available which, however, provide limited information because they can measure only limited areas of the vibrating structures.

The aim of this study is to design measurement methods, using a standard Scanning Laser Doppler Vibrometer (SLDV) and to integrate it into a software platform which will be able to handle a series of measurement tasks both under stationary and rotating conditions. The main contribution of this thesis is to extend the use of Continuous Scanning LDV (CSLDV) to the rotating structures, such as bladed discs, thus to perform synchronous measurements. Hence, a bladed disc is needed to be designed to perform vibration predictions and measurements and a mathematical model of the measurement test to control, critically, all possible sources of errors involved in measurement under rotating

conditions; all these to produce a robust measurement method. While the primary focus is the measurement method, the study also extends to evaluation of the sensitivity properties of the bladed disk test pieces that are the object of the measurement tool.

Acknowledgements

I would like to express my gratitude to my supervisor Professor David J. Ewins. As a *Master and Commander*, he gave me the guide and the freedom to experience the passion for the scientific research during these years. I also acknowledge his great patience and guidance during the writing up of this thesis.

Special thanks are due to Mr. D. Robb, Mr. A. B. Stanbridge, Mr J. Miller and P. Woodward for sharing with me their professional and working skills, from which I could gain such useful experiences.

Thanks to A. Tuchinda, E. Wing, M. Martarelli, H. Elizalde, M.Cand, W. Liu, G. Chen, E. Petrov, I. A. Severe, S. Nayagam, C. Zang, S. Huang, M. Nikolic, G. Girini, C. Schwingshackl, Professor J. Griffin, D. Feiner, all ERASMUS students and many others for having shared with me this wonderful inter-cultural experience.

Thanks to Professor Enrico P. Tomasini and Dr. L. Scalise for having given to me the chance to start this long journey.

I acknowledge the financial support of the US Air Force which entirely funded this research.

Special thanks are due to my parents because without them I would not be here enjoying this life. Finally, thanks to S. Montagnino and D.D.M.

Nomenclature

V_{Rn}	Real component of the vibration
V_{In}	Imaginary component of the vibration
Ω	Rotational speed
ω	Vibration frequency
t	Time
R	Radius
Ω_{r-LDV}	Radial LDV scan rate
$\Omega_{\theta-LDV}$	Circumferential LDV scan rate
$\varepsilon_x, \varepsilon_y$	Mirrors' rotation angles
S_x, S_y	Mirror's constants
V_x, V_y	Mirrors' voltages
α	Generic angle
λ	Rotation of the laser head around Y axis
ρ	Rotation of the laser head around X axis
d_x	Offset of the laser head along X axis
d_y	Offset of the laser head along Y axis
L	Distance of the laser head from the target
c	Distance between X and Y mirrors
τ	Initial angle
δ_x, δ_y	X-Y mirrors phase lag
$\varphi(t)$	Phase along the circumferential direction
F	Force
χ	Coordinate in the rotating frame of reference
$\{\phi\}$	Eigenvector
$[K]$	Stiffness matrix

$[M]$	Mass matrix
$[D]$	Damping matrix
η	Damping loss factor
Ω_{LDV}	LDV scan rate
$v_z(t)$	Vibration in z-direction
$\vec{\omega}$	Rotation vector

Abbreviations

<i>BL</i>	Buffer length
<i>NS</i>	Number of samples
<i>UR</i>	Update rate
<i>P</i>	Pulses
<i>ODS</i>	Operational Deflection Shape
<i>LDV</i>	Laser Doppler Vibrometry
<i>CSLDV</i>	Continuous Scanning LDV
<i>T-CSLDV</i>	Tracking-CSLDV
<i>MF</i>	Magnification factor
<i>DAC</i>	Digital Analogue Converter
<i>EO</i>	Engine Order
<i>DC</i>	Direct Current
<i>AC</i>	Alternate Current
<i>TTL</i>	Transistor-Transistor-Logic

Contents

1	Introduction	19
1.1	Overview	19
1.2	Definition of problem	21
1.3	Objectives of the study	24
1.4	Overview of the thesis.....	26
2	Literature review	29
2.1	Overview	29
2.1	Introduction	31
2.2	Continuous Scanning Laser Doppler Vibrometry	32
2.2.1	Introduction	32
2.2.2	Vibration measurements of moving structures using the CSLDV technique	32
2.3	Tracking Laser Doppler Vibrometer	36
2.3.1	Introduction	36
2.3.2	Application of the Scanning Laser Doppler Vibrometer to tracking a target point on a moving structure (Tracking LDV- TLDV).....	37
2.3.3	Tracking-Continuous Scanning LDV, TCSLDV	40
2.4	LDV measurements of rotating blade vibrations	41
2.4.1	Introduction	41
2.4.2	Blade vibration measurements by non-intrusive techniques	41
2.5	LDV vibration measurements on rotating shafts	43
2.5.1	Introduction	43
2.5.2	Laser vibrometer in torsional and bending vibration measurements	
	43	
2.6	Conclusions.....	45

3	The path to Tracking-CSLDV: X-Y scanning mirrors, study of X-Y mirror waveforms and sources of misalignment.....	46
3.1	Overview	46
3.2	Scanning device characterization and synchronization method	47
3.2.1	X-Y mirrors scanning device	47
3.2.2	Scanning device of Polytec PSV-300.....	50
3.2.3	Synchronization method.....	52
3.3	Tracking accuracy	54
3.3.1	Misalignment due to shaft and Blisk mounting.....	57
3.3.2	Mathematical description	58
3.4	Point tracking.....	65
3.4.1	Waveform study.....	65
3.4.2	Scanning device driver control	66
3.5	Line Tracking.....	68
3.5.1	Waveform study.....	68
3.5.2	Scanning device driver control	70
3.6	Area Tracking	71
3.6.1	Waveform study.....	71
3.6.2	Scanning device driver control	73
3.7	Conclusions.....	74
4	Blisk and Test rig: design and instrumentation.....	76
4.1	Overview	76
4.2	Blisk design	76
4.2.1	24-Bladed Disk Testpiece	78
4.3	Development of the rotating test rig	86
4.3.1	Original <i>ADTURB</i> test rig description.....	86
4.3.2	<i>USAF</i> test rig updating.....	89
4.3.3	Excitation Systems; DC and AC magnets.....	90
4.4	Conclusions.....	100

5	Virtual Test Simulation (VTS) using Tracking-Continuous Scanning LDV methods	101
5.1	Overview	101
5.2	Virtual Test Simulation (VTS) concepts.....	102
5.2.1	Structure of a VTS for the CSLDV method	103
5.3	ODS theory.....	104
5.4	Polynomial Curve Fitting	105
5.4.1	Polynomial curve fitting inaccuracy	106
5.5	Point Tracking method VTS	110
5.5.1	Point Tracking-VTS, Polynomial curve fitting	110
5.5.2	Point Tracking-VTS, LDV time history.....	112
5.6	Line Tracking method VTS.....	117
5.6.1	Line Tracking-VTS, Polynomial curve fitting.....	118
5.6.2	Line Tracking-VTS, LDV time history	119
5.6.3	ODS reconstruction.....	125
5.6.4	VTS simulations and real measurement test results.....	129
5.7	Area Tracking method VTS.....	132
5.7.1	Area Tracking-VTS, LDV time history.....	133
5.7.2	Area Tracking-VTS, ODS.....	137
5.7.3	VTS simulations and real measurement test results.....	138
5.8	Conclusions.....	140
6	Tracking-CSLDV measurement methods: applications.....	142
6.1	Overview	142
6.2	CAISER MYMESIS software platform.....	143
6.3	Point Tracking method: applications.....	145
6.3.1	Experimental validation of the effect of Coriolis force on the dynamics of bladed disk	145
6.3.2	USAF IBR FRFs measurements under rotating conditions.....	150
6.4	Line Tracking method: applications.....	153

6.4.1	USAF IBR and measurement results.....	154
6.5	Area Tracking method: applications.....	155
6.5.1	USAF IBR measurement results.....	156
6.6	Conclusions.....	162
7	Geometrical sensitivity study of a bladed disk	163
7.1	Overview	163
7.2	Introduction	163
7.3	Forced response calculation method.....	165
7.4	Inter-blade tip slot width variation	167
7.4.1	Stationary Conditions.....	168
7.4.2	Rotating Conditions.....	172
7.5	Blisk thickness variation	173
7.5.1	Stationary conditions.....	175
7.5.2	Rotating conditions.....	178
7.6	Conclusions.....	179
8	Conclusions and Suggestion for Further Work.....	181
8.1	Summary and Conclusions.....	181
8.1.1	Overview of Tracking-CSLDV methods.....	181
8.1.2	Test rig and USAF IBR design.....	183
8.2	Future Work.....	185
	References.....	187
	Bibliography.....	191

List of figures

Figure 3.1	Schematic representation of the mirrors rotation.....	48
Figure 3.2	Flow-chart of the feedback control action	49
Figure 3.3	X-Mirror, technical drawing	50
Figure 3.4	Y-Mirror, technical drawing	50
Figure 3.5	X-Mirror; FRF, Amplitude	51
Figure 3.6	X-Mirror; FRF, Phase	51
Figure 3.7	Y-Mirror; FRF, Amplitude	51
Figure 3.8	Y-Mirror; FRF, Phase	51
Figure 3.9	Alignment system	56
Figure 3.10	Alignment method	57
Figure 3.11	Ideal alignment.....	58
Figure 3.12	Sources of misalignment	58
Figure 3.13	Laser head aligned	59
Figure 3.14	Initial laser spot position ($\alpha=0$ degree).....	59
Figure 3.15	Offset of the laser head along X axes.....	60
Figure 3.16	Offset of the laser head along Y axes.....	61
Figure 3.17	Rotation of the laser head around X axes	61
Figure 3.18	Rotation of the laser head around Y axes	61
Figure 3.19	Path traced around the designed position.....	63
Figure 3.20	Path traced in rotating frame of reference.....	63
Figure 3.21	LDV output signal polluted by pseudo vibration.....	64
Figure 3.22	Generated pattern in red and the actual traced in blue.....	66
Figure 3.23	Output X-Y waveforms	66
Figure 3.24	Point Tracking front panel.....	68
Figure 3.25	Generated pattern in red and the actual traced in blue.....	70
Figure 3.26	X-Y waveforms	70

Figure 3.27 Line Tracking front panel.....	71
Figure 3.28 Triangular scan pattern	72
Figure 3.29 Generated pattern in red and the actual traced in blue.....	73
Figure 3.30 X-Y waveforms	73
Figure 3.31 Area Tracking front panel.....	74
Figure 4.1 Variation of the blade tip width and disc thickness.....	80
Figure 4.2 Veering study for blade sector	80
Figure 4.3 FEM blade sector	81
Figure 4.4 FEM blade sector; zoomed.....	81
Figure 4.5 24-Bladed disc.....	82
Figure 4.6 Dimensions of the USAF 24-Bladed disc	82
Figure 4.7 1T and 2F natural frequencies plot calculated at rest	83
Figure 4.8 Modal content of the two families of model at rest.....	83
Figure 4.9 1T and 2F natural frequencies plot calculated at 2400 rev/min.....	83
Figure 4.10 Modal content of the two families of model at 2400 rev/min	83
Figure 4.11 Curves 1T and 2F calculated for rotational speeds of 0 rev/min and 2400rev/min	84
Figure 4.12 Result of the Steady Stress analysis calculated at rotational speed of 2400 rev/min	84
Figure 4.13 Series of curves for 2F and 1T families.....	85
Figure 4.14 Stepper motor	87
Figure 4.15 Front and rear of test rig.....	87
Figure 4.16 Index mechanism	88
Figure 4.17 The self-tracking system scheme	88
Figure 4.18 Measurement test set-up	89
Figure 4.19 Fixed AC exciter, left hand side; Rotating AC exciter, right hand side	90
Figure 4.20 DC magnet	91
Figure 4.21 Example of a typical train of magnet pulses	92

Figure 4.22 Harmonics of a magnet pulse and its reconstruction through these harmonics	93
Figure 4.23 AC magnet	93
Figure 4.24 AC operational scheme	94
Figure 4.25 Rotating exciter and slip ring; prototype.....	97
Figure 4.26 FRF data using rotating and fixed AC magnet; sine sweep excitation	98
Figure 4.27 Slip rings, rotating exciter and overall assembly.....	99
Figure 4.28 Measured force produced by the exciter with 1mm gap inputting sinewaves at 6V (blue) and 12V (red)	99
Figure 5.1 Flow chart scheme of simulator panel	104
Figure 5.2 ODS; 2 nd flexural mode shape.....	107
Figure 5.3 Zoom of dotted circle.....	107
Figure 5.4 Zoom of dotted circle when the curve fitting is good.....	108
Figure 5.5 LDV time data; poor fitting	108
Figure 5.6 LDV time data; good fitting.....	108
Figure 5.7 ODS of a blade	109
Figure 5.8 LDV time data; bad fitting	109
Figure 5.9 LDV time data; improved fitting	109
Figure 5.10 Front panel of Point Tracking VTS-Polynomial Curve Fitting tab ..	111
Figure 5.11 ODS simulations with excitation and response positions.....	112
Figure 5.12 Front panel of Point Tracking VTS-LDV time history simulator	112
Figure 5.13 Path traced by the laser beam around the targeted location	116
Figure 5.14 LDV output time signal of Point Tracking-simulation.....	116
Figure 5.15 Frequency spectrum of LDV output time signal	116
Figure 5.16 LDV output time signal of Point Tracking-measured	117
Figure 5.17 Frequency spectrum of the measured LDV output time signal	117
Figure 5.18 Polynomial curve fitting for Line Tracking VTS; straight-line in white	119

Figure 5.19 Front panel of Line Tracking VTS, time history simulator; graph plots tab	119
Figure 5.20 Possible scan path traced by laser beam due to misalignment	124
Figure 5.21 Measured and simulated LDV time data; left hand side and right hand side, respectively	124
Figure 5.22 Frequency spectrum of measured and simulated LDV time data; left hand side and right hand side, respectively	125
Figure 5.23 Flowchart of ODSs comparison	126
Figure 5.24 Line Tracking-ODS section. Parameters settings, top. ODS plots, bottom.....	127
Figure 5.25 ODSs reconstructed from straight-line and small line loop scan.....	130
Figure 5.26 ODSs obtained from simulated LDV time data.....	131
Figure 5.27 ODSs obtained from measured LDV time data.....	132
Figure 5.28 Front panel of Area Tracking-VTS, time history simulator; Laser patterns.....	133
Figure 5.29 Simulated (left) and measured(right) of LDV time history; X-Y area scan.....	136
Figure 5.30 Frequency spectrum of simulated (left) and measured(right)time history	136
Figure 5.31 Area Tracking-ODS section, ODS settings and plots.....	137
Figure 5.32 MAC, ODS_s/ODS_{REF}	139
Figure 5.33 MSE, ODS_s/ODS_{REF}	139
Figure 5.34 ODS at 127Hz; X=20, Y=1.1	140
Figure 5.35 ODS at 127 Hz; X=21, Y=1.1	140
Figure 5.36 ODS at 127Hz; X=20, Y=1.1	140
Figure 5.37 ODS at 127 Hz; X=21, Y=1.1	140
Figure 6.1 CAISER MYMESIS front panel	144
Figure 6.2 USAF 24-bladed disk with straight and swept blades respectively ..	147
Figure 6.3 Straightening of the blade due to the centrifugal load	148

Figure 6.4 Frequency split of the 3ND mode measured at 0 rev/min, 120 rev/min and 180 rev/min, respectively	149
Figure 6.5 Measurement and predictions for the 2 ND and 3 ND mode, respectively	150
Figure 6.6 FRF measurement of tuned USAF 24 bladed disk at 0 rev/min, 600 rev/min and 1000 rev/min, respectively.	151
Figure 6.7 FRF measurement of tuned USAF 24 bladed disk at 0rev/min (red), 600 rev/min (black) and 1000 rev/min (blue), respectively. Zoom on 2ND mode	151
Figure 6.8 FRF measurement of mistuned USAF 24 bladed disk at 0rev/min, 600 rev/min and 1000 rev/min, respectively.	152
Figure 6.9 FRF measurement of mistuned USAF 24 bladed disk at 0rev/min (red), 600 rev/min (black) and 1000 rev/min (blue), respectively. Zoom on 3ND mode	153
Figure 6.10 Series of tracking line scans	155
Figure 6.11 Series of tracking line scans	155
Figure 6.12 FRFs measured at 0 (top left), 240 (top right) and 900 (bottom) rev/min, respectively	157
Figure 6.13 ODSs measured at rest for resonances (1), (2) and (3), respectively	158
Figure 6.14 ODSs measured at 240 rev/min for resonances (1), (2) and (3), respectively	158
Figure 6.15 ODSs measured at 900 rev/min for resonances (1) and (3), respectively	159
Figure 6.16 ODSs reconstructed form measurements performed at rotational speed range between 60 to 2400 rev/min.....	160
Figure 6.17 ODS of the USAF IBr 24-bladed disk, measured (left) and simulated (right) at 225.12 Hz and 60 rev/min.....	161
Figure 6.18 LDV output time data on the left hand side and zoom of the time signal on the right hand side	161

Figure 7.1 Change of 2 nd flap-wise and 1 st torsional family of modes to inter-blade tip slot width variation	165
Figure 7.2 Random mistuning pattern applied and geometrical dimensions	168
Figure 7.3 Tuned frequencies (top); FRF of blisk model with slot width of 5mm	169
Figure 7.4 Magnification Factor plots for each damping level.....	170
Figure 7.5 Magnification factor results of 12ND mode for all 14 blisk models ..	171
Figure 7.6 Magnification factor results of 12ND mode for all 14 blisk models; increased mistuning.....	172
Figure 7.7 Magnification factor plots calculated at 600 rev/min and 1200 rev/min, respectively for the 12 ND mode	173
Figure 7.8 Magnification factor plots calculated at 1800 rev/min and 2400 rev/min, respectively for the 12 ND mode	173
Figure 7.9 Random mistuning pattern applied and geometrical dimensions	174
Figure 7.10 Tuned frequencies (top); FRF of blisk model with 1.9mm thickness	176
Figure 7.11 Magnification Factor plots for each damping level.....	177
Figure 7.12 Magnification factor plots calculated at 0 rev/min; 12 ND mode	177
Figure 7.13 Magnification factor plots calculated at 600 rev/min and 1200 rev/min, respectively, for the 12 ND mode.....	178
Figure 7.14 Magnification factor plots calculated at 1800 rev/min and 2400 rev/min, respectively, for the 12 ND mode.....	179

List of tables

Table 4.1 Geometry dimensions of the 24-bladed blisk	81
Table 4.2 FEM construction parameters.....	81
Table 5.1 Parameter setup for the simulation	115
Table 5.2 Parameter setup for the simulation	123
Table 5.3 LDV mirror scan rate used both for the simulations and measurements	129
Table 5.4 Measurement tests parameters settings	129
Table 5.5 Parameter setup for the simulation and measurement of Area scan..	136
Table 5.6 LDV mirror scan rate used both for the simulations and measurements	138
Table 6.1 Mistuning pattern applied on the USAF IBr 24-bladed disk	152
Table 6.2 Radial LDV scan frequency.....	155
Table 6.3 Radial LDV scan frequency.....	155
Table 6.4 Rotational speeds set up for ODS measurement tests	159
Table 7.1 Geometrical dimensions of FE blisk models	168
Table 7.2 Geometrical dimensions of FE blisk models	175

1 Introduction

1.1 Overview

The research described in this thesis aims to develop a new vibration measurement methodology using the Laser Doppler Vibrometry (LDV) principle to investigate the vibrations pattern of the bladed discs which are used in gas turbines, both under stationary and rotating conditions. Bladed disc vibration amplitudes are known to be seriously amplified and varied from blade to blade due to the scatter in blade geometry or due to the variation in material properties. The phenomenon of having non-identical blades due to these kinds of variations is called *mistuning* and the distribution around a bladed disc is called a *mistuning pattern*. This pattern is generally random and unknown to the manufacturer and the user when installed. This problem has been the primary concern of many research studies and researchers working on this topic have developed several numerical models to represent the bladed disc assemblies to facilitate prediction of the relevant behaviour. All the numerical models produced need to be validated against real data acquired from real bladed discs to check the reliability of the numerical models. Different vibration measurement transducers have been used during the past to acquire the

response of the blades during their operating conditions but the process is difficult. The transducer that would offer a great advantage in the study of the mistuning problems is the LDV system thanks to the contact-less feature of the vibration measurement which does not affect the dynamic behaviour of the blades and the mistuning pattern of the bladed discs. Since the installation and the enhancement of scanning mirrors into the head of the laser, two important measurement techniques have been developed in recent years: the Continuous Scanning LDV (CSLDV) and the Tracking LDV technique (TLDV).

Blade vibration response prediction has been extensively studied at Imperial College, and, as a result, several numerical models have been developed. The Continuous Scanning LDV (CSLDV) technique is a relatively new innovative vibration measurement method developed in the past 8 years at Imperial College. The purpose of the present study is to ensure that mistuning analyses, such as those carried out at Imperial College, are effective for the design and manufacture of bladed discs. In order to achieve this, a new powerful vibration measurement tool has to be designed to perform vibration measurements of bladed discs during rotating conditions running in a well-controlled test rig. This is essential since testing at full-scale level is generally difficult and inadequately controlled and that could lead the measurements analysis to an improper interpretation of the results.

1.2 Definition of problem

The laser Doppler vibrometry (LDV) method operates by detection of a Doppler frequency shift, f_D , in the light backscattered from a vibrating surface. This backscattered light from the target is optically mixed with a mutually coherent reference beam and heterodyned on the photodetector surface. Frequency demodulation of the photodetector signal produces a time-resolved voltage of the target component vibration. The traditional way to use the LDV is as a single point sensor which measures the spatial vibration pattern by discretely stepping the laser beam through a succession of predefined grid points marked on the target. The introduction of the scanning device, made up of two mirrors having orthogonal axes which deflect the laser beam towards the target, and a video camera into the head of the laser head constitute the so-called Scanning Laser Doppler Vibrometer (SLDV). The SLDV system enhanced the performance of the measurement tests. Actually, now, over the image of the target, acquired by the video camera, a grid of points can be defined which can be scanned one-by-one automatically by the laser beam driven by the scanning mirrors. The Continuous Scanning LDV (CSLDV) method is a vibration measurement method that has been developed at Imperial College and is a step forward of the use of the SLDV system. CSLDV is a type of spatial field measurement where the SLDV system is employed as a velocity transducer whose laser beam can be **continuously** scanned over the vibrating surface of the target so that, ideally, all the points

constituting the surface are addressed and measured. The main concept behind the CSLDV method is that the laser beam, scanned continuously along a path of a structure vibrating sinusoidally at any excitation frequency, ω , will give a modulated LDV signal output whose frequency spectrum contains a set of sidebands which describe the vibration pattern. Then, the LDV output signal acquired can be post-processed to obtain the Operating Deflection Shape (ODS) of the structure under study. The CSLDV technique overtakes some limitations of the traditional acquisition point-by-point performed using the SLDV system in step scan mode, the most important of which is the time consumption of the full measurement test.

A brief overview of the deliverables and milestones of the project supporting this study will help the reader to have a better understanding of: (i) the Dynamic field on which the CSLDV method will have to operate and (ii) how this method has to be enhanced to achieve the final goals. The project is divided into a set of hard deliverables, some of them as reported below:

- 1) Literature survey of CSLDV methods for Rotating Structures
- 2) Numerical simulation of the CSLDV method for stationary and rotating Structures in order to understand and to optimize its application in practice
- 3) Blisk Testpiece design

-
- 4) Suite for CSLDV measurement methods of Stationary and Rotating Structures
 - 5) Vibration Tests on Non-Rotating and Rotating Mistuned Testpieces

This study must aim to move a further step forward on the development of the CSLDV technique for the vibration measurement of structures under rotating conditions, in order to provide measured data and so to validate the numerical models of the structures under study. The new measurement tool must be able to perform vibration measurements of rotating machines during operating conditions which are, for the actual study, rotating bladed discs. The SLDV system will have to track a rotating target and to measure its vibrations continuously during the rotation of the target. It has to work both at fixed point on the structure or simultaneously scanning across its surface and, for the specific case of rotating bladed discs, up and down the length of the blade. Therefore, in order to define paths, such as a straight-line, to be scanned on the surface of the rotating target, some functions have to be studied and coded to feed the scanning mirrors. Actually, whatever path chosen to be scanned on a rotating target, a rotating frame of reference coordinate system, will be achieved by coding such functions in a stationary frame of reference coordinate system. Then, according to the functions developed to drive the scanning mirrors, it will be possible to check both the performance of the scanning device and those

problems which will arise at different frequency scan rates. Once the SDLV system can perform tracking measurements, it will be necessary to post-process the data acquired using the CSLDV technique. The acquired data will be analysed and studied carefully in order to understand which sources of noise or/and additional components can pollute and lead to misinterpretation of the data for the reconstruction of the ODSs of the structures under tests. When the enhanced CSLDV technique for vibration measurements of rotating structures is reliable, it will also be possible to use the CSLDV measurement method to gain valuable info for validating models (of bladed discs).

1.3 Objectives of the study

The solution strategy to achieve the final goal, which is represented by the CSLDV method for vibration measurements of rotating structures, can be divided in a series of phases:

- 1) A literature review of measurement techniques based on the LDV method has to be produced, focussing the review for vibration measurement studies of structures under rotating conditions.
- 2) A detailed FE model of the test piece will have to be prepared. At this stage, the model will be assumed to be verified since none of the dynamic characteristics of the structure are compromised during the modelling. However, the bladed disk must satisfy a number of important criteria which were set at the beginning of the design process:

-
- 2.1) The family of 1st torsional modes has to be 'above' the family of 2nd flap-wise modes by a few tens of Hertz at 0 rev/min.
 - 2.2) The veering region has to be localized at around 4-6 nodal diameters at 0 rev/min.
 - 2.3) The two families of curves have to be fully separated, meaning no overlap between them, at 2400 rev/min.

The surfaces of the blades have to be wide enough to easily perform a scan using the CSLDV method.

- 3) A Virtual Test Simulation (VTS) software package has to be developed so to be able to reduce the level of uncertainty of the LDV signal output and to have all the parameters which have to be taken into consideration under optimal control.
- 4) The next phase of this study will consist in the conversion of the numerical models, developed under the simulation processes, into the actual functions feeding the scanning mirrors and thus in the production of panels to control the scanning laser device itself. All the information gathered by the simulation processes will be used in order to reduce the time consumption both during the real measurement set-up in the laboratory and during the analysis of the data acquired.

5) The final stage of the thesis will present true applications of all measurement methods developed. Results of vibration measurements under rotating conditions will be produced.

1.4 Overview of the thesis

This thesis presents a theoretical and, consequently, an experimental approach to the development of the continuous scanning LDV techniques under rotating conditions. Besides the main focus of the thesis, the design of the test piece, a 24-bladed disk, and the updating of an existing test rig are also presented. During the design process, a study focussed on the bladed disk geometrical optimization could be explored and one chapter is dedicated to that.

Chapter 2 presents an overview of CSLDV methods developed during the past years and some possible applications. This chapter, then, introduces all tracking techniques performed on moving structures using LDVs, to conclude with some applications on bladed disk measurements.

Chapter 3 focuses on three main aspects of the synchronous measurement methodology: 1) Scanning mirrors description and the role played by an external time base clock for sampling the X-Y mirrors waveforms, 2) possible sources of misalignment presented as mathematical models and 3) the study of X-Y waveforms and their codification into a control panel for performing tracking tasks.

Chapter 4 is focused on the design of the test piece, a 24-bladed disk, and on the description of the test rig design. The geometrical shape of the blades forced the development of a specific laser beam pattern to be traced over the surface in

order to measure the Operational Deflection Shape (ODS) under rotating conditions. Then, the chapter evolves through the description of the test rig presenting the original design and the updated one to meet the new measurement requirements such as ODS and FRFs measurements at speed. Three possible ways to perform the excitations on rotating targets are also explored.

Chapter 5 introduces briefly the software platform CAISER MYMEASIS. The main focus of this chapter is on the virtual test simulations (VTS). These are a reproduction of real vibration measurement tests but resolved in mathematical models to be run in any computer. To help the understanding of the simulator panels, the chapter develops along an introduction of VTS to go into the Operational Deflection Shape (ODS) mathematical concept followed by Polynomial curve fitting concept to conclude into the simulator panels' explanation and practical use of them for time signal predictions.

Chapter 6 provides some examples of tracking CSLDV measurement methods used during the past years. The chapter logic path follows the order of tracking methods complexity and starts from the Point Tracking to conclude with Area Tracking method. Several examples of measurements are provided for all three techniques and for the first time an ODS of whole 24-bladed disk, measured under rotating conditions, is shown. The software platform, CAISER MYMESIS, designed to control all measurement methods is presented, at this time, and the acronym of the software name is explained in detail.

Chapter 7 focuses on the study of the geometrical sensitivity of bladed disk to geometrical variations when a datum random mistuning pattern under both stationary and rotating conditions is superimposed. The research focuses on the

change of forced response ratio between mistuned and tuned FE models of which a high number was constructed. By plotting the highest forced response ratios of all FE models we should be able to see whether a geometrical variation can affect amplitude response of mistuned models

The overall conclusions are summarized in **Chapter 8**. The degree of success in achieving the task undertaken is discussed and some recommendations in the furthering of the work performed here are presented.

2 Literature review

2.1 Overview

The aim of this chapter is to present a survey of vibration measurement methods for moving components based on the laser Doppler vibrometry (LDV) concept. Since the 1960s, the laser Doppler system has been continuously developed to meet the needs of industries requiring a reliable transducer for non-contact vibration measurement, especially for measurements on moving structures. That goal has been achieved by enhancement of the performance of the scanning LDV system installed into the head of the laser and the consequent development of two important measurement techniques: the Continuous Scanning LDV technique (CSLDV) and the Tracking LDV technique (TLDV).

The laser Doppler vibrometer operates by the detection of a Doppler frequency shift, f_D , in the light backscattered from a vibrating surface. This backscattered light from the target is optically mixed with a mutually coherent reference beam and heterodyned on the photodetector surface. Frequency demodulation of the photodetector signal produces a time-resolved voltage analogue of the target component vibration.

The traditional way to use the scanning LDV is as single-point sensor which measures the vibration pattern by discretely stepping the laser beam through a predefined grid of points marked on the target. By coupling the LDV with a scanning device, made up of two mirrors having orthogonal axes, the laser beam

can be precisely deflected towards pre-selected measurement points. The assembly of the two systems, laser sensor and scanning device, constitutes the so-called Scanning Laser Doppler Vibrometer (SLDV). The SLDV system performs point-by-point scan that means the predefined acquisition points on the target are measured by the laser beam one-by-one. At each stage the acquired information is saved therefore, there is a high time consumption.

The Continuous Scanning LDV is a type of spatial field measurement that aims to overcome the limitations of conventional contacting transducers. The SLDV system is employed as a velocity transducer whose laser beam can be continuously scanned over the vibrating surface of the target. Ideally, with CSLDV method all the points constituting the surface are addressed and measured in few seconds.

Tracking LDV (TLDV) is a type of measurement that opens a new era in the measurements of moving structures. Actually, making use of its scanning mirrors, the laser beam in a conventional SLDV can be moved to perform measurements tracking a point of the structure under operating conditions.

The possibility of combining these two methods, performing continuous scan measurements tracking a structure during its operating conditions such as rotating bladed discs, could offer enormous advantages.

Hence the CSLDV and TLDV can easily overtake the limitations occurred using other measurement methods for rotating structures.

2.1 Introduction

During the last few years, automotive industries and aero engine manufacturers required to perform tests on moving components. New measurement methods able to save time and new transducers able to measure whatever target without contact have been always required. Since 1960s, Laser Doppler system has been developed to satisfy the needs of these industries and new measurements methods have been designed to work with such a device. The Laser Doppler vibrometer offers a great advantage to measure the velocity of a vibrating target without contact. It is an effective alternative of a traditional contacting transducer which is unable to be used on hot, light or rotating components. The aim of this document is to offer an overview of vibration measurement methods developed in the last decade based on the LDV concept. Continuous scanning LDV (CSLDV) and tracking LDV (TLDV) methods will be presented in the first two parts of this paper. The introduction of scanning mirrors into the head of the laser opened a new era in approaching to the measurement methodologies. They offer a reliable possibility to measure the vibrations while the laser beam is scanned over a grid of points, previously defined over the surface. That technology has been further developed, allowing the system to perform a continuous scan over the target, comparing to the traditional, SLDV, discrete point-by-point approach. The fastest signal processing to get the ODS of the investigated test piece has been also developed [1]. When the scanning mirrors are driven by particular software that permit to the laser beam to track a point on a moving structure, then a Tracking LDV has been yielded. The system operating in tracking measurements opens a wide range of applications over the investigation of moving structures. A survey of the turbo machinery blades vibrations measurement by LDV and fibre-optic LDV will be illustrated in the third section. Last part of this document will illustrate the employ of the LDV

and its developments in torsional and bending vibrations occurring in rotating shafts.

2.2 Continuous Scanning Laser Doppler Vibrometry

2.2.1 Introduction

Often it is important to investigate the vibration of moving components during their operating conditions in order to understand what vibration mechanisms are at work. Even if the actual measurements are very difficult to perform, they may be of considerable importance in, for instance, rotating discs such as turbine bladed discs or brake discs or gear-wheels. The Scanning Laser Doppler Vibrometer offers a great advantage in such measurements thanks to the particular capability of being able to measure the vibration of a moving object while the acquisition point is being scanned over the surface. The scanning device, installed into the head of the LDV, allows us to scan the laser beam continuously along a straight line, or around a circle, or in an arc, or over an area if it is properly driven by sinusoidal functions. Measurements performed using CSLDV techniques are applicable equally for targets in stationary condition and in rotating condition. All the parameters to perform continuous scanning LDV are controlled by the user, hence no external input from other transducers are needed.

2.2.2 Vibration measurements of moving structures using the CSLDV technique

In general case [1], a straight line scan on a stationary structure vibrating at frequency, ω , will give a modulated LDV signal output whose frequency spectrum contains a set of sidebands. The straight-line scan is achieved by imposing to the scanning device a co-sinusoidal signal: $x(t) = A \cos(\Omega_{LDV}t)$ where

Ω_{LDV} is the frequency scan rate and A is the amplitude. The vibration response of the LDV beam direct to trace a straight-line scan at frequency of Ω_{LDV} will be:

$$v_z(t) = \sum_{n=0}^p V_{Rn} \cos^n(\Omega_{LDV}t) \cos(\omega t) + \sum_{n=0}^p V_{In} \cos^n(\Omega_{LDV}t) \sin(\omega t) \quad (2.1)$$

Expanding out trigonometrically, multiple terms arise at frequencies $(\omega \pm n\Omega_{LDV})$, which are called upper and lower sidebands and they are symmetrical respect to the central frequency ω . Their values, in magnitude and phase, can be used to derive the Operating Deflection Shape (ODS) of scanned pattern. That measurement method can be applied to the vibration measurement of the moving timing belt [2]. The spectrum of the measured LDV signal will have a symmetrical set of sidebands spaced about the frequency scan rate.

A circular scan on a stationary circular structure vibrating at frequency, ω , will give a modulated LDV output whose frequency spectrum contains a couple of sidebands corresponding to several different nodal diameter components in the measured vibration pattern (an ODS) [1]. When the laser beam is driven by horizontal and vertical mirrors fed by two sinewaves equations $x(t) = R \cos(\Omega_{LDV}t)$ and $y(t) = R \sin(\Omega_{LDV}t)$, respectively, a circle of radius, R, is traced. The vibration response of the LDV beam direct to trace a circle scan at frequency of Ω will be:

$$v_z(t) = V_{R0} \cos(\omega t) + V_{I0} \sin(\omega t) + \sum_{n=1}^p \left\{ \frac{V_{R0} + V_{I0}}{2} \cos(\omega - n\Omega_{LDV})t + \frac{V_{R0} - V_{I0}}{2} \cos(\omega + n\Omega_{LDV})t \right\} \quad (2.2)$$

The vibration velocity then consists of harmonic components at frequencies $(\omega \pm n\Omega_{LDV})$ and its spectrum can be seen as a collection of sideband pairs spaced at $(\omega \pm n\Omega_{LDV})$ about the vibration frequency, ω .

This technique can be extended to the measurements of vibrating of rotating disc [3], [1]. Since the rotation of the disc about, Ω , the response frequencies are modified. Actually, if a sinusoidal excitation at frequency, ω , in a non-rotating frame of reference can be applicable to the rotating disc, n-diameter ODSs are excited, in the local, rotating disc coordinates at two distinct frequencies $(\omega \pm n\Omega)$. When the laser beam scan a circle at a frequency rate, Ω_{LDV} , the actual scan speed over the vibrating surface of the rotating disc will be $(\Omega_{LDV} - \Omega)$. Under that circumstance the vibration response of the LDV signal will be:

$$\begin{aligned}
 v_z(\alpha, t) = & \frac{V_{Rn}^- + V_{I0}^-}{2} \cos\left[(\omega - n(2\Omega - \Omega_{LDV}))t\right] + \\
 & + \frac{V_{Rn}^- + V_{I0}^-}{2} \cos\left[(\omega - \Omega_{LDV})t\right] + \\
 & + \frac{V_{Rn}^+ + V_{I0}^+}{2} \cos\left[(\omega + \Omega_{LDV})t\right] \\
 & + \frac{V_{Rn}^+ + V_{I0}^+}{2} \cos\left[(\omega + n(2\Omega - \Omega_{LDV}))t\right]
 \end{aligned} \tag{2.23}$$

As result, there are four frequency components in the SLDV output spectrum for each diametral order. They appear as sidebands, spaced by multiples of the laser beam speed relative to the disc, $n(\Omega_{LDV} - \Omega)$, centred on the disc frequency $(\omega \pm n\Omega)$.

The application, [2], of the circular-scan LDV is also suitable to wheel-road contact deflection measurements on automotive tyres.

Sometimes under certain circumstances, it can happen that the optical access to the disc is restricted and then it could be convenient to scan around an arc of a circle arranging the scan to be sinusoidal, so that the scan position α is described by the equation $\alpha(t) = \Theta \cos(\Omega_{LDV}t)$, [2]. That is equivalent to a sinusoidal straight line-scan where the line is curved around into an arc. The spectrum of the measured LDV signal will have two symmetrical sets of sidebands, equispaced about the scan frequency, Ω_{LDV} .

The circular-scan LDV and the arc-scan LDV are also suitable for vibration measurements on irregular rotating structures, such as rotating square plate [2]. The arc-scan spectrum is much more complicated comparing it to the circular-scan spectrum.

Last continuous scan technique, [3], that can be presented for vibration measurements of rotating disc it is area-scan LDV. When the scanning mirrors are driven by two equations $x(t) = (R_a + R_b \cos(\Omega_{r-LDV}t)) \cos(\Omega_{g-LDV}t)$ and $y(t) = (R_a + R_b \cos(\Omega_{r-LDV}t)) \sin(\Omega_{g-LDV}t)$, respectively, where Ω_{g-LDV} is the circle-scan frequency and Ω_{r-LDV} is the radial-scan frequency then two different area-scans can be performed. Actually, if $\Omega_{r-LDV} > \Omega_{g-LDV}$ the scanning circle will then spiral in and out to cover an annular area or, if $\Omega_{r-LDV} < \Omega_{g-LDV}$ then a 'daisy' scan is produced in which the laser beam scans to and fro along a radius which sweeps at lower frequency around the circular area.

Speaking about this vibration measurements approach, it is appropriate to refer to some problems which can arise when using the laser beam scanned continuously. One of them, [1], is speckle noise that it is noted at certain points in the spatial field of the velocity information measured by the LDV, it appears

as occasional velocity drop-outs. Speckle can cause several problems because it can become synchronous with the vibration, leading to a severe harmonic distortion. Another problem using the circular-scan LDV method is that the laser beam is deflected by two scanning mirrors separated by some distance, d_s , driven by cosine and sine functions. This arrangement will not necessarily yield a perfect circle for the scan but an ellipse carrying some additional components in the signal measured by the LDV [4]. Nevertheless, this problem can be resolved by employing different amplitudes for cosine and sine mirror drive signals.

2.3 Tracking Laser Doppler Vibrometer

2.3.1 Introduction

As illustrated in the previous section, a rotating structure such as a disc can be measured using CSLDV approach. In some other situations to investigate the dynamic behaviour of a moving object it is necessary to measure a point or some points on the structure during operating conditions. That could be done tracking these acquisition points. A tracking system can be arranged by enhancing the performance of the Scanning Laser Doppler Vibrometer (SLDV), making use of its scanning mirrors to move the laser beam during measurements to follow the motion of the target structure. As mentioned in the previous section, all the parameters to perform continuous scan are totally controlled by the user. Using the tracking measurement approach, the user needs of additional devices, such as state sensors, to provide external input to the functions driving the scanning mirrors. In this section, we shall present an overview of the vibration measurements carried out using such as approach.

2.3.2 Application of the Scanning Laser Doppler Vibrometer to tracking a target point on a moving structure (Tracking LDV-TLDV)

The enhancement of the performance of the scanning laser Doppler system offers many advantages both for the suitability of monitoring the target under operating condition and because it could allow to eliminate any relative velocity between the laser spot and the surface, thus reducing the optical noise like the speckle noise and improving the Signal-to-Noise ratio (SNR) [5]. Depending of the specific application different configurations of TLDV can be developed.

Tracking LDV approach was used to measure rotating disc vibrations, [6] and rotating bladed disc vibrations, [7]. The laser beam was controlled so as to follow a fixed point both on the rotating disc and on the rotating blade. Those arrangements required driving the scanning mirrors respectively by sine and cosine signals causing the laser to trace a circle on the surface of the projection. The rate at which the laser control signals were updated was controlled by a pulse-train rate coming from the shaft encoder. It assured that perfect tracking of the rotating target is achieved even when speed variations occur.

An important application where the TLDV approach has being used is in the vibration measurements of the automotive components such as timing belts, tyres and windscreen wipers.

The timing belt, [8], covers a wide range of applications in the transmission of the motion between two rotors. In order to track a linear motion that is realised by the belt for a certain period of its revolution between two pulleys, both scanning hardware and control software have been designed.

A test bench, made up of a drum on which surface a tyre was rolling, has been used to study the vibration occurring on the side-wall of the tyres. Hence SLDV configuration had to be configured to track a point on the side-wall of the rotating target [9].

Even a circular-scan LDV approach can be used to track a point on a rotating structure as carried out for the previous task. Actually if the scan frequency, Ω_{LDV} , of the cosine and sine functions driving our scanning mirrors is set equal to the frequency Ω of the rotating tyre it makes us able to perform tracking measurements [4].

Three different Tracking LDV system versions have been developed to perform vibration measurements on the windscreen wipers.

For the first method, [10], an advanced version of the TLDV has been developed for specific applications. In particular the so configured TLDV system is able to work with unknown a-priori motions through the application of a couple of sensors able to detect the actual position of the target point. In this way the rigid body motion of the object is subtracted and the vibration time history on each point of the grid can be measured with high sensitivity and accuracy.

A second system, [11], proposes an innovative approach to the tracking task. The arrangement of the system is more complicated because of an additional CCD camera employed with the SLDV system. Two scanning mirrors are the actuators of a closed loop control system and a high speed camera has been used as feedback sensor. Actually while the target object moves, the control system, PC, provides to correct the position of the laser beam using the information coming from the camera which observes the moving object.

The last method, [12], works with a different approach from those adopted for previous tracking systems. It has been designed as an open loop tracking system for arbitrary motions. The basic concept of following an arbitrary motion consists in a teaching phase and in a measurement phase. During the teaching phase the position of some reference points on the test piece relative to the vibrometer are used to interpolate the complex motion of the structure. The positions of these reference points are detected by a state sensor installed on the moving object. In the measurement phase, the trajectory of the actual measurement point is calculated online from trajectory of adjacent reference point.

Source of noise, performing tracking measurements, can be cause of uncertainty in vibration measurements and they can be presented as follow. Misalignment can occur between the optic axis of the tracking system and the axis of the rotation of the object and when it is present then it will produce a additional velocity components measured by the vibrometer. Some additional velocity components are also measured by the LDV when the scanning mirrors are driven by cosine and sine signal at uniform frequency scan rate as already illustrated at the end of the section (2.2.). Speckle noise problem can play an important rule in this type of acquisition. It can appear when the laser spot is not fixed on a precise point on the vibrating target but has a relative motion to the vibrating surface. Kinematics of the mirrors and vibration of the body of the vibrometer induced by oscillation of the scanning system inside the measurement head can be cause of noise sources.

2.3.3 Tracking-Continuous Scanning LDV, TCSLDV

It is reported in literature an additional step forward in laser Vibrometry technology from the simple point track technique [13]. In this Synchronized-Scanning technique, the scan amplitude and frequency may be continuously modulated during the tracking to perform a synchronized scan across the area of the rotating target.

A straight-line scan profile is achieved by imposing to the scanning mirror functions which have the generic form:

$$\theta_s(t) = \Theta_s \cos(\Omega t + \phi_s) \quad (2.4)$$

in which Θ_s is the scan amplitude and Ω is the scan frequency equal to the rotational speed of the target. To achieve the line scan, for example of a rotating blade, r_s , which would be constant in a circular tracking measurement, becomes a function of time, thereby modulating the scan amplitude:

$$r_s(t) = \bar{r}_s + \Delta r_s \cos(m\Omega t + \phi_{r_s}) \quad (2.5)$$

where \bar{r}_s and Δr_s are the mean and time dependent components of the scan radius, m is the number of radius cycles per revolution and ϕ_{r_s} is the initial phase. When one dimensional scan cannot provide enough information about the vibration of the structure, for example the measurement of torsional mode shapes, then a bi-dimensional scan has to be performed. In such a case, the area scan can be achieved by considering a simultaneous phase modulation of mirror drive signals:

$$\phi_s(t) = \bar{\phi}_s + \Delta\phi_s \cos(mn\Omega t + \phi_{\phi_s}) \quad (2.6)$$

where $\bar{\phi}_s$ and $\Delta\phi_s$ are the mean and time dependent of the scan phase, n is the number of phase cycles per radius and ϕ_{ϕ_s} is the initial phase.

2.4 LDV measurements of rotating blade vibrations

2.4.1 Introduction

One of the important design factors in the modern turbo machinery is the vibration of bladed discs. The blades are usually subjected to enormous stresses during operating conditions and they are the principal cause of the turbine failure. Different measurement techniques have been used in the investigation of the blade vibrations through the past years, from the use of the strain gauge-telemetry method to the employment of the LDV system.

2.4.2 Blade vibration measurements by non-intrusive techniques

Fiber-optic-laser-Doppler probes, [14], [15], [16], [17], are one possible solution to perform non-intrusive measurements on vibrating blades. These probes work in manner that the laser light is transmitted down to the target through the fibre-optic and the scattered light is returned in the same way up to the photo-detectors. Different measurement set-ups can be arranged with these probes, for example Blade Tip Timing (BTT) measurement methods, as well as different possible methods for signal processing.

BTT measurement methods aim at determining the time at which a point on a rotating blade tip passes a stationary optical laser probe. In absence of any structural vibration, the blade arrival time would be dependent only on the rotational speed. However, when the tip of the blade is vibrating, the blade

arrival times will depend on both the amplitude and the frequency of vibration, and hence the blade motion can, in principle, be characterized from knowledge of such data. The BTT systems need an optical access to the vibrating structure as well as the SLDV systems in order to perform the measurement. However, the BTT systems can be installed at any stage of an engine casing while the SLDV system can only operate facing the structure under measurement.

The potential of the LDV methods for non-contact measurement, during the last decade, have appeared very promising. The LDV technique allows for all the blades of a particular group to be monitored and an experimental set-up has been developed in measuring rotating blades vibration frequencies and amplitudes, [18]. In this set-up the LDV was placed in front the rotating bladed disc and the intermittent LDV signal was detected as result of rotating the blade through the laser beam. The blade vibration frequency and amplitude have been estimated from a least-square curve-fitting procedure and by applying a modal filtering in the signal processing, the limitations due to the curve-fitting process have been overcome.

In the vibration measurements of a rotating blisk reported in [19], the LDV system has been used in two different ways to investigate the complexities of forward- and backward-travelling waves and circumferentially regular and irregular blade vibration response pattern occurring in bladed-disc under rotating conditions. One these two methods employed the LDV as single-point transducer where the laser beam was directed along the rotation axis of the blisk's rotor, on which tip was fixed a small 45° mirror, and then redirected in a radial direction to encounter an annular, 45° mirror that turns the measurement beam onto a point near the tip of one of the blisk's blades. That arrangement allowed the measurement point to rotate with the blisk and to measure

vibrations at the tip of the given blade in a rotating frame of reference, in a direction parallel of the rotation axis. The alignment of the LDV in this method is very critical: in fact, any misalignment with respect to the axis of rotation is detected by the LDV as additional component in the signal measured and at the same time it is also necessary to maintain the measurement point at a designated position on the blade throughout the rotation cycle. In the second measurement method, a circular-scan LDV, already presented in section (2.2), has been used to perform an acquisition on the blisk equally in the stationary and in the rotating conditions. The latter requires the LDV scan rate to be set suitably close to, but not identical with, the blisk rotation speed.

2.5 LDV vibration measurements on rotating shafts

2.5.1 Introduction

In the previous sections we referred to different applications and measurement methods of moving structures where the LDV system offers great advantages with respect to other transducers. The LDV system has also been shown to be useful in investigations of the dynamic behaviour of the rotating shafts.

2.5.2 Laser vibrometer in torsional and bending vibration measurements

One of the first arrangements adopted to carry out those measurements was a cross-beam laser Doppler velocimeter, [20]. The laser beam, once split in two beams, was addressed to a converging lens which focused the beams on the rotating shaft. In this way, the system was capable in measuring tangential surface velocities and hence torsional vibration. With this optical geometry the backscattered light produced a Doppler beat frequency on the photo detector

output equal to: $f_D = \left(\frac{2U}{\lambda}\right) \sin\left(\frac{\theta}{2}\right)$; where U is the tangential surface velocity at the point of intersection of the beams, λ is the wavelength of the laser light and θ is the included angle between the incident laser beams. Demodulating the Doppler signal produced a time-resolved voltage analogue of U , the fluctuating part of which was proportional to the torsional vibration velocity.

The cross-beam laser velocimeter suffered from two major disadvantages: one was because the target had to have a circular cross-section and, secondly, it was unable to distinguish the torsional oscillation from solid body movement.

Since this is not a practical use, the actual optic geometry has been modified. The laser beam has been split into two equal intensity parallel beams of separation, d , which measure two points, A and B, on the shaft surface, [21]. In this case the Doppler frequency detected was: $f_D = \left(\frac{4\pi d}{\lambda}\right) \cos(\theta)N$; where N is the rotational speed of the shaft and θ is the angle between the normal to the plane of the incident beams and the rotational axis of the shaft. Disadvantages suffered by this system configuration were due to the multiplication of the two very small intensities in the backscattered beams, such that the amplitude of the AC signal was very small. For this reason the surface of the test piece required to be covered with retro-reflective paint or tape to increase the amplitude of the signal. In addition, that was a lack of directional information, due to the absolute peak value produced in the frequency domain, [22]. To improve that arrangement a dual interferometer has been developed requiring only one laser and one Bragg cell to introduce a frequency f_{Bragg} into both interferometers. This revised configuration solved aforementioned problems and wide ranges of measurements were achieved [23].

However, research using the system employing just one interferometer with the laser beam split in two beams has also been carried out. It produced the first comprehensive theory to describe the velocity sensed by a multiple laser beam incident on a rotating structure requiring three translational and three rotational co-ordinates to describe its vibratory motion fully, [24], [25], [26], [27].

2.6 Conclusions

In this chapter we have presented a survey of vibration measurement methods applicable to moving structures. We have seen how by improving the performance of the scanning mirrors in a conventional SLDV device, two new measurement methodologies have been developed: Continuous Scanning LDV (CSLDV) and Tracking LDV (TLDV). With the CSLDV technique we can achieve a spatial field measurement on a disc under rotating conditions. By the TLDV technique, we are able to perform tracking measurements on moving target. These two new methodologies offer an improvement to a wide area of vibration studies that includes the rotating turbo machinery bladed discs. In practice the possibility of combining these two techniques and performing continuous scan measurements while tracking a structure during operating condition, could offer enormous advantages. In particular, they can help to study the circumferentially regular and irregular blade vibration response pattern occurring in bladed-disc under rotating conditions. It is believed that the CSLDV and TLDV methods can easily overcome the limitations which other measurements methods encountered in performing tests of rotating structures.

3 The path to Tracking-CSLDV: X-Y scanning mirrors, study of X-Y mirror waveforms and sources of misalignment

3.1 Overview

This chapter focuses on three main aspects of synchronous measurement methodology: 1) description of the scanning mirrors and the role played by an external time base clock, such as an encoder, 2) possible sources of misalignment presented as mathematical models and 3) the study of X-Y waveforms and their codification into a control panel for performing tracking tasks. The description of the scanning mirrors is presented in depth in combination with the use of the encoder, these being the main contributors of the synchronous measurement development. Having gone through those two essential devices, the interest moves to one of the more unwanted issues represented by problem of alignment of the laser head with the rotating target followed by all possible sources of misalignment due to the inability to control all the degrees of freedom involved into the measurement chain system. Finally, we present a study of the waveforms required to achieve the final goal of the tracking process and the scan patterns developed to perform the Continuous Scanning LDV measurement under rotating conditions.

3.2 Scanning device characterization and synchronization method

The introduction of the scanning mirrors and a video camera into the head of the laser head constitutes the so-called Scanning Laser Doppler Vibrometry (SLDV). SLDV is a method used to perform synchronous measurement of rotating targets. Another important contributor to the tracking process is played by an encoder that provides the time base clock for sampling the output X-Y waveforms, thereby keeping the laser beam synchronous to the target at all times, no matter the rotational speed.

3.2.1 X-Y mirrors scanning device

Laser Doppler Vibrometry (LDV) is one of the best methods to perform measurements of bladed discs which are known to be very sensitive to any structural modification such as attaching even very light transducers to measure their vibrations. The introduction of a pair of movable mirrors in front of the laser head has aided its capabilities very much. The mirrors, called scanning mirrors, allow the laser beam to be moved anywhere over the surface of a target, either discretely or continuously. The two mirrors are mounted orthogonally, as shown in **Figure 3.1**, and they are driven by two galvanometer actuators: by applying a voltage to each of these, the mirrors can be rotated about their axes by two angles related to the voltages and some constants defined via a prior calibration of the scanning system. The voltages supplied to the horizontal mirror and vertical mirrors, V_x and V_y respectively, and the mirrors' rotation angles (indicated as ε_x and ε_y) will be described by the following relationship:

$$\begin{aligned}\varepsilon_x &= S_x V_x \\ \varepsilon_y &= S_y V_y\end{aligned}\tag{3.1}$$

S being the galvanometer static sensitivity.

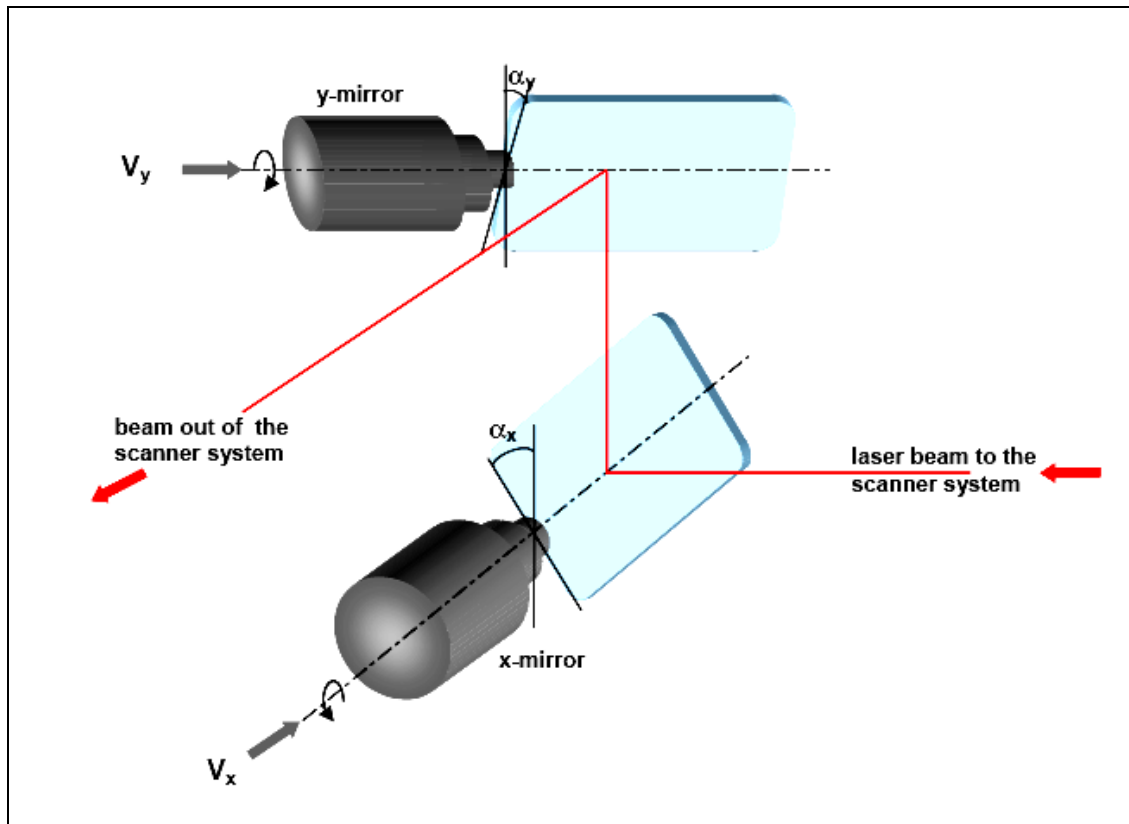


Figure 3.1 Schematic representation of the mirrors rotation

The scanning angles, α_x and α_y , can be specified by software and used as inputs for the scanner control which is basically an interface between the data acquisition/processing computer and the mirror driver motors and consists of a digital-to-analogue converter (DAC). This transforms the specified values of the angles into voltages. The latter are applied to the galvanometer actuators to give the specific rotation to the mirrors and to deflect the laser beam to the sought position on the test item. The galvanometer scanner consists not only of the mirrors and the actuators, but two further components are included in the device: a built-in capacitive rotation sensor to measure the actual angular shaft position of the mirror and a PID (Proportional, Integrative, Derivative) control system to generate a feedback control signal. This means that the galvanometers

work within a closed loop control, as shown in the flow-chart illustrated in **Figure 3.2**, which allows it to determine precisely the spatial relationship between the test structure and the SLDV system. It then accurately positions the laser beam on the desired location.

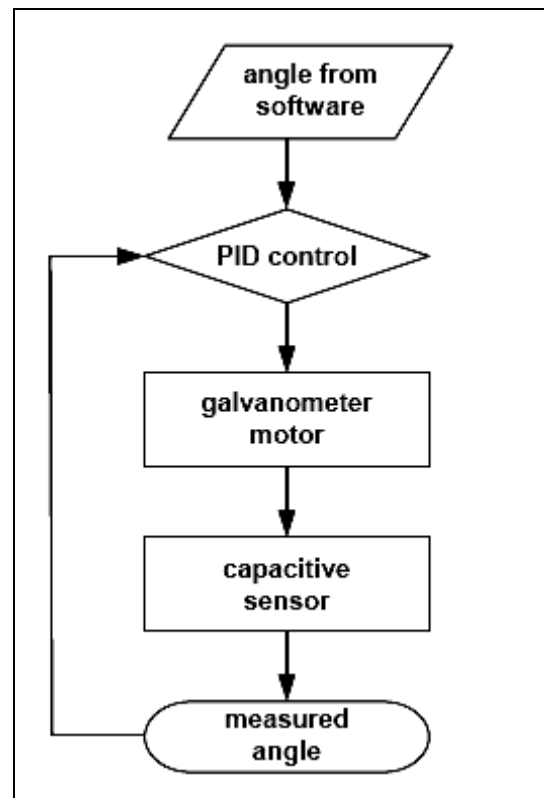


Figure 3.2 Flow-chart of the feedback control action

The dynamic performance of the scanner system is related to the rotor and mirror inertias, actuator torque and PID control algorithm. Response time in step mode depends on torque to inertia relationship and PID parameters. Mirror dimensions should be chosen as a compromise between the need for a large optical aperture for the scanning, and low mirror inertia, in order to have a fast response of the mirror itself. Unfortunately, using a built in scanning device, the only compromise possible would be to design the test piece whose dynamic properties, to be studied under rotating conditions, are shown within a rotational speed range suitable for the mirrors.

3.2.2 Scanning device of Polytec PSV-300

The development of the tracking measurement technique was based on the use of a standard commercialized Polytec scanning Vibrometer. Polytec is a provider of industries standard laser transducer products and one segment of those it is represented by scanning laser Vibrometer (SLDV) which is sold with inbuilt scanning mirrors. The Polytec PSV-300 mounts a couple of mirrors of different sizes; the biggest, whose inertia is 1332 gmm^2 , is mounted vertically and it scans in x-direction while the smaller, whose inertia is 515 gmm^2 , is mounted horizontally and it scans vertically. The mirrors, having large areas, are able to collect more back scattered light thus to increase the ratio of Signal-To-Noise (SNR) however their dimensions penalize the performance when they are used to carry out synchronous measurement at high rotational speed. **Figure 3.3** and **Figure 3.4** show the shape and dimensions (mm) of the X and Y mirrors, respectively [28].

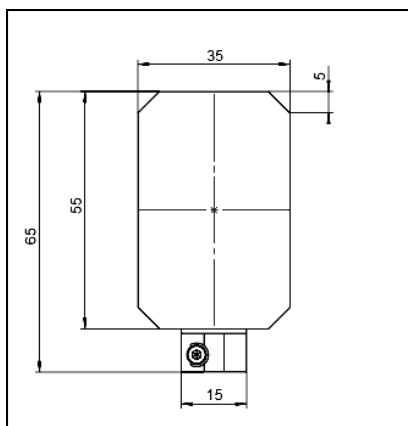


Figure 3.3 X-Mirror, technical drawing

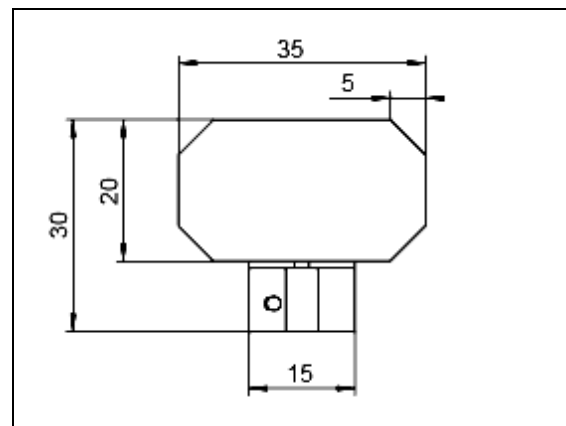


Figure 3.4 Y-Mirror, technical drawing

The scanning device, galvanometer motor and mirror, is affected by two problems: (i) a time delay, generally known as *phase lag*, between the input waveform into the scanning device and the actual rotation of the mirror, the phase delay is frequency dependent and it increases with that and (ii)

nonlinearity of the galvanometric motor at high oscillation frequency where a large input voltage is not converted into an equivalent angular rotation but into a smaller one. Hence, whenever a waveform is built and is output to one of the scanning devices it must take into account the *phase lag* to compensate that time delay and the reduced output angular rotation delivered, both of these being related to the input oscillation frequency. A series of plots were produced for both of the scanning mirrors to outline what was explained and **Figure 3.5** and **Figure 3.6** show a measured FRF of X-mirror, Amplitude and Phase respectively, while **Figure 3.7** and **Figure 3.8** show a measured FRF of the Y-mirror. Because the X-mirror size is bigger than the Y-mirror one that leads to a loss of performance confirming that smaller mirrors are preferable for the tracking measurement methods.

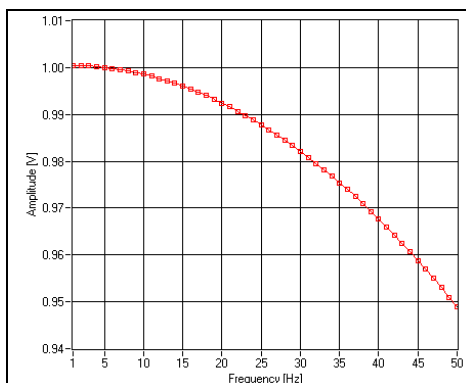


Figure 3.5 X-Mirror; FRF, Amplitude

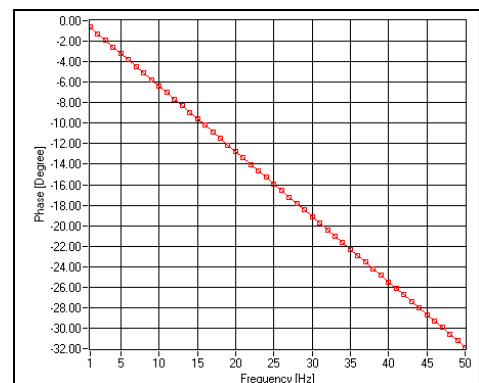


Figure 3.6 X-Mirror; FRF, Phase

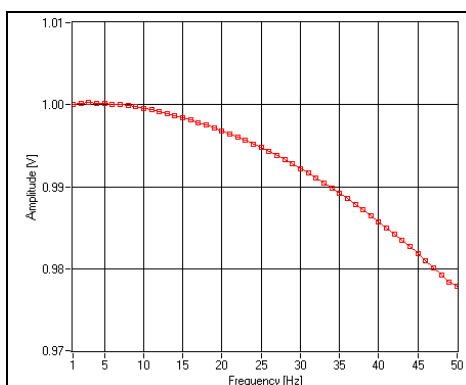


Figure 3.7 Y-Mirror; FRF, Amplitude

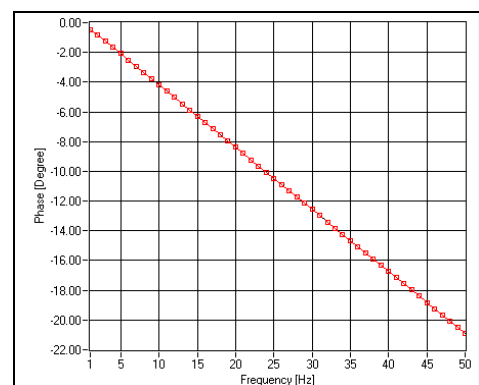


Figure 3.8 Y-Mirror; FRF, Phase

An aim of the research reported in this thesis was to develop a robust measurement technique for validation of methods for prediction of vibration amplitude of forced response and so the SLDV was used as delivered with its inbuilt scanning device, even though the dynamic properties are not optimal for the type of measurement method being developed.

3.2.3 Synchronization method

We previously mentioned briefly the important role played by the encoder. This device is one of the transducers used to measure the rotational speed of rotors and the one employed for this research is a rotary encoder. This is an electro-mechanical device used to convert the angular position of a shaft or axle to a digital code, making it a sort of transducer. This type of encoder outputs a Transistor-Transistor Logic (TTL) signal. The encoders can be classified according to one of its most important specification which is the number of pulses emitted per revolution. However, they can also provide one pulse per revolution from one of the output. Once the encoder is mounted on the shaft it will provide two TTL output signals to the output DAC card controlling the scanning device. The encoder used for this study is able to supply a maximum of 2000 pulses per revolution from one output plus an additional one pulse per revolution from another one. The DAC card used to control the scanning device is a National Instrument output card NI 6711 with four output channels. That card has the feature either to use its internal time clock base to sample the output waveform or to use an external clock for waveform sampling. Obviously, for this application the card is used in the second mode and the waveform sampling rate will depend on the number of pulses per revolution emitted by the encoder. Now we need to make a very short introduction about the functioning of the DAC output card. Any digital waveform needs to be defined by the number of samples which are sampled at some frequency rate. When we use a DAC output

card we have to allocate some of its memory, called a buffer, defined by the number of samples that will be used to build the waveform. When the buffer length, BL (number of samples), is divided by the update rate, UR (Samples/sec), we obtain the length of the buffer expressed in seconds and depending on the number of cycles in that buffer, we can define the LDV scan rate. Having decided to use an external time base clock for waveform sampling rate the update rate will be dependent on the rotation speed of the shaft and is given by the equation:

$$UR = RS * P \quad (3.2)$$

RS being the rotational speed expressed in rev/min and P the maximum number of pulses per revolution of the encoder expressed in Pulses/rev. The encoder employed for this study was able to deliver 2000 pulses/rev. Then, the time length of the DAC buffer no longer coincides with the actual time length of waveforms because it is variable with the rotational speed. The LDV scan rate defined as a number of cycles in the waveform time length will be variable with the rotational speed of the target. Accordingly to the time length of the DAC buffer we can scan a number of times the path length as given by the relation:

$$Cycles = \frac{BL}{LDV_{scan-rate}} \quad (3.3)$$

Unfortunately, the BL is related to the number of samples, NS , by the following relation:

$$BL = \frac{NS}{UR} \quad (3.4)$$

which means that the number of samples on the DAC is function of the rotational speed, RS , as shown by the following relation:

$$NS = BL * UR = BL * RS * P \quad (3.5)$$

the rotational speed, RS , being the only parameter to set up.

3.3 Tracking accuracy

One of the first challenges to be tackled in develop synchronous measurement techniques was to identify and to study the sources of uncertainty introduced by any external typical matter deriving by the use of a non contact measurement transducer. It is well known that LDVs are prone to be sensitive to speckle noise which is present for tests carried out under both stationary and rotating conditions. The fact the laser beam is now involved in a “double test”: meaning, the measurement of the vibration and the tracking of the same target while it is moving increases the number of unknown measured quantities contained in the LDV output signal. One of these unwanted factors was clearly identified in the misalignment issue and so the first task to accomplish in practice is the alignment of the laser beam with the rotational axis of the rotating testpiece. If the alignment is not well performed, it is likely that the measured data will be polluted by ‘pseudo’ vibrations and any LDV output signal post-processing can lead to wrong conclusions about the dynamic properties of the structure. Experience gained working with LDV transducers and the work performed using vibration force response prediction tools, helped to developed a sensitivity to anything that might appear ‘unusual’ with the measured data. Misalignment of the laser head with a rotating testpiece can introduce two sources of inaccuracy into the measured data. The first, and more evident inaccuracy, seen using a point tracking method was that the LDV time signal could contain a

spurious sinewave whose vibration frequency depends on the rotational speed of the target, which frequency content could clearly be seen in the frequency domain. As those undesired frequency harmonics are related to the rotational speed at which the measurement is performed, it is desirable when possible to avoid any proximity of them with frequency harmonics of the real vibration, as can be the case of sidebands used to reconstruct the Operational Deflection Shape (ODS) of the measured surface. Any overlap of those spurious frequency harmonics with the real ones can result in a failure of post processing of the acquired data. Unfortunately, one less obvious inaccuracy caused by a bad alignment is the position of the laser spot on the structure while it is rotating. When a case of first type, described above, occurs it can be immediately spotted by looking at the LDV time signal, but just how precisely it is possible to track the same point on the rotating structure would be more difficult to determine. A couple of questions can be raised about this type of inaccuracy: does it introduce significant amount of unwanted frequency harmonics into the measured data? If the answer is negative, why does this parameter need to be evaluated? From experience, it can be said that the frequency content is very small and is unlikely to produce any type of serious corruption of the time data. However it was necessary for it to be studied. Actually, during the design phase of any type of structural model it is possible to predict the amplitude of the vibration for any point of the model and this task is achievable both under stationary and rotating conditions. When a real measurement is performed under rotating conditions, the position of the laser spot is very important because any previous prediction can be validated only if there is a match between the position on the model and the measured position on the testpiece and this is a first answer to a aforementioned question. Another answer comes from the inability to predict LDV scanning parameters adequately, and to avoid speckle noise pollution of the time data, because the designed scanning path would actually be different

due to the misalignment. This concept will become clearer below. There are a number of ways by which misalignment occurs between the laser beam and the structure and the most important ones will be included will be shown and mathematically modeled, to predict the effect on the measured data. The way to perform alignment of the laser head with the target is now presented. The laser head is placed on a tilting table which sits on a rotating table and all three are placed on the table of a milling machine. The blue, red and grey arrows represent the degrees of freedom controllable by rotation of knobs.

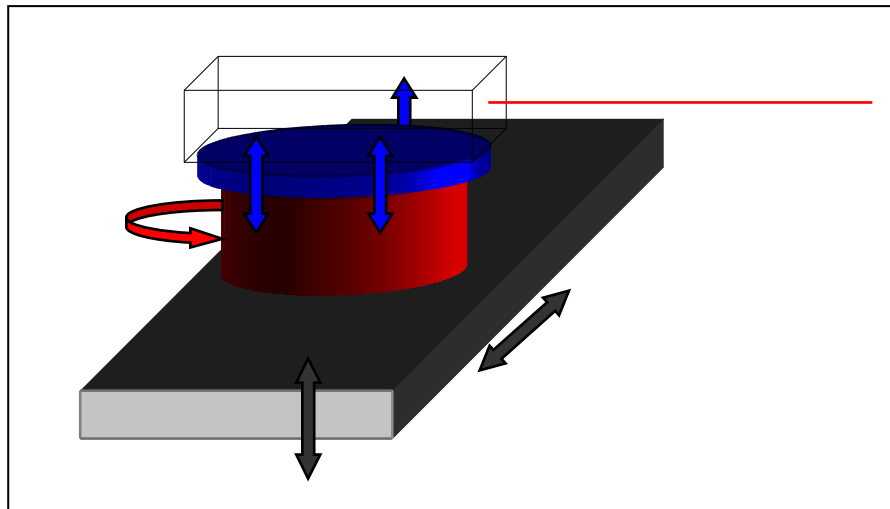


Figure 3.9 Alignment system

A practical and rapid way of achieving the LDV alignment by utilising the adjustments shown in **Figure 3.9** is given in **Figure 3.10**. A flat mirror tilted by a few degrees is attached at the tip of the shaft. The LDV beam is fired through a small hole, barely the size of laser beam, in the middle of the suspended plate and onto the centre of the tilted mirror (i.e., the centre of the drive shaft). When the mirror is rotated at a very slow speed, the reflected LDV beam tracks a circle on the plate. By making use of the adjustment controls, the LDV beam can be forced to follow one of the concentric circles on the plate. This, assuming that the

axis of rotation is normal to the suspended plate, will successfully align the LDV beam with the axis of rotation.

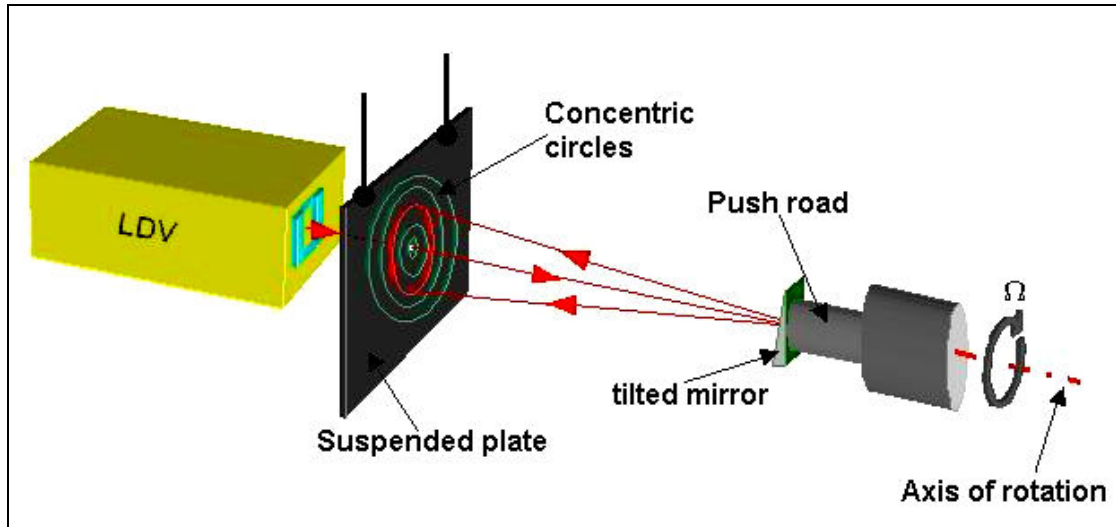


Figure 3.10 Alignment method

3.3.1 Misalignment due to shaft and Blisk mounting

The technique shown in the **Figure 3.9** and **Figure 3.10** can produce a good alignment whenever the shaft is perfectly straight, as shown for the ideal case in **Figure 3.11**. When the shaft is not straight the tilted mirror mounted at the tip of the shaft, as shown in **Figure 3.10**, to reflect the laser beam towards the plate might already contain an initial misalignment error which is unknown. However, we hypothesized that error very small thus to focus on errors introduced by a poor alignment of the laser head. Given that, we assume that the system of reference is set on the target and so the laser head must be aligned with respect to that reference. We set up four degrees of freedom to define the misalignment of the laser head such as to have offsets along the X and Y axis and rotations around the X and Y axis, as shown by the red arrows in **Figure 3.12** and as reported in **Table 3.1**.

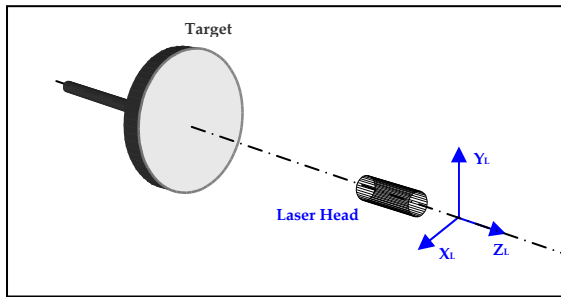


Figure 3.11 Ideal alignment

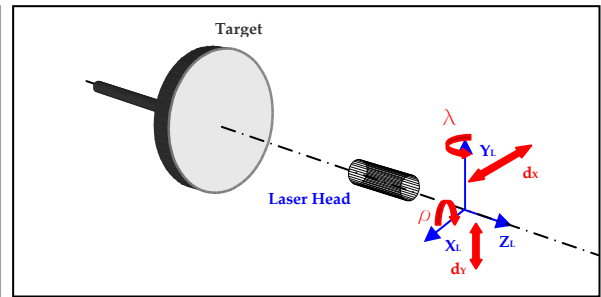


Figure 3.12 Sources of misalignment

Rotation around X	ρ	Translation along X	d_x
Rotation around Y	λ	Translation along Y	d_y

Table 3.1 Table of misalignment parameters

When problems like those just described are encountered, the position of the laser spot is no longer fixed at the same point during tracking but will trace a small path around the desired position. In the end this can result in poor agreement with predictions made for the target point, which is supposed to be measured.

3.3.2 Mathematical description

Although we introduced qualitatively the two types of misalignment, we did not provide any mathematical model to describe their effect on a simulated LDV output signal. In this paragraph, mathematical descriptions are introduced and described to quantify the effect of this inevitable problem which is found in synchronous measurement techniques. The equations refer to the path traced by the laser spot when point tracking is performed and they are expressed in the Cartesian system of reference.

3.3.2.1 Laser head aligned

It is important to define the equations of an aligned laser head before to start with the mathematical description of the sources of misalignment. **Figure 3.13** and **Figure 3.14** the laser head aligned and the initial laser spot position, $\alpha=0$ degree, respectively. The equations representing the motion of the laser spot while is performing a point tracking are:

$$\begin{aligned} X &= R \cos(\alpha) \\ Y &= R \sin(\alpha) \end{aligned} \quad (3.6)$$

where R is the radius.

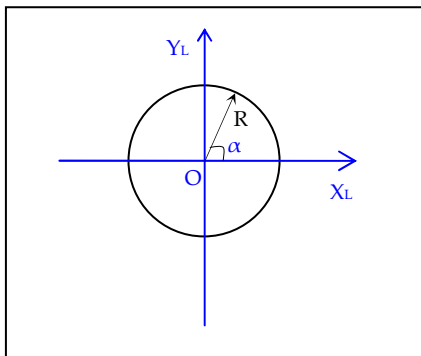


Figure 3.13 Laser head aligned

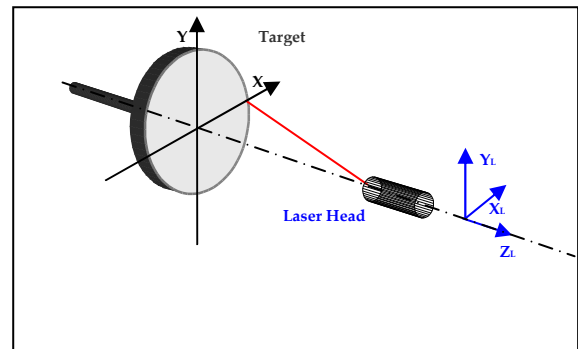


Figure 3.14 Initial laser spot position ($\alpha=0$ degree)

3.3.2.2 Misalignment cause by the offsets of the laser head along X and Y axis

The laser head can be offset, with respect to the system of reference (X, Y, Z), along either the X or Y axis, as shown in **Figure 3.15** and **Figure 3.16**, or like a combination of those. When this type of misalignment occurs the laser beam will trace a small path around the initial target position. The path traced by the laser beam, for a misalignment cause by an offset along the X axes, is expressed by the equations:

$$\begin{aligned}\Delta X &= X - X_{d_x} = R \cos \tau - r \cos \tau_{d_x} \\ \Delta Y &= Y - Y_{d_x} = R \sin \tau - r \sin \tau_{d_x}\end{aligned}\quad (3.7)$$

where the coordinates of the laser spot in the misaligned condition are expressed by equations:

$$\begin{aligned}X_{d_x} &= r \cos \tau_{d_x} \\ Y_{d_x} &= r \sin \tau_{d_x}\end{aligned}\quad (3.8)$$

where r and $\tau_{d_x} = a \tan\left(\frac{R - d_x}{L}\right)$ are the radius and the laser beam angle aperture of the misaligned configuration.

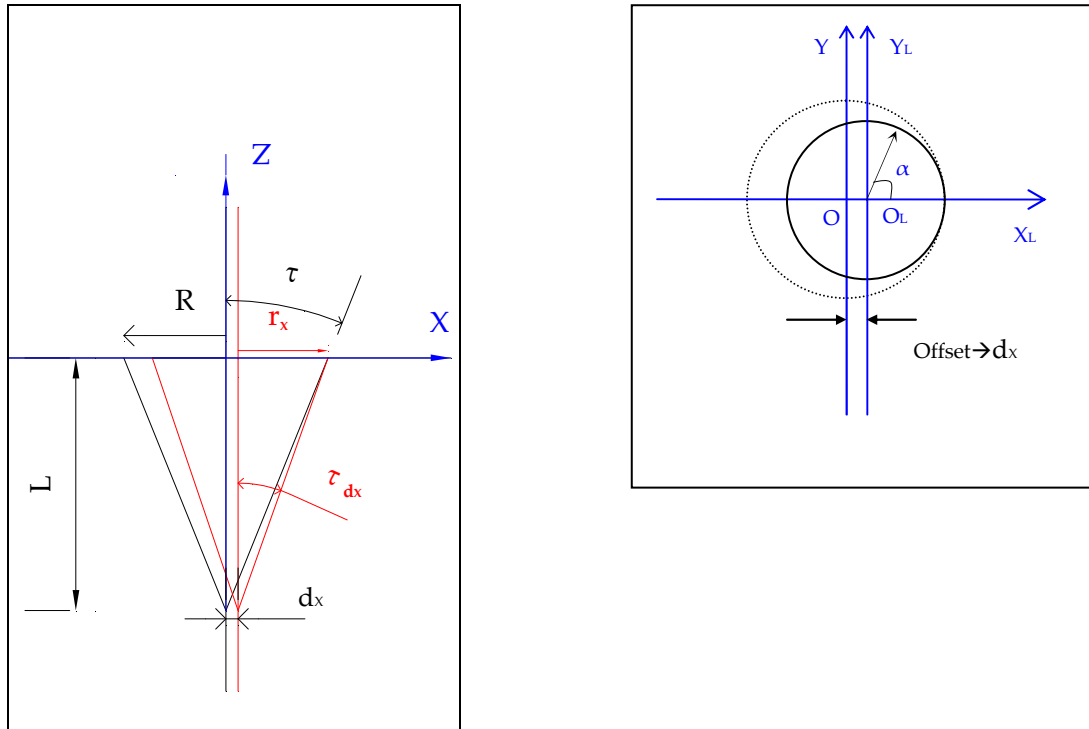


Figure 3.15 Offset of the laser head along X axes

When the misalignment is caused by an offset along the Y axes the radius of the misaligned condition, r_y , can be approximated to the radius of the aligned condition, R , and so ΔX can be approximated to zero. The path traced by the laser beam can be expressed by the equations:

$$\begin{aligned} \Delta X &= X - X_{d_y} = R \cos \alpha - r_{d_y} \cos \alpha \simeq 0 \\ \Delta Y &= Y - Y_{d_y} = R \cos \alpha - r_{d_y} \cos \alpha + d_y \simeq d_y \end{aligned} \tag{3.9}$$

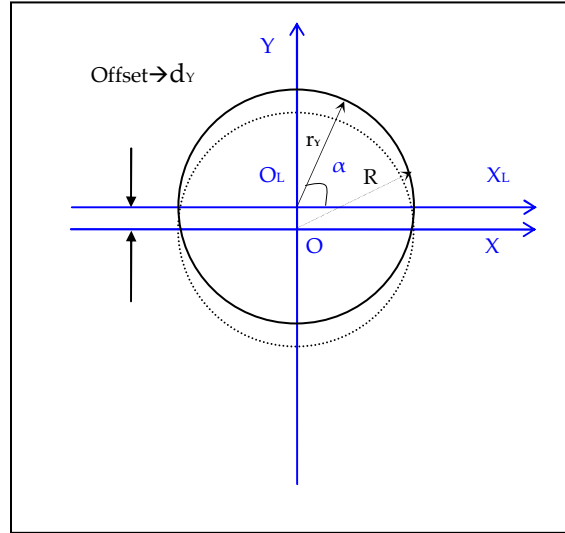


Figure 3.16 Offset of the laser head along Y axes

Generally, both the sources of misalignment are present therefore the superimposition of equations (3.7) and (3.9) is needed to describe the path traced by the laser beam.

3.3.2.3 Misalignment caused by the rotation of the laser head around X and Y axis

Other undesired sources of misalignment are caused by the rotation of the laser head around either around X or Y axis, even though a combinations of both of those is always expected to occur. **Figure 3.17** and **Figure 3.18** show the rotation of the laser head around the X and Y axis, respectively.

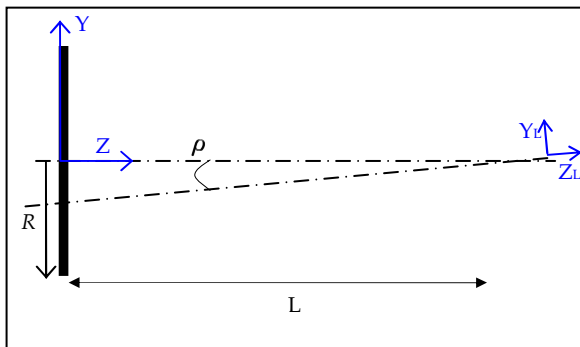


Figure 3.17 Rotation of the laser head around X axis

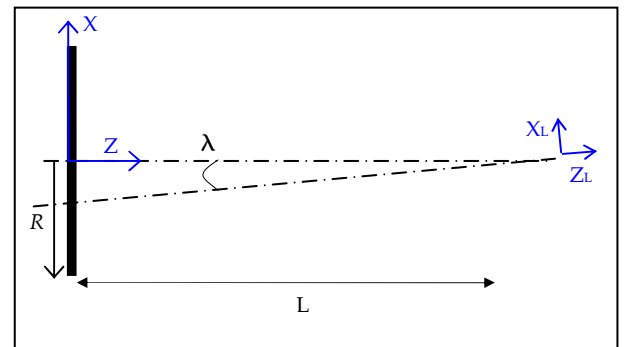


Figure 3.18 Rotation of the laser head around Y axis

The equations describing the motion of the laser spot when the laser head is rotated around the X axes are:

$$\begin{aligned} X &= \left[\frac{\left(\frac{R}{L} + \operatorname{tg} \rho\right) \left(1 - \frac{R}{L} \operatorname{tg} \rho \cos \alpha\right)}{1 - \frac{R}{L} \operatorname{tg} \rho} - \operatorname{tg} \rho \right] L \cos \alpha \\ Y &= \left[\frac{\left(\frac{R}{L} + \operatorname{tg} \rho\right) \left(1 - \frac{R}{L} \operatorname{tg} \rho \cos \alpha\right)}{1 - \frac{R}{L} \operatorname{tg} \rho} \right] L \sin \alpha \end{aligned} \quad (3.10)$$

where L is the distance of the laser head from the target and ρ is the rotation of the laser head. When there is a rotation of the laser head around the Y axes the equations become:

$$\begin{aligned} X &= \left[\frac{\left(\frac{R}{L} + \operatorname{tg} \lambda\right) \left(1 - \frac{R}{L} \operatorname{tg} \lambda \sin \alpha\right)}{1 - \frac{R}{L} \operatorname{tg} \lambda} \right] L \cos \alpha \\ Y &= \left[\frac{\left(\frac{R}{L} + \operatorname{tg} \lambda\right) \left(1 - \frac{R}{L} \operatorname{tg} \lambda \sin \alpha\right)}{1 - \frac{R}{L} \operatorname{tg} \lambda} - \operatorname{tg} \lambda \right] L \sin \alpha \end{aligned} \quad (3.11)$$

where λ is the rotation of the laser head. As already mentioned, all these configurations can occur simultaneously and so the laser beam, while it is tracking the target, will also trace a very small path around the targeted position. It is very difficult to measure precisely the rotation of the blisk plane around its axis and the degree of bending of the shaft and, even if that rotation is measured once the testpiece is installed in the test rig, it should be repeated every time it is

dismounted and reassembled again in the rig. Having said that, it is possible to provide an example to show the path traced by the laser spot around the designed position during the tracking both in a fix and rotating frames of reference as shown in **Figure 3.19** and **Figure 3.20**, respectively.

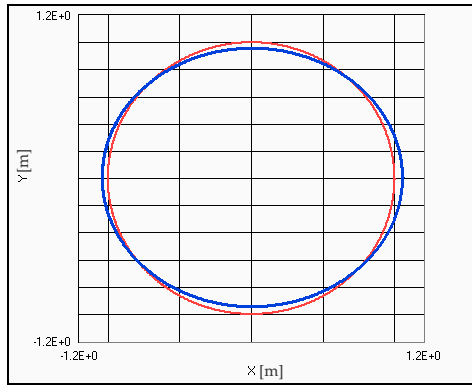


Figure 3.19 Path traced around the designed position

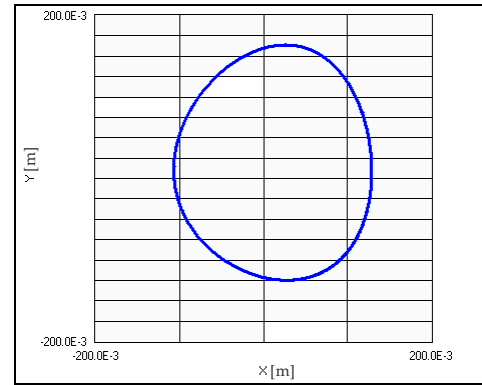


Figure 3.20 Path traced in rotating frame of reference

When the sources of misalignment are caused by the rotation of the laser head the laser beam will measure a 'pseudo' vibration, from the not excited structure, which can be expressed by the equation:

$$v_z(t) = 2\pi\Omega_{LDV}L \left(\frac{1}{\cos\lambda \cos\kappa} + \frac{1}{\cos\rho \cos\kappa} - \frac{2}{\cos\psi} \right) \sin(2\pi\Omega_{LDV}t) \quad (3.12)$$

where $\kappa = a \tan \frac{R}{L} + \lambda$, $\psi = a \tan \frac{R}{L}$ and $\alpha = 2\pi\Omega_{LDV}t$. All the illustrated cases can happen simultaneously, the equations reported can be combined to simulate the pseudo vibration polluting the LDV time signal whenever a misalignment is present, as shown in **Figure 3.21**. The real vibration is carried by a sinewave whose frequency content depends by the rotational speed of the blisk.

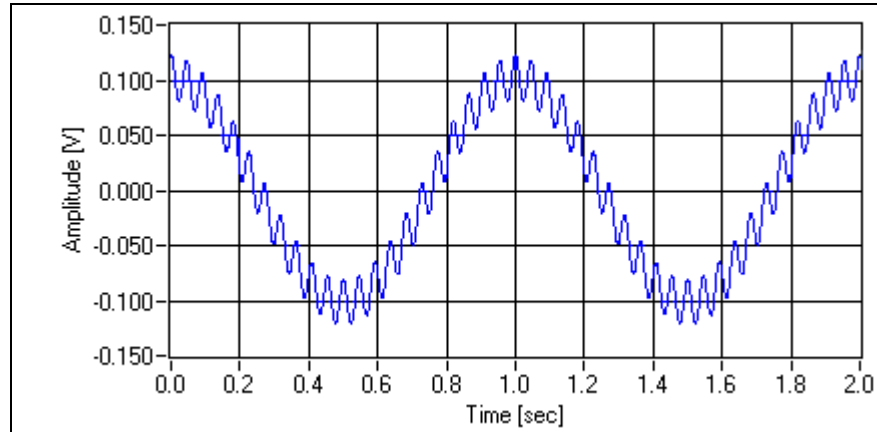


Figure 3.21 LDV output signal polluted by pseudo vibration

3.3.2.4 Misalignment caused by the X-Y mirrors scanning device

An additional source of misalignment comes from the scanning device which is made of two mirrors mounted orthogonally to one another. Having the mirrors at a certain distance apart also makes the laser beam also to travel on the mirrors when they are scanning continuously [4]. Therefore, for example, performing a circular-line scan whose input radius is for both of the mirrors R , the output radii are expressed by equations:

$$R_x = \frac{1}{2} \operatorname{arctg} \left(\frac{R}{d+c} \right)$$

$$R_y = \frac{1}{2} \operatorname{arctg} \left(\frac{R}{d} \right)$$
(3.13)

where R is the input radius, d is the distance between the laser head and the target and c is the distance between the mirrors. This will result in an elliptical pattern rather than the circular one that was meant to be traced and the LDV output time signal will show a series of harmonics in the frequency spectrum which are multiples of the LDV scanning rate frequency. Because this type of problem is inherent for any type of scanning device devised with two mirrors, it is important to take it into account.

3.4 Point tracking

The point tracking measurement method is the first synchronous measurement method that was performed and it involves one measurement point at a time. The technique is fairly simple to implement and it suits very well for the vibration measurement of bladed disks because one measurement point per blade is generally enough. Combining this method with a rotating exciter, it is possible to measure Frequency Response Functions (FRFs) under rotating conditions and thus can be very useful in many case studies where otherwise such a measurement would be very long and tedious to perform. In this section, a study of the X-Y mirrors waveforms is presented and an explanation given for how the output waveforms can be generated and the scanning device can be controlled by using a very simple control panel.

3.4.1 Waveform study

Point tracking is the simplest synchronous measurement to perform because the laser beam needs to address only one point of the structure at the time. Actually, a circle traced by the laser beam synchronized to the rotating blisk will perform a point track. The waveforms to drive X-Y mirrors in a circle are expressed by the equations:

$$\begin{aligned} x(t) &= R \cos(2\pi\Omega_{LDV}t + \tau) \\ y(t) &= R \sin(2\pi\Omega_{LDV}t + \tau) \end{aligned} \tag{3.14}$$

where R is the radial position of the measurement point and Ω_{LDV} is the LDV scan rate which is synchronous with the rotational speed of the blisk and τ is the initial phase angle. However, the above equations are for an ideal system because they do not take into account the possibility of a delay between the

output of the sine waves and the actual rotation of the mirrors due to their inertia as was explained in section 3.2.2. The equations are then rewritten:

$$\begin{aligned} x(t) &= R \cos(2\pi\Omega_{LDV}t + \delta_x + \tau) \\ y(t) &= R \sin(2\pi\Omega_{LDV}t + \delta_y + \tau) \end{aligned} \quad (3.15)$$

where δ_x , δ_y are the phase delays due to the inertia of the X and Y mirrors, respectively. Some SLDV systems mount mirrors of the same size and for them, $\delta_x = \delta_y = \delta$. The LDV scan rate is dependent on the rotational speed of the target, the phase lag of the mirrors will increase accordingly. The sine waveforms, constructed taking into account the phase lags at the corresponding speed of the target, will trace a slightly distorted circle as shown in red in **Figure 3.22**, while the actual circle traced by the laser beam is as shown in blue in **Figure 3.22**. **Figure 3.23** shows the X-mirror sinewave in blue and the Y-mirror sinewave in red.

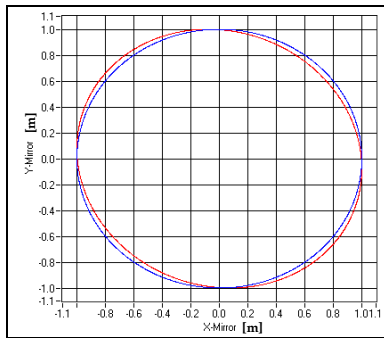


Figure 3.22 Generated pattern in red and the actual traced in blue.

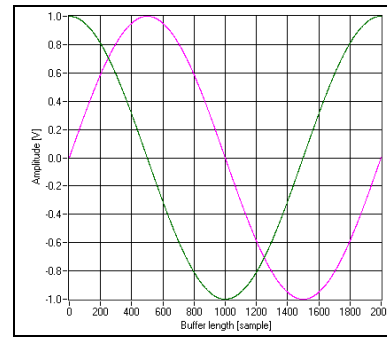


Figure 3.23 Output X-Y waveforms

3.4.2 Scanning device driver control

Having studied the X-Y sine waveforms to feed to the scanning device, it was important to design a panel which could control all the parameters to drive the

output card and to carry out a point tracking measurement. This is made of one front panel where we input all the values necessary to drive the scanning mirrors and one back diagram panel where all the inserted values are used to build the waveforms and to set up the driver of the output card. One of the requirements of the design is to have a control panel which is very versatile for use everywhere with several computers and test rig configurations. The first check to perform on the test rig is to determine the number of pulses per revolution output by the encoder attached to the shaft. Actually, a ring control sets up that parameter and it is of vital importance to insert the right number otherwise the tracking may fail because a wrong waveform sampling frequency. Another small check to be performed on the test rig is to assess the direction of the shaft rotation otherwise laser beam rotation direction could be inverted. The panel can be run on different computers where the identification number of the DAC cards could be assigned differently, by the Operating System, than the original configuration, and then a ring control is used to input the right *id* number to the DAC driver. Once those preliminary checks are done, the blisk can be spun and the initial phase angle for tracking found to address the laser spot position on the blade. That phase angle is given by the one pulse/rev, emitted by one of the outputs of the encoder, which triggers the output waveforms. Another important parameter to insert is the radial amplitude of the laser spot position. Last parameter to insert in the panel is the actual rotational speed of the target thus to adjust the phase delays of the X-Y mirrors. **Figure 3.24** shows the Point Tracking front panel.

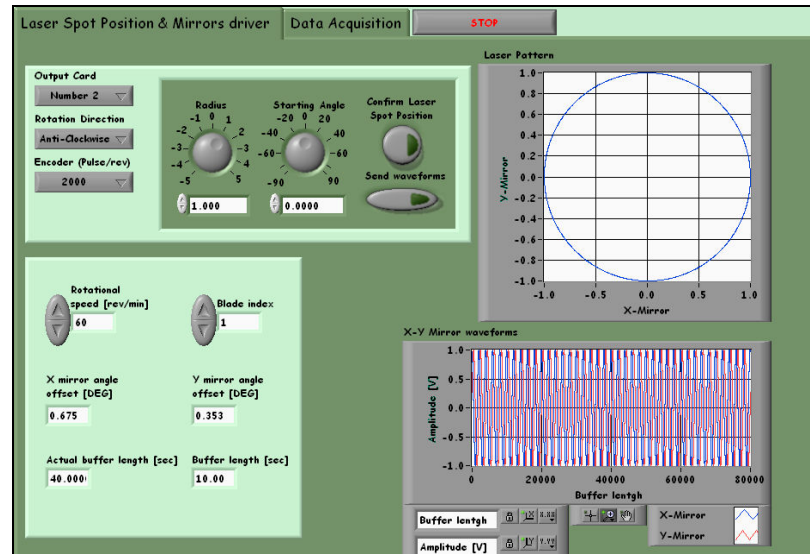


Figure 3.24 Point Tracking front panel

3.5 Line Tracking

Straight line tracking measurement method is a further development of the continuous scanning technique for measuring the deformation of the scanned line of a bladed disk under rotating conditions. Clearly, this technique is more complicated than a single point measurement for a number of reasons, one of which could be the line traced by the laser beam can drift off the designed path. The waveforms to drive the scanning mirrors have to synchronize the laser spot with the rotating target as done for point track but at the same time must allow the laser spot to travel up and down along the blade. This technique provides more information than a single measured point and functioning in very short time. Also in this section, we present a study of the X-Y waveforms needed to drive the mirrors properly and, finally, we show the control panel to control the scanning device.

3.5.1 Waveform study

The next step to the point tracking method is to be able to scan across the blade along one line. The laser beam will now travel along one dimension of the

structure and this translation will complicate the waveform definitions. Considering one point, situated initially at the tip of the rotating blade, that starts to travel down the blade along a straight line, the motion of that point in a fixed frame of reference will trace a spiral pattern. Therefore the task is to synchronize a spiral pattern, scanned in stationary conditions by the laser beam, to the rotating blade. To achieve a spiral pattern the laser spot travels simultaneously both circumferentially and radially and the terms that control the motion circumferentially must be synchronized with the rotational speed of the shaft. The sinewaves to drive both mirrors in a spiral pattern are expressed by the following equations:

$$\begin{aligned}
 x(t) &= \left[\frac{R_f - R_i}{2} \cos(2\pi\Omega_{r-LDV}t) + \frac{R_f + R_i}{2} \right] \cos(2\pi\Omega t + \delta_x + \tau) \\
 y(t) &= \left[\frac{R_f - R_i}{2} \cos(2\pi\Omega_{r-LDV}t) + \frac{R_f + R_i}{2} \right] \sin(2\pi\Omega t + \delta_y + \tau)
 \end{aligned} \tag{3.16}$$

where R_f and R_i are the final and initial radial position amplitudes, Ω_{r-LDV} is the LDV scan rate at which the laser beam travels along the path, Ω is the rotational speed of the target, δ_y is the phase lag of the Y mirror, δ_x is the phase lag of X mirror and τ is the initial phase angular position. Figure 3.25 shows the spiral pattern built taking into account the phase delays of the two mirrors depicted in red while the actual pattern traced is depicted in blue. Figure 3.26 shows the X-Y waveforms needed to drive the scanning mirrors.

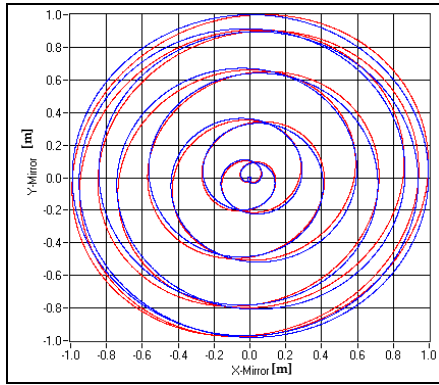


Figure 3.25 Generated pattern in red and the actual traced in blue

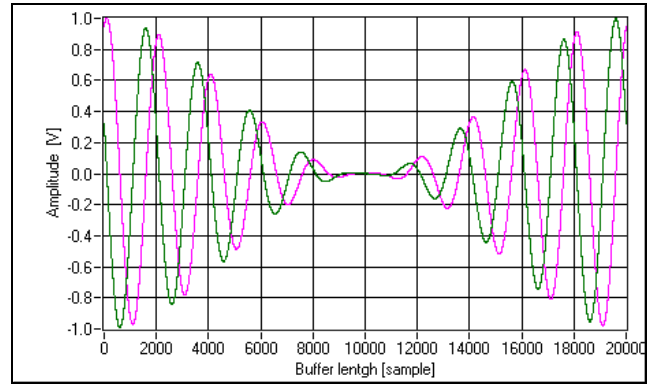


Figure 3.26 X-Y waveforms

3.5.2 Scanning device driver control

The front panel of straight Line Tracking method is similar to the Point Tracking one except for two additional input parameters required to control the length of the line scan and its scan rate, while the coding diagram, where the waveforms are programmed, is much more complicated. So, by defining the starting radial position, as was done for the previous panel, and the ending radial position, we obtain the line scan length. The parameter to control the rate at which the line is scanned depends strongly on the rotational speed of the target which has to be inserted to adjust the phase delays of the mirrors although this parameter is more important than the simple phase correction. In fact in section 3.2.3 we have defined that the number of samples allocated into the DAC output card is related to the rotational speed of the target. **Figure 3.27** shows the front panel to perform straight line tracking.

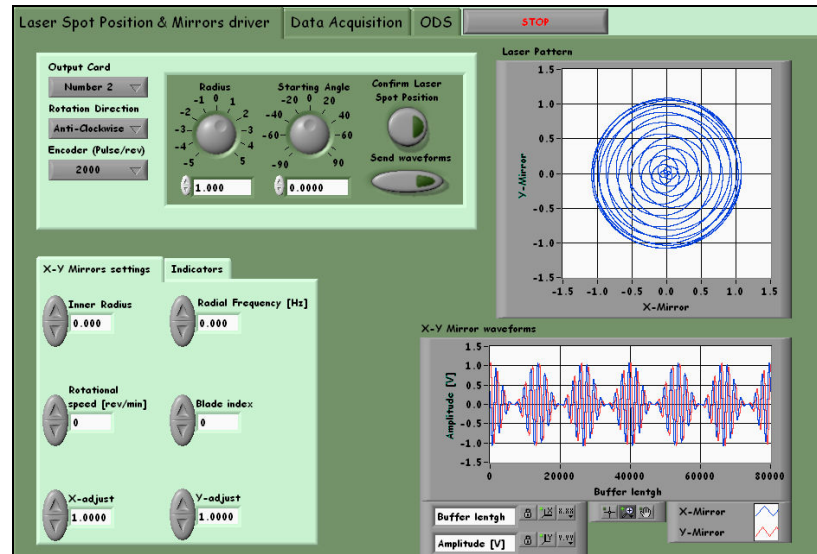


Figure 3.27 Line Tracking front panel

3.6 Area Tracking

The Area Tracking method is the top of all the methods considered in this research because the laser beam, sweeping all the surface of the vibrating blade, measures all its vibration and not just that of one point or along a line of it. Without doubt, this technique is also the most difficult to perform because when the scanned area is not synchronized very well with the rotating blade the laser beam can drift off the surface, thereby producing sharp spikes in the LDV time signal. Nevertheless, it is the only method that can measure the vibration of the blade area in a matter of a minute just using a standard SLDV.

3.6.1 Waveform study

When performing an area scan, the laser beam will travel both along the length of the blade and across its surface. The mirror drive waveforms to achieve this type of scanning will be more complicated than the others because the laser beam will need to maintain synchronous with the rotating blade and simultaneously travel over its surface. Depending on the shape of the blade, it is possible to design a scanning pattern such as a rectangular pattern (if the shape

of the blade is rectangular) or a triangular pattern (when the blade has a triangular shape). The blisk used for this study was designed to have blades of essentially triangular shape and so the scan pattern, shown in **Figure 3.28**, was chosen to be of the same form so to scan the full area.

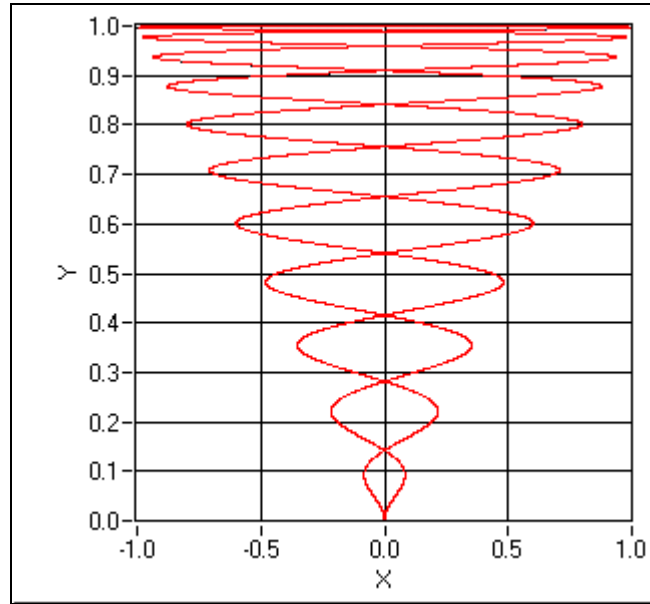


Figure 3.28 Triangular scan pattern

Because of the triangular shape of the scan pattern the output waveforms to drive X-Y mirrors are much more complicated the previous ones, as shown by the equations:

$$\begin{aligned}
 x(t) &= \left(\frac{R_f - R_i}{2} \cos(2\pi\Omega_{r-LDV}t) + \frac{R_f + R_i}{2} \right) * \cos(2\pi\Omega t + \varphi(t) + \delta_x + \tau) \\
 y(t) &= \left(\frac{R_f - R_i}{2} \cos(2\pi\Omega_{r-LDV}t) + \frac{R_f + R_i}{2} \right) * \sin(2\pi\Omega t + \varphi(t) + \delta_y + \tau)
 \end{aligned}
 \tag{3.17}$$

where R_f is the final radius, R_i is the initial radius, Ω_{r-LDV} is LDV scan rate in radial direction, Ω is the rotational speed of the blisk, δ_x and δ_y the phase lags of

X and Y mirrors, respectively, while $\varphi(t)$ is the phase which is described by the equation:

$$\varphi(t) = Ed \sin 2\pi t \quad (3.18)$$

Ed being the edge amplitude of the blade. **Figure 3.31** shows the scan pattern in a fixed frame of reference. The figure shows both the scan patterns when the phase lag of the mirrors are taken into account for the construction of waveforms, in red, and when the same is not taken into account, in blue. **Figure 3.30** shows one period of the X-Y waveforms, blue for the X-mirror and red for the Y-mirror.

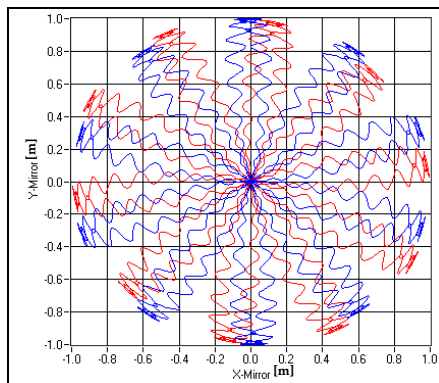


Figure 3.29 Generated pattern in red and the actual traced in blue

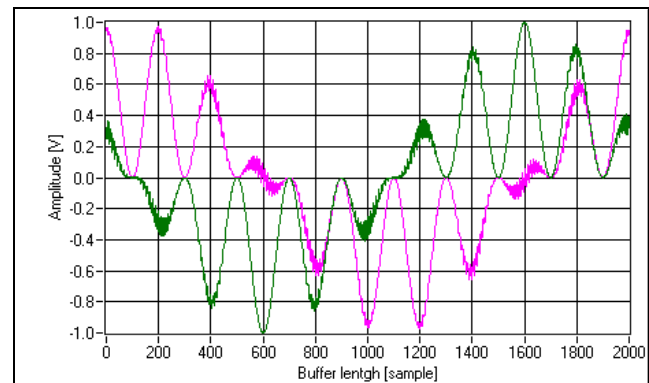


Figure 3.30 X-Y waveforms

3.6.2 Scanning device driver control

For the Area Tracking front panel, many features are similar to those described earlier for the Line Tracking panel and so common features will not be repeated here. Now, the laser beam moves both along the blade and sidewise across it and motion occurs at two different LDV scan rates so that two parameters control the length of the scan lengthways and edgewise and two control the rate at which the blade is scanned. Having two parameters controlling the speed at which the

beam scans the area of the blade means that it is crucial to have their actual output values corrected. The initial radial position, together with the initial phase angle, is to be specified with maximum care so that the laser spot falls at the middle of the blade otherwise the laser beam will fall off the blade because the scanned triangular pattern is not overlapping the area of the blade.

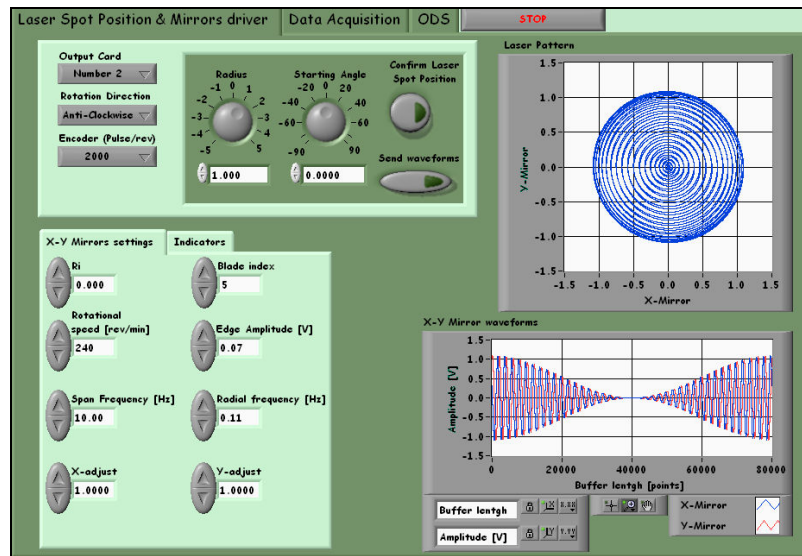


Figure 3.31 Area Tracking front panel

3.7 Conclusions

The aim of this chapter has been to present a complete overview of all the practical issues encountered when performing any of several types of synchronous measurement. We have studied the scanning mirrors, the main contributors of this measurement methodology, and the limitations of using an inbuilt scanning device because the dimensions of the mirrors. We have explained the important role of the encoder used to trigger the waveform output and its use of an external time base clock for the waveform sampling rate output from the DAC card. A wide overview of all possible sources of misalignment, together with a technique for alignment of the laser head with testpiece was presented and mathematically modelled to predict pseudo vibrations. Finally, all

three tracking methods were presented through the study of the waveforms to achieve one specific scanning pattern and the explanation of how the waveform was coded into a control panel to drive the scanning mirrors.

4 Blisk and Test rig: design and instrumentation

4.1 Overview

This chapter describes the design of the testpiece, a 24-bladed disk, and the test rig. The blisk design specifications were decided in order to study an interesting phenomenon concerning the forced response in the veering region of the 2nd Flap-wise and 1st Torsional families of modes, both at rest and under rotation. The shape of the blades forced the development of a specific laser beam pattern to be traced over the surface in order to measure the Operational Deflection Shape (ODS) under rotating conditions. Then, the chapter evolves through the development of the test rig previously employed for another project and the modifications needed to meet the new measurement requirements such as ODS and FRF measurements at speed. The chapter presents three possible ways to perform the excitation, focussing on the description of a rotating exciter.

4.2 Blisk design

Bladed disks are designed to be cyclically symmetric. However, variations due to manufacturing tolerances and wear cause each blade to be slightly different from the rest. Since these blade-to-blade variations alter the frequencies of the blades, they are generally referred to as mistuning.

Mistuning is a concern in the gas turbine industry because it can significantly increase the vibratory stress of a blade relative the stress it would have if all the blades were identical. As a result, researchers have developed reduced order models to efficiently determine the mistuning of a bladed disk and predict its vibratory response in the engine. However, much of this research has focused on families of modes that are isolated in frequency, i.e. neighbouring mode families are far enough away as to have little effect on their dynamic response. This is frequently true of first bending modes. But when two mode families of a bladed disk are close in frequency, they can interact.

We recall the matter of frequency veering because the interest in that phenomenon has led to a specific blisk design, before to introduce the 24-bladed disk design mechanical specification. Frequency veering, sometimes called 'curve veering' represents a phenomenon in which the locations of the eigenvalues of a system converge and then veer apart without crossing when the eigenvalues are plotted as a function of a characteristic parameter. In bladed turbine discs, this phenomenon can be clearly observed in conjunction of nodal diameters. In fact, it can be easily located in a plot of frequencies against nodal diameter modes where some families of modes can approach and veer apart, apparently without crossing one on other. This phenomenon, associated with rotor speed, involves interaction between blade modes that occurs because of the change of the rotational speed and, consequently, due to the change of centrifugal force acting on the blades. When one flap-wise family of modes veers away from a torsional family of modes, any change of centrifugal load, due to rotor speed change, forces the flap-wise family to cross the torsional family because that is less sensitive to that load. That above explained physically by an increase of stiffness, and then of the natural frequency, of the bending modes while torsional modes do not have a so sharp increase of stiffness, [29]. This type of interaction between modes produces many difficulties for modal

identification and forced response interpretation, especially when the bladed disk shows a strong modal localization due to mistuning. Because of the nature of the phenomenon, the bladed disk design had to be carefully selected to exhibit curve veering and a complete crossing of the two families of modes at a reasonable rotational speed, compatible with the LDV scanning mirrors operation limit.

Recently, researchers at Carnegie Mellon University have developed the ID&Predict analysis method, which is capable of identifying mistuning of a bladed disk in a veering region, analytically adjusting for centrifugal stiffening effects, and predicting its response under rotating conditions. In order to experimentally validate the ID&Predict method, researchers at Imperial College and Carnegie Mellon worked together to design a test piece which exhibited a veering behaviour. The blisk was also designed so that the relative spacing of the bending and torsion modes would change significantly between 0 and 2400 rev/min, thus changing the interaction between the bending and torsion modes.

The test plan was to first measure the FRFs of the blisk in stationary conditions. These FRFs would be evaluated by ID&Predict to determine the blisk's mistuning. Once the mistuning is determined, ID&Predict could then predict the forced response of the blisk at various operating points between 0 and 2400 rev/min. The FRFs would be re-measured under rotating conditions, and compared with the predicted response.

4.2.1 24-Bladed Disk Testpiece

This testpiece is designed to allow study of vibration response levels of the 1st torsional modes and of 2nd flap-wise modes in the veering region using the

Continuous Scanning LDV measurement method, as introduced in the previous chapter. The simplified bladed disk will be subjected to vibration excitation while rotating, and the blade responses will be measured and studied. The test disc is to be such that the blades can be ‘tuned’ to have near-identical dynamic properties to each other, and also mistuned in specific mistune patterns. A number of important criteria were set at the beginning of the design process:

- 1) The family of 1st torsional modes has to be ‘above’ the family of 2nd flap-wise modes by a few tens of Hertz at 0 rev/min.
- 2) The veering region has to be localized at around the 4-6 nodal diameter modes at 0 rev/min.
- 3) The two families of curves have to be fully separated, meaning no overlap between them, at 2400 rev/min.
- 4) The surfaces of the blades have to be wide enough to easily perform a scan using the CSLDV method.

Before starting with the blisk FE modelling, an initial study of the single blade sector was needed to estimate which geometrical parameters were driving the two families of modes to veer apart. After several attempts it was found that the veering phenomenon could be obtained varying two geometrical parameters: the disc thickness and the width of the blade tip. **Figure 4.1** shows the variation of the blade tip width, on the left hand side, and the variation of the disc thickness, on the right hand side. **Figure 4.2** shows results of several FE simulations where we can see the influence of the two geometrical parameters on the 2nd flap-wise and 1st torsional modes. We can see that the blade tip width was varied in the range of 65.5 (0.5) 59 mm and three values of disc thickness

were used: $t_{kns-1} = 1.8\text{mm}$, $t_{kns-2} = 3\text{mm}$ and $t_{kns-3} = 5\text{mm}$ as shown on the plot legend. The veering region is outlined by a red circle.

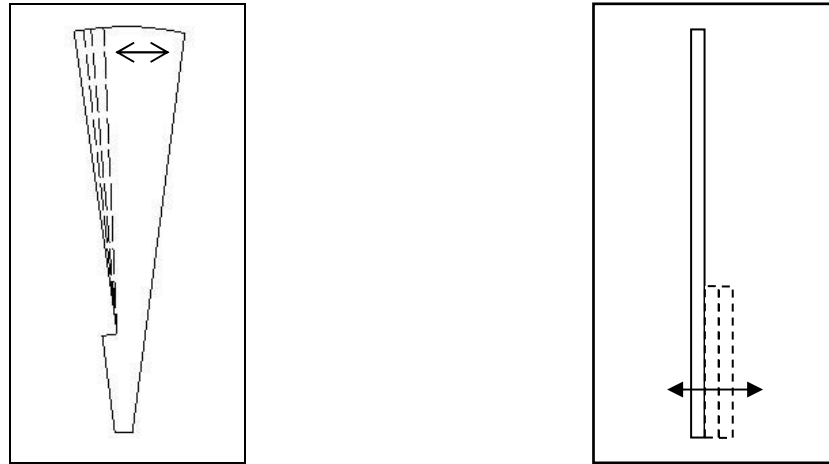


Figure 4.1 Variation of the blade tip width and disc thickness

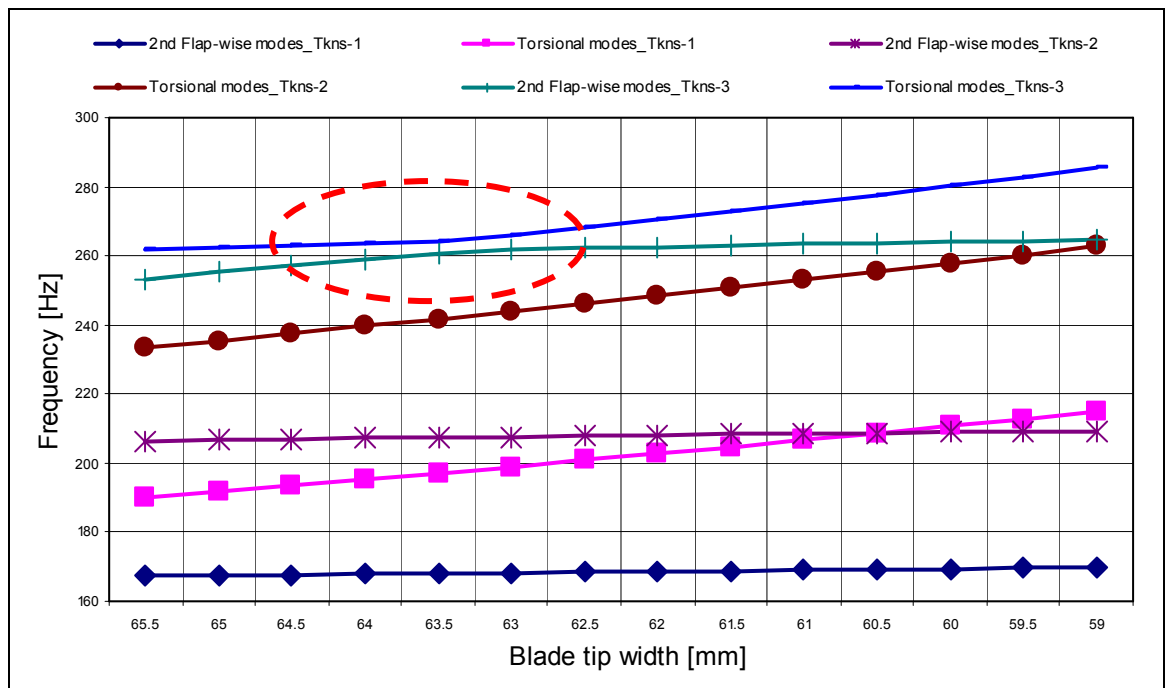


Figure 4.2 Veering study for blade sector

After the initial study of blade sector, several FE blisk models were simulated to meet the foresaid requirements and using the indications provided by the previous study. The results produced by the FE model of the final design

matched closely the initial requirements. The geometry dimensions of the blisk are reported in **Table 4.1** :

Overall Disc Diameter:	540 mm	Blade Gap at the Tip:	8 mm
Inner Disc Diameter:	188 mm	Blade root	14 Deg
Thickness Inner Disc	3.79 mm	Thickness Blades	1.89 mm
Bore	60 mm		

Table 4.1 Geometry dimensions of the 24-bladed blisk

The FE model was constructed in ANSYS using the following parameters, as shown in **Table 4.2** :

Element Type:	SHELL element	Young Modulus:	207 MPa
N. of Nodes:	659	Poisson ratio:	.33
N. of Elements:	643	Density:	7594 Kg*m ⁻³
Analysis Type:	Cyclic Symmetry	N. of Blades	24

Table 4.2 FEM construction parameters

Figure 4.3 and **Figure 4.4** show a basic sector of the blisk, as used in the cyclic symmetry analysis using ANSYS software, and the zoomed region where the clamping mechanism will work so a suitable number of nodes were locked to simulate the locked area. **Figure 4.5** shows the overall bladed blisk which resembles a fan blisk because the shape of its blades.

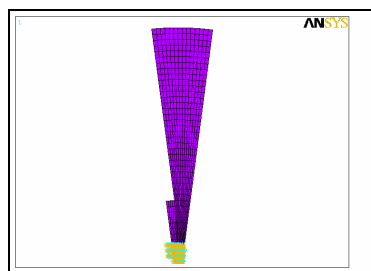


Figure 4.3 FEM blade sector

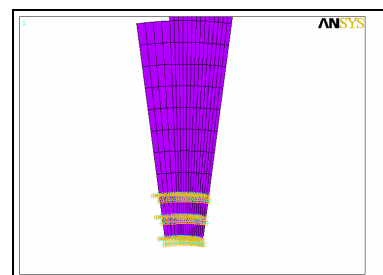


Figure 4.4 FEM blade sector; zoomed

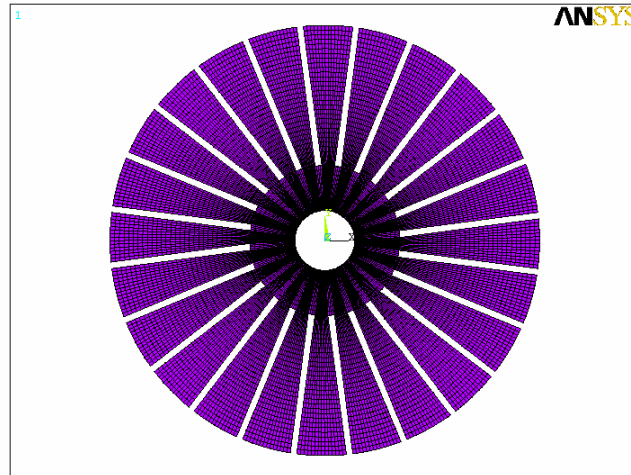


Figure 4.5 24-Bladed disc

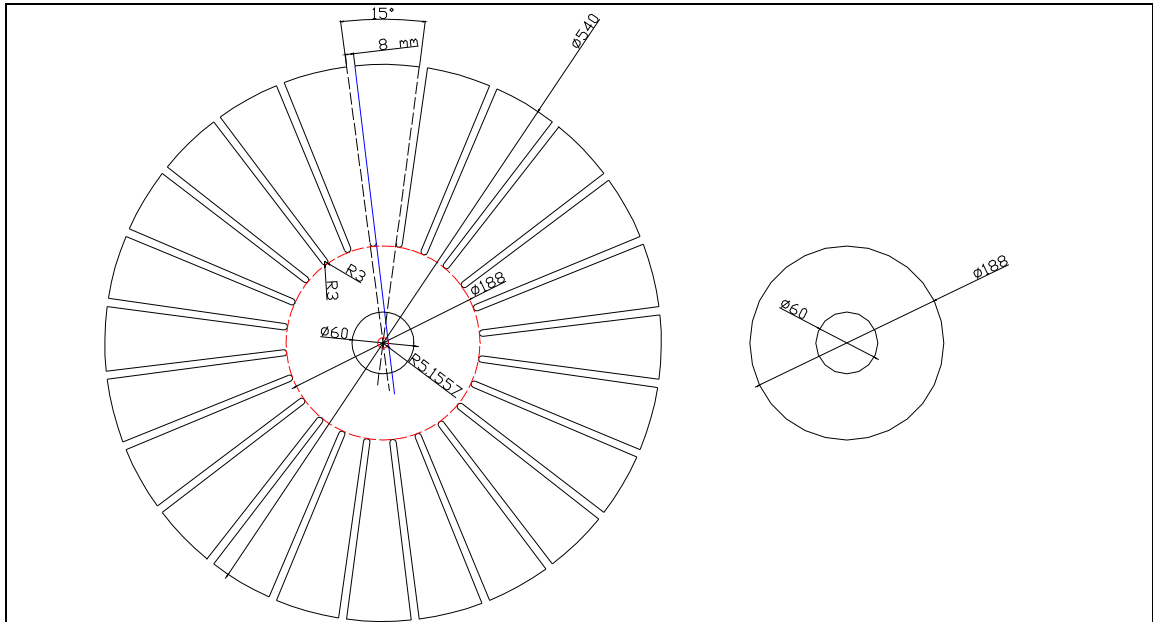


Figure 4.6 Dimensions of the USAF 24-Bladed disc

Some basic dimensions of this USAF 24 Bladed Disc testpiece are shown in **Figure 4.6**. FE analysis was used to predict tuned-blade natural frequencies and mode shapes for the blisk, using ANSYS cyclic symmetry analysis for modelling. **Figure 4.7** shows the two families of modes, 1T and 2F, which are separated by about 20Hz on the left hand side. While, **Figure 4.8**, on the right hand side,

shows the modal content (Flap Vs Twist) of the two families of modes where the nodal diameter at which veering occurs can be seen clearly.

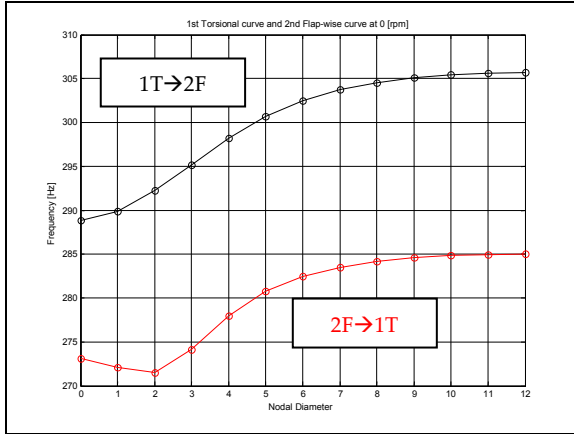


Figure 4.7 1T and 2F natural frequencies plot calculated at rest

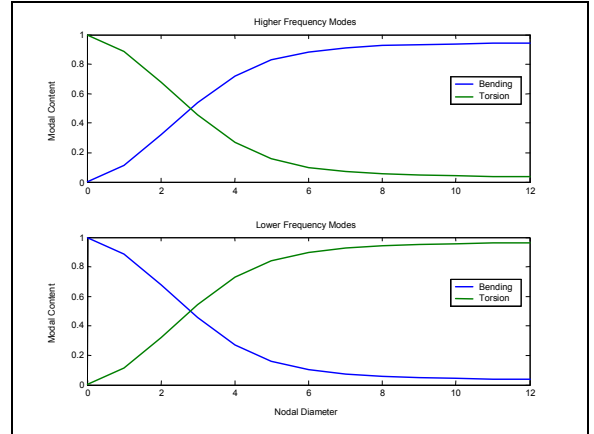


Figure 4.8 Modal content of the two families of model at rest

Figure 4.9 shows the corresponding curves calculated for a rotational speed of 2400 rev/min. **Figure 4.10** shows the modal content calculated at 2400 rev/min.

Figure 4.11 shows the 1T and 2F curves calculated for rotational speeds of 0 rev/min and 2400 rev/min.

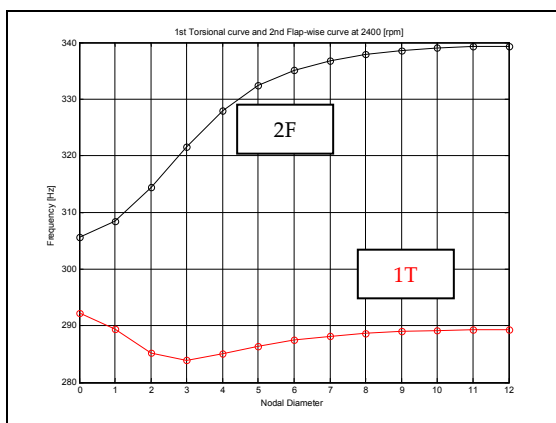


Figure 4.9 1T and 2F natural frequencies plot calculated at 2400 rev/min

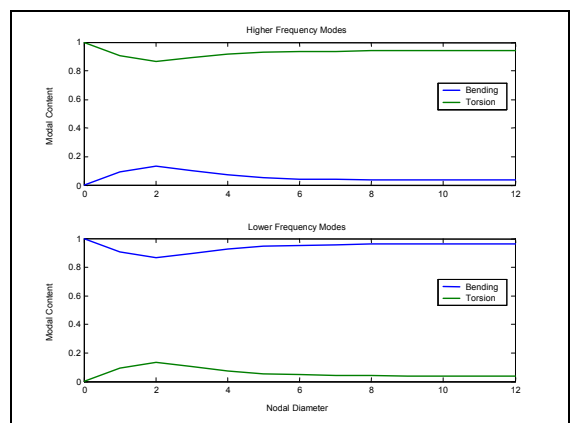


Figure 4.10 Modal content of the two families of model at 2400 rev/min

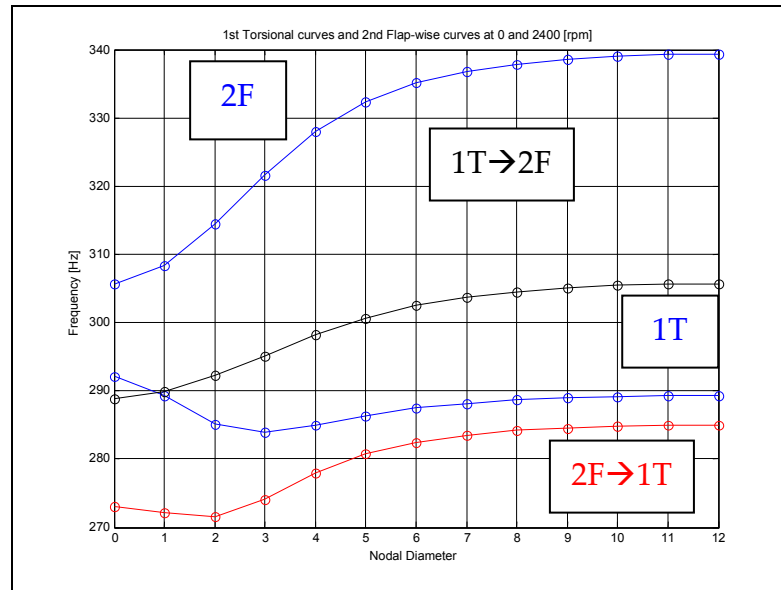


Figure 4.11 Curves 1T and 2F calculated for rotational speeds of 0 rev/min and 2400rev/min

Considering the geometry of the blade, which shows a sharp corner at the blade root, it was necessary to carry out a detailed stress analysis. The steady stress, calculated using Von Misses formulas, at the root of the blade for a rotational speed of 2400 rev/min is 59.4 MPa, which is lower than the yield stress of the steel. **Figure 4.12** shows the result of the stress analysis.

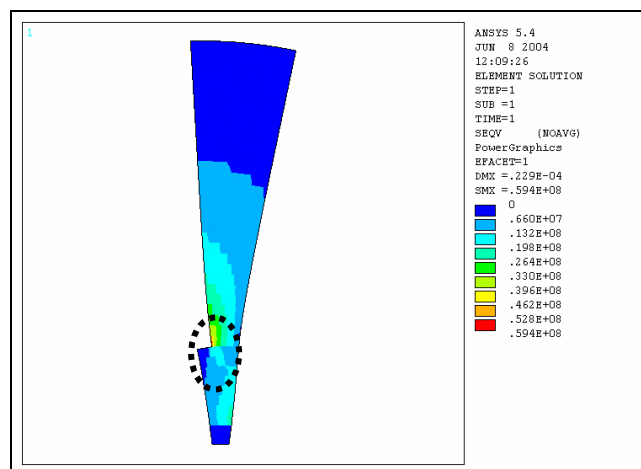


Figure 4.12 Result of the Steady Stress analysis (Von Misses) calculated at rotational speed of 2400 rev/min

Despite the fact that the geometrical shape of the blisk appears very simple, the parameters governing the proximity of those families of modes were hard to find: in fact the overall design took nearly six months. Several attempts were made, often unsuccessfully, until one of the key geometrical parameters was found to be the inter-blade tip slot width and, surprisingly, its variation showed very well how the two families could be controlled, as shown in **Figure 4.13** where the blade gap was varied in the range 5 (0.5) 11 mm. That design experience triggered an important thought about the relationship between geometrical sensitivity and mistuning perturbation which can be easily summarized by the following question: ‘How sensitive would be a blisk to a datum mistuning pattern when one of its geometrical dimensions is varied. Hence, this simple blisk design offered the possibility to study two phenomena: (i) the curve veering effect, studied from an experimental point of view, and (ii) geometrical sensitivity, studied for a datum mistuning pattern. The latter point will be explored in a separate chapter.

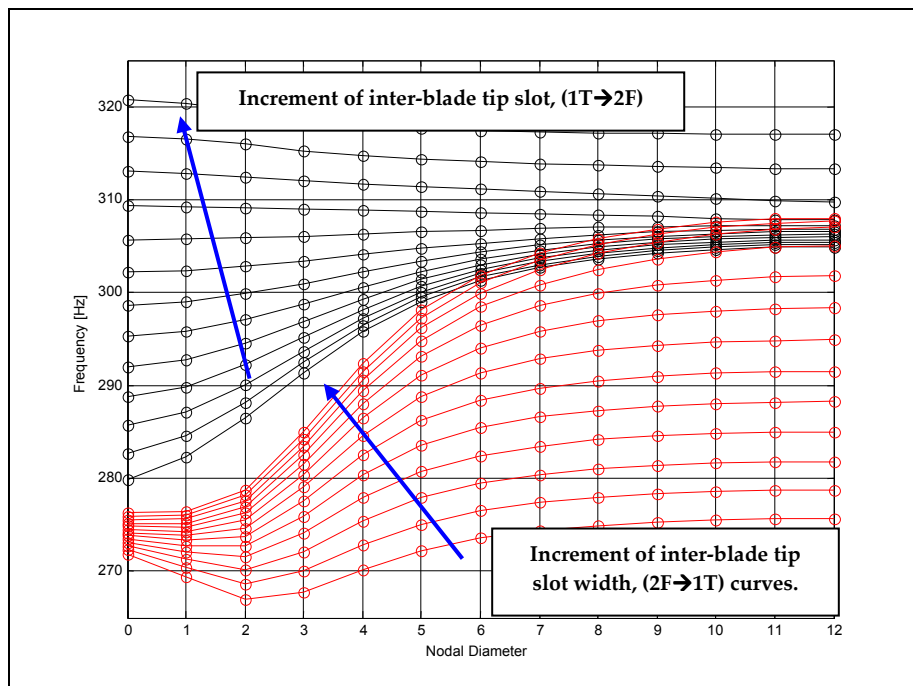


Figure 4.13 Series of curves for 2F and 1T families

4.3 Development of the rotating test rig

The vibration measurement tests on the 24-bladed disk were carried out on a well controlled test rig. That had been designed and built, in the past, to perform experimental investigations of the sensitivity of bladed disk to mistuning. That specific phenomenon presents a wide range of difficulties for measurements therefore it was important that all unwanted phenomena but not the one being studied were eliminated by designing a well-controlled test rig. Most of the original structure and features were retained; however, some parts of the rig were removed or substituted by others, included the measurement technique for the vibration measurements, developed to be independent of mechanical components.

4.3.1 Original *ADTURB* test rig description

The *Adturb* test rig was designed to meet several demanding requirements. In fact, it could operate under vacuum conditions, the rotor being enclosed in a chamber whose front side could be closed by a glass window allowing full operational conditions to the LDV laser beam. This feature proved to be very useful to perform measurements without the presence of aerodynamic effects such as damping due to the air. The rig was equipped with an electric motor whose maximum achievable speed was 6000 rev/min. The motor could be electronically controlled via software which could perform several tasks, such as setting up the rotational speed. The chamber could be equipped with up to six exciters, although only one is usually used for the measurements. The exciter consisting of a DC magnet was mounted on a stepper motor, schematically shown in **Figure 4.14**, which could be controlled electronically to adjust the clearance between the magnet and the blade tip, thus controlling the level of force [30].

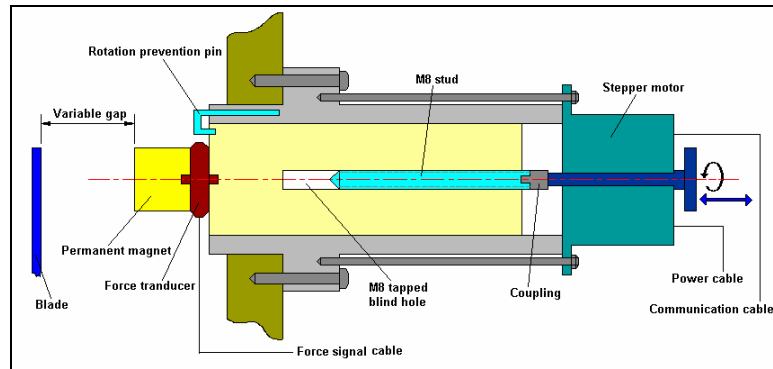


Figure 4.14 Stepper motor

Figure 4.15 shows the front and the rear faces of the test rig where it is possible to see one of the rotors used in the past for measurement tests.

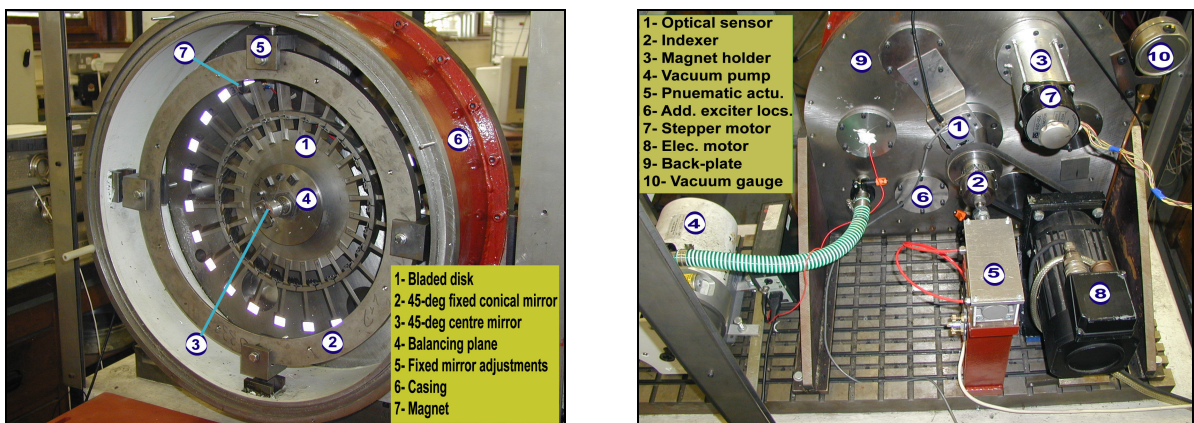


Figure 4.15 Front and rear of test rig

Bladed disks are very complex and sensitive structures and any type of contacting transducer can significantly change their dynamic behaviour, so the only transducers usable for accurate measurements are contact-less ones, such as the Laser Doppler Vibrometer (LDV) which was then used in all the Adturb project measurements. Despite the use of a Scanning LDV, that transducer was employed as a single point device because the measurement method employed consisted of self-tracking measurement system. The system consisted of an index 45 degree mirror mounted on a push-rod inserted into a hollowed shaft, as

shown in **Figure 4.16**. The mirror could be rotated in increment of 15 degrees, thereby aligning with any of the 24 blades, by a pneumatic actuator which, electronically controlled, could push forward the push-rod to allow its incremental rotation. That tracking method delivered a robust single point measurement technique in fact the laser spot located on the target position could be always synchronous with the target. A crucial feature was the positioning of the 45 degree annulus mirror and its alignment in order to properly deflect the laser beam, the operational working scheme is shown in **Figure 4.17**.

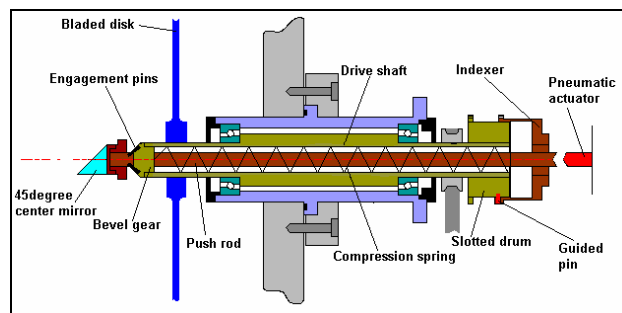


Figure 4.16 Index mechanism

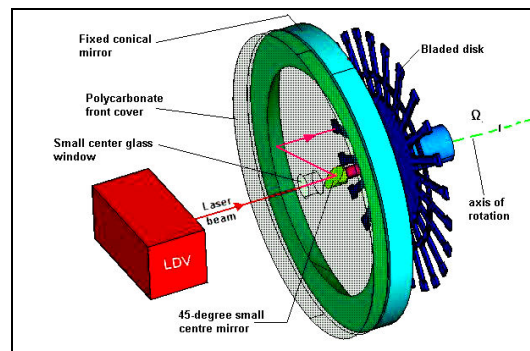


Figure 4.17 The self-tracking system scheme

Finally, Figure 4.18 show in detail the measurement set-up used in the past.

the original. The output card was an NI 6711 PCI with 4 output channels two of them used for driving the LDV scanning device. That card has the option to use an external time base clock to sample the output waveform, represented by the TTL output signal of the encoder. One of the features of the test rig which is now exploited more than in the previous design, and it is the possibility to have a greater variety of excitation methods. Previously, the excitation system consisted of one or more, up to 6, DC magnets placed right behind the blade tips. However, this excitation method, called Engine Order (EO) excitation, is speed-dependent and therefore excitation of some blisk resonances can be only obtained at rotational speeds beyond the operational frequency limit imposed by the scanning device. To overcome this limitation, the test rig should be equipped with either a fix AC exciter or a rotating one to achieve two different excitation configurations as shown in **Figure 4.19**. Following paragraphs describe the excitation methods.

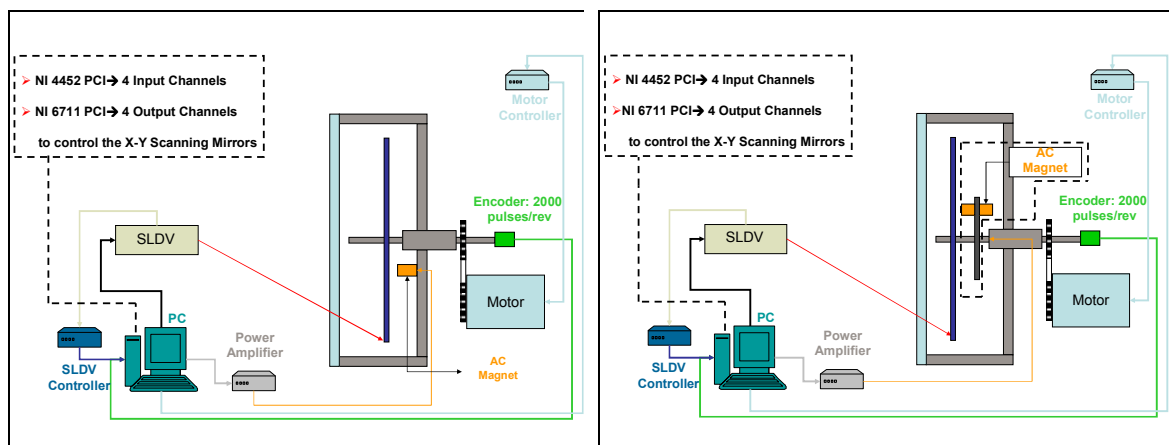


Figure 4.19 Fixed AC exciter, left hand side; Rotating AC exciter, right hand side

4.3.3 Excitation Systems; DC and AC magnets.

We have seen that the test rig offers several options to produce an excitation of the rotating blisk. By using a fixed DC magnet, placed behind the blade tip, an

EO excitation method can be performed which is very similar to the one experienced by real rotors under operating conditions. However, that excitation method is speed-dependent, and that may cause some problems for the scanning device performances, when the blisk resonances to be studied are only achievable at high rotational speeds. Any way, the excitation frequency can be easily controlled by mounting an AC magnet, thus removing the dependency of the resonance excitation on the rotational speed. This feature offers the chance to carry out measurement tests under rotating conditions at lower speed. A useful solution for using the AC excitation method was to mount the exciter on a disc support clamped at the shaft thus to have the exciter and the laser spot in the same system of reference, a clear picture of this excitation system will be given in the next sub-paragraph.

4.3.3.1 DC excitation system

The blisk excitation can be achieved through a permanent magnet fixed in space as shown in **Figure 4.20**.



Figure 4.20 DC magnet

Using this type of excitation arrangement the bladed blisk experiences a phased pulse excitation whenever a blade passes the exciter magnet and, in fact, the excitation force fluctuates from near-zero when the magnet is between blades, to a maximum when the magnet is centred on a blade tip. In the present case, the

magnet only attracts the blades; therefore, all the force values are positive. An example of a train of magnetic pulses is shown in **Figure 4.21**.

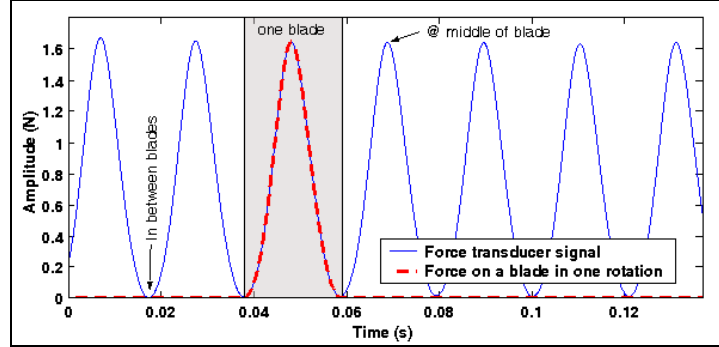


Figure 4.21 Example of a typical train of magnet pulses

Given a magnet pulse such as the one given in red in **Figure 4.21**, the amplitude of the force exciting different EOs can be calculated by performing a Fourier series analysis. Assuming that the discrete force signal, f , is defined at N time points, $t = t_k$ ($k = 1, 2, \dots, N$) and is periodic, with a period T , in the form $f(t) = f(t + T)$, it can be represented by a finite series:

$$f_k = \sum_{n=0}^{N-1} F_n e^{2\pi i n k / N} \quad (4.1)$$

where:

$$F_n = \frac{1}{N} \sum_{k=0}^{N-1} f_k e^{-2\pi i n k / N} \quad , \quad n = 1, 2, \dots, N \quad (4.2)$$

Here the absolute value of the complex F_n , $|F_n|$, gives the amplitude of the n th harmonic, or the amplitude of the nEO excitation. The first 48 harmonics of a typical magnet pulse, together with the reconstructed pulse using these harmonics in ((4.1), are given in **Figure 4.22**.

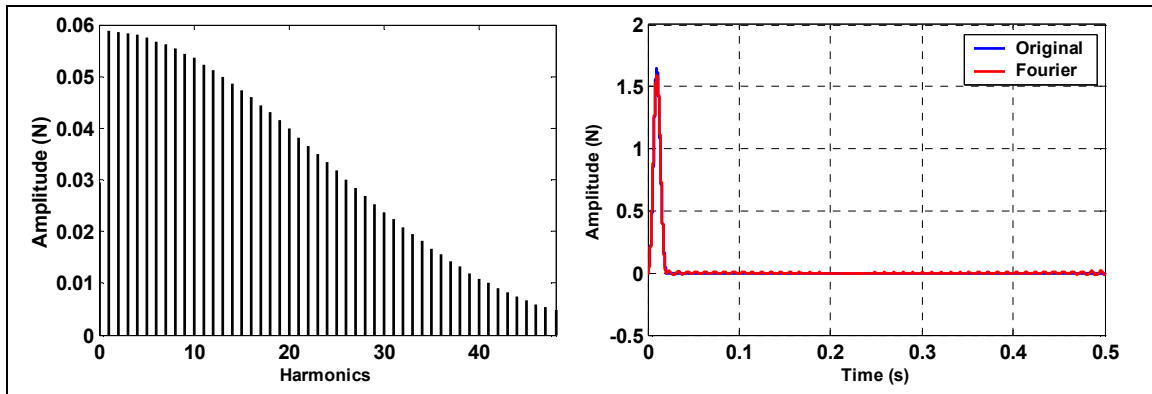


Figure 4.22 Harmonics of a magnet pulse and its reconstruction through these harmonics

4.3.3.2 AC excitation

Another way to excite the blisk is to use an AC magnet, such as the one shown in **Figure 4.23**.



Figure 4.23 AC magnet

The AC magnet can be used in two ways to excite the blisk, either fixed in space or rotating with the disc, thus to always excite the blisk at a fix point. It is important to note that the magnetic force is related to the gap by the inverse square, and so the exciter must be set up very close to the structure to input enough exciting force. When measurements are carried out with the blisk at rest, there are no problems about safety which may arise whenever the blisk is rotating and the vibrating blades can hit the exciter being very close to them. A solution to overcome that is to mount the exciter either the root of blade or at a

location at which the exciter can still transfer enough energy to the structure but whose vibration amplitude is small enough to avoid unwanted contacts between the test structure and the exciter. **Figure 4.24** shows the operational scheme of the AC magnet.

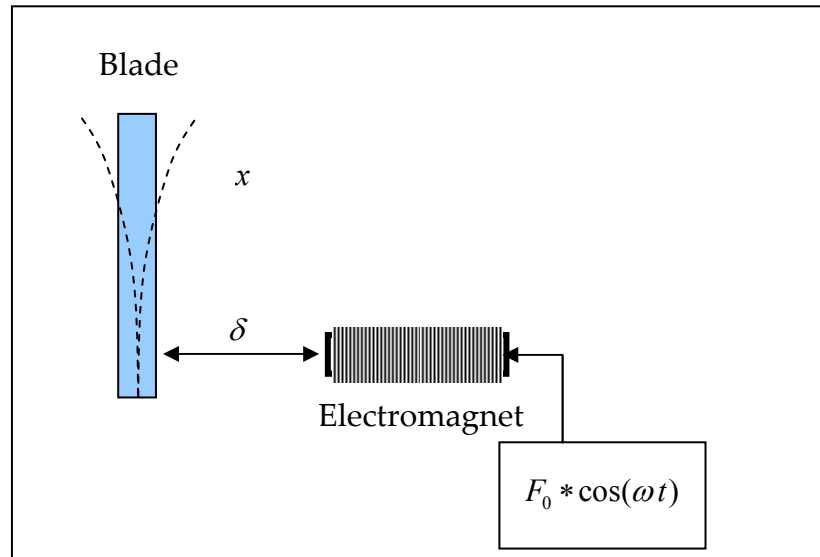


Figure 4.24 AC operational scheme

Supposing that the magnet is driven at the frequency, ω , in the form:

$$f(t) = F_0 * \cos(\omega t) \quad (4.3)$$

and recalling that the magnet force is always positive, the force experienced by the blade may be related to the gap and be described as follows:

$$F(t) \rightarrow \left| \frac{1}{\delta^2} F_0 * \cos(\omega t) \right| \quad (4.4)$$

Having a fixed AC exciter mounted behind the blisk turned out to be very practical because the excitation frequency could be easily controlled using a signal generator to excite any desired ODS at any rotational speed. However,

that solution was not helpful when a Frequency Response Function (FRF) had to be measured under rotating conditions because the excitation and the response are not measured in the same system of reference. Under these circumstances, the coordinate of any point of a bladed blisk rotating at speed of Ω can be related to the coordinate of fixed frame of reference by the following equation:

$$\chi = \chi_0 + \Omega t \quad (4.5)$$

where χ is the coordinate in the rotating frame of reference and χ_0 is the coordinate in the fixed frame of reference. With the exciter being fixed in the space, a harmonic stationary point force is represented by the equations (4.3), and the force acting on a bladed blisk can be represented by:

$$F(\vartheta, t) = (F_0 \cos \omega t) \delta(\chi - \Omega t) \quad (4.6)$$

where δ , the Kronecker delta, satisfies:

$$\begin{aligned} \delta(\chi - \Omega t) &= 0 && \text{for } (\chi - \Omega t) \neq 0 \\ \int_{-\infty}^{+\infty} \delta(\chi - \Omega t) d\chi &= 1 \end{aligned} \quad (4.7)$$

When the pair of n -th nodal diameter (ND) bladed blisk modes have the form of mode shapes:

$$\begin{aligned} \phi_1(\chi) &= \sin(n\chi) \\ \phi_2(\chi) &= \cos(n\chi) \end{aligned} \quad (4.8)$$

the generalized forces for the assumed modes become:

$$\begin{aligned}
 Q_{1n} &= \int_0^{2\pi} F(\chi, t) \phi_1(\chi) d\chi \\
 Q_{2n} &= \int_0^{2\pi} F(\chi, t) \phi_2(\chi) d\chi
 \end{aligned}
 \tag{4.9}$$

which after integration can be expressed as:

$$\begin{aligned}
 Q_{1n} &= \frac{F_0}{2} \sin(\omega - n\Omega)t + \frac{F_0}{2} \sin(\omega + n\Omega)t \\
 Q_{2n} &= \frac{F_0}{2} \cos(\omega - n\Omega)t + \frac{F_0}{2} \cos(\omega + n\Omega)t
 \end{aligned}
 \tag{4.10}$$

Thus, it can be seen that the excitation experienced by the bladed disk in rotating the frame of reference is at two distinct frequencies, $(\omega \pm n\Omega)$, for each n ND mode. It was decided to mount the exciter on a disc which could be locked onto the shaft right behind the bladed blisk so as to be fixed in the same frame of reference. One of the main concerns was to feed the exciter with the appropriate signals during rotation. The solution was to install two brushes on the disc which could slide on two slip rings attached on a fixed support to finally transfer the signal into the AC exciter. Any loss of signal voltage level due to the slippery contact was not affecting the performance of the exciter which could deliver enough force to excite the blisk. The first prototype was assembled using scrap materials as shown in **Figure 4.25**.

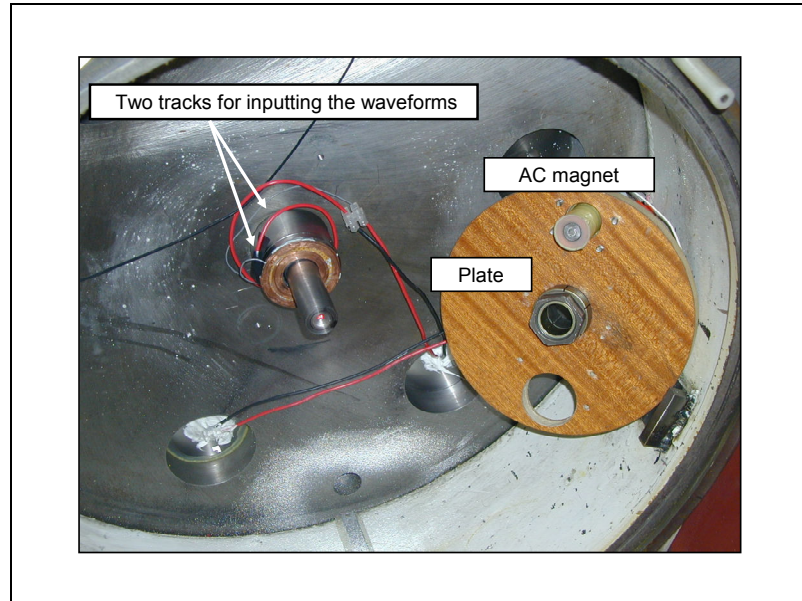


Figure 4.25 Rotating exciter and slip ring; prototype

Having designed such an exciter, the use of chirp signal as excitation force could speed up the FRF measurement which was not possible when using the exciter fixed in space. An example of FRF data measurement using rotating and fixed AC exciters is shown in **Figure 4.26**. Because of the prototype arrangement, the measurements could only be performed at 6 rev/min and 60 rev/min, as shown on the left hand and right hand side, respectively. The input signal was a sine sweep signal in the range of 15-35 Hz whose sweeping time was 10 sec. The picture shows clearly that when the AC magnet is used fixed in space the frequency spectrum of the measured LDV output signal was unreadable whereas by using the rotating exciter the measurements show up clearly.

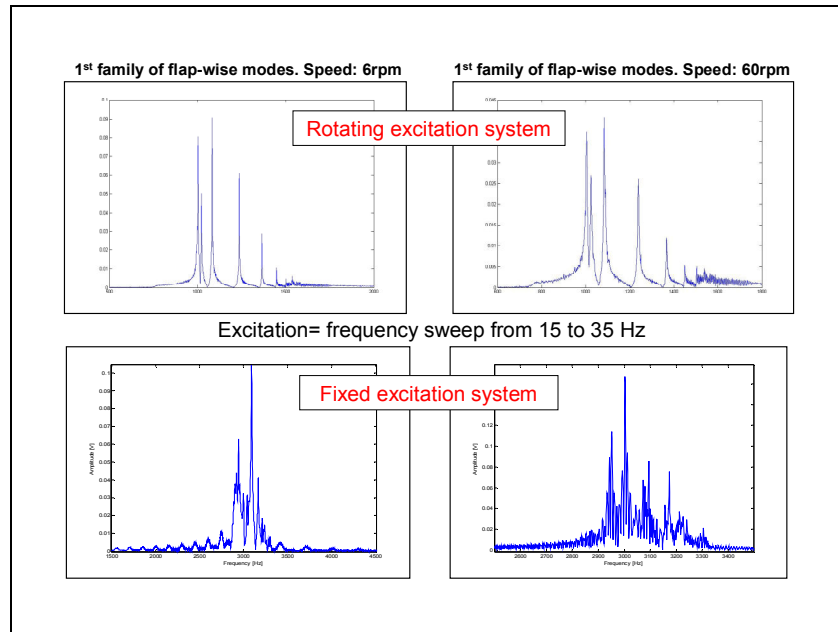


Figure 4.26 FRF data using rotating and fixed AC magnet; sine sweep excitation

Encouraged by results measured using a temporary prototype device, it was decided to design and manufacture a more robust one able to accomplish tasks at higher rotational speeds. The results of measurements made using that excitation method will be presented in Chapter 6. **Figure 4.27** shows the slip rings mounted on a fixed support and connected to the signal generator, the rotating AC magnetic exciter installed into a disc plate counter balanced by a weighted mass and the overall assembly which shows the position of the AC magnet respect to the blisk. All tests were carried out by setting up the gap between the exciter and the blisk at 1.5mm. However, when using such an assembly it was necessary to perform a force measurement to assess the level of force delivered by the exciter. The exciter was fed with sine waves in the frequency range between 20 (1) 300 Hz whose amplitude was set for the first measurement test at 6V, and for the second measurement test at 12V. **Figure 4.28** shows the results of the force measurements.

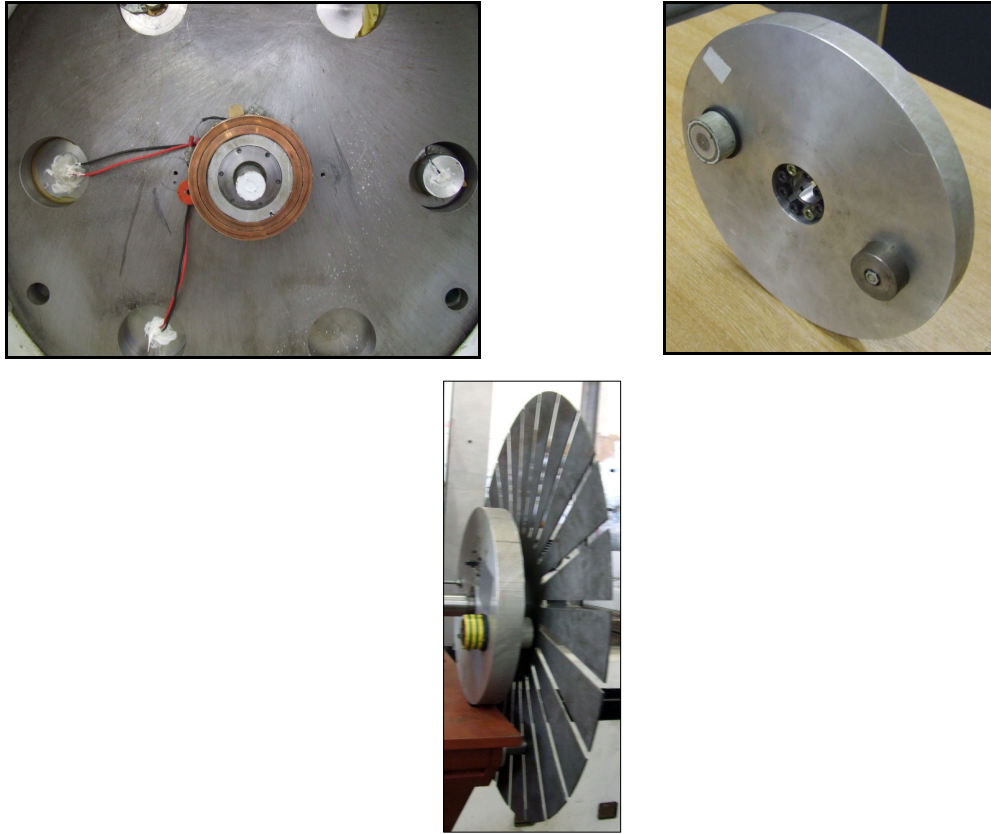


Figure 4.27 Slip rings, rotating exciter and overall assembly

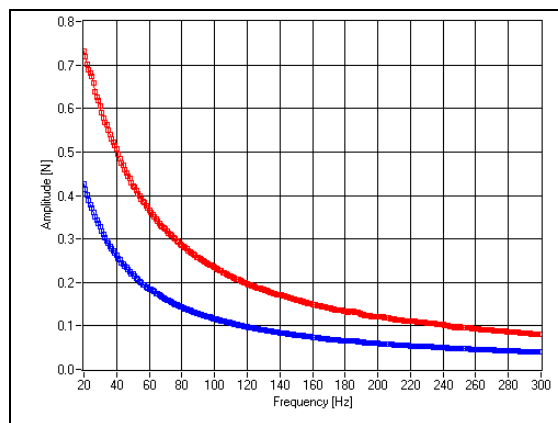


Figure 4.28 Measured force produced by the exciter with 1mm gap inputting sinewaves at 6V (blue) and 12V (red)

4.4 Conclusions

In this chapter we have presented the design of the 24-bladed disk test piece. A series of criteria were set for the rotor design to be able to study the dynamic behaviour of the blisk at the veering region both under stationary and rotating conditions. Some of these criteria can be recalled by saying that the 2nd flap-wise and 1st torsional families of modes had to be very close in frequency at rest and well separated at 2400 rev/min, the maximum rotational speed agreed, and the geometrical shape of the blade should allow the laser beam to sweep the surface easily. The designed blisk was similar to a fan blisk and it was also used for other research studies. Having presented the testpiece, the chapter also described the developed test rig used to carry out vibration tests. We have seen that the *USAF* test rig was a modification of an existing one previously used for another project. We have shown the differences between the two configurations, outlining the possibility of the later one to use a wider variety of excitation methods. A detailed explanation of the rotating exciter was provided and thanks to that excitation method it was possible and very easy to measure FRFs under rotating conditions.

5 Virtual Test Simulation (VTS) using Tracking-Continuous Scanning LDV methods

5.1 Overview

This chapter is focussed on the Virtual Test Simulations (VTS). The simulators performing such tasks are coded into panels which are part of a software platform, called CAISER MYMESIS, which can perform several tasks in the CSLDV measurement process. VTSs are reproduction of real vibration measurement tests but resolved in mathematical models to be run in any computer. One of the aims of these simulators is to provide a software tool to mechanical designers to experience ‘virtually’ measurement tests using CSLDV methods. In addition, this software aims to help those who periodically work with experiments, in the identification of the best measurement parameters to obtain optimum measurement results, such as ODS, of reliable quality. Virtual test simulation (VTS) is presented through the explanation of some software panels which can perform virtual measurements both under stationary and rotating conditions using continuous scanning LDV techniques. To help the comprehension of the simulator panels, the chapter develops along an introduction of VTS to go into the Operational Deflection Shape (ODS)

mathematical concept followed by Polynomial curve fitting concept to conclude into the simulator panels' explanation and practical use of them for predictions.

5.2 Virtual Test Simulation (VTS) concepts

Any vibration test requires both lot of experience to be properly carried out and a lot of time to set it up. Experience is without doubt an important attribute for any person dedicated to that type of work. In fact, non experts are to make trivial mistakes, even in setting up the measurement system. Any little error accidentally introduced anywhere in the test set up will inevitably be reported in the final measured output data. Even when the test rig is ready to run, some time can be required to set up the right measurement parameters such as instrument sensitivity and others. All this "experience" is something gathered from many years of practice, step by step, and of course this preparation costs time and money. Unfortunately, time is increasingly critical and everything is being sped up faster and faster. However, tests can be improved, at least to avoid an improper use of measurement parameters. Here, Virtual Test Simulations (VTS) can help, even experts, to test virtually on computers in order to assess what would be the best parameter choices to use in the laboratory. The main aim of VTS is to simulate the intended output measured data as close to the real situation as possible by mathematically modelling the output behaviour and, based on that, to perform a virtual test to obtain the best measurement parameters. With the LDV transducer used in this study, the challenge was to code and structure into a software platform a detailed mathematical model of the LDV and its output signal. That is not the only model involved because in reality we do not have a measurement without noise pollution and sources of signal corruption, hence the aim is to include models of any source of noise introduced by the scanning mirrors, roughness of the tested surface which is linked with the speckle noise, laser misalignment and any many others. Once

mathematical models are coded to describe sources of noise, we can superimpose them on the LDV output signal model. This *modus operandi* turns to be very useful for the Continuous Scanning LDV method. Because of the nature of LDV techniques, mathematical modelling can be used to perform simulations under several “operative” conditions in order to optimize the real measurement test set up, once in laboratory. On the other hand, the VTS method is also useful for training non experts to use a measurement method such as CSLDV by providing a basic knowledge of its use before application of the test rig itself. In the next paragraph it will become clearer how the VTS can be employed for the CLSDV method under stationary and rotating conditions for the test piece and the tracking methods, such as Point Tracking, Line Tracking and Area Tracking, introduced in Chapter 3, will be seen from a mathematical point of view.

5.2.1 Structure of a VTS for the CSLDV method

Before presenting an explanation of the VTS for the different tracking methods, it is important to introduce the structure of the simulator codes and to show how a common basic scheme is shared by all simulated methods. Schematically, the simulators are composed of panels divided into three tabbed sections working sequentially. The first one is generally called “ODS simulator and polynomial fitting” because it uses data from an FEM model to produce a desired ODS in the frequency range of the calculated solutions. The second section is called the “LDV output signal simulator” and is dedicated to simulate the LDV output signal (time history) using polynomial coefficients as input, which have been produced in the previous section by polynomial curve fitting. The last section, “ODS contractor”, post processes the LDV time signal simulated to reconstruct the ODS. **Figure 5.1** shows the flow chart of a general simulator panel in order to make clearer the process summarized above.

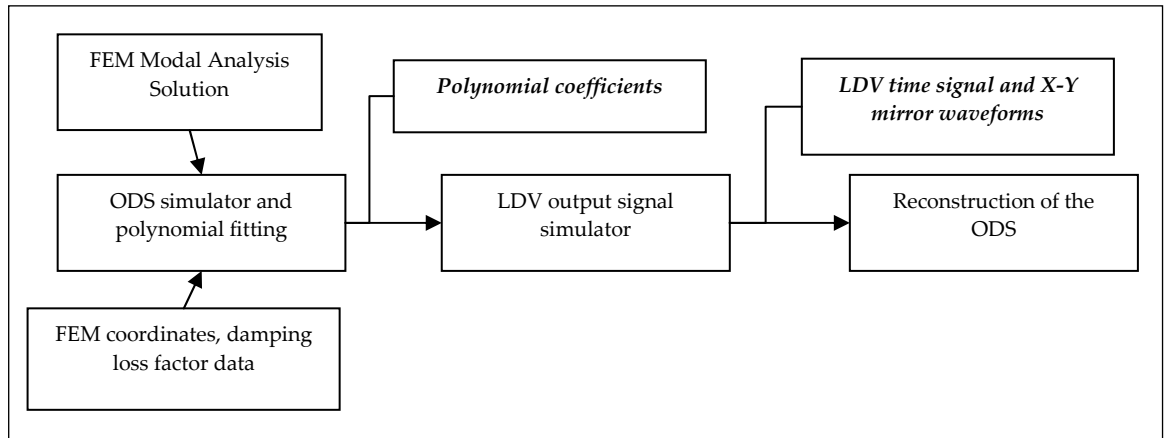


Figure 5.1 Flow chart scheme of simulator panel

5.3 ODS theory

CSLDV is a structural vibrations measurement method which allows rapid determination of the Operational Deflection Shape (ODS) of a vibratory structure. Accordingly VTS simulators calculate any ODS at any excitation frequency and excitation location as their first task. The initial simulated ODS will then become the reference data used to validate the subsequently reconstructed ODS from a simulated LDV time signal. If we consider the general equation of forced vibration for the particular case of harmonic excitation and response of a MDOF system with general hysteretic damping:

$$\left([K] + i[D] - \omega^2[M] \right) \{X\} e^{i\omega t} = \{F\} e^{i\omega t} \quad (5.1)$$

and the hysteretic damping matrix $[D]$ is, typically:

$$[D] = \beta[K] + \gamma[M] \quad (5.2)$$

the solution of the general equation is:

$$\{X\} = ([K] + i[D] - \omega^2[M])^{-1} \{F\} = [\alpha(\omega)] \{F\} \quad (5.3)$$

but this equation is not efficient for numerical application and so a more helpful form of this solution may be derived by modal analysis:

$$\{X\} = \sum_{r=1}^N \frac{\{\phi\}_r^T \{F\} \{\phi\}_r}{\omega_r^2 - \omega^2 + i\eta_r \omega_r^2} \quad (5.4)$$

where $\eta_r = \beta + \frac{\gamma}{\omega_r^2}$ is damping loss factor for that mode. Equation ((5.4) may be used to study an ODS in terms of mode shapes, force vectors, excitation frequencies and damping factors [31].

5.4 Polynomial Curve Fitting

This section will describe the polynomial curve fitting used in the simulators to curve fit a simulated ODS to recover polynomial coefficients. It should be noted that, the reason why curve fitting is essential for the VTS, and why any error produced by that process will have repercussions on the simulated LDV output time signal, is a consequence, explained in this section, of the measurement methodology and time data post-processing. When a structure is excited sinusoidally the LDV output signal, when laser beam is travelling continuously across the surface of the structure, is an amplitude-modulated signal whose frequency spectrum includes a series of sidebands, equally spaced apart the excitation frequency. The amplitudes of those sidebands can be transformed into coefficients of a polynomial series which will describe the ODS of the structure. Hence, the polynomial coefficients are key points both for the actual reconstruction of the ODS from real time data and for the simulation of the LDV time history. Whenever we want to simulate time data, the initial task is to

There are several algorithms to improve the polynomial curve fitting but this is not the place to discuss it where the primary intention is to show how a poor fitting reflects on the next stages of the LDV time data simulation.

5.4.1.1 Inaccuracy of polynomial curve fitting and LDV simulation

Consider a simulated ODS of the second flexural bending motion, as shown in **Figure 5.2**. A poor polynomial curve fitting will produce coefficients containing errors and then the reconstruction of the polynomial is poor, as shown in **Figure 5.3**. When the curve fitting is properly performed, the polynomial coefficients will fit a polynomial matching the simulated ODS perfectly, as shown in **Figure 5.4**.

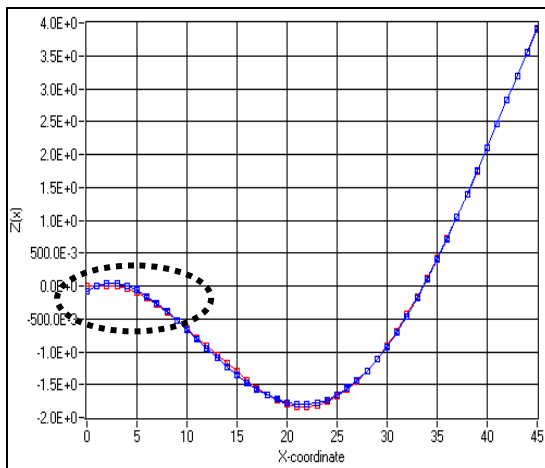


Figure 5.2 ODS; 2nd flexural mode shape

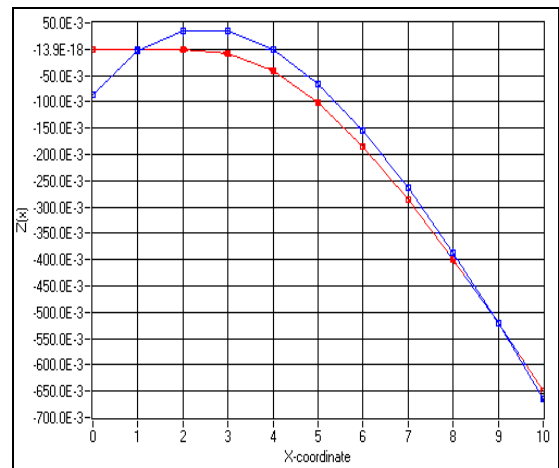


Figure 5.3 Zoom of dotted circle

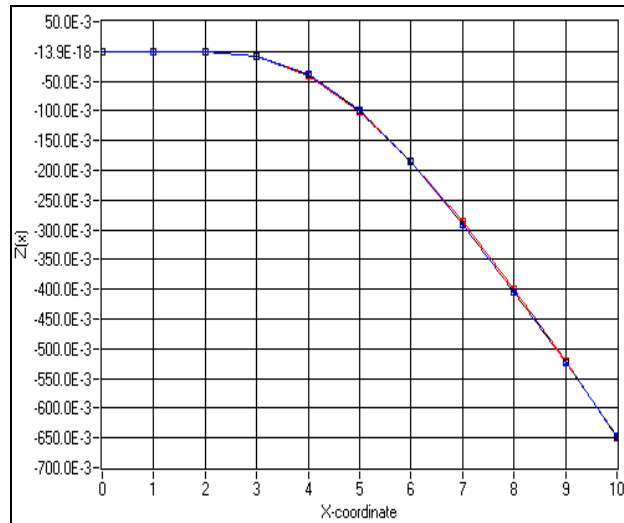


Figure 5.4 Zoom of dotted circle when the curve fitting is good

Good or poor polynomial curve fitting will reflect on the simulation of the LDV time history, and eventually on the reconstruction of the ODS. **Figure 5.5** shows a simulated LDV time data from a poor polynomial curve fitting where these errors can be seen as ‘pseudo vibration’ by the constrained root, as already shown in **Figure 5.4**. In fact, a good curve fitting returns clearly the simulation of the LDV time data, as shown in **Figure 5.6**.

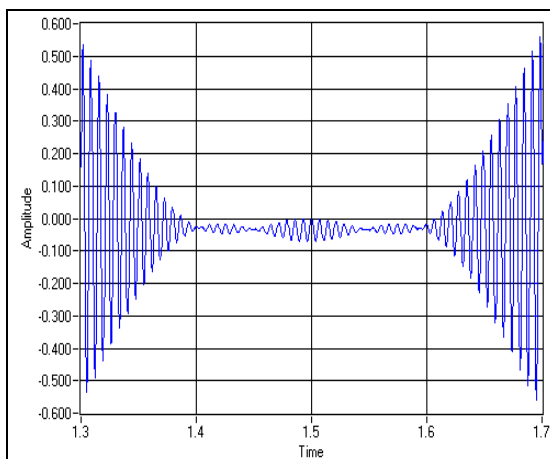


Figure 5.5 LDV time data; poor fitting

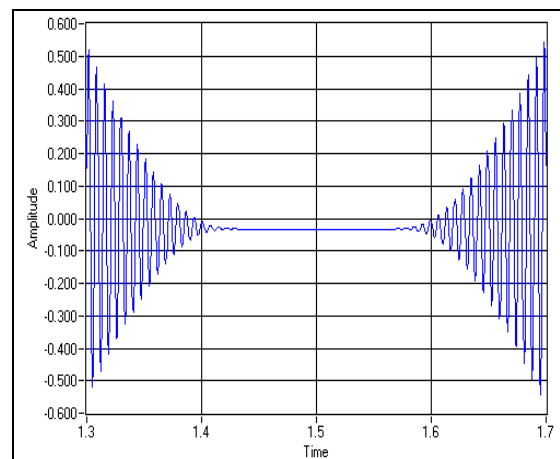


Figure 5.6 LDV time data; good fitting

If we now simulate the ODS of a blade sector for the 1st flexural bending motion, as show in **Figure 5.7**, a poor polynomial fitting will affect the simulation of the LDV time signal. **Figure 5.8** and **Figure 5.9** show simulations of LDV time data from poor polynomial coefficients and from refined polynomial coefficients. The main problem of curve fitting any ODS, both for 1D and 2D scan, is due to the constrained nodes, with zero displacement, of some coordinates of the ODS. As a result the solutions of equation (5.5), even when the polynomial order is correct, will contain small errors which can be reflected in the LDV time data simulation.

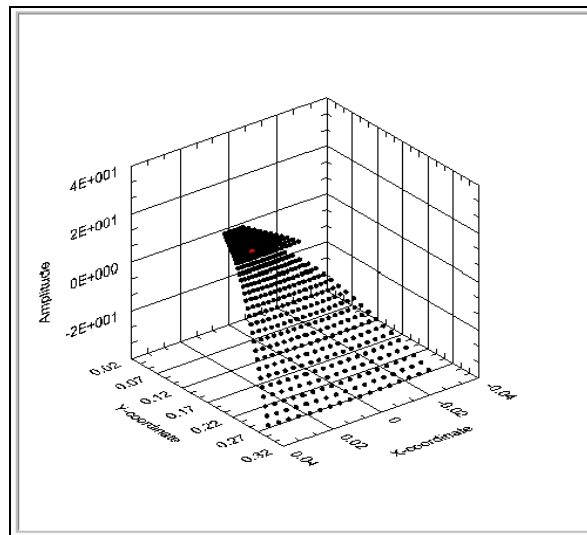


Figure 5.7 ODS of a blade

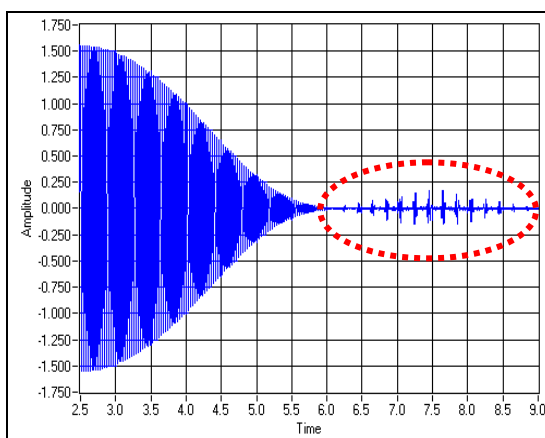


Figure 5.8 LDV time data; bad fitting

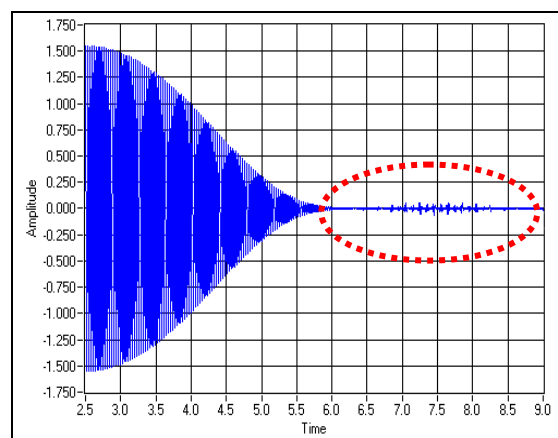


Figure 5.9 LDV time data; improved fitting

5.5 Point Tracking method VTS

'Point Tracking VTS' is one of the three panels dedicated to the simulation of LDV output time signal of synchronous measurement methods of rotating structures. This software panel is used to perform simulations of single point measurement time data of rotating structures. Despite the simplicity of the method, the Point Tracking panel must help to reproduce a real measurement including all sources of noise and any misalignment, which can cause a series of problems. One unwanted feature is an overload of the decoder which occurs when a resonance of the vibrating structure is encountered; however, that is not the case met during the measurements. It was already noticed in the previous chapter that when misalignment is present the laser spot position is not fixed at the specified location but it traces a small path around it. Generally, only a visual inspection of the laser spot during slow rotation of the blisk can determine if the level of misalignment is acceptable or not, whether the spot stays in a reasonable area around the target position. The simulator can only predict the effect of misalignment on the LDV output signal. Unfortunately, sources of misalignment such as offsets and rotations of the laser head are rarely input correctly because they are extremely difficult to measure. Speckle noise is always part of laser light but can become more severe when the laser beam travels on the structure surface thus the Point Tracking simulator takes into account those unwanted conditions for LDV time history predictions.

5.5.1 Point Tracking-VTS, Polynomial curve fitting

We already noted that all simulator panels are designed from a common basis as shown schematically in **Figure 5.1**. In modern mechanical design, one of the first tasks to accomplish is the construction of an FE model of the structure in order to study its mechanical characteristics, including its dynamic properties. This study can be extended to provide a virtual test simulation using the same FE

model. This way, bridging experimental and theoretical approaches can be considered quite interesting because analysts can have the opportunity to run a virtual measurement using the model they are developing and, at the same time, they can approach by numerical simulation the work often done by experimentalists in the laboratory. The panel, shown in **Figure 5.10**, offers options to set up the excitation frequency, location and force level as well as the response location by using a cursor to decide where to calculate it and eigenvalues are also listed. When all the parameters have been input, the ODS is calculated and presented in a 3D graph plot to show the deflection of the structure: this can be animated to visualize it. Some examples of calculated ODSs are shown in **Figure 5.11** where both the excitation and response locations can be seen. The excitation position is assumed to be at one node despite the fact that in real tests the exciter generally acts on an area rather than at a single point. It could be possible to adjust the simulation of the excitation, but this extra mathematical modelling effort was not considered necessary, the ODS simulations being in good agreement with the measured ones.

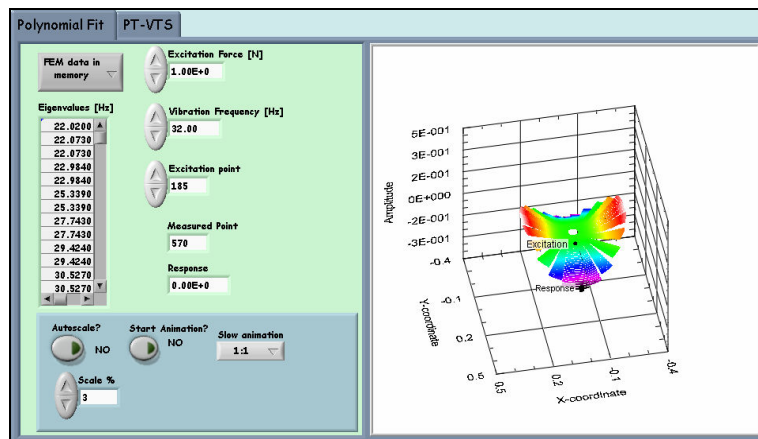


Figure 5.10 Front panel of Point Tracking VTS-Polynomial Curve Fitting tab

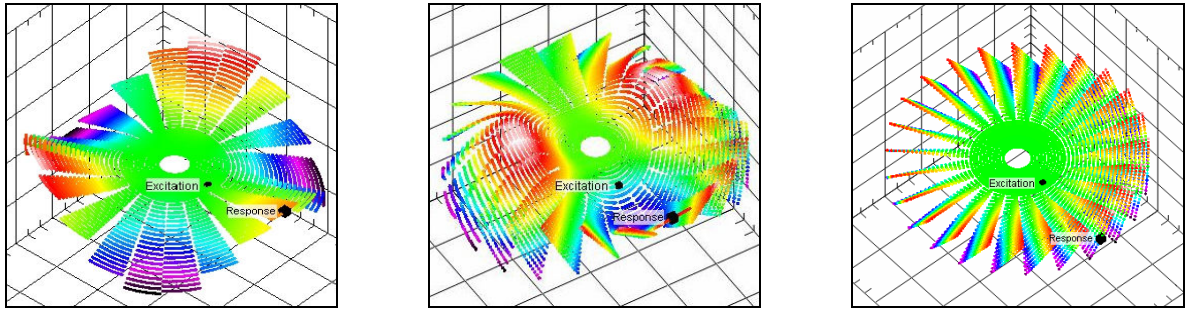


Figure 5.11 ODS simulations with excitation and response positions

5.5.2 Point Tracking-VTS, LDV time history

Once the response at the desired location is calculated, the value of the displacement is used in the next section of the Point Tracking panel, as shown in Figure 5.12, to simulate the vibration at that location. This section of the panel has to reproduce as accurately as possible a measurement test procedure from virtual control of the scanning device by inputting the values to generate the X-Y mirror waveforms to control the acquisition of the LDV time history by setting up input parameters.

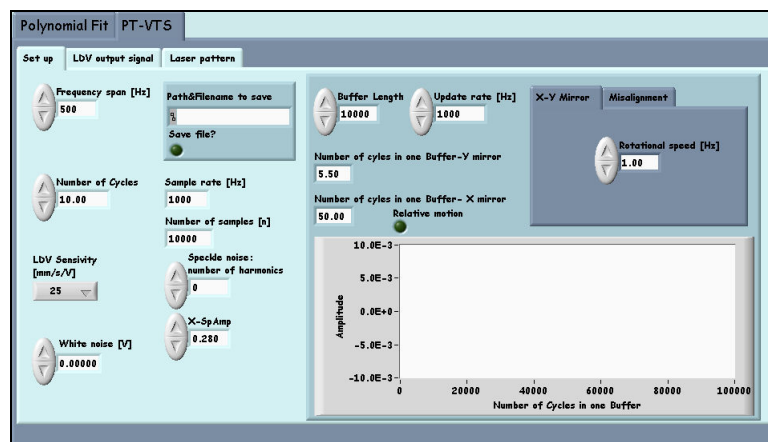


Figure 5.12 Front panel of Point Tracking VTS-LDV time history simulator

The panel has to provide a series of controls to generate sources of speckle noise, white noise and sources of misalignment to be superimposed on the virtual vibration. Finally, the result of the simulation can be seen on two plots, in the

time and frequency domains respectively. The main achievement of this simulator panel is to allow anyone to actively act on the controls and to simulate as much as LDV output time signals as are desired. By doing this it is possible to assess the ideal parameters with which eventually to run measurements on real structures.

5.5.2.1 *Mathematical formulation*

The vibration, which is expressed here as a velocity in the z-direction, is perpendicular to the structure surface in the X-Y plane:

$$v_z(t) = V_{zR} \cos \omega t + V_{zI} \sin \omega t \quad (5.7)$$

where V_{zR} and V_{zI} are the Real and Imaginary components of the vibration in z-direction, ω is the vibration frequency and t is time. For simplicity, we consider the vibration real and so the equation (5.7) becomes:

$$v_z = V_{zR} \cos \omega t \quad (5.8)$$

This equation is not taking into account any source of noise or misalignment therefore it could not be representative of real LDV time signal data. We have already introduced the problem of misalignment which is seen by the transducer as a pseudo vibration and which forces the laser beam to travel along a very small path around the designed measurement position. The frequency at which the small path is travelled depends on the rotational speed of the structure and because of that the laser beam will be more sensitive to speckle noise. It is now important to introduce a mathematical model to simulate the speckle noise and which was used for all the tracking methods simulations [1]. That mathematical model is based on the fact that the laser beam travels sinusoidally always on the

same path, such as backward and forward along lines. Thus its motion is periodic with a frequency which is governed by the rotational speed of the testpiece. This means that the speckle changes are also periodic and their frequency content is concentrated at the fundamental motion frequency (the rotational speed) and its harmonics. The most influential parameter for the speckle noise is the scan speed and so the speckle model was built on the basis of this since, when varying the scan speed, the noise characteristic changes accordingly. The speckle model superimposed on the velocity response is:

$$Spk = A_{\text{SPECKLE at } \Omega_L} \left[\cos(2\pi\Omega_{LDV}t) + b \sum_{n=2}^{\text{n.of harm}} v(n) \cos(n2\pi\Omega_{LDV}t) \right] \quad (5.9)$$

$$A_{\text{SPECKLE at } \Omega_L} = 7.34e^{-5}\Omega_{LDV}^3 - 1.17e^{-3}\Omega_{LDV}^2 + 3.57e^{-2}\Omega_{LDV} + 1.11e^{-3} \quad (5.10)$$

Ω_{LDV} being the scan frequency of the measuring laser beam, $v(n)$ a normalised random variable which represents the amplitudes of the LDV spectrum at the harmonics of the scan frequency, n is an integer which it depends on the number of harmonics of the scan frequency that is decided to be included, $A_{\text{SPECKLE at } \Omega_{LDV}}$ is the amplitude of the speckle noise at the scan frequency and b , assumed to have the value of 0.28, is a parameter which links the noise level at the scan frequency with the noise level at its harmonics. On the actual velocity response model produced it is superimposed an additional source of uniform white noise which is to allow for the spurious sources of noise that can, generally, affect the measurement data. The speckle noise is present with or without misalignment since the LDV technology is sensitive to that and when the laser beam is forced to trace a path that issue could become not negligible at all. Using the equations expressed in paragraph 3.3.2 and equation (5.9) above superimposed on vibration expressed by equation (5.8), we can now perform simulations of LDV

output time history whenever a single point synchronous measurement is carried out. It is important to note that the parameters to be set up in equations of sections 3.3.2 are arbitrary because it is difficult, if not impossible, to measure the exact amount of misalignment of the laser head. Therefore, for the simulations, values are used which make the LDV time history closest to the real measured ones. Assuming that we have set up the excitation location and the response location as shown in **Figure 5.11**, we can perform a simulation of Point Tracking using the parameters reported in **Table 5.1**:

Excitation Frequency:		24 Hz
LDV sensitivity		25 (mm/s)/V
Frequency Span:		500 Hz
Number of speckle noise harmonics		500
Rotational speed		60 rev/min
Laser Head Misalignment	Rotation around X-axis(*)	0.1 Degree
	Rotation around Y-axis(*)	1 Degree
	X-Offset(*)	4 mm
	Y-Offset(*)	2 mm
Table 5.1 Parameter setup for the simulation (*) <i>arbitrary value</i>		

Thus, we obtain a path of the laser beam across the targeted location, as shown in **Figure 5.13**, and a simulated LDV output time history, as shown in **Figure 5.14** while **Figure 5.15** shows the frequency content of the simulated signal.

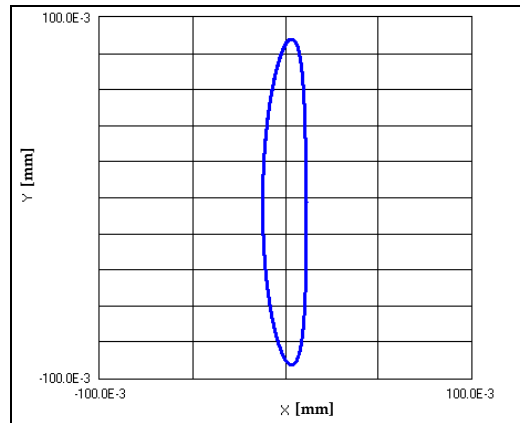


Figure 5.13 Path traced by the laser beam around the targeted location

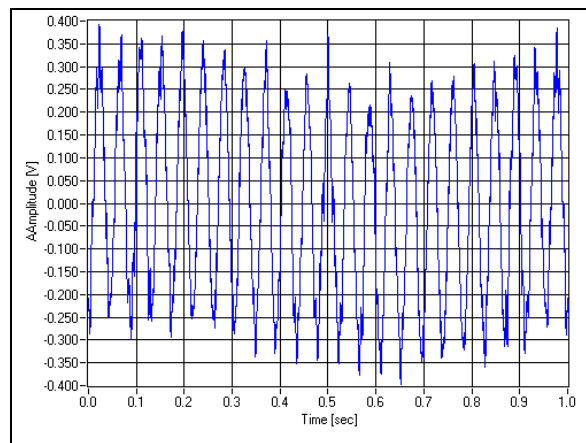


Figure 5.14 LDV output time signal of Point Tracking-simulation

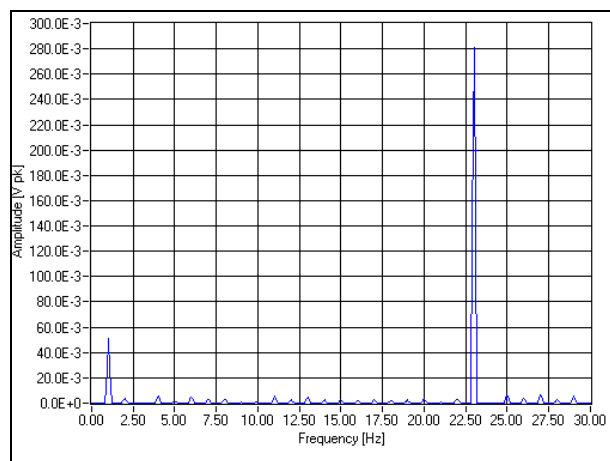


Figure 5.15 Frequency spectrum of LDV output time signal

When we perform a real test we find that our measurement prediction is close to the measured one but it cannot be an exact representation of the measured data.

Actually, looking **Figure 5.16**, the LDV output signal is distorted by the presence of the misalignment but it shows also a slight modulation. This is due to the unwanted excitation of other near by modes, as shown by red circles and square boxes in **Figure 5.17**. Even if the modes are lightly excited, they add a contribution to the time signal making it different from the simulated one.

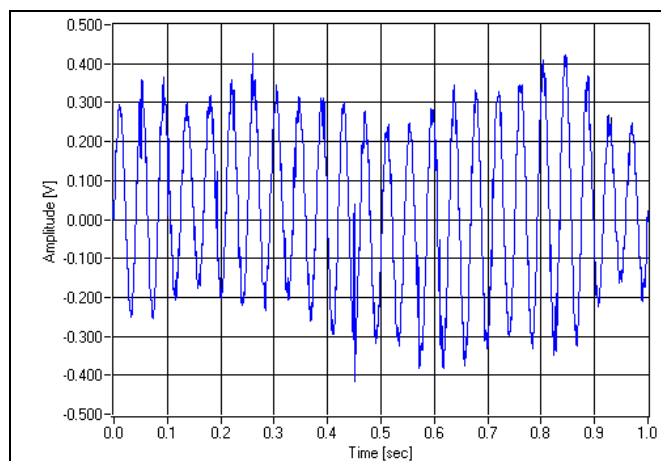


Figure 5.16 LDV output time signal of Point Tracking-measured

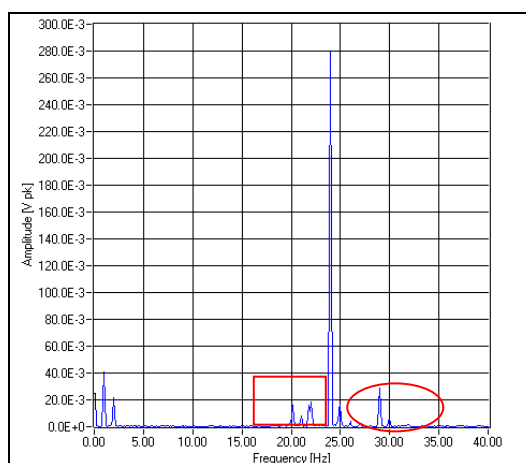


Figure 5.17 Frequency spectrum of the measured LDV output time signal

5.6 Line Tracking method VTS

We presented the X-Y mirrors waveforms to perform continuous straight-line synchronous measurement in the Chapter 3. Despite the complication of the

waveforms involved in practical tests, the laser beam being synchronous with rotating target sees that as stationary therefore that method can be readdressed to a mere line scan under stationary conditions and LDV output time signal is simulated accordingly. Clearly, also for this method, sources of misalignment add their contribution to distort slightly the designed straight line. However, the ability to simulate the LDV time history, and to add any kind of noise pollution, help us to predict the right parameters to scan the structure in order to avoid corruption of the LDV time signal because of noises and, consequentially, to fail data post processing. Finally, the aim is to help the user of this technique to perform measurement tests easily and more effectively.

5.6.1 Line Tracking-VTS, Polynomial curve fitting

The first task to accomplish, also for the Line Tracking VTS, is to calculate the ODS for which we wish to simulate the LDV output time signal. Using one point track simulator, the displacement of a selected point of the ODS was enough to reproduce the LDV time signal. Now, a straight line scan method is involved and to reconstruct the time signal we need to obtain the polynomial coefficients of the blade sector we wish to test. Once the ODS is calculated by inputting the desired excitation force, location and frequency parameters, the polynomial curve fitting can be performed by choosing both the blade and the number of polynomial coefficients for the curve fitting, as explained in section 5.4. **Figure 5.18** shows the Polynomial Fit front panel where on the right hand side is shown the projection of the blisk ODS with the chosen blade in colourful spectrum, the straight-line is in white colour. The calculated coefficients are then transferred to next panel section to be used in the LDV time signal simulator.

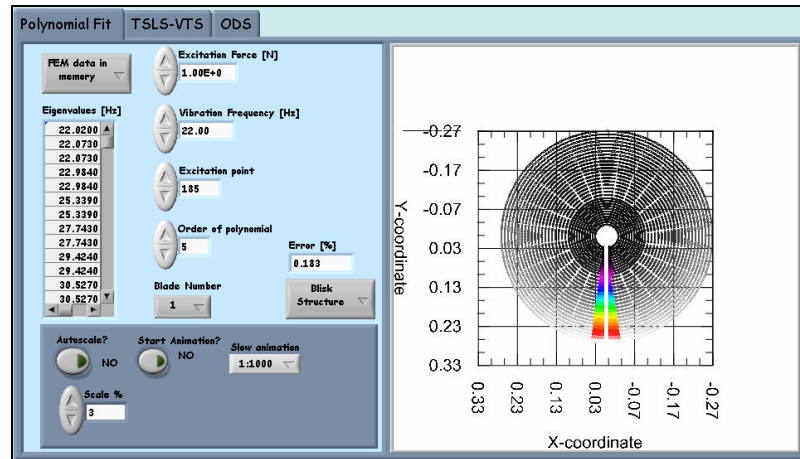


Figure 5.18 Polynomial curve fitting for Line Tracking VTS; straight-line in white

5.6.2 Line Tracking-VTS, LDV time history

The time signal simulator of the second section of the panel presents the same input parameters of the Point Tracking time signal simulator with an additional one corresponding to the X/Y-LDV mirror scan rate, meaning the frequency rate at which the laser beam travels the path length. **Figure 5.19** shows the tab where the simulated time signal is plotted in the time domain, on the left hand side, and its frequency content is plotted on the right hand side. An additional tab for this section is also provided to plot a possible line path when misalignment is included.

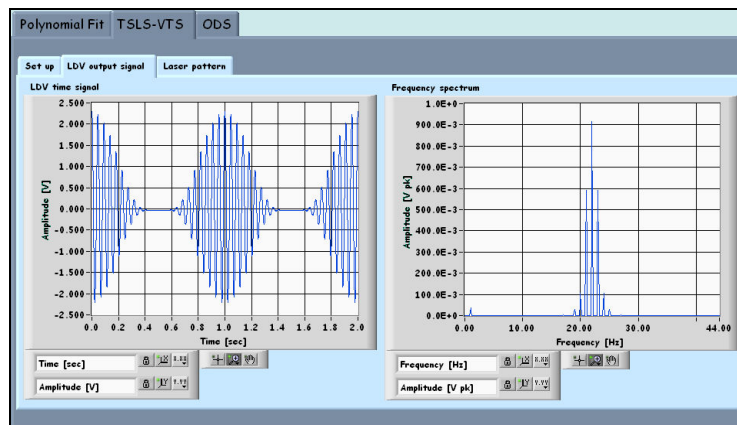


Figure 5.19 Front panel of Line Tracking VTS, time history simulator; graph plots tab

The Line Tracking-VTS simulator panel has two very important aims to achieve: (i) to be a training console for non experts in CLSDV method and (ii) to be a prediction software tool. Obviously, the second one could offer a valuable contribution for designing a measurement test procedure however the number of, known and unknown, variables involved in any vibration test under rotating conditions is, generally, too wide to be assessed and mathematically modelled therefore some disagreements between simulations and measurements data tests might be possible.

5.6.2.1 *Mathematical formulation*

The straight-line scan involves a one-dimensional scan along a line that can be swept by the laser moving with sinusoidal-varying velocity, and the scan is performed under stationary or rotating conditions, for which case a spiral scan is created whose circumferential frequency rate is synchronous with the rotational speed of the target. In the general case, a straight-line scan on a structure vibrating at frequency, ω , will give a modulated LDV output signal whose frequency spectrum contains a symmetrical set of sidebands spaced about the frequency scan rate, Ω_{LDV} . The Line Tracking simulator can also perform time signal simulations under stationary conditions by setting the rotational speed equal to zero. Whether the test is performed at the rest, or under rotation, the structure will see, in its frame of reference, a straight-line hence all the simulations, whether or not rotational speed is superimposed, are treated for simplicity as de-rotated. The straight-line scan is achieved by imposing, either to X-mirror or to Y-mirror, a waveform signal of zero amplitude expressed by equations:

$$\begin{aligned} x(t) &= 0 \\ y(t) &= \cos(2\pi\Omega_{LDV}t) \end{aligned} \tag{5.11}$$

where Ω_{LDV} is the scan rate frequency. Expressing the velocity in the z-direction as follow:

$$v_z(t) = V_{zR} \cos \omega t \quad (5.12)$$

where V_{zR} is the Real component of the vibration in z-direction, ω is the vibration frequency and t is time. Now, V_{zR} is function of the instantaneous position of the laser spot as expressed by equation:

$$V_{z,R}(x) = \sum_{n=0}^p V_{z,Rn} x^n \quad (5.13)$$

x being the normalized position vector representing all the points along the line. It goes from -1 to 1, considering the zero position as the centre of the line and normalizing at 2 its total length. $V_{z,Rn}$ is the n^{th} polynomial coefficient describing the velocity pattern along the line, which were calculated in the section of the panel where the ODS of the selected blade is curve fitted. The vibration response of the LDV beam directed to trace a straight-line scan on the test piece at frequency, Ω_{LDV} , will be:

$$v_z(t) = \sum_{n=0}^p V_{z,Rn} \cos^n(2\pi\Omega_{LDV}t) \cos(\omega t) \quad (5.14)$$

where ω is frequency vibration of the structure. Expanding out this expression trigonometrically, multiple terms arise at frequencies $(\omega \pm n\Omega_{LDV})$, referred to as 'upper and lower sidebands' which are symmetrical with respect to the central frequency, ω . Their values, in magnitude and phase, can be converted into polynomial coefficients, p , that later can be used to derive the Operating

Deflection Shape (ODS) of the scanned pattern. The LDV output signal simulated using the equation (5.14) is an ideal signal. Actually, it does not take in consideration the mirror phase lag which is always present because of the inertia of the mirrors, so that there is a time delay between the instant when the mirror signal driver is at zero and the instant when the laser spot is starting its scan on the surface. Thus equation (5.14) is modified by introducing a delay, δ , for the mirror and the mirror drive signal is given by a sinewave of equation:

$$x(t) = \cos(\Omega_{LDV}t + \delta)$$

Consequently, the vibration response as defined in equation (5.14) becomes:

$$v_z(t) = \sum_{n=0}^p V_{Rn} \cos^n(\Omega_{LDV}t + \delta) \cos(\omega t) \quad (5.15)$$

Now, a mathematical model of the speckle noise, expressed by equation (5.9), will be superimposed on the velocity response of the equation (5.15) to make the LDV signal similar to real experimentally measured data. That mathematical model is based on the fact that the laser beam travels sinusoidally always along the same path, such as backward and forward along a line, so that its motion is periodic with a frequency equal the scan rate. This means that the speckle changes are periodic as well, and their frequency content is concentrated at the fundamental scanning frequency (the scan frequency) and its harmonics. The most influential parameter of the speckle noise is the scan rate of the mirror and so the speckle model was built on the basis of this parameter since, when varying the scan rate, the noise occurrence changes consequently. The speckle model is then superimposed on the velocity response expressed by the equation (5.15). An additional source of noise, uniform white noise Φ_{wn} , is also

superimposed. This takes into consideration the spurious sources of noise that can, usually, affect the measured data. Having mathematical models for both LDV output signals, sources of noises and sources of misalignment, a simulation of LDV time history of a straight-line scan under rotating conditions can be performed and compared to a real measurement test data. Both simulation and measurement were performed at very low rotational speeds to be able to see the line path travelled, being the blisk slightly misaligned with the laser head. The simulation of the LDV time history was carried out by inputting the values listed in **Table 5.2**.

Excitation Frequency:		22 Hz
LDV sensitivity		25 (mm/s)/V
LDV scan radial scan rate		0.1 Hz
Frequency Span:		500 Hz
Number of speckle noise harmonics		500
Rotational speed		6 rev/min
Laser Head Misalignment	Rotation around X-axis(*)	1 Degree
	Rotation around Y-axis(*)	2 Degree
	X-Offset(*)	1 mm
	Y-Offset(*)	2 mm
Table 5.2 Parameter setup for the simulation (*) <i>arbitrary value</i>		

The misalignment parameters used to simulate a possible scan path have produced the laser locus shown in **Figure 5.20**. The decision to run the blisk at a very slow rotational speed, 6 rev/min, was necessary in order to visually inspect the laser path when it was set to travel along one edge of the blade, as this provided a fair reference for the comparison of the simulated and real laser scan paths. However, the path traced in **Figure 5.20** shows a very much exaggerated loop which is never experienced in real tests.

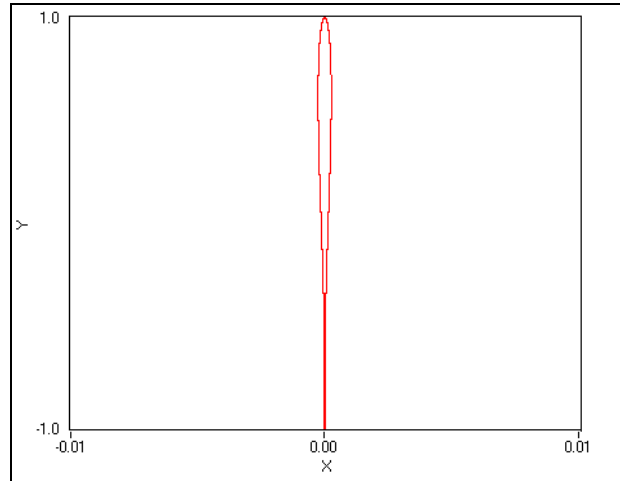


Figure 5.20 Possible scan path traced by laser beam due to misalignment

The simulated LDV output time signal is plotted on the left hand side of **Figure 5.21** and it reproduces very well the measured one plotted on the right hand side of **Figure 5.21**. **Figure 5.22** shows the frequency spectrum of both measured and simulated LDV time histories, left and right hand sides, respectively.

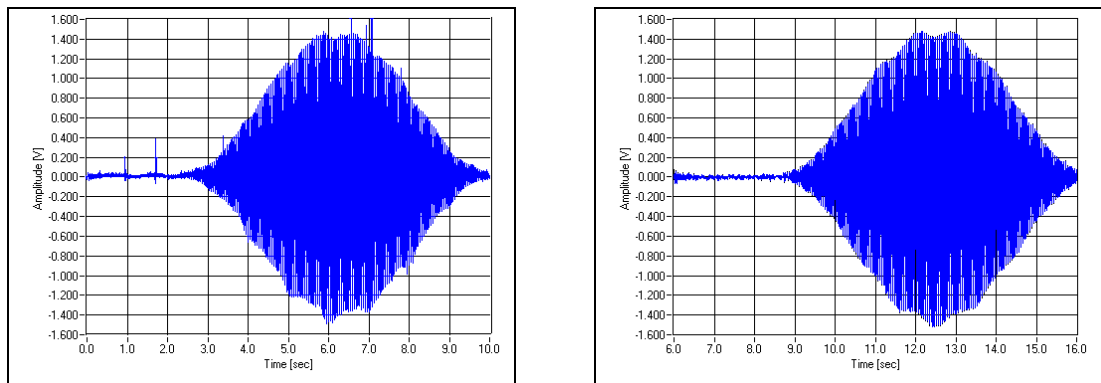


Figure 5.21 Measured and simulated LDV time data; left hand side and right hand side, respectively

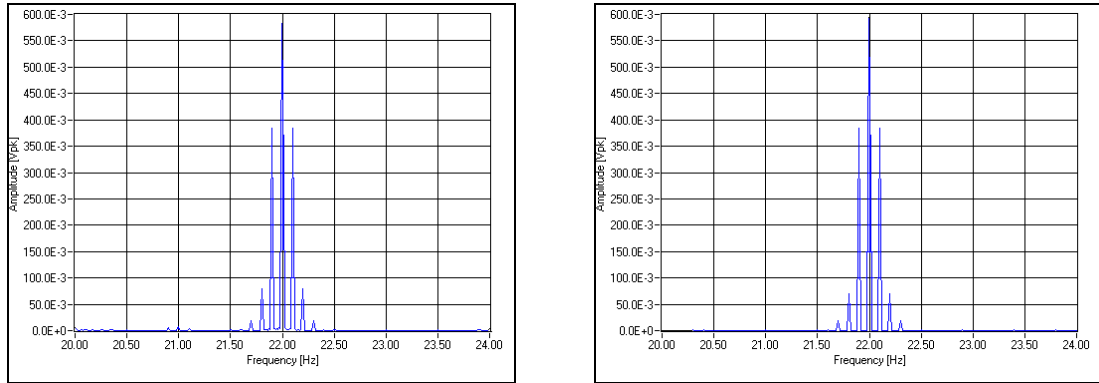


Figure 5.22 Frequency spectrum of measured and simulated LDV time data; left hand side and right hand side, respectively

5.6.3 ODS reconstruction

Once the LDV time history has been simulated, the data are exported to the last section of the Line Tracking panel for the reconstruction of the ODS. A series of options are offered here and one of those is the possibility to compare the ODS obtained from noisy simulated LDV time data with the original ODS simulated at the first section of the panel, the ODS Polynomial Fit. This feature is very useful to understand whether the LDV mirror scan rate chosen for the VTS was close to optimal, or not. In fact, two indicators such as Maximum Assurance Criterion (MAC) and Mean Square Error (MSE) are used to assess the quality of the reconstructed ODS with the simulated one, by inputting the eigenvectors of both ODSs into the formulas of the indicators. **Figure 5.23** shows a flow chart of how the software panel operates from the original ODS simulation of the FEM through to its reconstruction from the LDV time data corrupted by sources of noise. The reason for this type of procedure is due to the identification of the LDV scan rate at which the laser beam has to travel backward and forward along the structure. It was explained in the previous paragraph that the frequency content of the speckle noise is dependent on the frequency rate of the scanning and when harmonics of speckle noise overlap with the some of the sidebands,

then the reconstruction of the ODS fails because of corruption of the sideband magnitudes and phases. The possibility to select the LDV mirror scan rate independently from the excitation frequency gives an extra option for testing the structure and thus, the best parameter to set up during the measurements. All that can be carried out in laboratory, but these it is very time consuming. The Line Tracking panel might overcome that by allowing the user to simulate thousands of possible LDV output time signals using different LDV mirror scan rate values and to assess them immediately by comparisons of the ODSs.

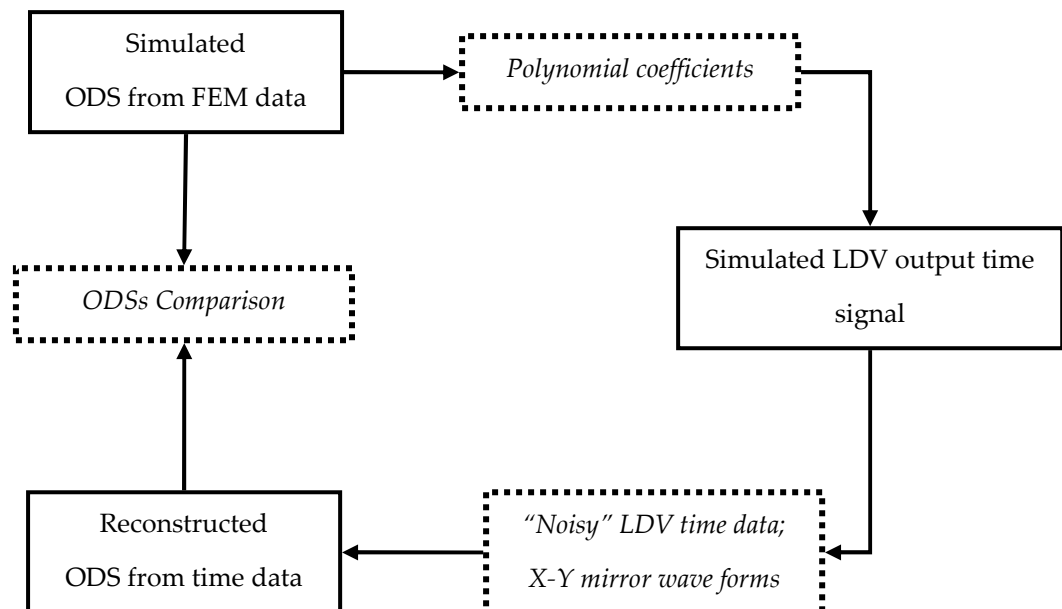


Figure 5.23 Flowchart of ODSs comparison

Another important feature offered by this section panel is the possibility to import time data actually measured during a test procedure and to reconstruct the ODS. The real measured ODS can be stored and used later for comparison with ones obtained from simulated time data: both ODS amplitudes can also be normalized whether or not the level of simulated excitation can be compared with the actual level. This additional comparison provides an “extra touch” to

the software because it can directly link experimental and analytical measurement test approaches and, ultimately, the mechanical design approach. **Figure 5.24** shows two tabs of the Line Tracking-ODS section. The top picture shows the tab where all parameter settings can be input, either by importing actual measured time data or by using simulated ones. Some parameters, such as excitation frequency and LDV mirror scan rate, are transferred from previous sections. The bottom pictures shows the ODS plot itself.

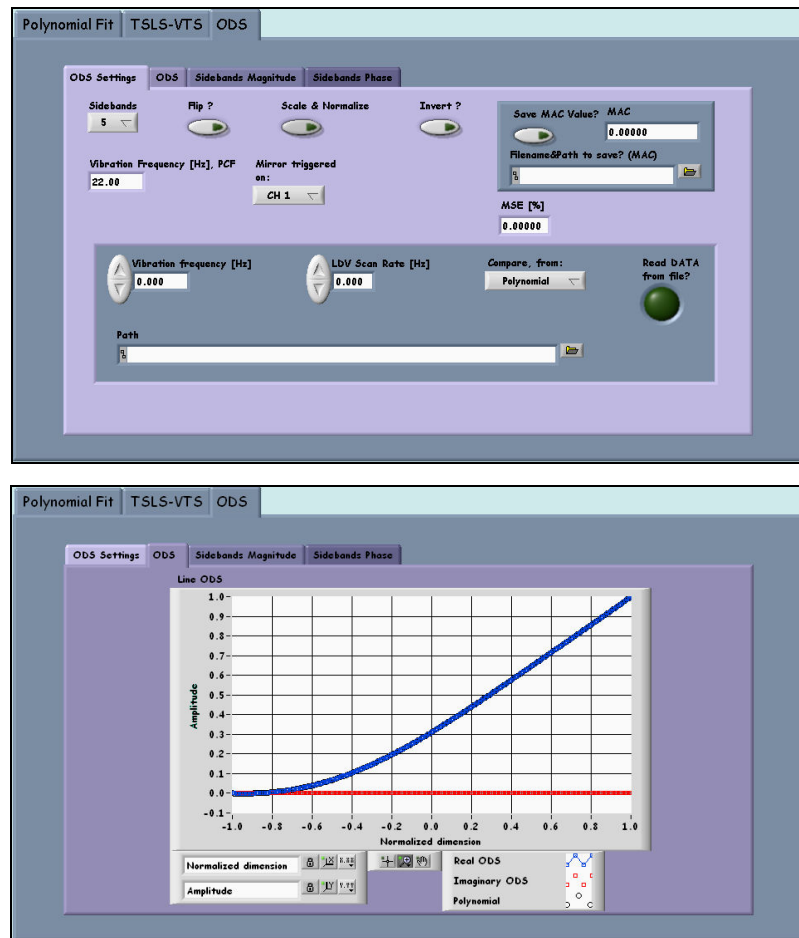


Figure 5.24 Line Tracking-ODS section. Parameters settings, top. ODS plots, bottom.

5.6.3.1 Mathematical description

We, now, provide a brief mathematical explanation for the reconstruction of the ODS from an LDV output time signal, this having already been fully explained [1]. The simulated LDV output signal can be expressed by the equation:

$$v_z(t) = \sum_{n=0}^p A_{R(\pm n)} \cos[(\omega \pm n\Omega_{LDV})t] \quad (5.16)$$

where A_{R0} is the amplitude of the spectrum component at the excitation frequency, ω and $A_{R\pm 1}$ are the spectrum sidebands amplitude at $(\omega \pm \Omega_{LDV})$, and so on up to $n = p$. However, it can be demonstrated that $A_{R,-1} = A_{R+1}$ and the equation (5.16) becomes:

$$v_z(t) = \sum_{n=0}^p A_{R(n)} \cos[(\omega \pm n\Omega_{LDV})t] \quad (5.17)$$

After some manipulations the sideband coefficients, A_R , can be seen to be related to the corresponding polynomial coefficients, V_R , by a simple matrix transform [T]:

$$\{V_R\} = [T]\{A_R\}[T]^T \quad (5.18)$$

where the matrix [T] is defined as:

$$[T] = \begin{bmatrix} 1 & 0 & -2 & 0 & 2 & 0 & -2 & 0 & 2 & 0 & -2 & 0 & 2 & 0 & -2 & 0 \\ 0 & 2 & 0 & -6 & 0 & 10 & 0 & -14 & 0 & 18 & 0 & -22 & 0 & 26 & 0 & -30 \\ 0 & 0 & 4 & 0 & -16 & 0 & 36 & 0 & -64 & 0 & 100 & 0 & -144 & 0 & 196 & 0 \\ 0 & 0 & 0 & 8 & 0 & -40 & 0 & 112 & 0 & -240 & 0 & 440 & 0 & -728 & 0 & 1120 \\ 0 & 0 & 0 & 0 & 16 & 0 & -96 & 0 & 320 & 0 & -800 & 0 & 1680 & 0 & -3136 & 0 \\ 0 & 0 & 0 & 0 & 0 & 32 & 0 & -224 & 0 & 864 & 0 & -2464 & 0 & 5824 & 0 & -12096 \\ 0 & 0 & 0 & 0 & 0 & 0 & 64 & 0 & -512 & 0 & 2240 & 0 & -7168 & 0 & 18816 & 0 \\ 0 & 0 & 0 & 0 & 0 & 0 & 0 & 128 & 0 & -1152 & 0 & 5632 & 0 & -19968 & 0 & 57600 \\ 0 & 0 & 0 & 0 & 0 & 0 & 0 & 0 & 256 & 0 & -2560 & 0 & 13824 & 0 & -53760 & 0 \\ 0 & 0 & 0 & 0 & 0 & 0 & 0 & 0 & 0 & 512 & 0 & -5632 & 0 & 33280 & 0 & -140800 \\ 0 & 0 & 0 & 0 & 0 & 0 & 0 & 0 & 0 & 0 & 1024 & 0 & -12288 & 0 & 78848 & 0 \\ 0 & 0 & 0 & 0 & 0 & 0 & 0 & 0 & 0 & 0 & 0 & 2048 & 0 & -26624 & 0 & 184320 \\ 0 & 0 & 0 & 0 & 0 & 0 & 0 & 0 & 0 & 0 & 0 & 0 & 4096 & 0 & -57344 & 0 \\ 0 & 0 & 0 & 0 & 0 & 0 & 0 & 0 & 0 & 0 & 0 & 0 & 0 & 8192 & 0 & -122880 \\ 0 & 0 & 0 & 0 & 0 & 0 & 0 & 0 & 0 & 0 & 0 & 0 & 0 & 0 & 16384 & 0 \\ 0 & 0 & 0 & 0 & 0 & 0 & 0 & 0 & 0 & 0 & 0 & 0 & 0 & 0 & 0 & 32768 \end{bmatrix} \quad (5.19)$$

The ODS of the scanned pattern can be derived from the simulated velocity response. In fact, the sideband coefficients can, now, be recovered from the LDV simulated output by multiplying the time signal by sine and cosine at $(\omega \pm n\Omega_{LDV})$.

5.6.4 VTS simulations and real measurement test results

The last part of the Line Tracking VTS procedure reports the results for the ODSs obtained from simulations of LDV output signals where the only parameter changed was the LDV mirror scan rate, as shown in **Table 5.3**.

LDV scan rate [Hz]	0.1	0.2	0.3	0.4	0.5	0.6	0.7	0.8	0.9	1	2	3	4	5
--------------------	-----	-----	-----	-----	-----	-----	-----	-----	-----	---	---	---	---	---

Table 5.3 LDV mirror scan rate used both for the simulations and measurements

The LDV time data, both simulated and measured, were obtained under rotating conditions and all parameters used for simulation and acquisitions are reported in **Table 5.4**.

	Simulation	Measurement
N. of LDV scan cycles	10	10
Sampling rate [Sample/sec]	1000	1000
Excitation frequency [Hz]	22	22
Number of speckle harmonics	500	---
White noise [V]	0.01	---
LDV sensitivity [mm/s/V]	25	25
ODS sidebands	6	6
Rotational speed [rev/min]	60	60

Table 5.4 Measurement tests parameters settings

Figure 5.21, in section 0, shows an example of measured and simulated LDV output time signals and we also noted that the laser beam does not trace a straight-line but something closer to a small loop because of the misalignment. We also noted that because of the slow rotational speed of the target, the path has been verified visually under running conditions. One obvious question can be raised because of that odd line shape whether the time data post-processing can be affected by that. To clarify this issue, one straight-line scan and one very small loop line scan were performed under non-rotating conditions for the same 2 ND mode resonance inspected under rotating conditions. The results of both scan type are shown in **Figure 5.25** where the ODSs are plotted together and they can be seen to overlap perfectly.

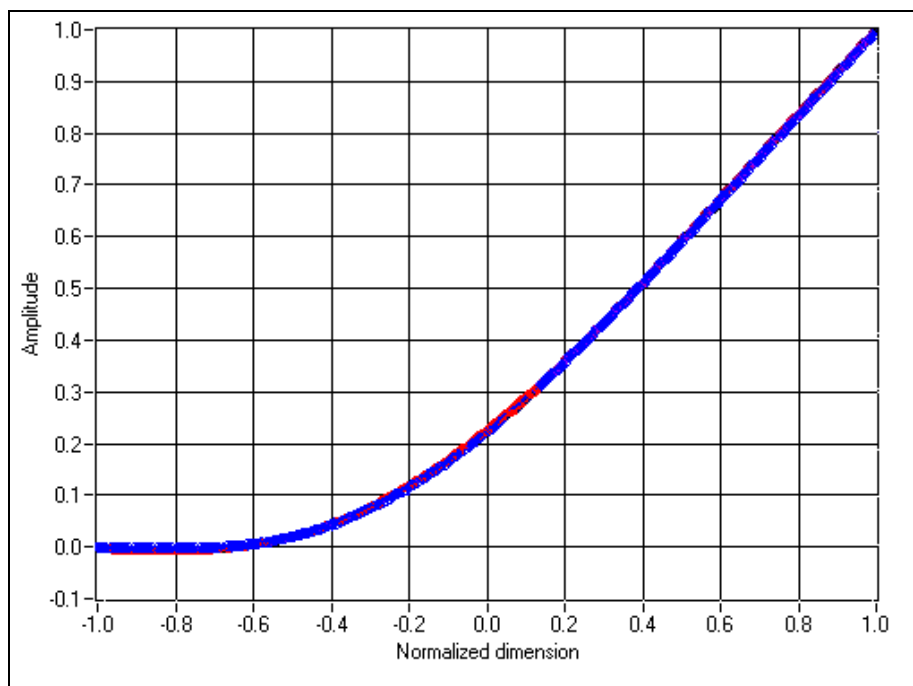


Figure 5.25 ODSs reconstructed from straight-line and small line loop scan

A series of LDV time data simulations were performed and afterward post processed to obtain ODSs, using the LDV mirror scan rate shown in **Table 5.3** and parameters shown in **Table 5.4**. All simulated and post-processed LDV time

signals yielded a good agreement with the reference simulated ODS from the first section of the Line Tracking panel. Therefore, the LDV mirror scan rate used was proved to be suitable for use in actual tests. **Figure 5.26** shows all the reconstructed ODSs from the LDV time data simulations and all of them overlap very well, being no differences of using a specific LDV mirrors scan rate. If the results of all simulations were correct, then all the LDV time data acquired according to **Table 5.4** should return a good ODS reconstruction. All ODSs obtained from the actual measurements returned good results. In fact, in this case also all of them overlap perfectly, as shown in **Figure 5.27**.

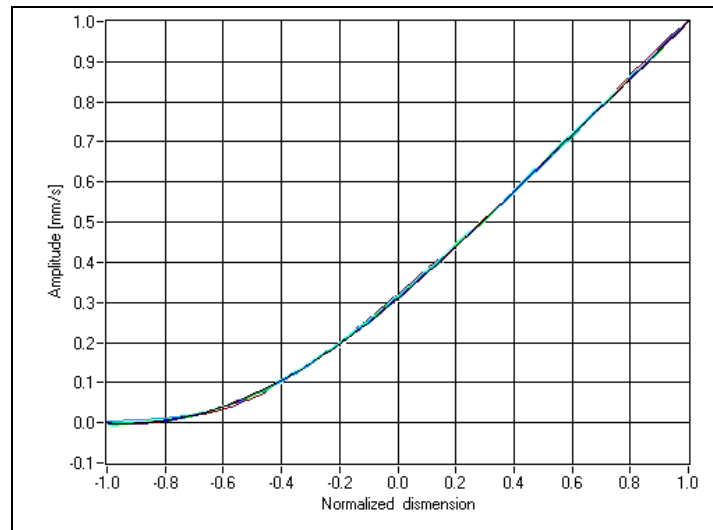


Figure 5.26 ODSs obtained from simulated LDV time data

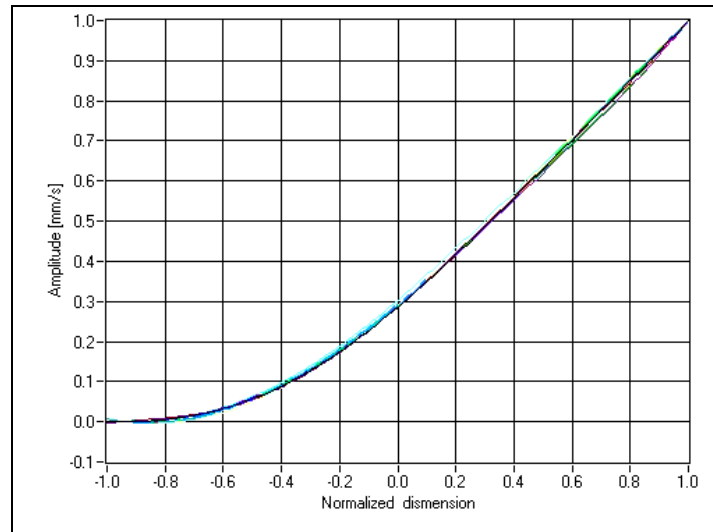


Figure 5.27 ODSs obtained from measured LDV time data

5.7 Area Tracking method VTS

The same comments can be repeated for Area Tracking-VTS, in spite of the very complicated X-Y mirror waveforms required to drive the scanning device. The virtual test simulation can be treated as if under stationary conditions, taking into account any possible sources of misalignment which could distort the prescribed laser path. However, having now the laser spot travelling across the whole area, the chance of encountering difficulties because of the speckle noise, or other general sources of noise, might be higher than might happen scanning along a line. Therefore, the Area Tracking-VTS plays a crucial role in the identification of the best X-Y LDV mirrors scan rates to perform any measurement test, either under stationary or rotating conditions, without incurring polluted LDV time data or the possibly of an incorrect ODS reconstruction. This software panel can also be used for both non-rotating and rotating conditions simply by inserting the appropriate rotational speed value. The Area Tracking-VTS panel has, like the previous ones, the ODS Polynomial Fit method to obtain the polynomial coefficients. It will not be described again in this last part of the chapter, having already been explained in detail previously.

5.7.1 Area Tracking-VTS, LDV time history

The Area Tracking-VTS panel has an LDV time signal simulator section which is very similar to the Line Tracking-VTS panel but, for the earlier case, the laser beam had to be both synchronous with the rotating target and travelling radially across the blade. Now, the laser beam must also sweep circumferentially across the blade as well as radially and an additional parameter which called “span frequency” rate is required to perform any Area-Tracking LDV time data simulation. This panel can work both for stationary and rotating conditions by inputting the relevant rotational speed of the bladed blisk. However, blade shapes can be different and so the panel can be set up to virtually perform a square/rectangular shape and triangular scanning pattern. In fact, there is a dedicated tab to allow the user define that. It is appropriate again to stress how the simulator panels were designed to minimize the gap between practical and theoretical vibration measurement procedures in order to provide a basic and efficient training for anyone not already expert. **Figure 5.28** shows the tab where laser patterns are plotted. Despite that we have to use radial and circumferential LDV scan rates, all are expressed in the Cartesian coordinate system so as to avoid any confusion whether, a square/rectangular plate or bladed blisk ODSs are used for the LDV time signal simulations.

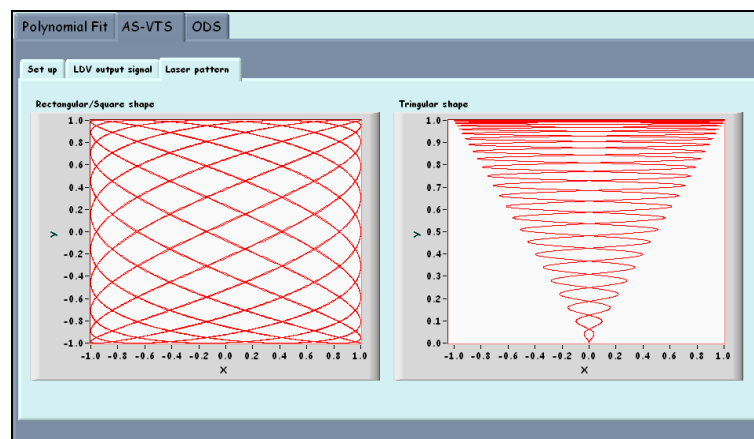


Figure 5.28 Front panel of Area Tracking-VTS, time history simulator; Laser patterns

5.7.1.1 Mathematical description

Also for the 2D scanning pattern, the mathematical description is performed using the reference system of the structure, and so the laser beam is either a square/rectangular or triangular shape. In order to perform an area scan of a square/rectangular shape, as shown on the left hand side of Figure 5.28, the laser beam of the LDV must scan at frequency of Ω_x in the x-direction and a frequency of Ω_y in the y-direction and those two frequencies must not be fractionally related to each other in order to describe a non-closed Lissajou pattern on the scanned surface. Taking into account the delays occurring on X-mirror, δ_x , and Y-mirror, δ_y , the sinusoidal signals feeding the scanning mirrors are:

$$\begin{aligned} x(t) &= \cos(\Omega_{x-LDV}t + \delta_x) \\ y(t) &= \cos(\Omega_{y-LDV}t + \delta_y) \end{aligned} \tag{5.20}$$

When a triangular shape is performed, as shown in the right hand side of Figure 5.28, the waveform equations to feed in the scanning mirrors are slightly more complicated and are expressed as follow:

$$\begin{aligned} x(t) &= \cos(\Omega_{y-LDV}t + \frac{\pi}{2}) * \cos(\Omega_{x-LDV}t + \delta_x + \frac{\pi}{2}) \\ y(t) &= \cos(\Omega_{y-LDV}t + \delta_y + \frac{\pi}{2}) \end{aligned} \tag{5.21}$$

The velocity in the z-direction is expressed by equation (5.12) where V_{zR} is expressed as follow:

$$V_R(x, y) = \sum_{n,m=0}^{p,q} V_{Rn,m} x^n y^m \quad (5.22)$$

x and y being the normalized position vectors representing all the points on the surface. As already stated for the straight-line scan, in the section 5.5.2.1, $V_{z,Rn}$ is the n^{th} polynomial coefficient describing the velocity pattern of the scanned line. Now, $V_{z,Rn,m}$ is the $(n^{\text{th}} \times m^{\text{th}})$ polynomial coefficients describing the velocity pattern of the scanned area. These coefficients are recovered, as explained for the straight-line scan, by surface curve-fitting the calculated ODS of either one blade sector of the bladed blisk or of the plate. The velocity response, when a square/rectangular shape laser pattern is performed, will be:

$$v_z(t) = \sum_{n,m=0}^{p,q} V_{Rn,m} \cos^n(\Omega_{x-LDV}t + \delta_x) \cos^m(\Omega_{y-LDV}t + \delta_y) \cos(\omega t) \quad (5.23)$$

otherwise, when a triangular pattern is performed, it will be:

$$v_z(t) = \sum_{n,m=0}^{p,q} V_{Rn,m} \cos^n(\Omega_{y-LDV}t + \frac{\pi}{2}) * \cos^n(\Omega_{x-LDV}t + \delta_x + \frac{\pi}{2}) \cos^m(\Omega_{y-LDV}t + \delta_y + \frac{\pi}{2}) \cos(\omega t) \quad (5.24)$$

According to equations (5.23) or (5.25), we are now able to simulate the LDV output signal on which sources of noise and misalignment can be superimposed. An example of an LDV time history, both measured and simulated, obtained from an X-Y area scan on a square plate under stationary conditions, is provided in **Figure 5.29** to show the good agreement of both time data. **Table 5.5** lists the parameters used to run both measurement and simulation of the continuous area scan. **Figure 5.29** shows just a small portion of the LDV output time signal, simulated on the left hand side and measured on the right hand side,

respectively. Both LDV time histories look very similar thus confirming the quality of the time data-simulator. **Figure 5.30** shows the frequency spectra of the LDV time histories, and the sidebands are clearly visible.

	Simulation	Measurement
X-LDV mirror scan rate [Hz]	20	20
Y-LDV mirror scan rate [Hz]	1.1	1.1
N. of X-LDV mirror scan cycles	100	100
Excitation Frequency [Hz]	127	127
Sampling rate [Sample/sec]	10000	10000
N. of speckle harmonics	1000	---
White noise [V]	0.1	---

Table 5.5 Parameter setup for the simulation and measurement of Area scan

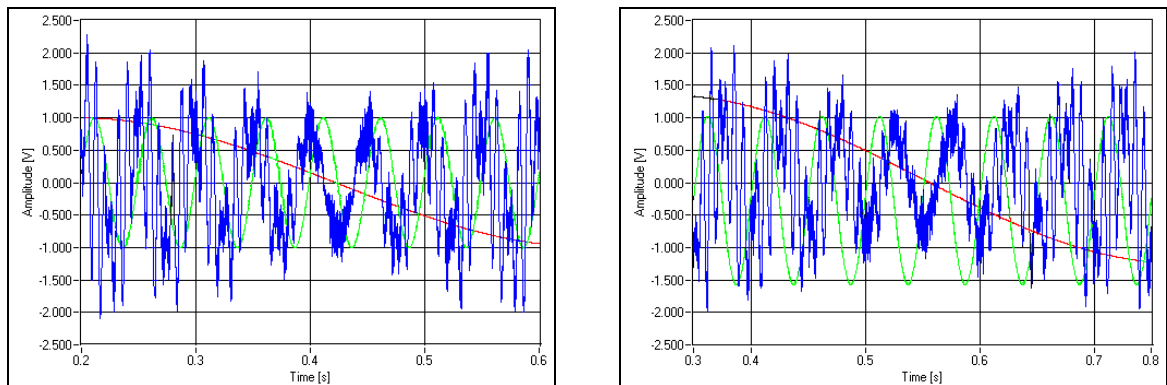


Figure 5.29 Simulated (left) and measured(right) of LDV time history; X-Y area scan

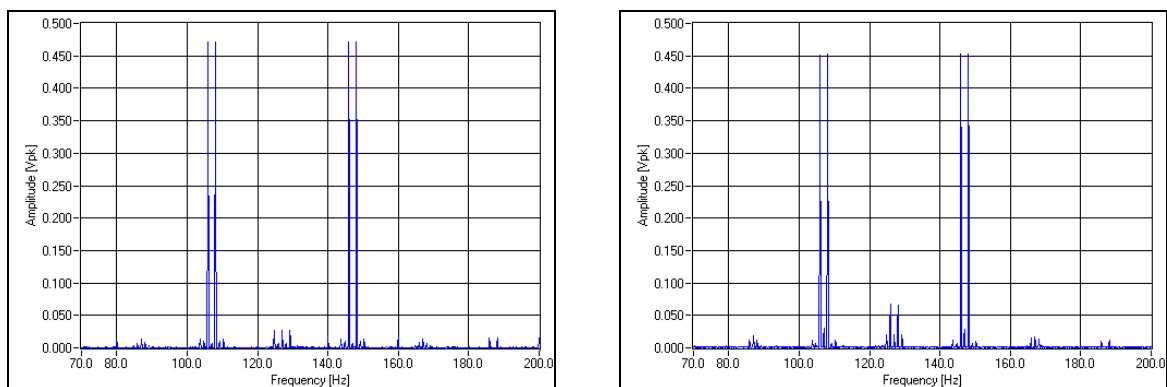


Figure 5.30 Frequency spectrum of simulated (left) and measured(right)time history

5.7.2 Area Tracking-VTS, ODS

The Area Tracking panel has one last section where the LDV output time signal, together with the X-Y LDV mirror signal, is transferred for post-processing. Conceptually, this panel works like the equivalent one on the Line Tracking panel and the flow chart shown earlier in **Figure 5.23** is still valid for 2D scanning method applied here. Accordingly, this last section is used to assess whether the measurement parameters used virtually for the time data simulation can produce a good reconstruction of the ODS which is always compared with the simulated one in the first section ODS Polynomial Fit. This panel provides the possibility of animating the reconstructed ODS to give a better visualization and comprehension of the vibration characteristic. Also, this section offers the feature of importing real measurement data. **Figure 5.31** shows the front panel of Area Tracking-ODS section.

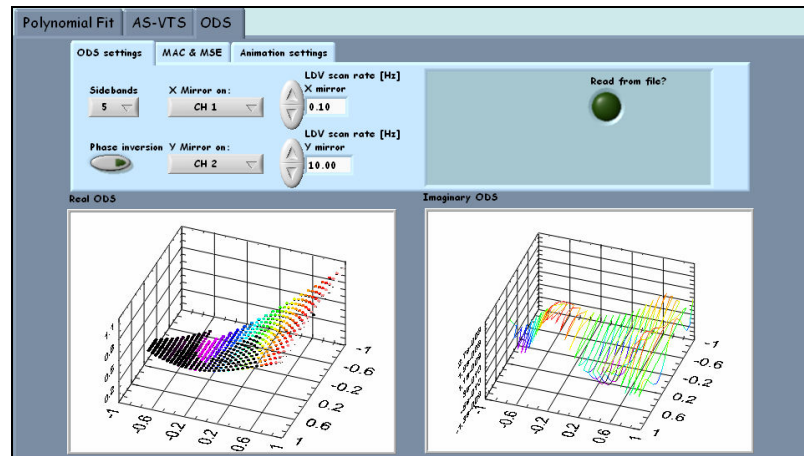


Figure 5.31 Area Tracking-ODS section, ODS settings and plots

5.7.3 VTS simulations and real measurement test results

This last paragraph reports simulations and actual measurements of continuous area scanning performed under stationary conditions on a square plate. The main reason for these series of simulations at rest, rather than under rotation, is to show effectively that the LDV time data simulator can easily predict the worst X-Y LDV mirrors scan rate without any the additional time signal pollutions due to the rotation. It was already noted that the speckle noise level depends by the LDV frequency scan rate at which the laser beam moves, and thus the higher the beam scans the area higher the level of noise will be. Obviously, the resolution of the ODS deflection depends on the number of polynomial coefficients we can use, and so on the number of sidebands we can use. If the background noise level is too high, the furthest sidebands will disappear into the noise level and possibly their use will produce a poor ODS quality. Under these conditions, it was decided to run the simulations as well as the tests at high LDV frequency scan rate as reported, in **Table 5.6**. Both simulation and measurement set up parameters used were already reported in **Table 5.5**.

X-LDV scan rate [Hz]	10	11	12	13	14	15	16	17	18	19	20	21	22	23	24
Y-LDV scan rate [Hz]	1.1	1.1	1.1	1.1	1.1	1.1	1.1	1.1	1.1	1.1	1.1	1.1	1.1	1.1	1.1

Table 5.6 LDV mirror scan rate used both for the simulations and measurements

All simulated LDV time histories were then post-processed to reconstruct the ODSs and these compared with the reference, ODS_{REF} plate obtained originally in the first section of the panel. Maximum Assurance Criterion (MAC) and Mean Square Error (MSE) were used to check the quality of the ODSs and **Figure 5.32** and **Figure 5.33** show the results, indicating which LDV frequency rates should

be avoided so as not to fail the measurement process in laboratory. Using the indications provided by the simulator, the same measurements were performed, using exactly the same parameters, on a real square plate under 'free-free' conditions as had been assumed for all simulations. The number of sidebands used to reconstruct the ODSs from measured time data and simulated time data was set to 5.

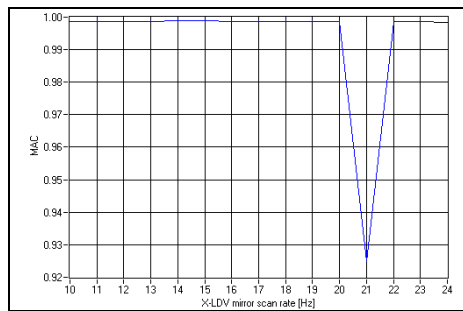


Figure 5.32 MAC, ODSs/ODS_{REF}

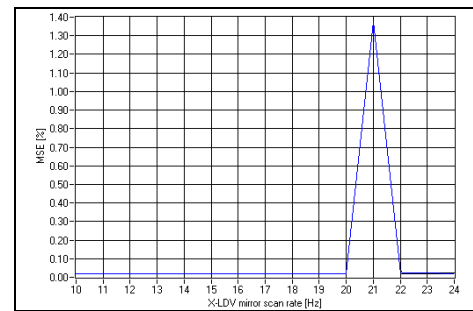


Figure 5.33 MSE, ODSs/ODS_{REF}

The VTS indications of the worst LDV mirror frequency rates to be avoided proved absolutely right and, in fact, the area scan measurement performed using 21 Hz and 1.1 Hz for X-Y LDV frequency rates, respectively, produced a poor quality ODS result. To outline the difference of using one LDV frequency rate rather than another is shown in **Figure 5.34** and **Figure 5.35** where the X-Y LDV scan rate used were [20,1.1] Hz and [21, 1.1] Hz, respectively. It is clear that the ODS in **Figure 5.35** shows poorer quality than the one in **Figure 5.34**. This is also confirmed by inspecting the ODSs reconstructed from measured time data as shown in **Figure 5.36** and **Figure 5.37**, respectively.

From simulated LDV output time signal

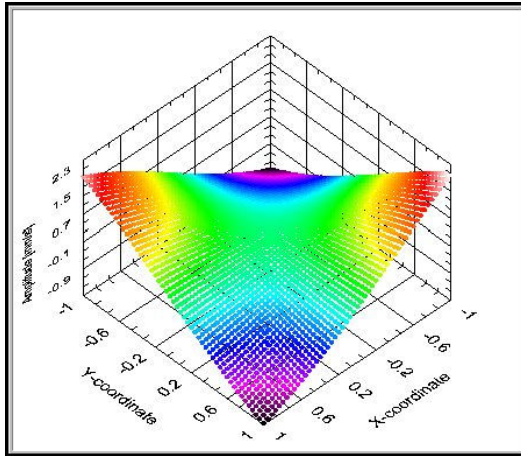


Figure 5.34 ODS at 127Hz; X=20, Y=1.1

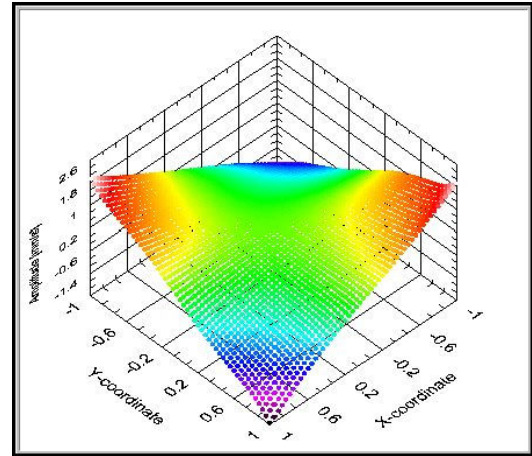


Figure 5.35 ODS at 127 Hz; X=21, Y=1.1

From measured LDV output time signal

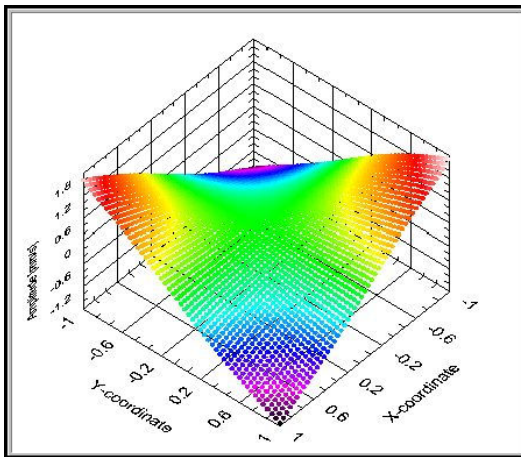


Figure 5.36 ODS at 127Hz; X=20, Y=1.1

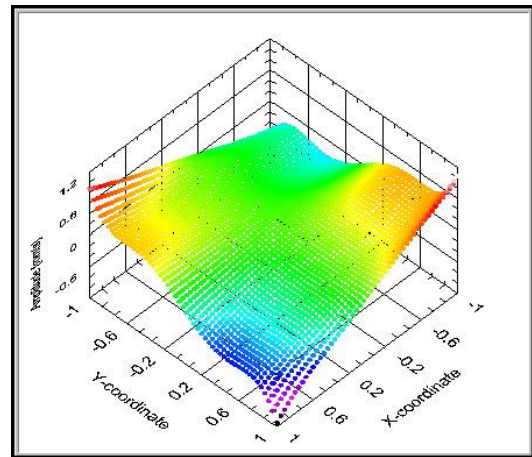


Figure 5.37 ODS at 127 Hz; X=21, Y=1.1

5.8 Conclusions

We have presented in this chapter some of the simulator panels featuring the CAISER MYMESIS software platform. We have provided detailed explanations of the Virtual Test Simulation (VTS) as powerful mathematical approach to represent vibration measurement tests, introducing the double role of: (i) teaching continuous tracking scanning methodologies, and (ii) helping to identify the best measurement parameters. The entire philosophy is focused on

the reconstruction of ODSs from simulated LDV output time signals and the choice of optimum measurement parameters. Inevitably, ODS theory had to be explained, being the starting point of LDV time history simulation, and the next connection to the modal solutions calculated during the design FE modelling phase. The ODS is a consequence of the transformation of measured sidebands magnitudes into polynomial coefficients; therefore, any calculated ODS needed to be polynomial curve fitted to obtain coefficients. Any sources of errors deriving from that curve fitting process may affect the simulation of LDV time data. Using some example of 1D and 2D ODSs, it was demonstrated that poor coefficients may affect the LDV output time signal simulation by generating pseudo vibrations when they do not really exist. The Chapter concludes with the presentation of the Point Tracking, Line Tracking and Area Tracking VTS panels. All are explained in detail and results of simulations and measurements are provided to confirm the effectiveness of the simulator panels in helping the user to identify right measurement parameters.

6 Tracking-CSLDV measurement methods: applications

6.1 Overview

This chapter presents all three types of tracking CSLDV measurement method used for validation of vibration predictions. The logical path of the chapter reflects the degree of complexity involved in performing synchronous measurements, so it starts with the simplest one, the Point Tracking method and concludes with the most complex one, the Area Tracking method. The software platform, CAISER MYMESIS, designed to control all measurement methods is presented (and the acronym of the software is explained in detail). The Point Tracking technique, combined with the use of a rotating exciter, was employed in two different studies for FRF measurements. Examples of the Line Tracking technique are presented in spite of the fact that there were no specific studies requiring the use of such a method. The two-dimensional scan, Area Tracking technique, was successfully used to measure the ODSs of rotating blades and thus to simplify modal identification in the veering region of two close families of modes. Examples of blade ODSs are provided for a maximum rotational speed of 2400 rev/min and, for the first time, the measurement of an ODS of a whole bladed disc is presented and compared with a simulated one.

6.2 CAISER MYMESIS software platform

CAISER MYMESIS is the synthesis of all Continuous Scanning LDV procedures developed in this work, some presented in Chapter 3 and also in Chapter 5. Why such a name for a software? Basically, it is an acronym from Continuous scAnning laSEr DoppleR vibroMetry thechnologY for MachinEry and Structural dynamIcs meaSurement. Obviously, the spellings of CAISER as well as MYMESIS are not correct, but it is perhaps interesting to give an explanation of the two words. The word CAISER, standing for Kaiser in German and Csar in Slavic, comes from the Latin name of Gaius Iulius Caesar, Roman emperor. This name would be awarded to every Roman emperor, and it became a signal of great power and authority far beyond the bounds of the Roman Empire. The word MYMESIS correctly spelled as '*mimesis*' is a Greek word and in its simplest contest means imitation or representation. However, both Plato and Aristotle use it to refer to the representation of nature. Thus, we could say that CAISER MYMESIS could indicate IMPERIAL SIMULATION.

CAISER MYMESIS is a software platform which can handle a series of tasks. Most of those are CSLDV measurement methods but also traditional measurement techniques can be performed. The software structure has been designed to guide the user along a logical path of performing measurements which can be summarized as follows:

1. Selection of measurement parameters using the Virtual Test Simulation (VTS) method, some of which are presented in Chapter 5.
2. Use of those parameters to set up the CSLDV panel, as shown in Chapter 3, to perform the vibration test.
3. Possibility to perform Step-SLDV measurement method when CSLDV methods are not required.

Hence, CAISER MYMESYS front panel shows a series of options which can be loaded dynamically, as required. **Figure 6.1** shows the front panel of the software where menus to run VTS simulators are shown on the left hand side, the centre of the panel shows the menus which call the CSLDV panels to perform tests under either stationary or rotating conditions and on the right hand side there are menus to call the panel used to perform the traditional Step-SDLV method, or other utilities, such as calling ICATS software or PSV Polyec software.

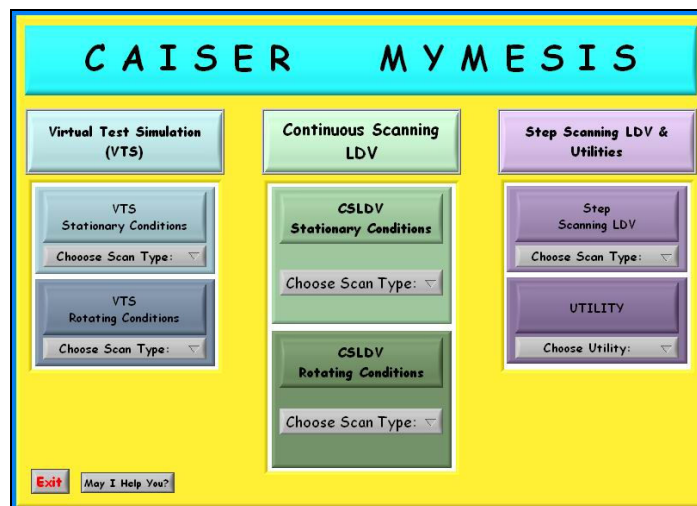


Figure 6.1 CAISER MYMESYS front panel

The design of the CAISER MYMESYS front panel, as well as all the individual CSLDV front panels, was made to be as simple as possible so as to avoid any difficulties during its use, while giving a degree of freedom to the user when needed.

The next sections will provide a series of examples of the use of the Point Tracking, Line Tracking and Area Tracking techniques, respectively. The Point Tracking technique was employed for two specific research studies: (i) the effect of the Coriolis forces acting on rotating bladed disc and (ii) a study of the bladed

disk dynamics in the veering region between two modes families by using measurements of FRFs under rotating condition. The Line Tracking did not have a specific target study, such as validation of predictions, during the research study as it was superseded by the more general Area Tracking method. However, some measurements were performed on a bladed disk to show the advantage of using such a technique when the blades width is narrow. The Area Tracking was actually used for blade vibration measurements under rotating conditions. The two-dimensional plot of the ODS obtained by that method provided helpful measurement tool to resolve complicated modal identification problems as they could occur for two families of modes at the veering region.

6.3 Point Tracking method: applications

The first practical use of the Point Tracking software panel was for the measurement of the frequency split of blisk modes due to the effect of the Coriolis force under rotating conditions. The excitation of backward and forward travelling waves of a rotating bladed disc could be achieved by using an AC magnet, as explained mathematically in Chapter 4. Hence, the validation of theoretical predictions could be obtained by a combination of those two methods. The same approach was also used for the measurements of FRFs at speed in the frequency range of the 2nd flap-wise and 1st torsional families of modes. In order to be able to measure FRFs at speed, both response and excitation must be in the same frame of reference, and this required adaptation of the original test rig.

6.3.1 Experimental validation of the effect of Coriolis force on the dynamics of bladed disk

For the first time, an experimental validation of the effect of Coriolis forces on the dynamics of a bladed disk was carried out. The test piece employed for the

tests was an existing 24-bladed disk which was slightly modified to incorporate a prominent radial flexibility to enforce the action of Coriolis force. The FE model of the modified bladed disk exhibited a phenomenon of natural frequency splits for all nodal diameter (ND) modes. This section will focus on the experimental validation of that phenomenon, however a short background to the effect is provided.

6.3.1.1 Background

In rotor dynamics analysis, mode shapes associated with 0 and 1 nodal diameters are considered important because these modes are the only ones which can interact with the motion of the shaft carrying the bladed disc. In fact, bladed discs with 0 nodal diameter are characterized by a resulting axial force that interact with the longitudinal and torsional deformation of the shaft while 1 nodal diameter modes are characterized by a transverse deformation which is related to the transverse bending deformation of the shaft. Thus both inertia and gyroscopic effects are taken into account in rotordynamics studies. Coriolis forces are experienced by rotating blades when there are components of motion orthogonal to the primary axis of rotation of the disc:

$$\vec{F}_{Coriolis} = -m(2\vec{\omega} \times \vec{r}') \quad (6.1)$$

where $\vec{F}_{Coriolis}$ is the Coriolis force, normal to the blade frame velocity, \vec{r}' , and to the rotation vector, $\vec{\omega}$, and m is the blade mass. Generally, the effect of Coriolis forces is not taken into account in vibration analysis, it being considered negligible with respect to other forces. Here, it is appropriate to note that all nodal diameter (ND) modes, except 0 ND and 1 ND, have the bending moments balanced at the centre of the disc and such a feature allows us to perform an analysis of bladed disc vibration in isolation from the supporting shaft. It should

be noticed that the dynamic properties of the bladed disc changed significantly when the Coriolis forces were included in the analysis. Perfectly-tuned cyclically-symmetric bladed discs are characterized by having double modes with identical natural frequencies for each number of nodal diameters. When the Coriolis forces are included, each pair of double modes was found to split into two single modes with different natural frequencies corresponding to forward and backward travelling wave mode shape. The Point Tracking measurement method, combined with the rotating exciter, was employed to demonstrate that a bladed disc designed to exhibit a strong Coriolis effect shows the predicted frequency split in the n nodal diameter modes.

6.3.1.2 Measurement results

Tests were carried out using a modified design of the USAF 24-bladed disk. The original design did not exhibit any Coriolis forces because the blisk was flat. In fact, those forces can be generated when there is rotation combined with significant radial as well as tangential and/or axial components in the blade vibratory displacements. There are several ways to introduce such a coupling and the one used with this blisk was to bend the blades in the axial direction to give so-called “swept blades”. The higher the angle of inclination of the blades, the stronger is the effect of the Coriolis forces. The unmodified and modified bladed disks are shown in **Figure 6.2**

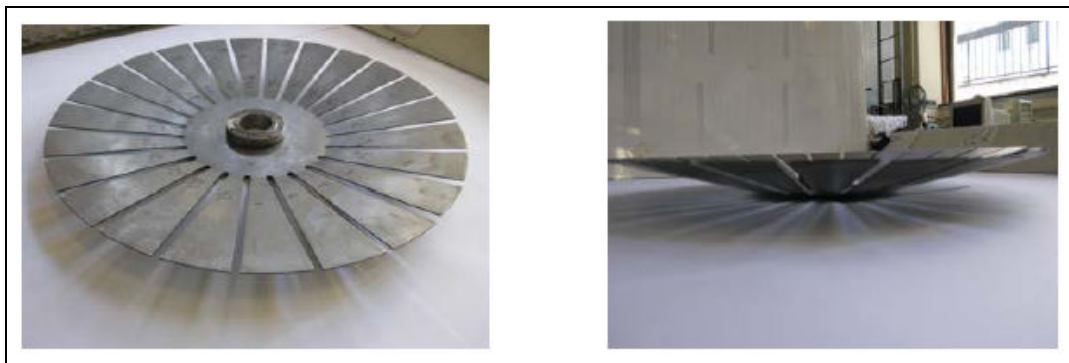


Figure 6.2 USAF 24-bladed disk with straight and swept blades respectively

The swept angle was chosen to be 15 degrees which was reduced to 7 degrees, at 1300 rev/min because the centrifugal forces acting on very flexible blades. **Figure 6.3** shows the measurement of the angle on the left hand side and the resulting angles measured at different rotational speed on the right hand side. As a result, hence the effect of Coriolis forces reduced while the blisk was rotating.

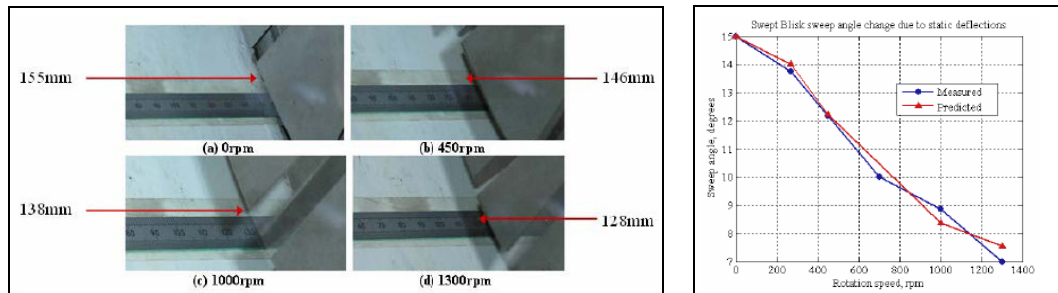
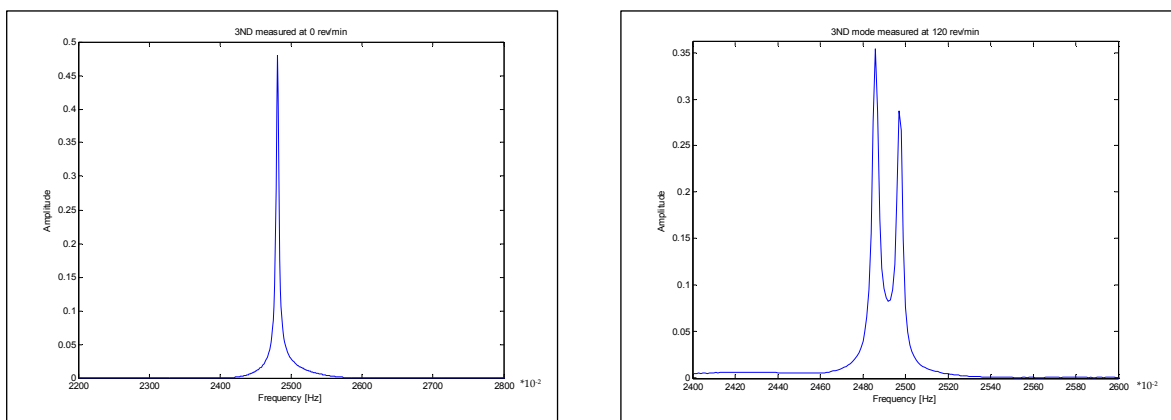


Figure 6.3 Straightening of the blade due to the centrifugal load

The combination both of the Point Tracking method and the rotating exciter made possible the measurement of the frequency split at speed by sweeping the excitation frequency around the resonance of interest. **Figure 6.4** shows the frequency split measured at 0 rev/min, 120 rev/min and 180 rev/min, respectively, of the 3ND mode for the tuned blisk configuration. It is noticeable, as expected, that at rest there is no frequency split.



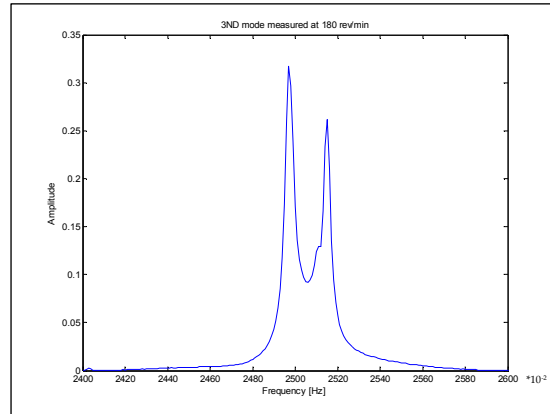


Figure 6.4 Frequency split of the 3ND mode measured at 0 rev/min, 120 rev/min and 180 rev/min, respectively

Predictions of the frequency split were made, [32] and [33], both for the tuned and mistuned blisk configuration for all ND modes of the first flap-wise family. Measurements were carried out on the 2ND and 3ND modes which were showing the highest splits at speed and were not presenting any frequency split due to inherent mistuning for the virtually tuned testpiece used. **Figure 6.5** shows a plot of the measurements carried out on the 2ND and 3ND modes, respectively. The left hand side presents results of frequency split measured between 240 and 900 rev/min of the 2ND mode. The red curve shows predictions of the frequency splits while the blue one presents the measured data. The shape of the latter curve shows that the frequency split grows up to a certain rotational speed and then it starts to decrease slightly. It was realised that this was because of a reduction in the sweep angle due to an increase of the centrifugal force acting on the blades at higher speeds. The same behaviour is observed for the 3ND mode on the right hand side plot of **Figure 6.5**.

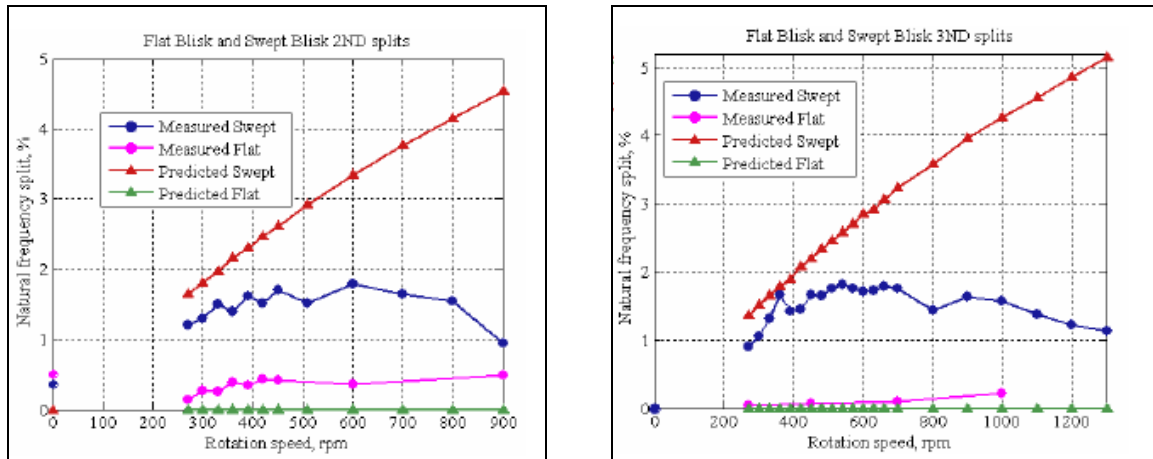


Figure 6.5 Measurement and predictions for the 2 ND and 3 ND mode, respectively

6.3.2 USAF IBR FRFs measurements under rotating conditions

Another interesting application of the Point Tracking method and the rotating exciter was to measure FRFs under rotating conditions for the USAF IBR 24-bladed disk, both for tuned and mistuned configurations. The FRFs were measured at both corners of each blade tip. These measurements were made because the proximity of the 2nd flap-wise and 1st torsional family so that only measuring both corners could assure the identification of both flap-wise and torsional modes. All measurements were carried out under vacuum conditions so as to avoid any air damping which could be very significant on this type of non-aerodynamic testpiece design. **Figure 6.6** shows the FRF data measured at rest, at 600 rev/min and at 1000 rev/min, respectively, for the tuned configuration. Centrifugal forces forced the flexural modes more than the torsional modes so that the frequency resonances of the flap-wise modes will grow faster than the others, and thus overlapping the torsional ones when the rotational speed is increased. **Figure 6.7** shows a zoom of the 2ND mode region FRFs presented in **Figure 6.6** where, clearly, the increase of the resonance frequencies due to the rotational speed can be seen.

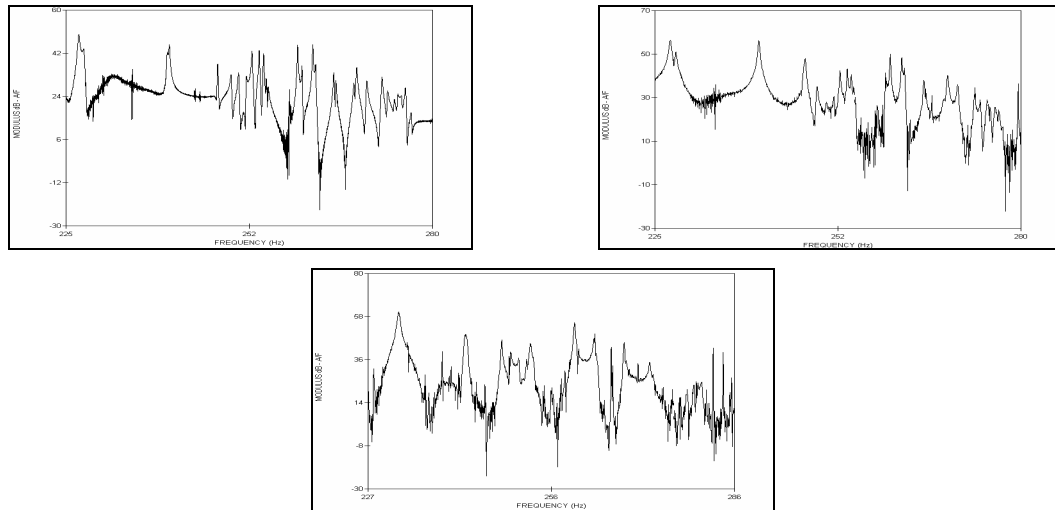


Figure 6.6 FRF measurement of tuned USAF 24 bladed disk at 0 rev/min, 600 rev/min and 1000 rev/min, respectively.

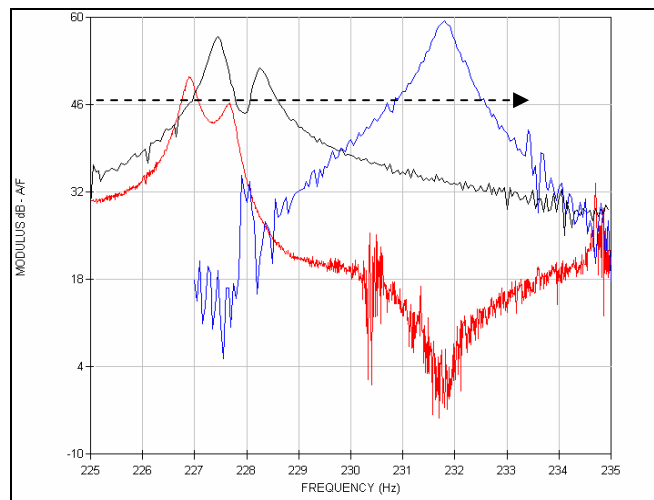


Figure 6.7 FRF measurement of tuned USAF 24 bladed disk at 0 rev/min (red), 600 rev/min (black) and 1000 rev/min (blue), respectively. Zoom on 2ND mode

Following the measurements of FRFs for the tuned blisk, a random mistuning pattern was introduced with very small cylindrical masses applied at the blade tip corners according to data given **Table 6.1**. The weights of the 24 masses had to be carefully chosen to avoid any unbalance of the blisk that could be seriously dangerous once at speed. **Figure 6.8** shows the FRF data measured at rest, at 600 rev/min and at 1000 rev/min, respectively, for the mistuned configuration.

Blade n.1	1.6g	Blade n.2	1.0g	Blade n.3	1.2g	Blade n.4	1.6g
Blade n.5	1.6g	Blade n.6	1.0g	Blade n.7	1.2g	Blade n.8	1.6g
Blade n.9	1.6g	Blade n.10	1.0g	Blade n.11	1.2g	Blade n.12	1.6g
Blade n.13	1.6g	Blade n.14	1.0g	Blade n.15	1.2g	Blade n.16	1.6g
Blade n.17	1.6g	Blade n.18	1.0g	Blade n.19	1.2g	Blade n.20	1.6g
Blade n.21	1.6g	Blade n.22	1.0g	Blade n.23	1.2g	Blade n.24	1.6g

Table 6.1 Mistuning pattern applied on the USAF IBr 24-bladed disk

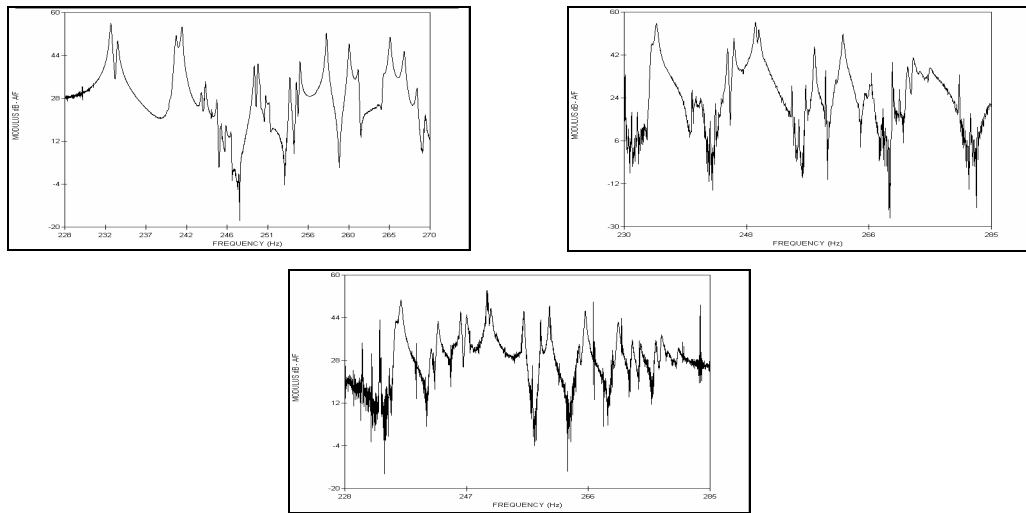


Figure 6.8 FRF measurement of mistuned USAF 24 bladed disk at 0 rev/min, 600 rev/min and 1000 rev/min, respectively.

Figure 6.9 shows a zoom of **Figure 6.8** for the 3ND mode region as outlined in the dotted rectangular area. Having mistuned the blisk, it is clear that each ND mode now presents two different natural frequencies, corresponding to backward and forward travelling waves, so that the plot looks very crowded.

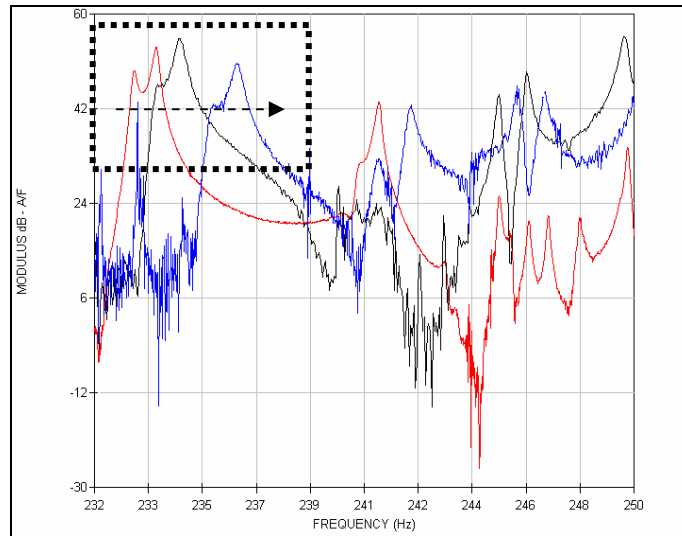


Figure 6.9 FRF measurement of mistuned USAF 24 bladed disk at 0 rev/min (red), 600 rev/min (black) and 1000 rev/min (blue), respectively. Zoom on 3ND mode

Some of the FRFs measured were post-processed to be sure that the measurements were correct. However, the aim of this study was to prove the ability of performing such measurements and further interpretation of the data was undertaken at the Carnegie Mellon University (CMU) which was involved in the study of the veering phenomenon [29].

6.4 Line Tracking method: applications

Line Tracking method is a one-dimension scan which, when the scanning path is radial, cannot provide information about torsional motion of a blade, unless several line scans are performed on the same blade. Nevertheless, it is very useful when the blade's profile is quite narrow, thus to justify the use of a one-dimension scan. The USAF IBR has a very wide blade profile, similarly to a fan bladed disk, which make the use of such a technique less effective. However, ODS measurements were performed on that blade which was not crossed by any nodal diameter lines, thus to avoid torsional component due to that.

6.4.1 USAF IBR and measurement results

The very first synchronous CSLDV measurement which was performed on the USAF IBR was Line Tracking method. Originally, the radial LDV scan rate input in the control panel was not the one at which the laser beam travelled along the blade. In fact, it was not defined the relationship between rotational speed, waveform sampling frequency and time length of the output buffer. However, measurements performed using the old control panel are presented in this section. Physical measurements were performed on a 24-bladed disk rotating at a speed of 457 rev/min. The 3ND modes of the 1st flap-wise family of modes were excited on the rotating blisk by a single DC magnet mounted behind the blisk at the blade tip radius. The reason for using a DC magnet as the excitation system, rather than the AC magnet was to show the versatility of the test rig. **Figure 6.10** shows the ODS obtained from line track scan performed at different radial LDV scan rates as reported in **Table 6.2**. It is clear from the graph that more reliable ODS reconstruction was obtained from slow radial scan frequencies than fast ones, as shown in **Figure 6.10**. Since the first use, the code was constantly updated and improved in order to deliver the simplest code possible. **Figure 6.11** and **Table 6.3** show ODS measurements and the radial scan frequencies at which they were performed. The last version of the code was able to control the radial scan frequency independently from the rotational speed of the target. The last example shows all ODS lines overlapping perfectly.

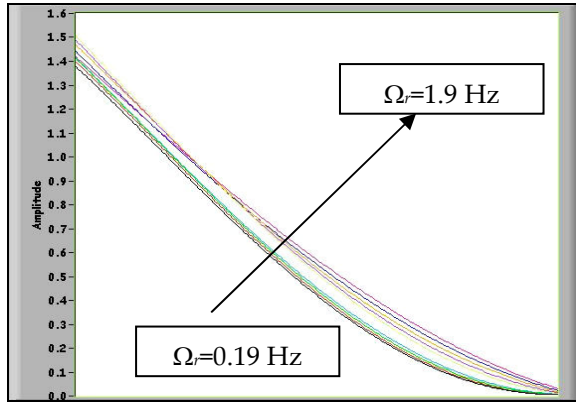


Figure 6.10 Series of tracking line scans

Frequency Scan rate (Radial direction) [Hz]
0.19
0.38
0.57
0.71
1.14
1.33
1.52
1.71
1.9

Table 6.2 Radial LDV scan frequency

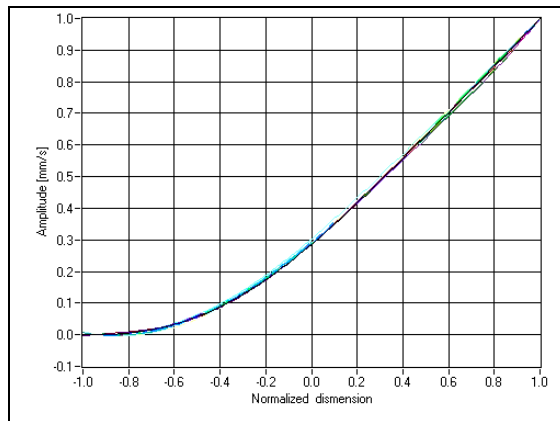


Figure 6.11 Series of tracking line scans

Frequency Scan rate (Radial direction) [Hz]	
0.1	0.8
0.2	0.9
0.3	1
0.4	2
0.5	3
0.6	4
0.7	5

Table 6.3 Radial LDV scan frequency

6.5 Area Tracking method: applications

The area scan method is the most powerful measurement technique available to date. The key points are: (a) a 2D full field measurement technique based on the use of a standard SLDV (class II laser) system, commercially available on the market, (b) extremely simple to perform, (c) limited time required both to perform and to post-process the time history data. This study was focussed on the development of a scanning path suitable for the geometrical design of the blade surface. However, other area scanning paths can easily be coded to accommodate any specific blade shape. In this final section, we will provide

examples of measured ODSs at different rotational speeds, concluding with an ODS of the whole bladed disk.

6.5.1 USAF IBR measurement results

The main achievement of this study was to provide a tool to perform an area scan of a blade's surface while it was rotating over a range of speeds between 0 and 2400 rev/min. The capability to perform such a measurement was helpful for performing modal identification of blisk which was specifically designed to have two families of modes, very close in frequency at rest and to show a high modal density at the veering region at speed. Although the rotating exciter is not designed to run beyond 1200 rev/min, and so unable to cope with the target maximum speed designed for the blisk, FRFs were anyway measured at different rotational speeds of 0, 240 and 900 rev/min, as shown in **Figure 6.12**. These measurements were carried out under vacuum conditions to avoid any air damping and using the rotating AC excitation magnet which swept sine waves in the range between 245 Hz to 260 Hz in 100 seconds. Both plots in the top left hand corner and top right hand corner in **Figure 6.12** show three circles outlining, respectively, three resonances (1), (2) and (3), while in the bottom plot, circles numbered as (1) and (3), are shown. Resonance number (2) is visible at rest but it becomes smaller at 240 rev/min, and suddenly disappears at 900 rev/min. A modal identification was then performed by measuring the ODS of the blade from which the FRFs were measured by the Point Tracking method. Hence, the resonance frequencies were measured and used to excite the bladed disk at the three rotational speeds previously run.

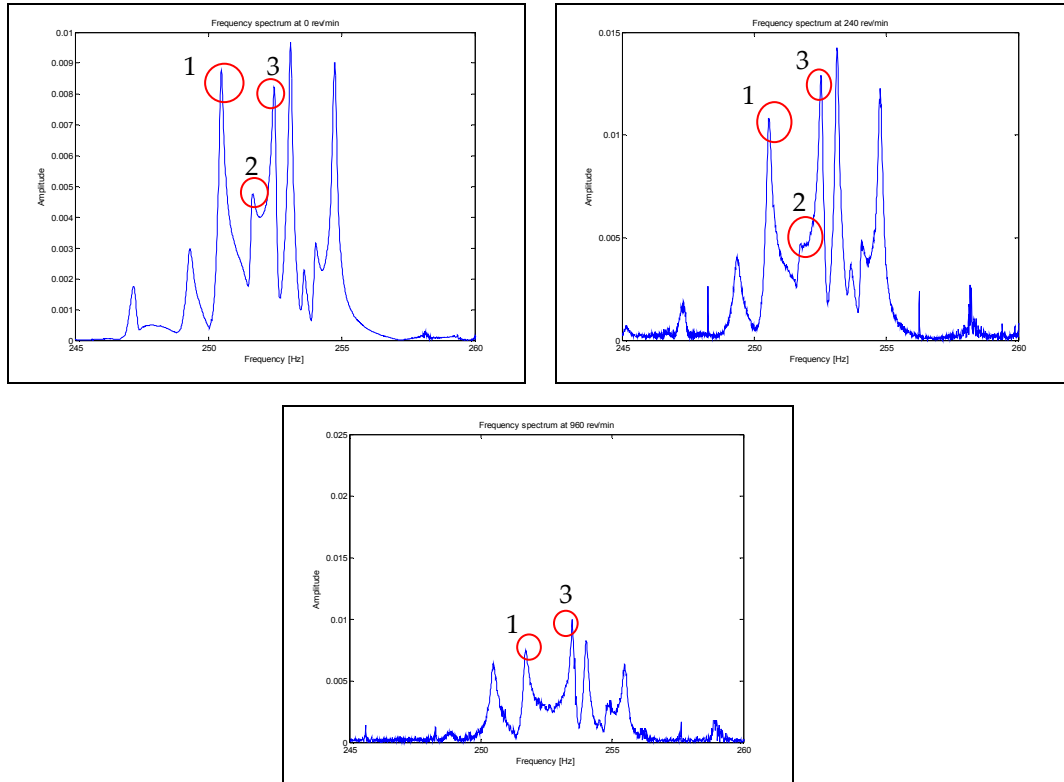


Figure 6.12 FRFs measured at 0 (top left), 240 (top right) and 960 (bottom) rev/min, respectively

Figure 6.13 shows ODS measurements performed under stationary conditions, exciting the bladed disk at resonances (1), (2) and (3), respectively. It is clear to observe that ODSs at both resonances (1) and (3) show contributions from the 2nd flexural and 1st torsional families of modes while the ODS at resonance (2) shows a contribution from the 2nd flexural mode shapes, only. When the measurement of ODSs was repeated at 240 rev/min, we still can see that the deflection shapes at resonances (1) and (3) present a contribution of both flexural and torsional mode shapes while the deflection shape at resonance (2) shows contribution of flexural mode shapes only, as shown in **Figure 6.14**.

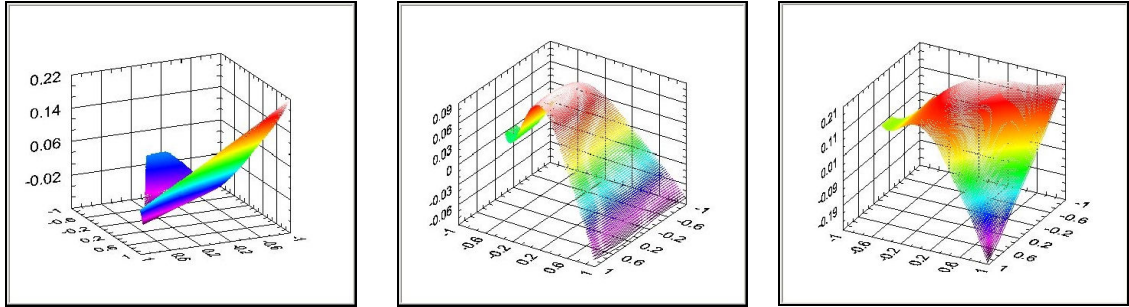


Figure 6.13 ODSs measured at rest for resonances (1), (2) and (3), respectively

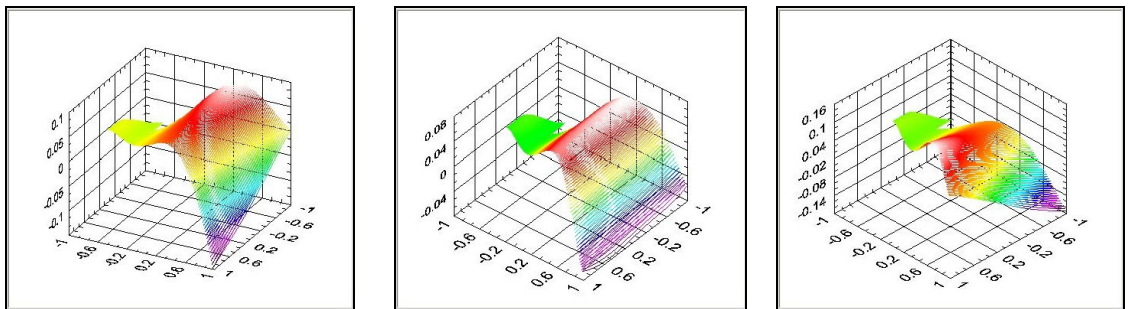


Figure 6.14 ODSs measured at 240 rev/min for resonances (1), (2) and (3), respectively

Repeating the ODS measurements at 900 rev/min, as shown in **Figure 6.15**, we can observe that the ODS at resonance (1) shows a combination of flexural and torsional mode shapes while ODS at resonance (3) shows the same combination but the contribution of flexural mode shapes is higher than the one experience at 240 rev/min. We could say that the Area Tracking method is a helpful measurement method for modal identification, especially for those families of modes veering towards/apart from one to each other where the measurement of few points per blade is not sufficient to give a clear understanding of the deflection shape of the blades.

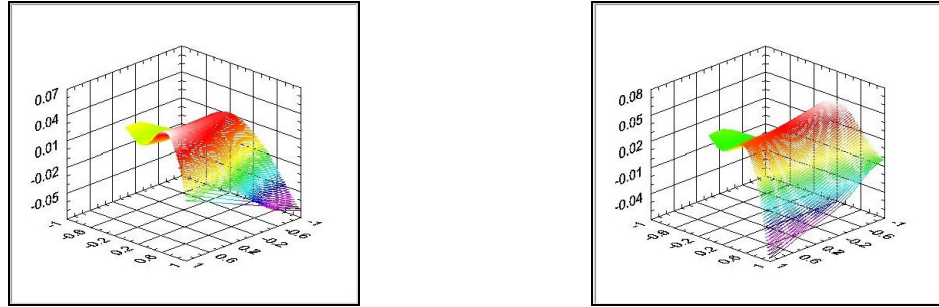


Figure 6.15 ODSs measured at 900 rev/min for resonances (1) and (3), respectively

We have now presented examples of ODSs measured at speed using the rotating exciter. However, another challenge was to carry out ODS measurements for rotational speeds beyond the ones achievable using the rotating exciter; in fact the maximum speed limit, for which the blisk was designed, is 2400 rev/min. These experiments were carried out under vacuum conditions using an AC magnet fixed so to be able to control the excitation frequency. The rotational speeds used for these tests are reported in **Table 6.4**.

Rev/min	Rev/min	Rev/min	Rev/min	Rev/min	Rev/min	Rev/min
60	120	240	480	960	1920	2400

Table 6.4 Rotational speeds set up for ODS measurement tests

Figure 6.16 shows the seven ODSs measured on the same blade at rotational speeds in the range between 60 and 2400 rev/min. There, we could demonstrate that the Area Tracking method was suitable for ODS measurements at higher rotational speeds than the ones previously presented.

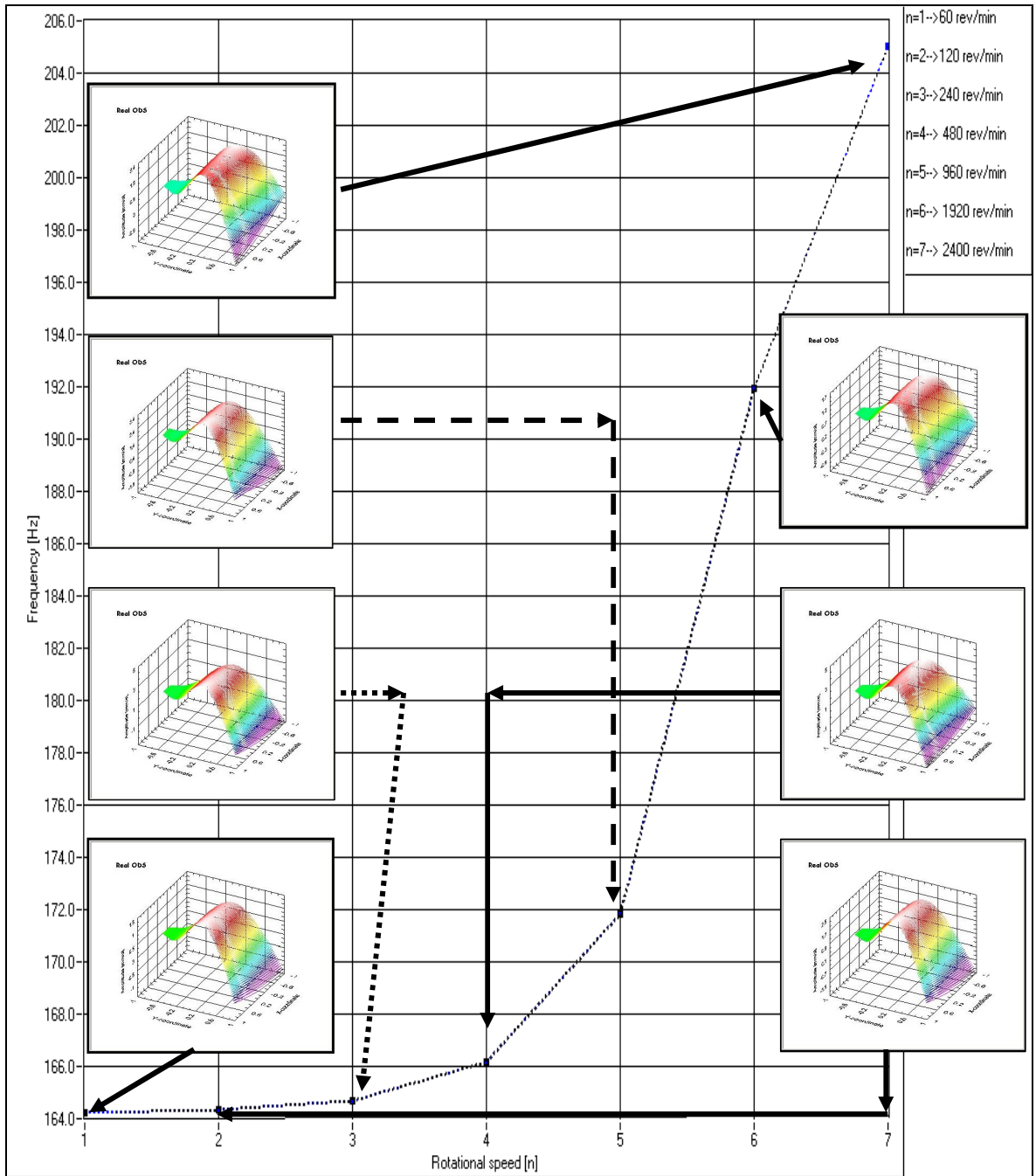


Figure 6.16 ODSs reconstructed from measurements performed at rotational speed range between 60 to 2400 rev/min

The very last example, we believe being the most impressive, is shown in **Figure 6.17**. That shows, on the left hand side, the ODS measurement of all 24-bladed disk at the rotational speed of 60 rev/min and excitation frequency of 225.12 Hz while, on the right hand side, it is shown the simulated ODS. Despite some differences between the measured and simulated ODSs, we can say that a full field measurement under rotating condition has been performed for the first time using a standard SLDV system. We can, finally, conclude that the ODS reconstruction was obtained from a single LDV time signal, as shown in **Figure 6.18**. Actually, the laser beam scanned continuously all the 24 blades and the red rectangular area, in **Figure 6.18**, shows the moment when the laser beam goes from one blade to next one continuously.

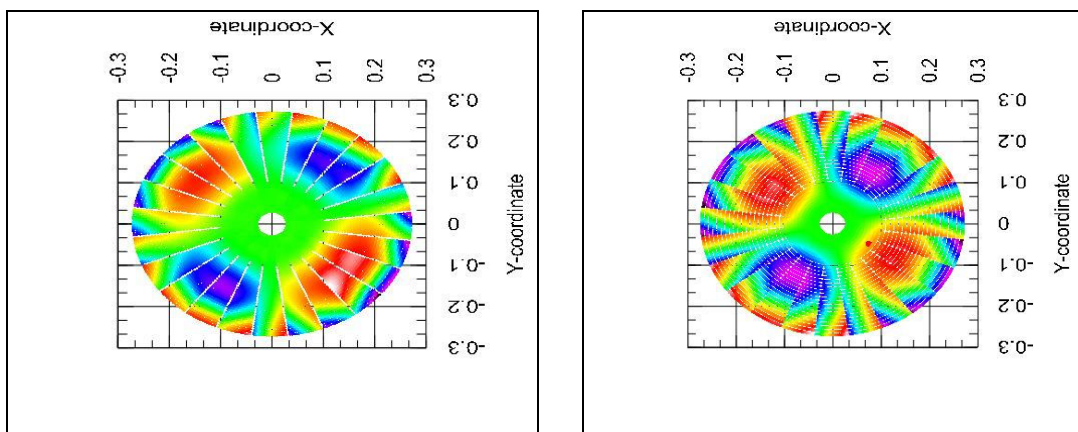


Figure 6.17 ODS of the USAF IBr 24-bladed disk, measured (left) and simulated (right) at 225.12 Hz and 60 rev/min

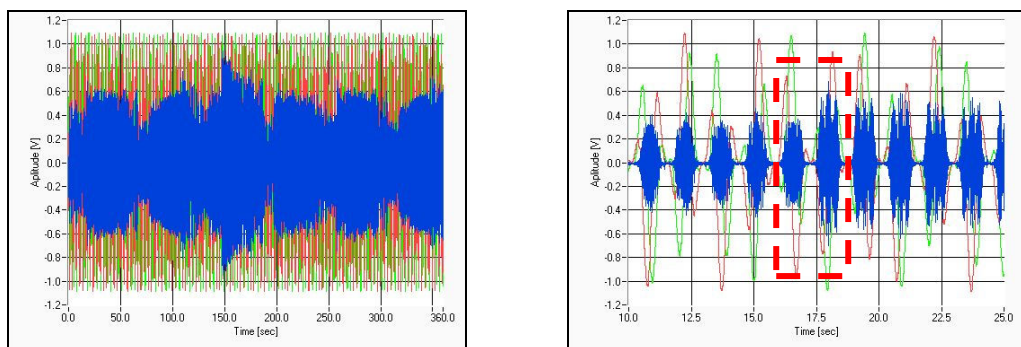


Figure 6.18 LDV output time data on the left hand side and zoom of the time signal on the right hand side

6.6 Conclusions

The aim of this chapter was to present results of tracking measurements methods and applications, and to introduce the software combining all the tracking CSLDV panels. We have presented the use of Point Tracking and the rotating exciter for FRFs measurements for two different studies. One of these was focussed on demonstration of the effect of Coriolis forces on bladed discs, where those forces can produce a frequency split of all nodal diameter modes resonances. We successfully measured that frequency split at several rotational speeds and the post-processing of the data showed the backward and forward travelling waves associated with each resonance. We have also presented some examples of Line Tracking measurement results, explaining the efficiency of that method whenever narrow blades are to be measured. We finally concluded the chapter by providing examples of ODSs measured on the vibrating surface of a single blade rotating in a range of speed between 0 and 2400 rev/min. Hence, this latter method could prove its ability of modal identifications, especially for two families of modes veering apart where a high modal density is present. The last example showed the ODS of the 24-bladed disc measured under rotating conditions and compared with a simulated one, thus to validate the measurement result.

7 Geometrical sensitivity study of a bladed disk

7.1 Overview

A bladed disk is very complicated structure and there are many parameters involved into the designing, manufacturing and testing processes. The aim of this study is to provide a sensitivity indication of bladed disk to geometrical variations when a datum random mistuning pattern, under both stationary and rotating conditions, is superimposed. The research focuses on the range or scatter of forced response level between mistuned and tuned FE models of when a large number, nominally identical are considered. By plotting the highest forced response level of all FE models we should be able to see whether a geometrical variation can affect the response amplitudes of mistuned assemblies.

7.2 Introduction

This thesis is not primarily focussed on the study of the mistuning phenomena that change the dynamic behaviour of symmetrical structures such as a bladed disk. That problem has an extensive literature produced over the past 40 years. However, the design of the USAF 24-bladed disk offered the chance to look at the interaction between mistuning and optimization of the structure design. The experience gained working on the structural design of 24-bladed disk has led to the creation of several FE models whose geometrical parameters were changed to study the variation in their modal properties. Hence, this chapter will present the results of simulations performed on a series of FE blisk models when a

mistuning pattern is superimposed on the tuned assembly. Section 4.2.1 ended with the question: "How sensitive would be a blisk to a datum mistuning pattern when one of its geometrical dimensions is varied?". We have seen that one of the requirements of that design was to obtain two families of modes which were very close in frequency: the 2nd flap-wise and 1st torsional families of modes, respectively. The main difficulty to design a blisk with such characteristics was to find a parameter which could drive these two families of modes apart to a greater or smaller frequency distance. During that research, it was noticed that the blisk was surprisingly sensitive to inter-blade tip slot width variations. **Figure 7.1** shows how the 2nd flap-wise and 1st torsional natural frequencies varied with variation of that parameter and, in fact, by varying the inter-blade tip slot width it was possible to design a blisk meeting the initial requirements. The proximity of those two families of modes suggested that any additional study performed in that area would have been extremely difficult especially for identification of the mode shapes. Hence, the idea formed to study first family of modes, reasonably distant in frequency from the others, for a series of blisk models where only one geometrical dimension would be changed and on which the same mistuning pattern would be superimposed. It is not the intention of this chapter to explore the physical phenomenon behind the variation of the vibration amplitude response of mistuned models. Nevertheless, this investigation aims to explore the influence of some parameters such as rotational speed and damping loss factor variations for whole series of forced response calculations. The study was performed under stationary and rotating conditions although in the latter case it was not Engine Order (EO) excitation that was used, rather, it was decided to run simulations at different rotational speeds. The reason was based on the need to be able to explore blisk models' behaviour in a wide range of rotational speeds while focussing attention only on the maximum response amplitudes achieved at resonance frequency induced by

the EO excitation method. This work is based on the influence of the variations of inter-blade tip slot width dimension and blisk thickness to the same mistuning pattern. Thus, one part of the study is focused on changes in the inter-blade tip slot width and the second part is focused on the variation of blisk thickness, both of which are performed under stationary and rotating conditions. Additionally, all forced response simulations were carried out using 6 different levels of damping loss factor. The latter was also included into the analysis to produce a more comprehensive understanding of the behaviour.

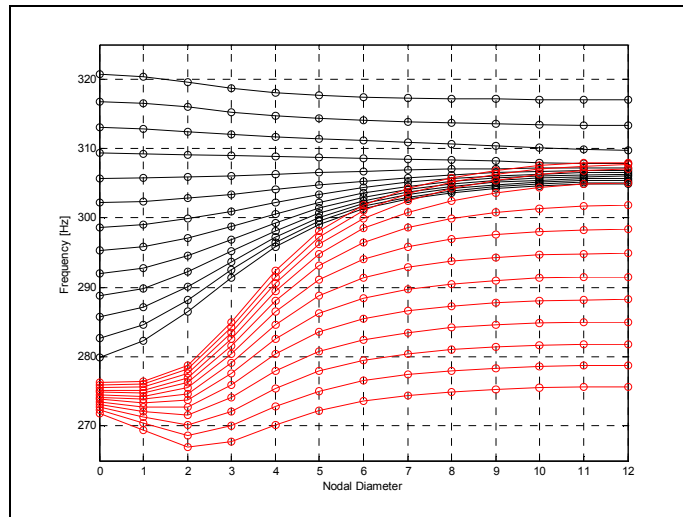


Figure 7.1 Change of 2nd flap-wise and 1st torsional family of modes to inter-blade tip slot width variation

7.3 Forced response calculation method

Having the modal data eigenvectors and eigenvalues calculated, these were used to calculate forced response characteristic of tuned and mistuned blisk models by using the following equation:

$$\{X\} = \sum_{r=1}^N \frac{\{\phi\}_r^T \{F\} \{\phi\}_r}{\omega_r^2 - \omega^2 + i\eta_r \omega_r^2} \quad (7.1)$$

where $\{X\}$ is the ODS displacement, $\{F\}$ is the applied Force, N is the number of modes included, $\{\phi\}_r$ is the eigenvector and ω_r is the eigenvalue of mode r , ω is the vibration frequency and η_r is the modal damping loss factor. The damping level was decided to be the same for all the 24 modes included and it was also decided to have 6 different levels between 10^{-6} and 10^{-1} . In fact, damping plays an important role in reducing the response amplitude of the blade vibrations thus it was interesting to investigate when that factor was varied too. Magnification factor (MF), ratio of $\{X_M\}/\{X_T\}$, was finally calculated where $\{X\}$ is displacement in z-directions. Having a 24-bladed disk, it was decided to choose 24 locations at the blade tips, one location per blade. The excitation force, $\{F\}$, was always applied at the location where the response was calculated and so the excitation was moved around all 24 blades in turn. The maximum amplitude response value, for both tuned and mistuned models, simulated at each eigenvalue of the mode “ r ” was selected to calculate the magnification factor (MF), as expressed by the following equations:

$$\{X_i\} = \sum_{r=1}^N \frac{\{\phi\}_r^T \{F_i\} \{\phi\}_r}{i\eta_r \omega_r^2} \quad (7.2)$$

$$D_i = \left(\frac{X_{i_Mist}}{X_{i_Tuned}} \right) \quad (7.3)$$

$$MF = Max(D_i) \quad (7.4)$$

where $i = 1, \dots, 24$ is the blade index and $r = 1, \dots, 24$ is the eigenvalue index, having calculated the first 24 modes. A set of data was finally produced [14, 24]. That ratio is the mean of assessing if the mistuning pattern has produced responses higher as produced by the tuned assembly. Hence, a magnification ratio equal to 1 means that the $(X_i)_{Mist} = (X_i)_{Tuned}$ so both systems respond equally while when that ratio is higher than 1, $(X_i)_{Mist} > (X_i)_{Tuned}$, the vibration amplitude of some, or

all, blades of the mistuned blisk model are higher than the tuned one. We have calculated the first 24 mode shapes of the first flap-wise family indexing them from 0 to 23 as it will be seen in the 3D plots of the next sections. Index labelled 0 represents the 0 ND mode, indexes labelled 1 and 2 represent 1⁽⁻⁾ ND mode and 1⁽⁺⁾ ND mode respectively and so on, index labelled 23 represents single 12 ND mode.

7.4 Inter-blade tip slot width variation

In the introduction we presented a plot where it was shown how the two families of modes changed by varying the inter-blade tip slot width, with those two families being very close in frequency. It was decided to use the first family of modes well separated from all others and so to avoid difficulties in mode shape identification. The first geometrical dimension varied was the inter-blade tip slot width in the range from 5mm (0.5mm) 11.5mm. A total of 14 FE models were constructed all with the same uniform blisk thickness of 1.897mm (16 SWG). All the FE models had the same number of nodes (13704) and all were constrained at the bore setting the displacement of the nodes at that boundary zero. All the models had the same material properties: Young's modulus (207GPa), Density (7594 Kg/m³) and Poisson's ratio (0.3) and all dimensions are shown in **Table 7.1**. A mistuning pattern was produced, creating a new element whose material density, 10000 Kg/m³, was set higher than the one used for the basic FE model. A specific pattern of mistuning weights was chosen randomly and was applied to all the FE models. The models were not constructed using cyclic symmetry, and so no modal solutions were calculated using that approach. **Figure 7.2** shows the FE model with a 5 mm inter-blade tip slot width where the overall blisk diameter and inner disc diameter are drawn in blue and green line, respectively, and elements circled by a dotted line represent the

mistuning pattern. The type of blisk design looks like a fan blisk whose blades are very flexible and the inner disc portion very stiff.

N.	D	d	inter-blade tip slot width	Thickness	N.	D	d	inter-blade tip slot width
1	540	195	5	1.897380	8	540	195	8.5
2	540	195	5.5	1.897380	9	540	195	9
3	540	195	6	1.897380	10	540	195	9.5
4	540	195	6.5	1.897380	11	540	195	10
5	540	195	7	1.897380	12	540	195	10.5
6	540	195	7.5	1.897380	13	540 <td 195	11	
7	540	195	8	1.897380	14	540	195	11.5

Dimensions in [mm]

Table 7.1 Geometrical dimensions of FE blisk models

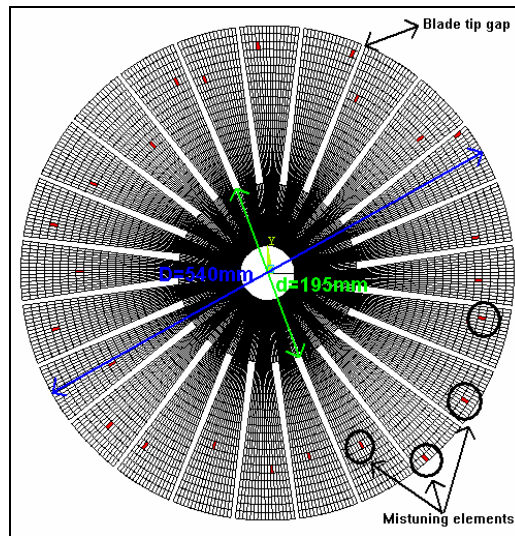


Figure 7.2 Random mistuning pattern applied and geometrical dimensions

7.4.1 Stationary Conditions

When all the FE models were constructed, 14 for the tuned blisk and 14 mistuned ones, a modal analysis solution was run to obtain the modal data for all the models. Then, all data produced were used to calculate the forced response and consequently the magnification factor. **Figure 7.3** shows natural

frequencies of all 14 tuned FE models. **Figure 7.3** also shows clearly that all modes are contained in about a 10Hz frequency span between 22 to 32 Hz. An heavy mistuning pattern could split the natural frequencies too much to introduce confusion with mode shape identification.

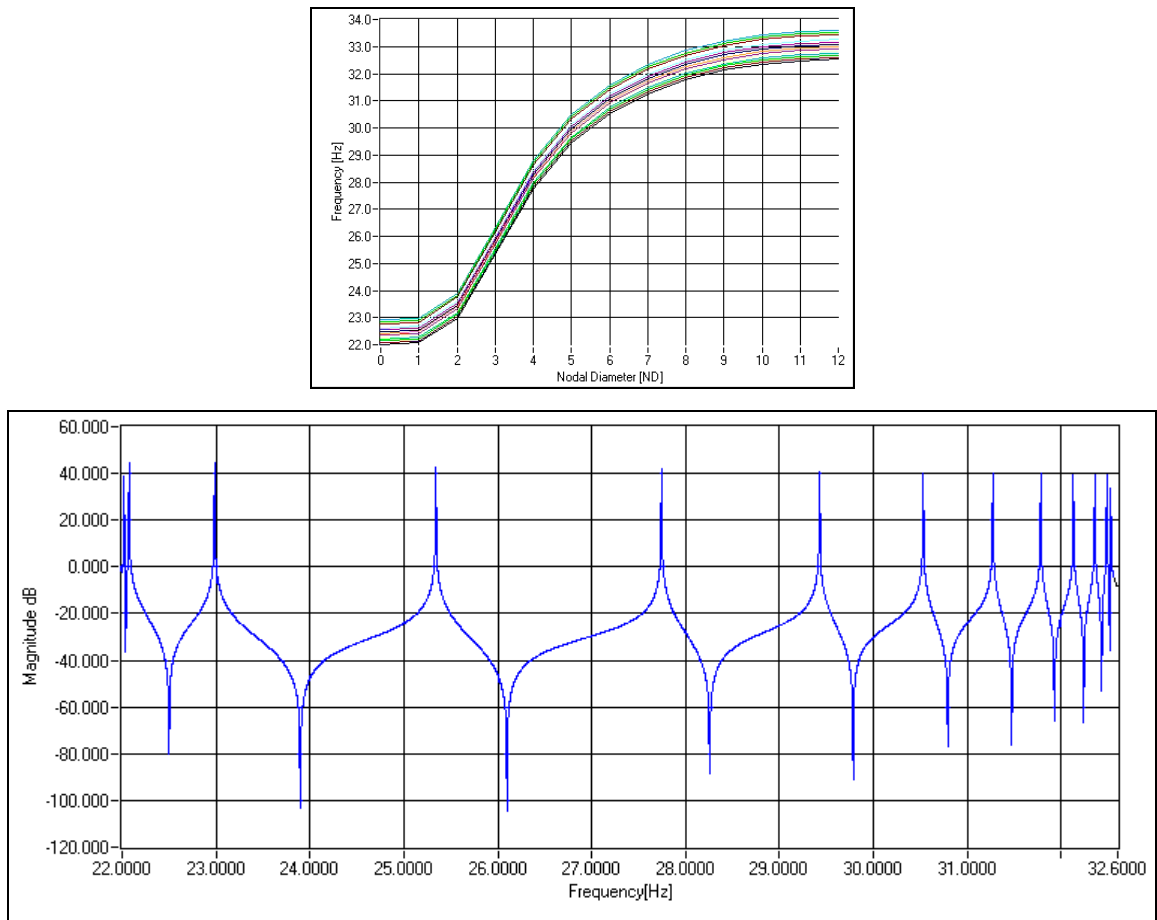


Figure 7.3 Tuned frequencies (top); FRF of blisk model with slot width of 5mm

Figure 7.4 shows the results of forced response calculations for the 6 levels of damping loss factor. The top left hand side corner shows the plot calculated for a damping level of $\eta_r=10\%$ continuing to the bottom right hand side where the plot calculated for the damping level of $\eta_r=0.0001\%$ is shown. Recalling what was said in section 7.3 about the index of the mode shapes, the magnification factor (MF) results are plotted, in **Figure 7.4**, for mode shapes (MD) against geometrical variation (Inter-blade tip slot width [mm])

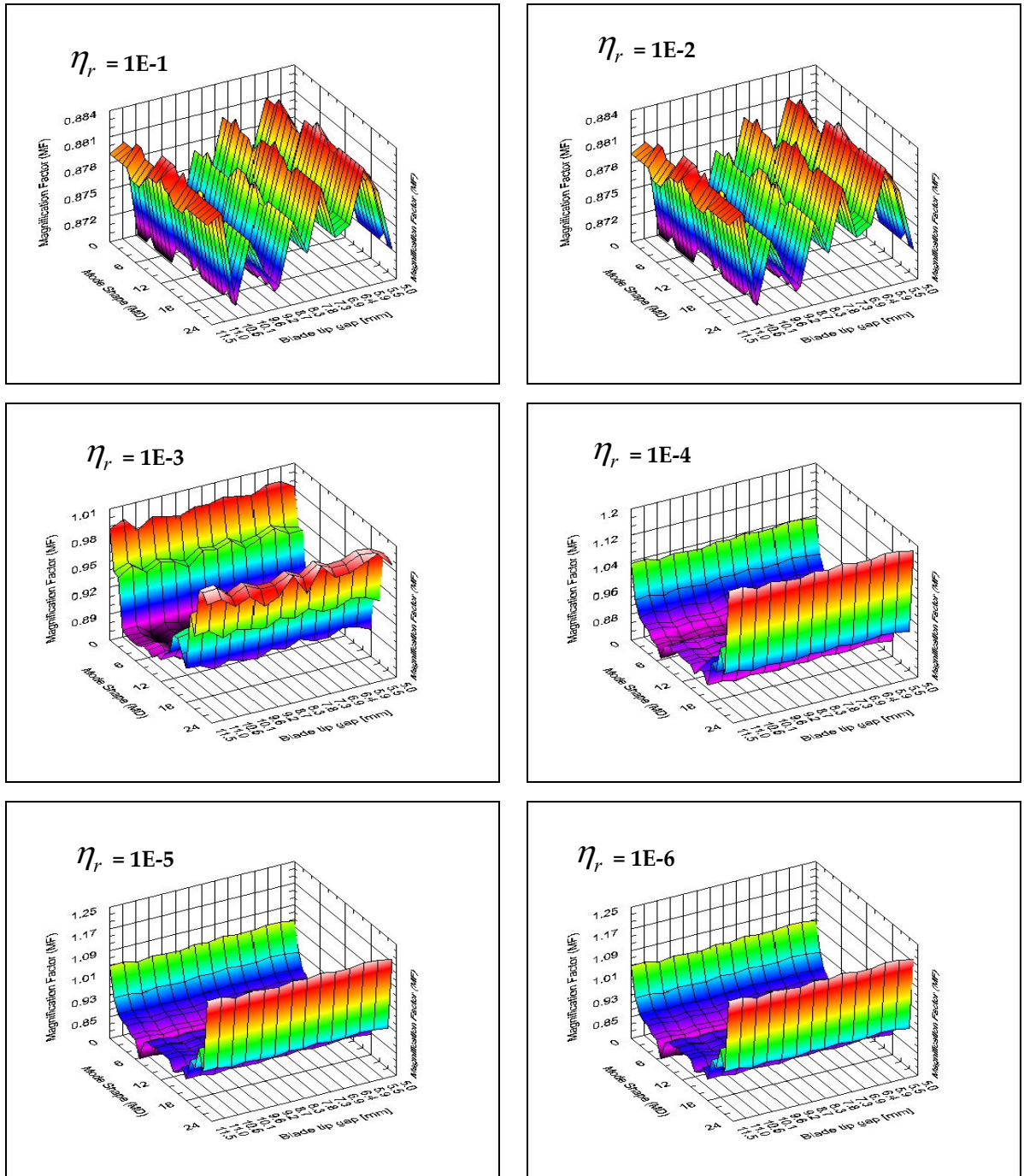


Figure 7.4 Magnification Factor plots for each damping level

If we focus on the magnification factor (MF) curves of the 12 ND mode, as shown in **Figure 7.5**, calculated for all damping levels, we can see that the responses of all FE models stay almost constant. The plot also suggests that the magnitude of the mistuning pattern, superimposed on all the models, produced

a response 20% higher of the tuned models ones for very small levels of damping otherwise negligible. An additional attempt, although only for these 14 blisk models, was to increase the amount of mistuning by 100% so the density of the mistuning element was set at 20,000 Kg/m³ instead of 10,000 Kg/m³. Modal analysis solutions were recalculated for all FE models thus to use the model data for forced response calculations using the same 6 levels of damping loss factor. Modification of all FE models, modal analysis solution, data manipulation and forced response calculations were extremely time-consuming, and that is the reason why there is only single attempt.

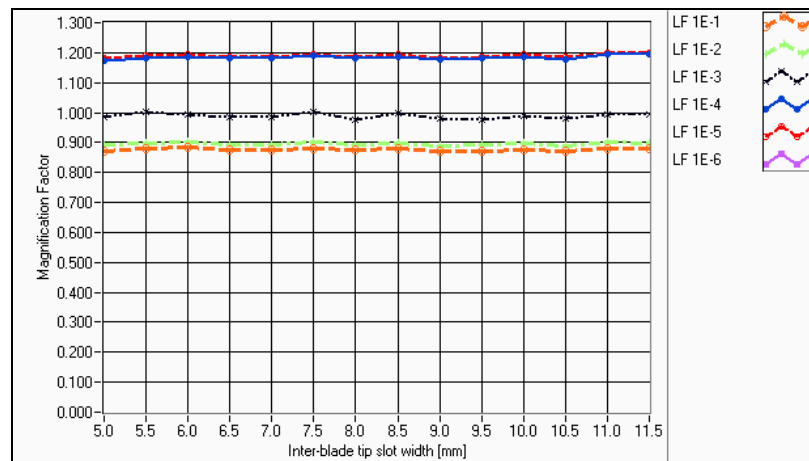


Figure 7.5 Magnification factor results of 12ND mode for all 14 blisk models

Despite such an effort the results of MF, shown in **Figure 7.6**, for all damping levels showed no differences from the previous calculation presented. The increased level of mistuning did not produce a significant fluctuation of responses between FE models. Hence, it can be concluded that the variation of amplitude responses between the mistuned assemblies was negligible.

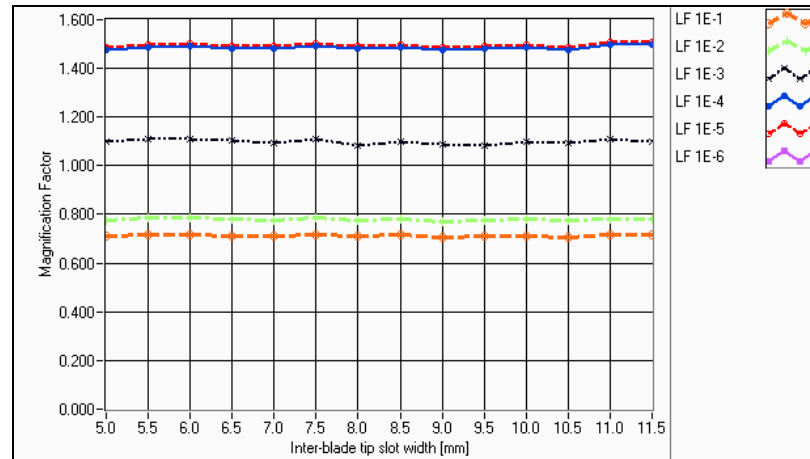


Figure 7.6 Magnification factor results of 12ND mode for all 14 blisk models; increased mistuning

7.4.2 Rotating Conditions

However, the results of the calculations under stationary conditions suggested performing calculations under rotating conditions to explore the behaviour of the same mistuned FE blisk models at speed. It is common practice to perform engine order excitation when the blisk is rotating, that being the actual excitation type most frequently experienced under operating conditions. However, this study focuses on exploring how sensitive the blisks are to small variations of geometrical parameters when a mistuning pattern is superimposed. Therefore, it was not targeted at a specific rotational speed but all FE models were run at 4 rotational speeds, [600, 1200, 1800, 2400] rev/min, and a modal analysis solution was repeated for each of these speeds. Also, for the simulation under rotating conditions, 6 levels of damping loss factor were used, as specified in section 7.3. We would only like to focus attention on the 12 ND mode for the rotational speeds of 600 rev/min, 1200 rev/min, 1800 rev/min and 2400 rev/min, respectively, as shown in **Figure 7.7** and **Figure 7.8**. The first comment regards the magnitude of the magnification factor, which decreases as the rotational speed increases. However, the magnification factor fluctuation can be still

considered negligible. This analysis would suggest that the response of mistuned models do not vary considerably from one model to another. The magnitude of the mistuning pattern adopted is probably too small to produce a significant responses change between FE models. The use of more and heavier mistuning patterns would improve the quality of the study.

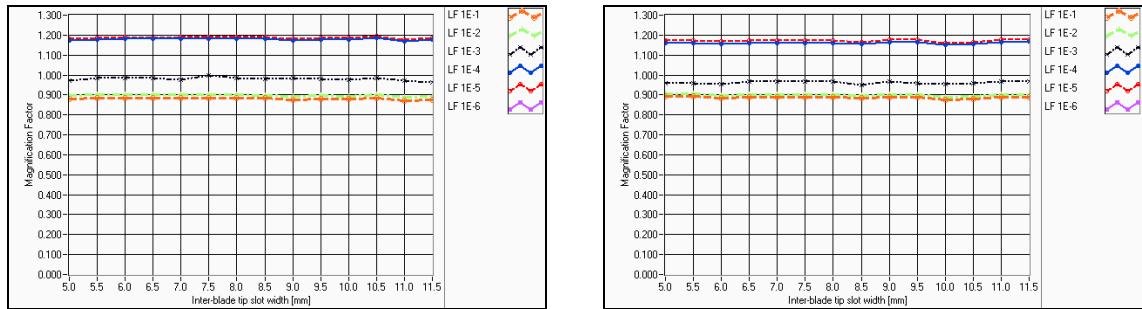


Figure 7.7 Magnification factor plots calculated at 600 rev/min and 1200 rev/min, respectively for the 12 ND mode

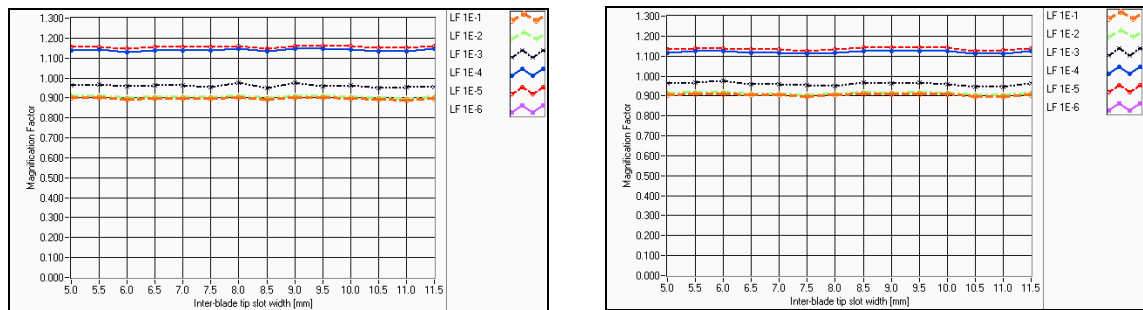


Figure 7.8 Magnification factor plots calculated at 1800 rev/min and 2400 rev/min, respectively for the 12 ND mode

7.5 Blisk thickness variation

In the previous section we presented the effect of varying one geometrical dimension of a bladed disk when a pattern of mistuning weights is applied to all FE models. Results of the forced responses calculated for all models showed that, at different damping levels, the amplitude of the response can change from

model to model. Having obtained a poor feedback about the sensitivity of the blisk to a geometrical variation about the mistuning, it was decided to pick one of 14 blisk models and to change a second dimension to see how the models would react to the same mistuning pattern already applied to the previous blisk models. The FE model with a 10.5mm blade tip gap was taken and its thickness was varied in the range from 1.9 mm (0.1 mm) 3.2 mm. The increment of the geometrical dimension is again small, at 0.1 mm, to study the vibration response amplitude of blisk models on which the given mistuning pattern was superimposed. The aim of this additional change is to broaden the exploration of the effect of geometrical variations on the dynamics of the structure. It is impossible to perform a study on all the geometrical dimensions of a bladed blisk; however, the hope is to extract more useful information which can address the study more precisely. An immediate output from such simulations could be to understand if, during the designing process, the decision to use one geometrical dimension within a range of choices, rather than another, can lead a worse forced response. **Table 7.2** shows geometrical dimensions of all the blisk models. **Figure 7.9** shows the mistuning pattern applied and the geometrical dimensions of the blisk model.

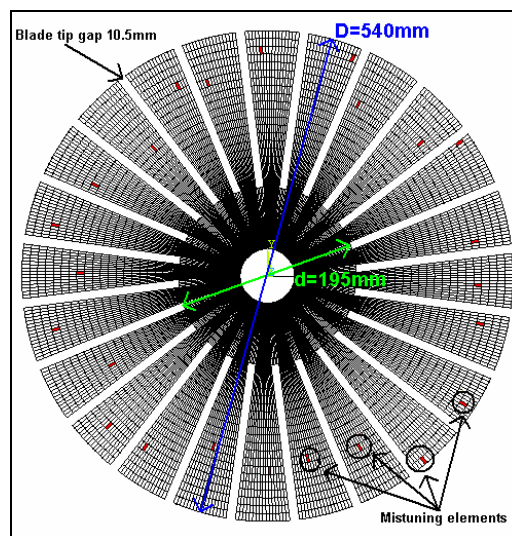


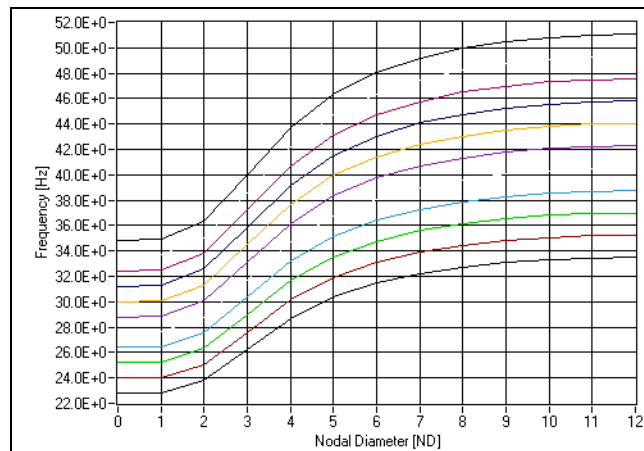
Figure 7.9 Random mistuning pattern applied and geometrical dimensions

N.	Thickness	D	d	Blade tip gap	N.	Thickness
1	1.9	540	195	10.5	8	2.6
2	2.0	540	195	10.5	9	2.7
3	2.1	540	195	10.5	10	2.8
4	2.2	540	195	10.5	11	2.9
5	2.3	540	195	10.5	12	3.0
6	2.4	540	195	10.5	13	3.1
7	2.5	540	195	10.5	14	3.2

Table 7.2 Geometrical dimensions of FE blisk models

7.5.1 Stationary conditions

Having constructed 14 FE blisk models, the modal solution under stationary conditions was calculated. Hence, the first 24 ND modes of the first family, eigenvectors and eigenvalues, were used to run forced response simulations to calculate the magnification factor using equation (7.1). All forced response simulations were again performed using 6 damping levels, as reported in section 7.3. Results for the natural frequencies of the tuned models are plotted in **Figure 7.10**.



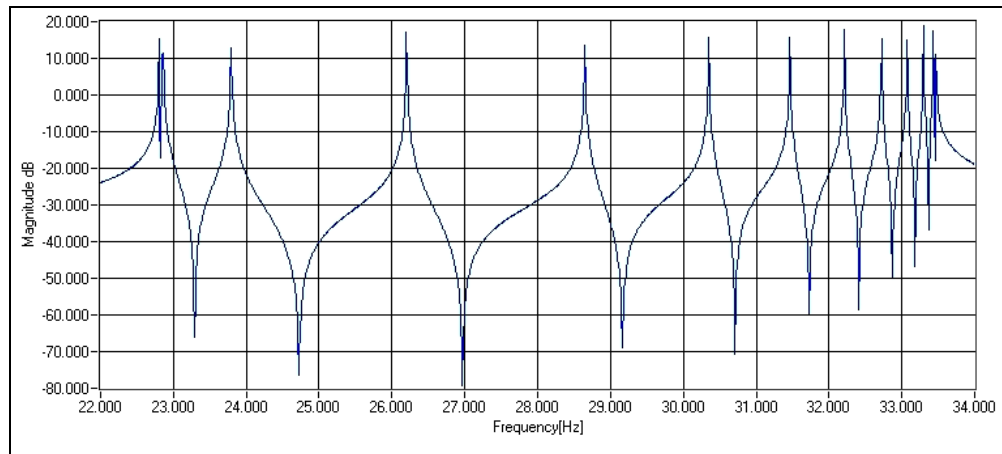
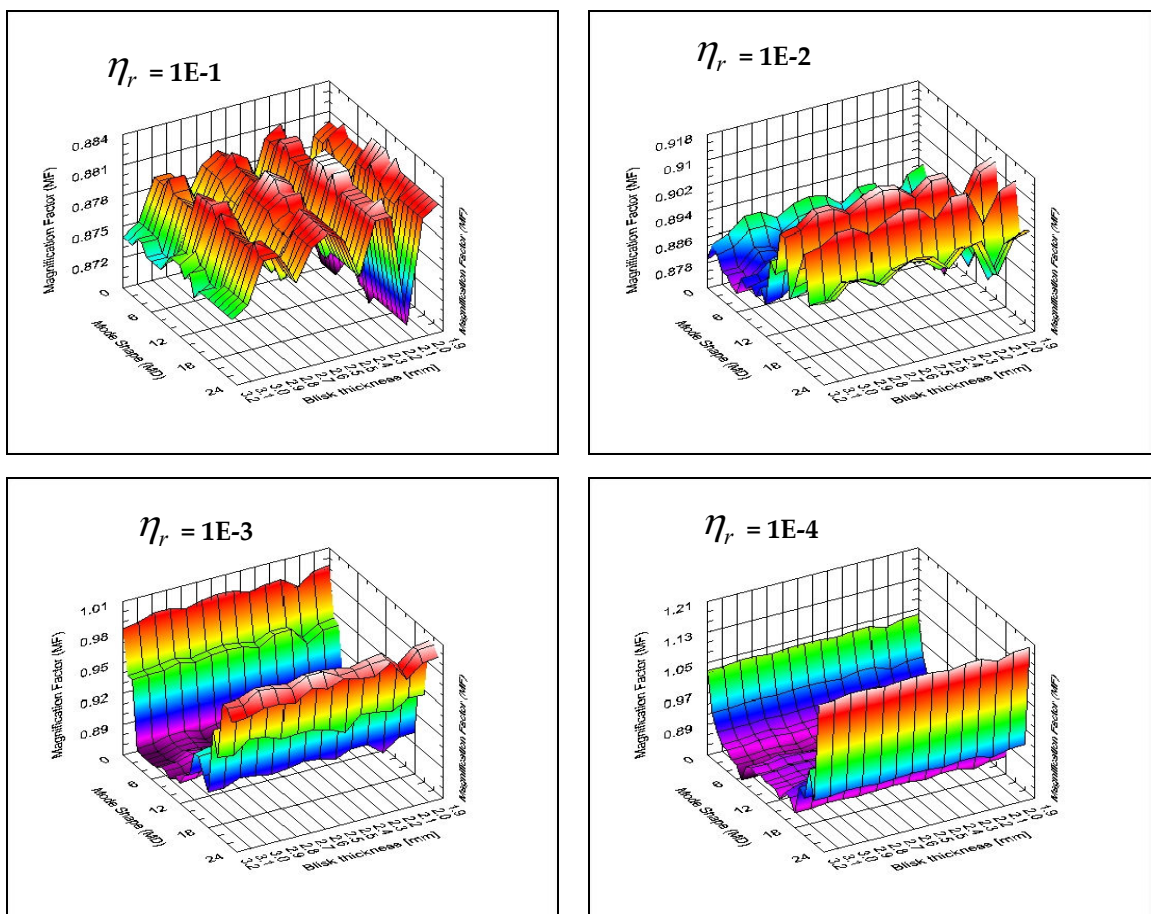


Figure 7.10 Tuned frequencies (top); FRF of blisk model with 1.9mm thickness

The results of all simulations are plotted in Figure 7.11.



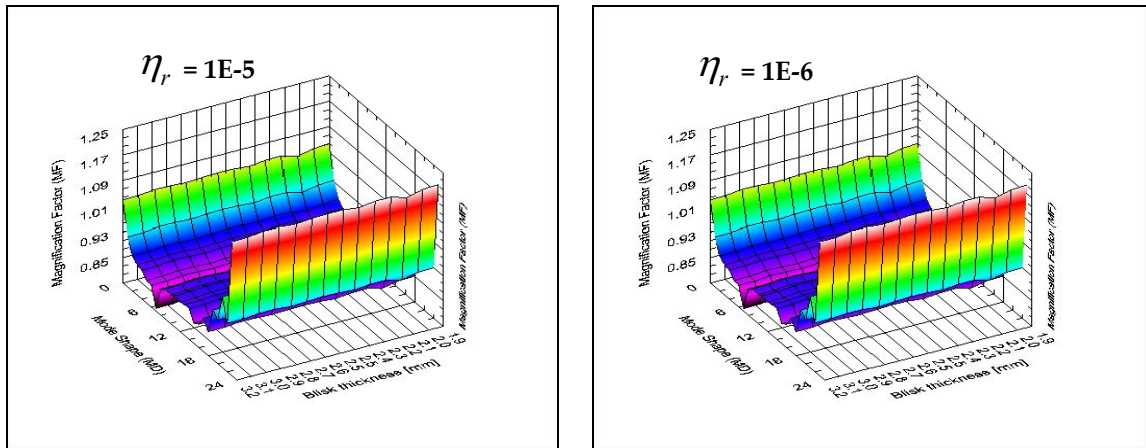


Figure 7.11 Magnification Factor plots for each damping level

Figure 7.12 shows responses of all models for the 12 ND mode for all damping values. Again, the mistuning pattern did not produce relevant changes of the response between models. All curves are practically constant. It will be interesting to see how those FE models respond when the rotational speed is superimposed, as is done in the next section.

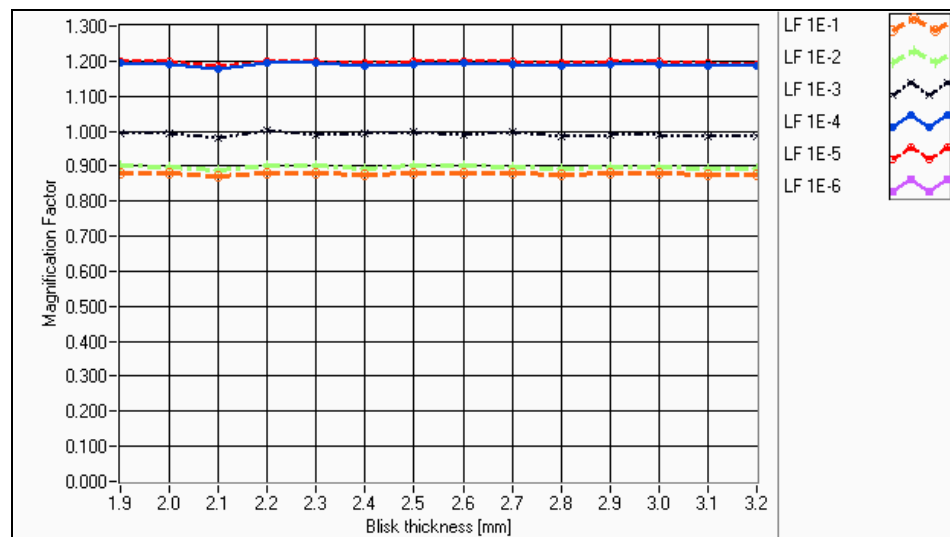


Figure 7.12 Magnification factor plots calculated at 0 rev/min; 12 ND mode

7.5.2 Rotating conditions

Repeating the same procedure used for the models with blade tip gap variation with this case, the modal analysis solution was run under rotating conditions. The set of rotational speeds were 600, 1200, 1800 and 2400 rev/min respectively. All modal data were used to run equation (7.1), using 6 damping loss factor levels, to obtain forced response levels then used to calculate the magnification factors. For this last section we would like to report only the results of 12 ND mode shape for all damping values. **Figure 7.13** shows results calculated at 600 rev/min and at 1200 rev/min, respectively. The results presented in both plots show equal responses between models and so the mistuning pattern adopted did not produced interesting results.

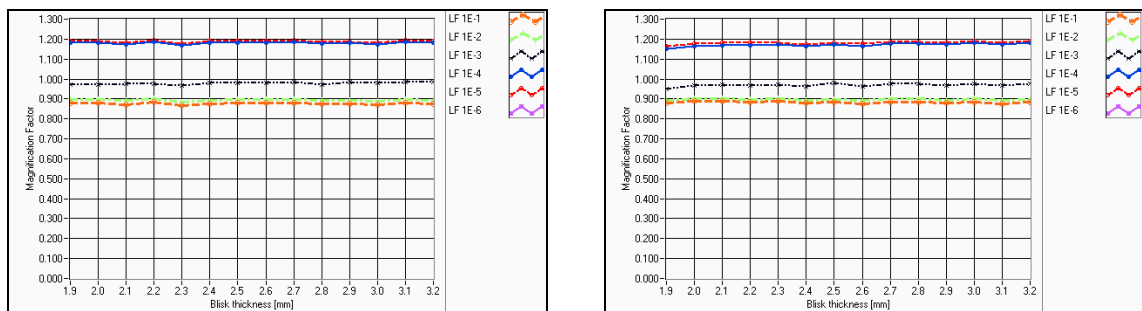


Figure 7.13 Magnification factor plots calculated at 600 rev/min and 1200 rev/min, respectively, for the 12 ND mode

Last two figures, **Figure 7.13** and **Figure 7.14**, respectively, show the calculation of forced response for rotational speed of 1800 rev/min and 2400 rev/min. Apparently, for these cases, the magnification factor grows as much as the blisk thickness.

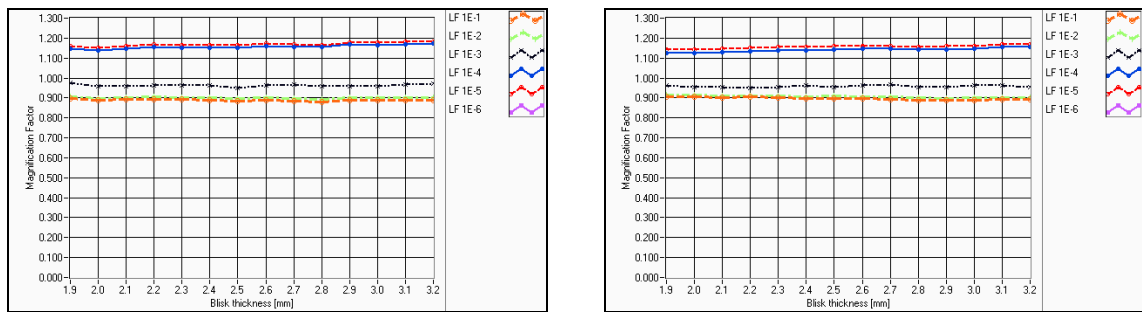


Figure 7.14 Magnification factor plots calculated at 1800 rev/min and 2400 rev/min, respectively, for the 12 ND mode

7.6 Conclusions

When this work was planned, it was not clear how interesting the results of the simulations might be or useful for a further stage of study. The large number of FE models considered limited a deeper study of this matter and this can only be considered an initial investigation. In fact, the numbers of modal analysis calculations, under stationary and rotating conditions, and the following forced response calculations were very extensive. Despite the effort, the plots presented did not give interesting insight, probably, because the light mistuning pattern superimposed to FE models which had one geometrical dimension varied such as blade tip gap or blisk thickness. Under stationary condition, both geometrical variations produced a flat magnification factor curves for any damping level adopted therefore the responses of mistuned models did not vary very much. The superposition of the rotational speed added an extra point of view on the analysis showing that the pattern of magnification factor curves could change from one speed to another. Therefore, blisk models more sensitive than others at one rotational speed flipped their dynamic behaviour at another speed. Even the analysis performed under rotating condition did not brought forward any interesting and useful information about the blisk sensitivity to geometrical

variation. Concluding this chapter, it can be said that this study was born from an intuition during the design stage of the 24-bladed disk. Despite the fact that the thesis is mainly focussed on measurement techniques for rotating structures such as bladed disks, we could obtain few answers from this additional investigation providing an initial direction for following studies on the interaction of the mistuning phenomenon and structural design optimization.

8 Conclusions and Suggestion for Further Work

8.1 Summary and Conclusions

The main goal of the presented study was to deliver a software platform which could perform a series of tasks using Continuous Scanning LDV methods, this software platform was called CAISER MYMESIS and the origin of the name was explained in Chapter 6. CAISER MYMESIS is a collection of all CSLDV methods which can be performed theoretically, via Virtual Test Simulation, and practically. The software platform was initially developed in combination with the design of a test piece, such as a 24-bladed disk, which was then used to carry out vibration measurements to prove the reliability of the CSLDV methods, under rotating and stationary conditions. Other important achievements obtained in this study are also summarized.

8.1.1 Overview of Tracking-CSLDV methods

In Chapter 2, we have seen how two new measurement methodologies have been developed by using an industrial standard Scanning LDV: Continuous Scanning LDV (CSLDV) and Tracking LDV (TLDV). It was anticipated that the possibility of combining these two techniques and performing continuous scan measurements while tracking a structure during operating condition, could offer enormous advantages. Hence, in Chapter 3 the way to combine those two methodologies into a Tracking-CSLDV was studied in detail and so the scanning

mirrors and encoder were presented as main contributors to this development. Finally, the waveforms required to achieve a specific scanning path, either mono-dimensional or bi-dimensional, were presented together with the control panels which actually drive the scanning mirrors via an output DAC card installed in the computer. The ability of performing a synchronous measurement over a rotating target by scanning the laser beam continuously over its surface led to describe a vibration measurement procedure mathematically, as presented in Chapter 5. Caiser Mymesis software platform can perform Virtual Test Simulations (VTS) which is a powerful mathematical approach to represent measurement procedures. All mathematical equations are coded in control panels of CAISER MYMESIS which play a double role of: (i) teaching continuous tracking scanning methodologies, and (ii) helping to identify the best measurement parameters. The entire philosophy is focussed on the reconstruction of ODSs from LDV output time signals. So, the VTS panels take into account sources of noise such as speckle noise, misalignment, mirror phase lag and other sources to reproduce an LDV time history which is realistic as possible a representation of a measured one. This allows selection of the optimum parameters to carry out a vibration measurement from which to obtain a reliable ODS reconstruction. The long path to the Tracking-CSLDV study ends with a presentation of the practical applications in which tracking methods were used to carry out measurements, as presented in Chapter 6. The simplest synchronous measurement technique is represented by a Point Tracking method which was mainly employed for the measurement of FRFs, under rotating conditions, in order to demonstrate the effect of Coriolis forces on bladed discs, where those forces can produce a frequency split of all nodal diameter modes' resonances. We successfully measured the frequency splits at several rotational speeds and the post-processing of the data showed the backward and forward travelling waves associated with each resonance. When blades have narrow

widths, and the torsional modes are not excited, then the Line Tracking method is a simple and powerful technique. Some examples were provided, despite the fact that Line Tracking was not necessary for most of the applications under study. The last and most impressive results of ODS measurements were obtained from the Area Tracking method. Examples of ODSs measured from the vibrating surface of a single blade rotating in a range of speed between 0 and 2400 rev/min are presented. Furthermore, this method could prove its ability of mode shape identification where high modal density is present, specifically when two families of modes veer together or/and apart. The most impressive example is the ODS measurement capability of the whole 24-bladed disc measured under rotating conditions and compared with a simulated one. The ODS recovery was obtained from one single measurement; in fact the laser beam scanned continuously all 24 blades while rotating.

8.1.2 Test rig and USAF IBR design

In Chapter 4 we have presented the original design of the test rig which was made during an earlier project. Clearly, the test rig had to be modified to fulfil the requirements of the new measurement technique developed here which required less mechanical components to perform the tracking and so the overall assembly was lighter. Although the Engine Order (EO) excitation method, achieved by using a fixed DC magnet, was retained, a new excitation method had to be developed in order to be able to measure FRFs under rotating conditions. The use of AC magnets is resulted to be very helpful for this purpose and it could be use either fixed in space or rotating. The rotating exciter was extremely useful for measurement of the FRFs which were used to measure the frequency split due to the effect of the Coriolis forces on the swept bladed disk and, once post-processed by modal analysis, to animate the backward and

forward travelling waves of the ND modes studied. The last component of the presented research study was the design of the 24-bladed disk which was produced during the development of the T-CSLDV methods and, in fact, the area pattern was decided upon the geometrical shape of the blade. The design of the blisk was made in collaboration with Carnegie Mellon University (CMU) which set a number of criteria, as presented in Chapter 4. Some of these can be summarized by saying that the 2nd flap-wise and 1st torsional families of modes had to be very close in frequency at rest and well separated at 2400 rev/min, the maximum rotational speed agreed, and the geometrical shape of the blade should allow the laser beam to sweep the surface easily. The designed blisk was of similar proportion to a fan blisk and was also used for other research studies, such as for the study of Coriolis forces. This specific design was so evaluated to study the dynamic behaviour of the blisk in the veering region. However, the measurement results obtained from this test piece are focussed on the achievement of the tracking capability up to 2400 rev/min and the reconstruction of the ODSs at different rotational speeds, as presented in Chapter 6. The large amount of time spent on the blisk design gave a chance to open the way to another study focussed on the geometrical sensitivity of a bladed disk when a mistuning pattern is superimposed. The results of this additional research study are presented in Chapter 7. Unfortunately, the large number of FE models considered limited a deeper study of this matter and this can only be considered an initial investigation. However, the results of several forced response calculations have indicated that when one geometrical parameter is varied, that can lead to a higher or a smaller level of forced response for a mistuned blisk model. Either varying the blade tip gap, or the blisk thickness dimensions, it is seen that the superimposition of a light mistuning pattern can produce different levels of forced response.

8.2 Future Work

The overall project was very extensive but all of the main objectives were achieved. Nevertheless, there are some aspects can still be studied further and improved. We would like to give some suggestions and directions for additional work which can be developed in future.

The scanning device is one of the main contributors to the achievement of the tracking capability. For the presented study an industrial-standard SLDV was used to develop the T-CLSDV methods. The laser head is already equipped with a scanning device which copes very well with all tasks requiring Step-Scanning LDV methodology. The performance of that device is still good when CSLDV methods are used for static measurements but when tracking must be performed then the performance could not be optimal. In fact, the large scanning mirrors mounted are important because the wider the mirror area is, the more back scattered light can be collected from the laser beam, thereby improving the Signal-To-Noise Ratio (SNR). Clearly, this means that there is more inertia and this may reduce the efficiency of the scanning system when a target must be followed at high speed. Another drawback of having a scanning device in-built in the laser head may be represented by the cost of a Scanning LDV system which, inevitably, might discourage buyers and limit the expansion of an alternative measurement technique. One suggestion would be to study a scanning device optimal for T-CSLDV methodologies and which may cover a wider range of applications as possible. Finally, the scanning device must be easily adaptable to any single point LDV system.

We have presented in Chapter 3 a possible alignment technique which was used to align the laser head to a rotating target. That method might be very tedious when carried out by users who have not experienced such an alignment method.

A suggestion for such a topic could be to study all degrees of freedom involved in the alignment process and, then, to design a procedure which can make simpler and faster the alignment procedure.

The rotating exciter was an innovative and helpful excitation method developed to measure FRFs under rotating conditions, for the first time. The actual design of the exciter has a speed limitation and, in fact, it is only functional up to a rotational speed of 1200 rev/min. However, the working speed range can be easily expanded by designing the exciter differently, especially the coupling between the brushes and slip-rings.

We have presented in Chapter 5 the significant potential of Virtual Test Simulations (VTS), especially when CSLDV methods are used, for simulation of LDV output time signal. We have explained that any simulation of LDV time history starts by using the polynomial coefficients obtained from the surface curve-fitting of a simulated ODS. One of the problems discovered during the simulations was due to the poor curve-fitting of an ODS when the structure is constrained and, in fact, it was showed that can lead to 'pseudo' vibrations. Hence, a suggestion in such a direction would be to recommend a study of a mathematical algorithm to improve the surface curve-fitting.

We have presented in Chapter 7 an initial study of geometrical sensitivity of a bladed disk when a mistuning pattern is superimposed. Time available to explore that idea further was very limited, and so it would be suggested to continue such a study trying, for example, to identify geometrical parameters which could make more sensitive the assembly to mistuning.

References

- [1] **Exploiting the laser scanning facility for vibration measurements**
Martarelli, -M.;
Dept. of Mech. Eng., Imperial Coll., London, UK
PhD Thesis
- [2] **Continuos-scan vibration measurements on moving components**
Stanbridge, -A. -B.; Martarelli, -M.; Ewins, -D. -J.
Dept. of Mech. Eng., Imperial Coll., London, UK
Proceeding of IMAC XX. A conference on structural dynamics. 4-7 February 2002; pp. 1519
- [3] **Rotating disc vibration analysis with a circular scanning LDV**
Stanbridge, -A. -B.; Martarelli, -M.; Ewins, -D. -J.
Dept. of Mech. Eng., Imperial Coll., London, UK
Proceeding of IMAC XIX. A conference on structural dynamics. 5-8 February 2001; pp. 464
- [4] **A comprehensive velocity sensivity model for scanning and tracking laser Doppler vibrometry on rotating structure**
Halkon, -B.; Rothberg, -S.
Wolfson Sch. Of Mechanical and Manufacturing Eng., Loughborough University (UK)
Proceedings-of-the-SPIE-The-International-Society-for-Optical-Engineering. 2002; 4827: 9-21
- [5] **Vibration measurements by tracking laser Doppler vibrometer on automotive components**
Castellini, -P.
Dipt. di Meccanica, Ancona Univ., Italy
Shock and Vibration, 2002; 9(1-2): 67-89
- [6] **Laser based measurement system for measuring the vibration of rotating discs**
I Bucher, P Schmiechen, D A Robb, D J Ewins.
Dept. of Mech. Eng., Imperial College, London, UK
First International Conference on vibration measurements by laser techniques.
Ancona, Italy, 3-5 October, 1994.
- [7] **Vibration measurements on blades of naval propeller rotating in water**
Castellini,-P.; Santolini,-C.
Dipt. di Meccanica, Ancona Univ., Italy
Proceedings-of-the-SPIE-The-International-Society-for-Optical-Engineering. 1996; 2868: 186-94
- [8] **Tracking laser Doppler vibrometer for linear motion: application to a timing belt**
Castellini,-P.; Cupido,-E.; Paone,-N.; Tomasini,-E.-P.
Dipt. di Meccanica, Ancona Univ., Italy
Proceedings-of-the-SPIE-The-International-Society-for-Optical-Engineering. 2000; 4072: 194-200
- [9] **Vibration measurements on rolling tyres by Tracking Laser Doppler Vibrometer**
Castellini,-P.; Cupido,-E.; Baldoni,-F.; Ingenito,-G.
Dipt. di Meccanica, Ancona Univ., Italy
Proceedings-of-the-SPIE-The-International-Society-for-Optical-Engineering. 2000; 4072: 169-75

-
- [10] **Vibration measurements on wind-screen wipers by tracking laser Doppler vibrometer**
Castellini, -P.; Cupido, -E.
Dipt. di Meccanica, Ancona Univ., Italy
Proceeding of IMAC-XIX. A conference on structural dynamics. 3-6 February 2003; pp.457
- [11] **Novel image tracking laser Doppler vibrometer for application on automotive field**
Castellini, -P.; Tomasini, -E. -P.
Dipt. di Meccanica, Ancona Univ., Italy
Proceeding of IMAC XX. A conference on structural dynamics.4-7 February 2002;
pp.1004
- [12] **Tracking scanning laser Doppler vibrometer: extending laser vibrometer to arbitrarily objects**
Bendel, -K; Scelles, -N.; Dietzhausen, -H.
Corporate research- Applied physics; Robert Bosh GmbH
Proceeding of IMAC-XXI
- [13] **Synchronized-Scanning Laser Vibrometry**
Halkon, -B.; Rothberg, -S.
Wolfson Sch. Of Mechanical and Manufacturing Eng., Loughborough University (UK)
Proceedings-of-the-SPIE-The-International-Society-for-Optical-Engineering. 2004; 5503:
260-271
- [14] **Large-bandwidth reflection fiber-optics sensor for turbomachinery rotor blade diagnostic**
Rossi,-G.-L.; Paone, N.; Andrelli, L.
Dipartimento di Meccanica, Ancona Univ., Italy
Sensors and Actuators A, 32. (1992); 539-542
- [15] **An improved single-parameter tip-timing method for turbomachinery blade vibration measurements using optical laser probes**
Heath, S.; Imrengun. M.
Dept. of Mech. Eng., Imperial College, London, UK
Int. Journal Mech. Sci. 1996 Vol.38, N.10;1047-1058
- [16] **A fiber-optics laser Doppler probe for vibration analysis of rotating machines**
Cookson,-R.-A.; Bandyopadhyay,-P.
Sch. of Mech. Eng., Cranfield Inst. Of Technology; Bedford (UK)
Journal of Engineering for Power July 1980, Vol.102; 607-612
- [17] **Noncontact vibration measurements on compressor rotor blades**
Zielinski,-M.; Ziller,-G.
Elect. And Measurement Technology division, MTU (Germany)
Meas. Sci. Technol. 11 (2000) 847-856
- [18] **Laser vibrometry measurements of rotating blade vibrations**
Reinhardt,-K.-A.; Kadambi,-R.-J.; Quinn,-R.-D.
Dep. Mech. And Aerospace Eng. Case Western Reserve University, Cleveland (USA)
Journal of Engineering for Gas Turbines and Power July 1995, Vol.117; 484-488
- [19] **Vibration measurements in a rotating blisk test rig using an LDV**
Stanbridge, -A.-B.; Sever, -I., A.; Ewins, -D.-J.
Dept. of Mech. Eng., Imperial Coll., London, UK
Proceedings-of-the-SPIE-The-International-Society-for-Optical-Engineering. 2002; 4827:
1-8
- [20] **Principles and practice of the laser Doppler anemometry (second edition)**
Durst,-F.; Melling,-A.; Whitelaw,-J.-H.
London: Academic Press

-
- [21] **The laser torsional vibrometer: a step forward in rotating machinery diagnostic**
Halliwell, N. A.
Wolfson Sch. Of Mechanical and Manufacturing Eng., Loughborough University (UK)
Journal of Sound and Vibration 1996; 190(3), 399-418
- [22] **Non-invasive measurements of damage of fresco paintings and icon by laser scanning vibrometer: experimental results on artificial samples and real works of art**
Castellini,-P.; Esposito,-E.; Paone,-N.; Tomasini,-E.-P.
Dipt. di Meccanica, Ancona Univ., Italy
Measurement-. 2000; 28(1): 33-45
- [23] **Measurement of rotational vibrations using a novel interferometric technique**
Lewin,-A.-C.; Volkmar,-R.; Siegmund,-G.
Polytec GmbH, (Germany)
Measurement 16 (1995); 81-90
- [24] **Laser rotational vibrometer and their application in the modal analysis**
Rothberg, -S.
Wolfson Sch. Of Mechanical and Manufacturing Eng., Loughborough University (UK)
Proceeding of IMAC XXI. A conference on structural dynamics. 3-6 February 2003; pp. 333
- [25] **Laser vibrometer and contacting transducer, target rotation and six degree-of-freedom vibration: what do we really measure?**
Bell, R. J.; Rothberg, S.
Wolfson Sch. Of Mechanical and Manufacturing Eng., Loughborough University (UK)
Journal of Sound and Vibration 2000; 237(2), 245-261
- [26] **Rotational vibration measurement using laser Doppler vibrometry: comprehensive theory and practical application**
Bell, R. J.; Rothberg, S.
Wolfson Sch. Of Mechanical and Manufacturing Eng., Loughborough University (UK)
Journal of Sound and Vibration 2000; 238(4), 673-679
- [27] **Torsional and bending vibration measurement on rotors using laser technology**
Hocknell, A.; Rothberg, S.; Lucas, A.; Halliwell, N. A.
Wolfson Sch. Of Mechanical and Manufacturing Eng., Loughborough University (UK)
Journal of Sound and Vibration 1999; 226(3), 441-467
- [28] **Polytec GmbH**
Private communication
- [29] **Sensitivity of tuned bladed disk response to frequency veering**
J.A.Kenyon, J.H.Griffin, N.E. Kim
Journal of Engineering for Gas turbine and Power, October 2005, Vol.127
- [30] **The effects of Coriolis forces on vibration properties of bladed discs**
M.Nikolic, D.J.Ewins, E.P.Petrov, Dario Di Maio
7th IFT0MM-Conference on Rotor Dynamics, Vienna, Austria, 25-28 September 2006
- [31] **Experimental of Turbomachinery blade vibration predictions**
I.A.Severe
PhD thesis, Imperial College London, March 2004
- [32] **Synchronized-Scanning Laser Vibrometry**
Halkon, -B.; Rothberg, -S.
Wolfson Sch. Of Mechanical and Manufacturing Eng., Loughborough University (UK)
Proceedings-of-the-SPIE-The-International-Society-for-Optical-Engineering. 2004; 5503: 260-271

References

- [33] **Coriolis Forces in Forced Response Analysis of Mistuned Bladed Discs**
M.Nikolic, E.P.Petrov, D.J.Ewins
Proceeding of ASME Turbo Expo 2006, Power for Land and Air.

Bibliography

- [1] **Vibration measurement on artificial heart valve by laser Doppler vibrometer**
Castellini,-P.; Huebner, -M.; Pinotti, -M.
Dipt. di Meccanica, Ancona Univ., Italy
Proceeding of IMAC XXI. A conference on structural dynamics. 3-6 February 2003; #171
- [2] **Laser Doppler vibrometry for the characterization of the dynamic behaviour of structures excited by piezoelectric exciters**
Martarelli,-M.; Revel,-G.-M.
Dipt. di Meccanica, Ancona Univ., Italy
Proceeding of IMAC XXI. A conference on structural dynamics. 3-6 February 2003; #167
- [3] **A new vibration measurement procedure for on-line quality control of electronic devices**
Revel,-G.-M.
Dipt. di Meccanica, Ancona Univ., Italy
Shock-and-Vibration. 2002; 9(1-2): 3-10
- [4] **Automotive components vibration measurements by tracking laser Doppler vibrometry: advances in signal processing**
Castellini,-P.; Montanini,-R.
Dipt. di Meccanica, Ancona Univ., Italy
Measurement-Science-&-Technology. 2002; 13(8): 1266-79
- [5] **Vibration measurements by tracking laser Doppler vibrometer on automotive components**
Castellini, -P.
Dipt. di Meccanica, Ancona Univ., Italy
Shock and Vibration, 2002; 9(1-2): 67-89
- [6] **New applications of scanning laser Doppler vibrometry (SLDV) to non-destructive diagnostics of artworks: mosaics, ceramics, inlaid wood and easel painting**
Castellini,-P.; Esposito,-E.; Marchetti,-B.; Paone,-N.; Tomasini,-E.-T.
Dipt. di Meccanica, Ancona Univ., Italy
Journal of Cultural Heritage, 2002
- [7] **Novel image tracking laser Doppler vibrometer for application on automotive field**
Castellini, -P.; Tomasini, -E. -P.
Dipt. di Meccanica, Ancona Univ., Italy
Proceeding of IMAC XX. A conference on structural dynamics.4-7 February 2002; pp.1004
- [8] **A new approach to the measurement of transverse vibration and acoustic radiation of automotive belts using laser Doppler vibrometry and acoustic intensity techniques**
Di-Sante,-R.; Rossi,-G.-L.
Dipt. di Meccanica, Ancona Univ., Italy
Measurement-Science-&-Technology. 2001; 12(4): 525-33
- [9] **Automated modal analysis by scanning laser vibrometry: Problems and uncertainties associated with the scanning system calibration**
Martarelli, -M; Revel, -GM; Santolini, -C
Dept. of Mech. Eng., Imperial College, London, UK
Dipt. di Meccanica, Ancona Univ., Italy
Mech Syst Signal Process. Vol. 15, no. 3, pp. 581-601. May 2001

- [10] **Vibration measurements on wind-screen wipers by tracking laser Doppler vibrometer**
Castellini, -P.; Cupido, -E.
Dipt. di Meccanica, Ancona Univ., Italy
Proceeding of IMAC-XIX. A conference on structural dynamics. 3-6 February 2003; pp.457
- [11] **Tracking laser Doppler vibrometer for linear motion: application to a timing belt**
Castellini,-P.; Cupido,-E.; Paone,-N.; Tomasini,-E.-P.
Dipt. di Meccanica, Ancona Univ., Italy
Proceedings-of-the-SPIE-The-International-Society-for-Optical-Engineering. 2000; 4072: 194-200
- [12] **Development of the tracking laser vibrometer: Performance and uncertainty analysis**
Castellini,-P.; Paone,-N.
Dipt. di Meccanica, Ancona Univ., Italy
Review-of-Scientific-Instruments. 2000; 71(12): 4639-47
- [13] **Measurement techniques for the acoustic analysis of synchronous belts**
Di-Sante,-R.; Revell,-G.-M.; Rossi,-G.-L.
Dipt. di Meccanica, Ancona Univ., Italy
Measurement-Science-&-Technology. 2000; 11(10): 1463-72
- [14] **Quality control of electronic devices by vibration analysis**
Di-Giulio,-G.; Nicolini,-A.; Revel,-G.-M.; Tomasini,-E.-P.
Dipt. di Meccanica, Ancona Univ., Italy
Proceedings-of-the-SPIE-The-International-Society-for-Optical-Engineering. 2000; 4072: 434-9
- [15] **Laser vibration measurement for damage detection on composite materials: advances in signal processing**
Castellini,-P.; Revel,-G.-M.
Dipt. di Meccanica, Ancona Univ., Italy
Proceedings-of-the-SPIE-The-International-Society-for-Optical-Engineering. 2000; 4072: 442-52
- [16] **Application of lasers for noncontact excitation and measurement of vibration**
Castellini,-P.; Revel,-G.-M.; Scalise,-L.
Dipt. di Meccanica, Ancona Univ., Italy
Proceedings-of-the-SPIE-The-International-Society-for-Optical-Engineering. 2000; 4072: 280-91
- [17] **Vibration measurements on rolling tyres by Tracking Laser Doppler Vibrometer**
Castellini,-P.; Cupido,-E.; Baldoni,-F.; Ingenito,-G.
Dipt. di Meccanica, Ancona Univ., Italy
Proceedings-of-the-SPIE-The-International-Society-for-Optical-Engineering. 2000; 4072: 169-75
- [18] **Non-invasive measurements of damage of fresco paintings and icon by laser scanning vibrometer: experimental results on artificial samples and real works of art**
Castellini,-P.; Esposito,-E.; Paone,-N.; Tomasini,-E.-P.
Dipt. di Meccanica, Ancona Univ., Italy
Measurement-. 2000; 28(1): 33-45
- [19] **SLDV (scanning laser Doppler vibrometry) for the analysis of defects in teeth cavity resin filling**
Esposito,-E.; Putignano,-A.; Rappelli,-G.; Scalise,-L.
Dipt. di Meccanica, Ancona Univ., Italy
Proceedings-of-the-SPIE-The-International-Society-for-Optical-Engineering. 1999; 3585: 378-88

- [20] **Non-destructive diagnostics of layered structures: advanced signal analysis algorithms applied to vibrometric data**
Tomasini,-E.-P.; Piazza,-F.; Esposito,-E.; Possanzini,-M.
Dipt. di Meccanica, Ancona Univ., Italy
Proceedings-of-the-SPIE-The-International-Society-for-Optical-Engineering. 1999; 3897: 272-82
- [21] **Non-invasive measurements of structural damage by laser scanning vibrometer: an experimental comparison among different exciters**
Castellini,-P.; Esposito,-E.; Paone,-N.; Tomasini,-E.-P.
Dipt. di Meccanica, Ancona Univ., Italy
Proceedings-of-the-SPIE-The-International-Society-for-Optical-Engineering. 1999; 3585: 304-15
- [22] **Experimental and numerical investigation on structural effects of laser pulses for modal parameter measurement**
Castellini,-P.; Revel,-G.-M.; Scalise,-L.; De-Andrade,-R.-M.
Dipt. di Meccanica, Ancona Univ., Italy
Optics-and-Lasers-in-Engineering. 1999; 32(6): 565-81
- [23] **Sound power estimation by laser Doppler vibration measurement techniques**
Revel,-G.-M.; Rossi,-G.-L.
Dipt. di Meccanica, Ancona Univ., Italy
Shock-and-Vibration. 1998; 5(5-6): 297-305
- [24] **Vibration measurements on blades of a naval propeller rotating in water with tracking laser vibrometer**
Castellini,-P.; Santolini,-C.
Dipt. di Meccanica, Ancona Univ., Italy
Measurement-. July 1998; 24(1): 43-54
- [25] **Dynamic characterization of teeth by laser vibrometry**
Castellini,-P.; Miglietta,-G.; Revel,-G.-M.; Scalise,-L.
Dipt. di Meccanica, Ancona Univ., Italy
Proceedings-of-the-SPIE-The-International-Society-for-Optical-Engineering. 1998; 3411: 581-9
- [26] **Damage detection and characterization by processing laser vibrometer measurement results: application to composite materials**
Castellini,-P.; Revel,-G.-M.
Dipt. di Meccanica, Ancona Univ., Italy
Proceedings-of-the-SPIE-The-International-Society-for-Optical-Engineering. 1998; 3411: 458-68
- [27] **The application of a laser scanning vibrometer for dynamic characterization of large impellers**
Rossi, G. L., Santolini C., Giachi M., Generosi S.
Dipt. di Meccanica, Ancona Univ., Italy
Nuovo Pignone S.P.A. (Italy)
Measurement 24 (1998) 33-41
- [28] **Vibration measurements on blades of naval propeller rotating in water**
Castellini,-P.; Santolini,-C.
Dipt. di Meccanica, Ancona Univ., Italy
Proceedings-of-the-SPIE-The-International-Society-for-Optical-Engineering. 1996; 2868: 186-94

- [29] **Hand-arm vibration measurement by a laser scanning vibrometer**
Rossi,-G.-L.; Tomasini,-E.-P.
Dipartimento di Meccanica, Ancona Univ., Italy
Measurement-. Oct. 1995; 16(2): 113-24
- [30] **Large-bandwidth reflection fiber-optics sensor for turbomachinery rotor blade diagnostic**
Rossi,-G.-L.; Paone, N.; Andrelli, L.
Dipartimento di Meccanica, Ancona Univ., Italy
Sensors and Actuators A, 32. (1992); 539-542
- [31] **Line coupling of axisymmetric substructures using a continuously-scan LDV**
Stanbridge, -A.-B.; Ind, -P.-R.; Ewins, -D.-J.
Dept. of Mech. Eng., Imperial Coll., London, UK
Proceeding of IMAC XXI. A conference on structural dynamics. 3-6 February 2003; pp. 165
- [32] **Vibration measurements in a rotating blisk test rig using an LDV**
Stanbridge, -A.-B.; Sever, -I., A.; Ewins, -D.-J.
Dept. of Mech. Eng., Imperial Coll., London, UK
Proceedings-of-the-SPIE-The-International-Society-for-Optical-Engineering. 2002; 4827: 1-8
- [33] **Using continuous-scan LDV data for FE model validation in the presence of 'Close' modes**
Stanbridge,-A.-B.; Ewins,-D.-J
Dept. of Mech. Eng., Imperial Coll., London, UK
International Conference on on Structural Dynamic Modelling; 3-5 June 2002 Madeira Portugal
- [34] **Measuring mode shapes with a continuously scanning laser vibrometer-Hilbert transform approach**
Kang,-M.-S.; Stanbridge,-A.-B.; Chang,-T.-G.; Kim,-H.-S.
Dept. of Mech. Eng., Kyungwon Univ., Kyunggi-Do, South Korea
Mechanical-Systems-and-Signal-Processing. March-May 2002; 16(2-3): 201-10
- [35] **Continuous-scan vibration measurements on moving components**
Stanbridge, -A. -B.; Martarelli, -M.; Ewins, -D. -J.
Dept. of Mech. Eng., Imperial Coll., London, UK
Proceeding of IMAC XX. A conference on structural dynamics. 4-7 February 2002; pp. 1519
- [36] **Automated modal analysis by scanning laser vibrometry: Problems and uncertainties associated with the scanning system calibration**
Martarelli, M; Revel, GM; Santolini, C
Dept. of Mech. Eng., Imperial College, London, UK
Dipt. di Meccanica, Ancona Univ., Italy
Mech Syst Signal Process. Vol. 15, no. 3, pp. 581-601.2001
- [37] **Rotating disc vibration analysis with a circular scanning LDV**
Stanbridge, -A. -B.; Martarelli, -M.; Ewins, -D. -J.
Dept. of Mech. Eng., Imperial Coll., London, UK
Proceeding of IMAC XIX. A conference on structural dynamics. 5-8 February 2001; pp. 464

- [38] **Reference-free mode shape identification with a continuously scanning laser Doppler vibrometer (SLDV)**
Ho,-Y.; Ewins,-D.-J.
Dept. of Mech. Eng., Imperial Coll., London, UK
Proceedings-of-the-SPIE-The-International-Society-for-Optical-Engineering. 2001; 4317: 604-9
- [39] **Exploiting the laser scanning facility for vibration measurements**
Martarelli, -M.;
Dept. of Mech. Eng., Imperial Coll., London, UK
PhD Thesis
- [40] **Measuring strain response mode shapes with a continuous-scan LDV**
Stanbridge,-A.-B.; Martarelli,-M.; Ewins,-D.-J.
Dept. of Mech. Eng., Imperial College, London, UK
Proceedings-of-the-SPIE-The-International-Society-for-Optical-Engineering. 2000; 4072: 160-8
- [41] **Measuring area vibration mode shapes with a continuous-scan LDV**
Stanbridge,-A.-B.; Martarelli,-M.; Ewins,-D.-J.
Dept. of Mech. Eng., Imperial College, London, UK
Proceedings-of-the-SPIE-The-International-Society-for-Optical-Engineering. 2000; 4072: 176-83
- [42] **Scanning laser Doppler vibrometer applied to impact modal testing**
Stanbridge, AB; Martarelli, M; Ewins, DJ
Dept. of Mech. Eng., Imperial College, London, UK
Shock and Vibration Digest Vol. 32, no. 1, 35 p. Jan 2000
- [43] **Modal testing using a scanning laser Doppler vibrometer**
Stanbridge,-A.-B.; Ewins,-D.-J.
Dept. of Mech. Eng., Imperial College, London, UK
Mechanical-Systems-and-Signal-Processing. March 1999; 13(2): 255-70
- [44] **Detecting damage in vibrating structures with a scanning LDV**
Khan,-A.-Z.; Stanbridge,-A.-B.; Ewins,-D.-J.
Dept. of Mech. Eng., Imperial College, London, UK
Optics-and-Lasers-in-Engineering. Dec. 1999; 32(6): 583-92
- [45] **Measuring area mode shapes with a scanning laser Doppler vibrometer**
Stanbridge A. B., Martarelli M., Ewins D. J.
Dept. of Mech. Eng., Imperial College, London, UK
Proceeding of IMAC XVII. A conference on structural dynamics. February 2003;
- [46] **Modal testing using impact excitation and a scanning LDV**
Stanbridge,-A.-B.; Khan,-A.-Z.; Ewins,-D.-J.
Dept. of Mech. Eng., Imperial College, London, UK
Proceedings-of-the-SPIE-The-International-Society-for-Optical-Engineering. 1998; 3411: 348-56
- [47] **Scanning laser Doppler vibrometer measurements for vibrating beam modal updating**
Stanbridge A. B., Ewins D. J.
Dept. of Mech. Eng., Imperial Coll., London, UK
Society for Experimental Mechanics, Inc., 16th International Modal Analysis Conference. Volume II (USA), pp. 1498-1504, 1998

-
- [48] **Measurement of total vibration at a point using a conical-scanning LDV**
Stanbridge,-A.-B.; Ewins,-D.-J.
Dept. of Mech. Eng., Imperial College, London, UK
Proceedings-of-the-SPIE-The-International-Society-for-Optical-Engineering. 1996; 2868:
126-36
- [49] **Measurement of translational and angular vibration using a scanning laser Doppler vibrometer**
Stanbridge, -A. -B; Ewins, -D., -J.
Dept. of Mech. Eng., Imperial College, London, UK
Shock and Vibration 1996 (3) 141-152
- [50] **An improved single-parameter tip-timing method for turbomachinery blade vibration measurements using optical laser probes**
Heath, S.; Imrengun. M.
Dept. of Mech. Eng., Imperial College, London, UK
Int. Journal Mech. Sci. 1996 Vol.38, N.10;1047-1058
- [51] **Modal testing of rotating discs using a scanning LDV**
Stanbridge A. B., Ewins D. J.
Dept. of Mech. Eng., Imperial College, London, UK
Proceedings Design Technical Conf: Acoustics Vibrations And Rotating Machines:
Volume 3 Part B DE -Vol. 84-2; 1202-1213 AMSE, Boston 1995
- [52] **Structural modal analysis using a scanning laser Doppler vibrometer**
Stanbridge A. B., Ewins D. J.
Dept. of Mech. Eng., Imperial College, London, UK
R. Ae. Soc. International Forum on Aerolasticity and Structural Dynamics. Manchester
26-28 June 1995
- [53] **Laser based measurement system for measuring the vibration of rotating discs**
I Bucher, P Schmiechen, D A Robb, D J Ewins.
Dept. of Mech. Eng., Imperial College, London, UK
First International Conference on vibration measurements by laser techniques.
Ancona, Italy, 3-5 October, 1994.
- [54] **Spatially continuous power flow using a scanning laser Doppler vibrometer.**
Blotter,-J.-D.; West,-R.-L.; Sommerfeldt,-S.-D.
Mech. Eng. Dept., Brigham Young Univ., Provo, UT, USA
Transactions-of-the-ASME.-Journal-of-Vibration-and-Acoustics. Oct. 2002; 124(4): 476-82
- [55] **Measuring mode shapes with a continuously scanning laser vibrometer-Hilbert transform approach**
Kang,-M.-S.; Stanbridge,-A.-B.; Chang,-T.-G.; Kim,-H.-S.
Dept. of Mech. Eng., Kyungwon Univ., Kyunggi-Do, South Korea
Mechanical-Systems-and-Signal-Processing. March-May 2002; 16(2-3): 201-10
- [56] **Two-axis-scanning laser Doppler vibrometer for precision engineering**
Venkatakrishnan,-K.; Tan,-B.; Ngoi,-B.-K.-A.
Sch. of Mech. & Production Eng., Nanyang Technol. Univ., Singapore
Optics-and-Lasers-in-Engineering. Sept. -Oct. 2002; 38(3-4): 153-71
- [57] **Noncontact acousto-optic scanning heterodyne laser vibrometer for measurement of dynamics parameter of hard disc**
Ngoi,-B.-K.; Venkatakrishnan,-K.; Tan,-B.; Chin,-C.-S.
Sch. of Mech. & Production Eng., Nanyang Technol. Univ., Singapore
Proceedings-of-the-SPIE-The-International-Society-for-Optical-Engineering. 2000; 4072:
2-7

- [58] **Two-axis-scanning laser Doppler vibrometer for microstructure**
 Ngoi,-B.-K.-A.; Venkatakrishnan,-K.; Tan,-B.; Noel,-N.; Shen,-Z.-W.; Chin,-C.-S.
 Nanyang Technol. Inst., Singapore
 Optics-Communications. 1 Aug. 2000; 182(1-3): 175-85
- [59] **Laser scanning heterodyne-interferometer for micro-components**
 Ngoi,-B.-K.-A.; Venkatakrishnan,-K.; Bo-Tan
 Sch. of Mech. & Production Eng., Nanyang Technol. Inst., Singapore
 Optics-Communications. 1 Jan. 2000; 173(1-6): 291-301
- [60] **Broadband vibration measurements using a continuously scanning laser vibrometer**
 Vanlanduit,-S.; Guillaume,-P.; Schoukens,-J.
 Dept. of Mech. Eng., Vrije Univ., Brussels, Belgium
 Measurement-Science-&-Technology. Oct. 2002; 13(10): 1574-82
- [61] **Linear and nonlinear damage detection using a scanning laser vibrometer**
 Vanlanduit,-S.; Guillaume,-P.; Schoukens,-J.; Parloo,-E.
 Dept. of Electr. Eng., Vrije Univ., Brussels, Belgium
 Proceedings-of-the-SPIE-The-International-Society-for-Optical-Engineering. 2000; 4072:
 453-66
- [62] **Damage detection using finite element and laser operational deflection shapes**
 Waldron,-K.; Ghoshal,-A.; Schulz,-M.-J.; Sundaresan,-M.-J.; Ferguson,-F.; Pai,-R.; Chung,-
 J.-H.
 Dept. of Mech. Eng., North Carolina A&T State Univ., Greensboro, NC, USA
 Finite-Elements-in-Analysis-and-Design. Jan. 2002; 38(3): 193-226
- [63] **Vibration suppression using a laser vibrometer and piezoceramic patches**
 Ghoshal,-A.; Wheater,-E.-A.; Ashok-Kumar,-C.-R.; Sundaresan,-M.-J.; Schulz,-M.-J.;
 Human,-M.; Pai,-P.-F.
 Dept. of Mech. Eng., North Carolina Univ., Greensboro, NC, USA
 Journal-of-Sound-and-Vibration. 10 Aug. 2000; 235(2): 261-80
- [64] **Structural health monitoring techniques for wind turbine blades**
 Ghoshal, Anindya; Sundaresan, Mannur J; Schulz, Mark J; Pai, Pfrank
 North Carolina A&T State Univ, Greensboro, NC, USA
 Journal of Wind Engineering and Industrial Aerodynamics [J WIND
 ENG IND AERODYN]. Vol. 85, no. 3, pp. 309-324. 2000
- [65] **Laser rotational vibrometer and their application in the modal analysis**
 Rothberg, -S.
 Wolfson Sch. Of Mechanical and Manufacturing Eng., Loughborough University (UK)
 Proceeding of IMAC XXI. A conference on structural dynamics. 3-6 February 2003; pp.
 333
- [66] **A comprehensive velocity sensitivity model for scanning and tracking laser Doppler
 vibrometry on rotating structure**
 Halkon, -B.; Rothberg, -S.
 Wolfson Sch. Of Mechanical and Manufacturing Eng., Loughborough University (UK)
 Proceedings-of-the-SPIE-The-International-Society-for-Optical-Engineering. 2002; 4827:
 9-21
- [67] **Laser vibrometer and contacting transducer, target rotation and six degree-of-freedom
 vibration: what do we really measure?**
 Bell, R. J.; Rothberg, S.
 Wolfson Sch. Of Mechanical and Manufacturing Eng., Loughborough University (UK)
 Sound and Vibration 2000; 237(2), 245-261

- [68] **Rotational vibration measurement using laser Doppler vibrometry: comprehensive theory and practical application**
Bell, R. J.; Rothberg, S.
Wolfson Sch. Of Mechanical and Manufacturing Eng., Loughborough University (UK)
Sound and Vibration 2000; 238(4), 673-679
- [69] **Torsional and bending vibration measurement on rotors using laser technology**
Hocknell, A.; Rothberg, S.; Lucas, A.; Halliwell, N. A.
Wolfson Sch. Of Mechanical and Manufacturing Eng., Loughborough University (UK)
Sound and Vibration 1999; 226(3), 441-467
- [70] **Remote vibration measurements: compensation of the wave form distortion due to the whole body translations**
Hocknell, A.; Rothberg, S.; Jones, R.
Wolfson Sch. Of Mechanical and Manufacturing Eng., Loughborough University (UK)
Sound and Vibration 1998; 214(2), 285-307
- [71] **The laser torsional vibrometer: a step forward in rotating machinery diagnostic**
Halliwell, N. A.
Wolfson Sch. Of Mechanical and Manufacturing Eng., Loughborough University (UK)
Sound and Vibration 1996; 190(3), 399-418
- [72] **Detection of defects in circular plates using a scanning Laser Vibrometer**
Franck Pai P., Yunje Oh, Seung-Yoon Lee
Dept. of Mech. & Aerosp. Eng., Missouri Univ., Columbia, MO, USA
Sage Publications, Vol. 1(1) : 0063-88
- [73] **Damage detection of beams using operational deflection shape**
Pai,-P.-F.; Young,-L.-G.
Dept. of Mech. & Aerosp. Eng., Missouri Univ., Columbia, MO, USA
International-Journal-of-Solids-and-Structures. May 2001; 38(18): 3161-92
- [74] **Structural damage detection and estimation using a scanning laser vibrometer**
Pai,-P.-F.; Seung-Yoon-Lee; Schulz,-M.-J.
Dept. of Mech. & Aerosp. Eng., Missouri Univ., Columbia, MO, USA
Proceedings-of-the-SPIE-The-International-Society-for-Optical-Engineering. 2001; 4335: 83-94
- [75] **Locating structural defects using operational deflection shapes**
Si-Jin; Pai,-P.-F.
Dept. of Mech. & Aerosp. Eng., Missouri Univ., Columbia, MO, USA
Journal-of-Intelligent-Material-Systems-and-Structures. Aug. 2000; 11(8): 613-30
- [76] **Circuit board operating shape and failure identification using a scanning laser velocimeter**
Roberts N., Kenkle S., Hansche B.
Sandia National Laboratories, California, USA
Dynamics Environments Workshop, 25-27 June 2002, El Segundo California
- [77] **Laser Doppler vibrometer-based anti-personnel mine detection**
Sabatier,-J.-M.; Ning-Xiang
Nat. Center for Phys. Acoust., Mississippi Univ., MS, USA
IGARSS-2001.-Scanning-the-Present-and-Resolving-the-Future.-Proceedings.-IEEE-2001-International-Geoscience-and-Remote-Sensing-Symposium-Cat.-No.01CH37217. 2001: 3093-5 vol.7









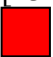

- [78] **An investigation of acoustic-to-seismic coupling to detect buried antitank landmines**
Sabatier,-J.-M.; Ning-Xiang
Nat. Center for Phys. Acoust., Mississippi Univ., MS, USA
IEEE-Transactions-on-Geoscience-and-Remote-Sensing. June 2001; 39(6): 1146-54
- [79] **Forward-looking acoustic mine detection system**
Costley,-R.-D.; Sabatier,-J.-M.; Ning-Xiang
Nat. Center for Phys. Acoust., Mississippi Univ., MS, USA
Proceedings-of-the-SPIE-The-International-Society-for-Optical-Engineering. 2001; 4394
pt. 1-2: 617-26
- [80] **Fusion of acoustic/seismic and ground penetrating radar sensors for antitank mine detection**
Bradley,-M.; Sabatier,-J.-M.; Witten,-T.; Duncan,-M.; Hawkins,-J.
Planning Syst. Inc., Long Beach, MS, USA
Proceedings-of-the-SPIE-The-International-Society-for-Optical-Engineering. 2001; 4394
pt. 1-2: 979-90
- [81] **Continuous scanning laser Doppler vibrometer for mine detection**
Costley,-R.-D.; Valeau,-V.; Ning-Xiang
Nat. Center for Phys. Acoust., Mississippi Univ., MS, USA
Proceedings-of-the-SPIE-The-International-Society-for-Optical-Engineering. 2000; 4038
pt. 1-2: 711-18
- [82] **Acoustic-to-seismic coupling and detection of landmines**
Sabatier,-J.-M.; Xiang,-N.
Nat. Center for Phys. Acoust., Mississippi Univ., MS, USA
IGARSS-2000.-IEEE-2000-International-Geoscience-and-Remote-Sensing-Symposium.-
Taking-the-Pulse-of-the-Planet:-The-Role-of-Remote-Sensing-in-Managing-the-
Environment.-Proceedings-Cat.-No.00CH37120. 2000: 1646-8 vol.4
- [83] **Increasing speckle noise immunity in LDV-based acoustic mine detection**
Goggans,-P.-M.; Smith,-C.-R.; Ning-Xiang
Dept. of Electr. Eng., Mississippi Univ., MS, USA
Proceedings-of-the-SPIE-The-International-Society-for-Optical-Engineering. 2000; 4038
pt. 1-2: 719-24
- [84] **Laser-Doppler vibrometer measurement of acoustic to seismic coupling**
Arnott,-W.-P.; Sabatier,-J.-M.
Nat. Center for Phys. Acoust., Mississippi Univ., MS, USA
Applied-Acoustics. 1990; 30(4): 279-91
- [85] **Laser Doppler, speckle and related techniques for blood perfusion mapping and imaging**
Briers,-J.-D.
Kingston Univ., Kingston-upon-Thames, UK
Physiological-Measurement. Nov. 2001; 22(4): R35-66
- [86] **High-speed 3D optical imaging and failure analysis of high- and low-frequency movements in micro-electro-mechanical systems (MEMS) with nanometer resolution**
Van-Spengen,-W.-M.; De-Wolf,-I.; Puers,-R.
IMEC, Leuven, Belgium
Proceedings-of-the-SPIE-The-International-Society-for-Optical-Engineering. 2001; 4558:
268-76


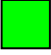
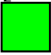
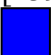
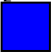

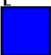
- [87] **On the number of measurement sites required to assess regional cerebral blood flow by laser-Doppler scanning during cerebral ischemia and reperfusion**
Soehle,-M.; Heimann,-A.; Kempfski,-O.
Inst. for Neurosurg. Pathophysiology, Johannes Gutenberg Univ., Mainz, Germany
Journal-of-Neuroscience-Methods. 30 Sept. 2001; 110(1-2): 91-4
- [88] **Development of a continuous scanning laser Doppler vibrometer with bow scanning compensation**
Kyhwan-Park; Sangyol-Yoon; Jongpil-La; Sukmin-Kim
Dept. of Mechatronics, Kwangju Inst. of Sci. of Technol., South Korea
ISIE-2001.-2001-IEEE-International-Symposium-on-Industrial-Electronics-Proceedings-Cat.-No.01TH8570. 2001: 359-63 vol.1
- [89] **Development of a continuous scanning laser Doppler vibrometer for vibration mode shape analysis**
Kyhwan-Park; Seonjae-Kim; Sangyol-Yoon; Jekil-Ryu
Dept. of Mech., Kwangju Inst. of Sci. & Technol., South Korea
Proceedings-of-the-2000.-IEEE-International-Conference-on-Control-Applications.-Conference-Proceedings-Cat.-No.00CH37162. 2000: 554-9
- [90] **Measurements of velocity distributions in the deformation zone in cold rolling by a scanning LDV**
Li,-E.-B.; Tieu,-A.-K.; Yuen,-W.-Y.-D.
Fac. of Eng., Wollongong Univ., NSW, Australia
Optics-and-Lasers-in-Engineering. Jan. 2001; 35(1): 41-9
- [91] **Fusion of acoustic/seismic and ground penetrating radar sensors for antitank mine detection**
Bradley,-M.; Sabatier,-J.-M.; Witten,-T.; Duncan,-M.; Hawkins,-J.
Planning Syst. Inc., Long Beach, MS, USA
Proceedings-of-the-SPIE-The-International-Society-for-Optical-Engineering. 2001; 4394 pt. 1-2: 979-90
- [92] **Moving vibrational measurement techniques, methodologies, and concepts from macroscopic applications to the microworld**
Bucaro,-J.-A.; Houston,-B.-H.; Photiadis,-D.-M.; Romano,-A.-J.; Sarkissian,-A.; Liu,-X.; Morse,-S.; Vignola,-J.; Williams,-E.-G.; Marcus,-M.-H.; Sekaric,-L.
Naval Res. Lab., Washington, DC, USA
IEEE-Ultrasonics-Symposium.-Proceedings.-An-International-Symposium-Cat.-No.00CH37121. 2000: 513-24 vol.1
- [93] **Evaluating quasi-self-sensing piezoelectric actuator by using an innovative laser Doppler interferometer**
Hsiao,-W.-H.; Lin,-T.-C.-H.; Chen,-S.-J.; Kon,-S.-C.; Lin,-C.; Shih,-H.-C.; Wu,-W.-J.; Lee,-C.-K.; Wu,-J.-G.-Y.
Inst. of Appl. Mech., Nat. Taiwan Univ., Taipei, Taiwan
Tenth-International-Conference-on-Adaptive-Structures-and-Technologies. 2000: 558-65
- [94] **A new computational remote acoustic impact NDT system for the inspection of composite materials and detection and quantification of corrosion**
Mew,-J.-M.; Webster,-J.-M.; Thevar,-T.; Schmidt,-T.
Div. of Comput. Sci., Portsmouth Polytech., UK
Insight-Non-Destructive-Testing-and-Condition-Monitoring. Jan. 2000; 42(1): 22-5

- [95] **Measured free vibrations of partially clamped, square plates**
Wilson,-J.-F.; Henry,-J.-K.; Clark,-R.-L.
Dept. of Civil & Environ. Eng., Duke Univ., Durham, NC, USA
Journal-of-Sound-and-Vibration. 13 April 2000; 231(5): 1311-20
- [96] **Experimental Robust Control of Structural Acoustic Radiation**
David E. Cox, Gary P. Gibbs, Robert L. Clark and Jeffrey S. Viperman
39th AIAA/ASME/ASCE/AHS/ASC Structures, Structural Dynamics, and Materials
Conference, Long Beach, California, AIAA 98-2023, April 20-23, 1998
- [97] **Validation of a new non-iterative method for accurate position determination of a scanning laser vibrometer**
Pauwels,-S.; Boucart,-N.; Dierckx,-B.; Van-Vlierberghe,-P.
Lms Int., Leuven, Belgium
Proceedings-of-the-SPIE-The-International-Society-for-Optical-Engineering. 2000; 4072:
266-71
- [98] **Normal mode testing using a scanning Laser Doppler Vibrometer**
Brehmer,-A.
Deutsches Zentrum fur Luft- und Raumfahrt e.V., Gottingen, Germany
Proceedings-of-the-SPIE-The-International-Society-for-Optical-Engineering. 2000; 4072:
184-93
- [99] **Review of 8-mm Piezoelectric Motor Connection Methods**
Barben, CL; Yerganian, SS
Kansas City Plant, Kansas City, MO (US); 8 Jun 2000
NTIS
- [100] **Tracking scanning laser Doppler vibrometer: extending laser vibrometer to arbitrarily objects**
Bendel, -K; Scelles, -N.; Dietzhausen, -H.
Corporate research- Applied physics; Robert Bosh GmbH
Proceeding of IMAC-XXI
- [101] **Positional calibration of galvanometric scanners used in laser Doppler vibrometers**
Stafne, -M. -A.(1); Mitchell, -L., -D.(2); West, -R., -L.(2)
(1)Electric Motor Development Division K4, Robert Bosh GmbH, Germany
(2)Dep. Of Mech. Eng., Virginia Polytechnic Institute and State University
Measurement 28 (2000) 47-59
- [102] **Structural vibration modes of a blown open organ pipe**
Runnemalm,-A.; Zipsler,-L.; Franke,-H.
Div. of Exp. Mech., Lulea Univ. of Technol., Sweden
Acustica-Acta-Acustica. Nov.-Dec. 1999; 85(6): 877-82
- [103] **Scanning laser Doppler is a useful technique to assess foot cutaneous perfusion during femoral artery cannulation**
Boyle N. H., Roberts P.C., Bernice Ng, Berkenstadt H., McLuckie A., Beale R. J., Mason C. R.
Dep. Of Surgery and Intensive Care, New Guy's House, Guy's Hospital London(UK)
Critical Care 1999, Vol. 3 No. 4
- [104] **Vibration of head suspensions for proximity recording**
Takahashi,-H.; Bogy,-D.-B.; Matsumoto,-M.
Dept. of Mech. Eng., California Univ., Berkeley, CA, USA
IEEE-Transactions-on-Magnetics. July 1998; 34(4) pt. 1: 1756-8

- [105] **Localizing energy sources and sinks in plates using power flow maps computed from laser vibrometer measurements**
Arruda,-J.-R.-F.; Mas,-P.
Univ. Estadual de Campinas, Sao Paulo, Brazil
Shock-and-Vibration. 1998; 5(4): 235-53
- [106] **Predicting and measuring flexural power flow in plates**
Arruda,-J.-R.-F.; Mas,-P.
Dept. de Mecanica Comput., Univ. Estadual de Campinas, Sao Paulo, Brazil
Proceedings-of-the-SPIE-The-International-Society-for-Optical-Engineering. 1996; 2868: 149-63
- [107] **Spatial domain modal analysis of lightly-damped structures using laser velocimeters**
Arruda,-J.-R.-F.
Dept. de Mecanica Comput., Univ. Estadual de Campinas, Brazil
Transactions-of-the-ASME.-Journal-of-Vibration-and-Acoustics. July 1993; 115(3): 225-31
- [108] **Comparison of accelerometer and laser Doppler vibrometer measurement techniques for a vibration test of a large aerospace structure**
Levin,-R.-I.; Lieven,-N.-A.-J.; Skingle,-G.-W.
Dept. of Aerosp. Eng., Bristol Univ., UK
Proceedings-of-the-SPIE-The-International-Society-for-Optical-Engineering. 1998; 3411: 502-13
- [109] **Pose estimation of a scanning laser Doppler vibrometer with applications to the automotive industry**
Xiandi-Zeng; Wicks,-A.; Allen,-T.-E.
Automated Anal. Corp., Ann Arbor, MI, USA
Optical-Engineering. May 1998; 37(5): 1442-7
- [110] **Improvement of ultrasonic testing of concrete by combining signal conditioning methods, scanning laser vibrometer and space averaging techniques**
Koehler, B; Hentges, G; Mueller, W
NDT and E International; 31 (4) Aug 1998, p.281-7
- [111] **Positional calibration of galvanometric scanners used in laser Doppler vibrometers**
Stafne, -M. -A.(1); Mitchell, -L., -D.(2); West, -R., -L.(2)
(1)Electric Motor Development Division K4, Robert Bosh GmbH, Germany
(2)Dep. Of Mech. Eng., Virginia Polytechnic Institute and State University
Measurement 28 (2000) 47-59
- [112] **Geometrical method for the determination of the position and orientation of a scanning laser Doppler vibrometer**
Xiandi-Zeng; Wicks,-A.-L.; Mitchell,-L.-D.
Dept. of Mech. Eng., Virginia Polytech. Inst. & State Univ., Blacksburg, VA, USA
Optics-and-Lasers-in-Engineering. Oct.-Nov. 1996; 25(4-5): 247-64
- [113] **Identification of energy sources and sinks in plates by means of a scanning laser Doppler vibrometer**
Blotter,-J.-D.; West,-R.-L.
Dept. of Mech. Eng., Virginia Polytech. Inst. & State Univ., Blacksburg, VA, USA
Noise-Control-Engineering-Journal. March-April 1996; 44(2): 61-8
- [114] **Acoustic radiation prediction of a compressor housing from three-dimensional experimental spatial dynamics modelling**
Montgomery,-D.-E.; West,-R.-L.; Burdisso,-R.-A.
Dept. of Mech. Eng., Virginia Polytech. Inst. & State Univ., Blacksburg, VA, USA
Applied-Acoustics. Feb. 1996; 47(2): 165-85

- [115] **Laser scanning system testing-errors and improvements**
William-Xinzuo-Li; Mitchell,-L.-D.
Dept. of Mech. Eng., Virginia Polytech. Inst. & State Univ., Blacksburg, VA, USA
Measurement-. Oct. 1995; 16(2): 91-101
- [116] **Visual statistical analysis of three-dimensional structural dynamics data**
Montgomery,-D.-E.; West,-R.-L.
Virginia Polytech. Inst. & State Univ., Blacksburg, VA, USA
Mechanical-Systems-and-Signal-Processing. May 1995; 9(3): 299-316
- [117] **A weighted least-squares discrete finite element formulation for modelling three-dimensional velocity response fields measured by a laser Doppler vibrometer**
Montgomery,-D.-E.; West,-R.-L.
Nomura Enterprise Inc., Chantilly, VA, USA
Mechanical-Systems-and-Signal-Processing. July 1996; 10(4): 471-95
- [118] **A rapidly scanning two-velocity component laser Doppler velocimeter**
Shinpaugh,-K.-A.; Simpson,-R.-L.
Dept. of Aerosp. & Ocean Eng., Virginia Polytech. Inst. & State Univ., Blacksburg, VA, USA
Measurement-Science-&-Technology. June 1995; 6(6): 690-701
- [119] **The calibration of a scanning laser vibrometer by a digital FM demodulation technique**
Xiandi-Zeng; Dominguez,-J.-L.; Wicks,-A.-L.
Dept. of Mech. Eng., Virginia Polytech. Inst. & State Univ., Blacksburg, VA, USA
NOISE-CON-94-Proceedings.-1994-National-Conference-on-Noise-Control-Engineering.-
Progress-in-Noise-Control-for-Industry. 1994: 799-804
- [120] **Computer vision techniques for comparing laser Doppler velocimeter scans of a vibrating plate to analytical plate modes**
Montgomery, David E; West, Robert L.
Virginia Polytechnic Inst and State Univ, Blacksburg, VA, USA
Proc Conf Digital Image Process Tech Appl Civ eng., ASCE, New York, NY(USA), 1993,
pp. 220-227
- [121] **Visualization of one-dimensional velocity fields over two-dimensional vibrating structures**
Lin, Wen Tang; West, Robert L
Virginia Polytechnic Inst and State Univ, Blacksburg, VA, USA
Proceedings-of-the-SPIE-The-International-Society-for-Optical-Engineering, Society of
Photo-optical Instrumentation engineers, Bellingham, WA (USA), 1993, vol. 1923, no. pt
2, pp. 1624-1628
- [122] **Computer animation of complex modal response of one-, two-, three-dimensional structures**
Montgomery, David E; West, Robert L
Virginia Polytechnic Inst and State Univ, Blacksburg, VA, USA
Proceedings-of-the-SPIE-The-International-Society-for-Optical-Engineering, Society of
Photo-optical Instrumentation engineers, Bellingham, WA (USA), 1993, vol. 1923, no. pt
2, pp. 1321-1327
- [123] **Signal-processing techniques for low signal-to-noise ratio laser Doppler velocimetry signals**
Shinpaugh,-K.-A.; Simpson,-R.-L.; Wicks,-A.-L.; Ha,-S.-M.; Fleming,-J.-L.
Virginia Polytech. Inst. & State Univ., Blacksburg, VA, USA
Experiments-in-Fluids. March 1992; 12(4-5): 319-28

- [124] **Three-Dimensional Rapidly Scanning Laser Doppler Velocimeter with Low SNR Signal Processing**
 Shinpaugh, KA; Simpson, RL
Virginia Polytechnic Inst. and State Univ., Blacksburg. Dept. of Aerospace and Ocean Engineering. 30 Nov 1990
- [125] **Experimental Robust Control of Structural Acoustic Radiation**
 David E. Cox, Gary P. Gibbs, Robert L. Clark and Jeffrey S. Viperman
39th AIAA/ASME/ASCE/AHS/ASC Structures, Structural Dynamics, and Materials Conference, Long Beach, California, AIAA 98-2023, April 20-23, 1998
- [126] **Angle resolved velocity distributions of sputtered medium Z atoms**
 Goehlich,-A.; Niemoeller,-N.; Doebele,-H.-F.
Inst. fur Laser- und Plasmaphys., Essen Univ., Germany
Journal-of-Nuclear-Materials. 1 Feb. 1997; 241-243: 1160-3
- [127] **Simultaneous measurement of the position and shape of a swimming fish by combining a fringe pattern projection method with a laser scanning technique**
 Zeng,-L.; Matsumoto,-H.; Kawachi,-K.
Japan Sci. & Technol. Corp., Tsukuba, Japan
Optical-Engineering. May 1998; 37(5): 1500-4
- [128] **Two-directional scanning method for reducing the shadow effects in laser triangulation**
 Zeng, L; Matsumoto, H; Kawachi, K.
Japan Sci. & Technol. Corp., Tsukuba, Japan
Measurement Science and Technology; 8 (3) Mar 97, p.262-6
- [129] **Problems of laser vibrometry of temporal bone specimens**
 Zahnert,-T.; Vogel,-U.; Hofmann,-G.; Huttenbrink,-K.--B.
Dept. of Oto-Rhino-Laryngology, Tech. Univ. Dresden, Germany
Proceedings-of-the-SPIE-The-International-Society-for-Optical-Engineering. 1996; 2868: 249-54
- [130] **The measurement of contact and grip force as reference for human hand transmitted vibration evaluation by laser scanning vibrometers**
 Marsili,-R.; Rossi,-G.
Ist. di Energetica, Perugia Univ., Italy
Proceedings-of-the-SPIE-The-International-Society-for-Optical-Engineering. 1996; 2868: 302-9
- [131] **Laser vibrometer analysis of sensor loading effects in underwater measurements of compliant surface motion**
 Caspall,-J.-J.; Gray,-M.-D.; Caille,-G.-W.; Jarzynski,-J.; Rogers,-P.-H.; McCall,-G.-S.-,II
Georgia Tech. Res. Inst., Georgia Inst. of Technol., Atlanta, GA, USA
AIP-Conference-Proceedings. 1996; (368): 411-30
- [132] **Scanning laser Doppler technique for velocity profile sensing on a moving surface**
 Sriram,-P.; Hanagud,-S.; Craig,-J.; Komerath,-N.-M.
Sch. of Aerosp. Eng., Georgia Inst. of Technol., Atlanta, GA, USA
Applied-Optics. 1 June 1990; 29(16): 2409-17
- [133] **A weighted least-squares discrete finite element formulation for modelling three-dimensional velocity response fields measured by a laser Doppler vibrometer**
 Montgomery,-D.-E.; West,-R.-L.
Nomura Enterprise Inc., Chantilly, VA, USA
Mechanical-Systems-and-Signal-Processing. July 1996; 10(4): 471-95

- [134] **Error evaluation of the structural intensity measured with a scanning laser Doppler vibrometer and k-space signal processing**
 Morikawa,-R.; Ueha,-S.; Nakamura,-K.
 Precision & Intell. Lab., Tokyo Inst. of Technol., Japan
 Journal-of-the-Acoustical-Society-of-America. May 1996; 99(5): 2913-21
- [135] **Experimental determination of bending strain power spectra from vibration measurements**
 Xu,-Y.; Miles,-R.-N.
 Roush Anatrol, Sunnyvale, CA, USA
 Experimental-Mechanics. June 1996; 36(2): 166-72
- [136] **Full-field random bending strain measurement of a plate from vibration measurements**
 Xu,-Y.; Miles,-R.-N.
 Dept. of Mech. Eng., State Univ. of New York, Binghamton, NY, USA
 Journal-of-Sound-and-Vibration. 18 April 1996; 191(5): 847-58
- [137] **Measurement of the transfer function between bending strain and a transient load using a scanning laser vibrometer**
 Moccio,-C.-A.; Miles,-R.-N.
 Dept. of Mech. Eng., State Univ. of New York, Binghamton, NY, USA
 Journal-of-Sound-and-Vibration. 8 Feb. 1996; 189(5): 661-8
- [138] **An identification algorithm for directing the measurement point of scanning laser vibrometers**
 Yanchu-Xu; Miles,-R.-N.
 Dept. of Mech. & Ind. Eng., State Univ. of New York, Binghamton, NY, USA
 Optics-and-Lasers-in-Engineering. 1995; 22(2): 105-20
- [139] **Estimation of random bending strain in a beam from discrete vibration measurements**
 Miles,-R.-N.; Bao,-W.; Xu,-Y.
 Dept. of Mech. & Ind. Eng., State Univ. of New York, Binghamton, NY, USA
 Journal-of-Sound-and-Vibration. 7 July 1994; 174(2): 191-9
- [140] **Transient strain response measurement using a scanning laser vibrometer**
 Moccio,-C.-A.; Miles,-R.-N.
 Dept. of Mech. & Ind. Eng., State Univ. of New York, Binghamton, NY, USA
 Advances-in-Electronic-Packaging-1993.-Proceedings-of-the-1993-ASME-International-Electronics-Packaging-Conference. 1993: 201-5 vol.1
- [141] **Global noise characteristics of a laser Doppler vibrometer. I. Theory**
 Streaan,-R.-F.; Mitchell,-L.-D.; Barker,-A.-J.
 Lexmark Int. Inc., Lexington, KY, USA
 Proceedings-of-the-SPIE-The-International-Society-for-Optical-Engineering. 1996; 2868: 2-11
- [142] **Global noise characteristics of it laser Doppler vibrometer. II. Experiments using beam dynamics**
 Streaan,-R.-F.; Mitchell,-L.-D.; Barker,-A.-J.
 Lexmark Int. Inc., Lexington, KY, USA
 Proceedings-of-the-SPIE-The-International-Society-for-Optical-Engineering. 1996; 2868: 97-105
- [143] **Dynamic characteristics of lens actuator for digital video disc**
 Takeshita,-N.; Fujita,-T.; Kime,-K.
 Imaging Syst. Lab., Mitsubishi Electr. Corp., Kyoto, Japan
 Proceedings-of-the-SPIE-The-International-Society-for-Optical-Engineering. 1995; 2514: 159-66

- [144] **The application of the laser scanning Doppler vibrometry in aero-engine development**
Hancox, J; Staples, B C; Parker, R J
Proceedings of the Institution of Mechanical Engineers. Pt.G. Journal of Aerospace Engineering; 209 (G1) 1995, p.35-42
- [145] **Structural imaging of an auto door for noise control purposes**
Yienger,-J.-M.; Mitchell,-L.-D.; West,-R.-L.
Swales & Associates, Beltsville, MD, USA
Sound-and-Vibration. July 1993; 27(7): 22-9
- [146] **Using a scanning laser vibrometer to investigate vibrating wire dynamics**
Maddux,-G.-E.
Wright Lab., Wright-Patterson AFB, OH, USA
Proceedings-of-the-SPIE-The-International-Society-for-Optical-Engineering. 1993; 1756: 134-45
- [147] **Turbulent Boundary Layer Inner-Outer Interactions**
Bogard, DG; Lim, C; Kohli, A.
Texas University at Austin. Dept. of Mechanical Engineering. 6 Dec 1993
- [148] **Detection of coherent structures in a turbulent boundary layer using a scanning LDV system**
Bolton, BL; Bogard, DG
Mech. Eng. Dep., Univ. Texas, Austin, TX, USA
Experimental Thermal and Fluid Science [EXP. THERM. FLUID SCI.], vol. 5, no. 3, pp. 274-280, 1992
- [149] **Scanning laser Doppler techniques for vibration testing**
Sriram,-P.; Craig,-J.-I.; Hanagud,-S.
Dept. of Aerosp. Eng., Wichita State Univ., KS, USA
Experimental-Techniques. Nov.-Dec. 1992; 16(6): 21-6
- [150] **Mode shape measurement using a scanning laser Doppler vibrometer**
Sriram, P; Hanagud, S; Craig, JI
Wichita State Univ, Wichita, KS, USA
INT J ANAL EXP MODAL ANAL., vol. 7, no. 3, pp. 169-178, 1992
- [151] **A laser Doppler scanner for imaging blood flow in skin**
Essex,-T.-J.-H.; Byrne,-P.-O.
Northern Regional Med. Phys. Dept., Newcastle Gen. Hospital, UK
Journal-of-Biomedical-Engineering. May 1991; 13(3): 189-94
- [152] **Estimation of velocity profiles for both laminar and turbulent unsteady flows in pipes**
Chunchen-Su; Uchiyama,-M.; Hakomori,-K.
Fac. of Eng., Tohoku Univ., Sendai, Japan
Transactions-of-the-Society-of-Instrument-and-Control-Engineers. May 1990; 26(5): 487-93
- [153] **A beam scanning LDV to measure velocity profile of unsteady flow**
Uchiyama,-M.; Hakomori,-K.
Faculty of Engng., Tohoku Univ., Aramaki, Sendai, Japan
Bulletin-of-the-Japan-Society-of-Precision-Engineering. June 1982; 16(2): 71-7
- [154] **Measuring automotive vibration with a scanning laser interferometer**
Townsend, G
Environmental Engineering; 3 (Sep 90) p.19, 22-3, 25, 29

- [155] **Application of a laser-Doppler scanning technique to the unstable flow field of a heated jet**
Lehmann,-B.; Mante,-J.
Inst. fuer Exp. Stromungsmech., Berlin, West Germany
ICIASF-'89-Record.-International-Congress-on-Instrumentation-in-Aerospace-Simulation-Facilities-Cat.-No.89CH2762-3. 1989: 254-62
- [156] **Computerized laser Doppler interferometric scanning of the vibrating tympanic membrane**
Konradsson,-K.-S.; Ivarsson,-A.; Bank,-G.
Dept. of Otolaryngology, Gen. Hospital, Lund Univ., Malmo, Sweden
Scandinavian-Audiology. 1987; 16(3): 159-66
- [157] **Measurements of instantaneous flow velocity distributions by a rapid beam scanning LDV**
Nakatani,-N.; Uehara,-A.; Maegawa,-A.; Sakabe,-T.; Yamada,-T.
Dept. of Precision Eng., Osaka Univ., Japan
Technology-Reports-of-the-Osaka-University. March 1987; 37(1865-1888): 143-50
- [158] **Flow measurements of proximity sensors with the beam scanning LDV**
Nakatani,-N.; Yamada,-T.
Dept. of Precision Eng., Osaka Univ., Japan
Fluid-Control-and-Measurement. 1986: 1021-6 vol.2
- [159] **Velocity profiles in decelerating turbulent pipe flows**
Van-de-Sande,-E.; Hiemstra,-W.
N.V. Kema, Arnhem, Netherlands
Fluid-Transients-in-Fluid-Structure-Interaction-1985.-Winter-Annual-Meeting-of-the-American-Society-of-Mechanical-Engineers. 1985: 19-24
- [160] **Fully automated quality control in the mass production of gasoline engines by means of laser-optical vibration measurement**
Schiffbaenker,-H.
ISATA-85:-In-Pursuit-of-Technical-Excellence.-International-Symposium-on-Automotive-Technology-and-Automation. 1985: 457-88 vol.1
- [161] **Scanning laser Doppler vibration analysis system**
Stoffregen,-B.
Volkswagenwerk AG, Wolfsburg, West Germany
Technisches-Messen-tm. Nov. 1984; 51(11): 394-7
- [162] **Convective pattern evolution and secondary instabilities**
Gollub,-J.-P.; McCarriar,-A.-R.; Steinman,-J.-F.
Phys. Dept., Haverford Coll., Haverford, PA, USA
Journal-of-Fluid-Mechanics. Dec. 1982; 125: 259-81
- [163] **Membrane vibration tests using surface-bonded piezoelectric patch actuation**
Gaspar, -L.-J.; Pappa, -S.R.
NASA Langley Research Center Hampton, VA
IMAC 2003
- [164] **Membrane Vibration Studies Using a Scanning Laser Vibrometer**
Gaspar, JL; Solter, MJ; Pappa, RS
National Aeronautics and Space Administration, Hampton, VA. Langley Research Centre. Feb 2001

- [165] **Experimental Robust Control of Structural Acoustic Radiation**
David E. Cox, Gary P. Gibbs, Robert L. Clark and Jeffrey S. Viperman
39th AIAA/ASME/ASCE/AHS/ASC Structures, Structural Dynamics, and Materials Conference, Long Beach, California, AIAA 98-2023, April 20-23, 1998
- [166] **Laser Doppler velocimeter development**
Seegmiller,-H.-L.; Bader,-J.-B.; Cooney,-J.-P.; DeYoung,-A.; Donaldson,-R.-W.-,Jr.; Gunter,-W.-D.-,Jr.; Harrison,-D.-R.
NASA Ames Res. Center, Moffett Field, CA, USA
IEEE-Aerospace-and-Electronics-Systems-Magazine. May 1986; 1(5): 16-20
- [167] **Development of a new laser Doppler velocimeter for the Ames high Reynolds channel no.11**
Seegmiller,-L.-H.; Bader,-J.-B.; Cooney,-J.-P.; DeYoung,-A.; Donaldson,-R.-W.-,Jr.; Gunter,-W.-D.-,Jr.; Harrison,-D.-R.
NASA Ames Res. Center, Moffett Field, CA, USA
ICIASF-'85-Record.-International-Congress-on-Instrumentation-in-Aerospace-Simulation-Facilities-Cat.-No.85CH2210-3. 1985: 36-47
- [168] **Laser Doppler Dust Devil Measurements**
Bilbro, JW; Jeffreys, HB; Kaufman, JW; Weaver, EA
National Aeronautics and Space Administration. Marshall Space Flight Center, Huntsville, Ala. Feb 1977
- [169] **Remote intensity fluctuation measurements with a laser Doppler radar [for rotational speed of disc and atmospheric measurements]**
Kennedy,-L.-Z.; Bilbro,-J.-W.
Marshall Space Flight Center, NASA, Huntsville, AL, USA
Applied-Optics. Sept. 1976; 15(9): 2008
- [170] **Development of a Laser Doppler System for the Detection, Tracking, and measurement of Aircraft Wake Vortices**
Huffaker, RM; Jeffreys, HB; Weaver, EA; Bilbro, JW
National Aeronautics and Space Administration Huntsville Ala George C Marshall Space Flight Centre. Mar 1975
- [171] **Development of a Laser Doppler System for the Detection and Monitoring of atmospheric Disturbances**
Jeffreys, HB; Bilbro, JW
National Aeronautics and Space Administration. Marshall Space Flight Center, Huntsville, Ala. 28 Nov 1975
- [172] **Axial flow measurements in trailing vortices**
Ciffone,-D.-L.; Orloff,-K.-L.
NASA, Moffett Field, CA, USA
AIAA-Journal. Aug. 1974; 12(8): 1154
- [173] **Laser Doppler Velocimeter Investigation of Trailing Vortices Behind a Semi-Span Swept Wing in a Landing Configuration**
Ciffone, DL; Orloff, KL; Grant, GR
National Aeronautics and Space Administration. Ames Research Center, Moffett Field, Calif. Aug 1973
- [174] **Aviation Safety Research and Transportation/Hazard Avoidance and elimination**
Sonnenschein, C; Dimarzio, C; Clippinger, D; Toomey, D
Raytheon Co., Sudbury, Mass. Dept. of Electro-Optics. Aug 1976

- [175] **Data Analysis Study and Performance Evaluation of the Scanning Laser Doppler System**
Sonnenschein, CM; Dimarzio, CA; Clippinger, DH
Raytheon Co., Sudbury, Mass. Advanced Development Lab.16 Dec 1974
- [176] **Scanning laser Doppler velocimeter system simulation for sensing aircraft wake vortices**
Thomson,-J.-A.-L.; Meng,-J.-C.-S.
Phys. Dynamics Inc., Berkeley, CA, USA
Journal-of-Aircraft. Aug. 1976; 13(8): 605-13
- [177] **Laser-Doppler velocity-profile meter**
Aponin,-G.-I.; Besshaposhnikov,-A.-A.
Instruments-and-Experimental-Techniques. July-Aug. 1976; 19(4) pt. 2: 1186-8;
Original: Pribery-i-Tekhnika-Eksperimenta. July-Aug. 1976; 19(4) pt. 2: 224-6
- [178] **Remote Measurement Utilizing NASA'S Scanning Laser Doppler Systems. Volume 1. Laser Doppler Wake Vortex Tracking at Kennedy Airport**
Krause, MC; Wilson, DJ; Howle, RE; Edwards, BB; Craven, CE
Lockheed Missiles and Space Co., Huntsville, Ala. Research and Engineering Centre.
Mar 1976
- [179] **Remote Measurement Utilizing NASA'S Scanning Laser Doppler Systems. Volume 2. Laser Doppler Dust Devil Velocity Profile Measurement Program**
Howle, RE; Krause, MC; Craven, CE; Gorzynski, EJ; Edwards, BB
Lockheed Missiles and Space Co., Huntsville, Ala. Research and Engineering Centre.
Mar 1976
- [180] **Conduct Overall Test Operations and Evaluate Two Doppler Systems to Detect, Track and Measure Velocities in Aircraft Wake Vortices**
Wilson, DJ; Krause, MC; Craven, CE; Edwards, BB; Coffey, EW
Lockheed Missiles and Space Co., Huntsville, Ala. Research and Engineering Centre. Dec 1974
- [181] **Constant doppler wide-angle laser beam scanning**
Farhat,-N.-H.
RCA, Camden, NJ, USA
Applied-Optics. May 1971; 10(5): 1180-1
- [182] **A laser Doppler velocimeter employing a scanning interferometer**
Kuriger,-W.-L.
Univ. Oklahoma, Norman, OK, USA
Proceedings-of-the-IEEE. Dec. 1969; 57(12): 2161
- [183] **Laser vibrometry measurements of rotating blade vibrations**
Reinhardt,-K.-A.; Kadambi,-R.-J.; Quinn,-R.-D.
Dep. Mech. And Aerospace Eng. Case Western Reserve University, Cleveland (USA)
Journal of Engineering for Gas Turbines and Power July 1995, Vol.117; 484-488
- [184] **Turbomachinery blade vibration and dynamic stress measurements utilizing nonintrusive techniques**
Kadambi,-R.-J.; Quinn,-R.-D.; Adams,-M.-L.
Dep. Mech. And Aerospace Eng. Case Western Reserve University, Cleveland (USA)
Journal of Turbomachinery October 1989, Vol.111; 468-474

- [185] **A fiber-optics laser Doppler probe for vibration analysis of rotating machines**
Cookson,-R.-A.; Bandyopadhyay,-P.
Sch. of Mech. Eng., Cranfield Inst. Of Technology; Bedford (UK)
Journal of Engineering for Power July 1980, Vol.102; 607-612
- [186] **Noncontact vibration measurements on compressor rotor blades**
Zielinski,-M.; Ziller,-G.
Elect. And Measurement Technology division, MTU (Germany)
Meas. Sci. Technol. 11 (2000) 847-856
- [187] **Measurement of rotational vibrations using a novel interferometric technique**
Lewin,-A.-C.; Volkmar,-R.; Siegmund,-G.
Polytec GmbH, (Germany)
Measurement 16 (1995); 81-90
- [188] **Principles and practice of the laser Doppler anemometry (second edition)**
Durst,-F.; Melling,-A.; Whitelaw,-J.-H.
London: Academic Press
- [189] **Synchronized-Scanning Laser Vibrometry**
Halkon, -B.; Rothberg, -S.
Wolfson Sch. Of Mechanical and Manufacturing Eng., Loughborough University (UK)
Proceedings-of-the-SPIE-The-International-Society-for-Optical-Engineering. 2004; 5503:
260-271
- [190] **Sensitivity of tuned bladed disk response to frequency veering**
J.A.Kenyon, J.H.Griffin, N.E. Kim
Journal of Engineering for Gas turbine and Power, October 2005, Vol.127
- [191] **Coriolis Forces in Forced Response Analysis of Mistuned Bladed Discs**
M.Nikolic, E.P.Petrov, D.J.Ewins
Proceeding of ASME Turbo Expo 2006, Power for Land and Air.
- [192] **The effects of Coriolis forces on vibration properties of bladed discs**
M.Nikolic, D.J.Ewins, E.P.Petrov, Dario Di Maio
7th IFT0MM-Conference on Rotor Dynamics, Vienna, Austria, 25-28 September 2006
- [193] **Experimental of Turbomachinery blade vibration predictions**
I.A.Severe
PhD thesis, Imperial College London, March 2004
- [194] **Modal Testing theory, practice and application (Second Edition)**
D.J.Ewins
Research Studies Press LTD.
- [195] **Polytec GmbH**
Private communication

Appendix

Legend:

 Innovation

 Method

 Application

- IC = Imperial College London (UK)
- UNIAN = Università degli Studi di Ancona (IT)
- VPI = Virginia Polytechnic Institute (USA)
- MU = Mississippi University (USA)
- NASA = National Aeronautics and Space Administration (USA)
- US NY = University State of New York (USA)
- UM = University of Missouri (USA)
- NTU = Nanyang Technology University (Singapore)
- NCSU = North Carolina State University (USA)
- UE de C = Universidade Estadual de Campinas (BR)
- LMSC = Lockheed Missiles and Space Co.
- Others = Other universities
- [...] = Refer to the paper number listed below the chart

Appendix

Year	IC			UNIAN							VPI					MU	NASA				
	CSLDV	SLDV Calibration	Tracking LDV	Human body	Electronic device	Tracking LDV	Damage detection	Automotive vibration	SLDV Calibration	Excitation source	General application	Flow measurements	Signal Processing	Visualization tech.	SLDV Calibration	ESPF & ESDM	Mine detection	Flow measurements	Noise control	Membrane vibration	
2003	[31]			[1]																	[163]
2002	[32]				[3]	[4]	[6]														
	[33]					[5]															
	[34]					[7]															
	[35]																				
2001		[36]				[10]		[8]	[9]								[77]				
	[37]																[78]				
	[38]																[79]				
2000	[40]				[14]	[11]		[13]		[16]				[111]							[164]
	[41]					[12]	[15]										[81]				
	[42]					[17]	[18]										[82]				
1999	[43]						[20]										[83]				
	[44]				[19]		[21]														
	[45]									[22]											
1998	[46]			[25]		[24]	[26]			[27]											
	[47]									[23]										[165]	
1997																					
1996	[48]					[28]								[112]	[113]						
	[49]														[114]						
1995	[51]			[29]																	
	[52]										[118]			[115]	[117]						
1994			[53]										[116]		[119]						
														[120]							
														[121]							
1993														[122]							
1992																					
1991													[123]								
1990												[124]					[84]				
1989																					
1988																					
1987																					
1986																				[166]	
1985																				[167]	
1984																					
1978																					
1977																				[168]	
1976																				[169]	
1975																				[170]	
																				[171]	
1974																				[172]	
1973																				[173]	
1969																					

Appendix

Year	US NY		UM	NTU	NCSU		UE de C		LMSC	Others										
	Strain measurements	SLDV Calibration	Damage detection	Micro-components	Damage detection	PZT	ESPF	Modal analysis	Flow measurements	System Innovation	Flow measurements	Quality control	Human body	Automotive vibration	Modal analysis	Boundary Layer	Application	Electronic device	Laser noise	Strain measurements
2003																				
2002			[72]	[56]	[62]										[55]		[54]	[76]		
2001																				
			[73]									[85]								
			[74]									[87]			[88]		[92]	[86]		
2000				[57]											[89]					
				[58]		[63]									[95]			[92]		
			[75]	[59]	[64]					[93]					[98]		[93]	[99]		
1999										[100]			[103]		[102]					
1998								[105]						[110]			[108]	[104]	[96]	
1997																				
										[128]							[126]			
1996	[136]												[129]						[134]	
	[137]						[106]					[130]							[141]	
																			[142]	[135]
1995																				
		[138]															[144]	[143]		
1994																				
	[139]																			
1993	[140]							[107]						[145]		[147]	[146]			
1992															[149]					
															[150]	[148]				
1991													[151]							
1990											[152]			[154]						
1989											[155]									
1988																				
1987											[157]	[156]								
1986											[158]									
1985											[159]	[160]								
1984										[161]										
1983																				
1982															[153]					
															[162]					
1977																				
1976								[178]		[166]										
								[179]	[177]	[165]										
1975																				
1974								[180]		[164]										
1972																				
1971										[181]										
1970																				
1969										[182]										

Appendix

Year	Others																	
	Moving object	SLDV Calibration	Tracking LDV	Damage detection														
2003			[100]															
2002																		
			[66]															
2001																		
	[90]																	
2000		[97]		[61]														
		[101]		[92]														
1999																		
1998	[127]																	
1997																		
1996																		
	[131]																	
1995																		
1994																		
1993																		
1992																		
1991																		
1990	[132]																	
1989																		
..																		
1969																		